Hyaluronic Acid-based Multifunctional Bioinks for 3D Bioprinting of Mesenchymal Stromal Cells for Cartilage Regeneration

-

Hyaluronsäure-basierte multifunktionale Biotinten für den 3D Biodruck von mesenchymalen Stromazellen zur Knorpelregeneration

Doctoral thesis for a doctoral degree
at the Graduate School of Life Sciences,
Julius-Maximilians-Universität Würzburg,
Section Biomedicine

submitted by

Julia Hauptstein

from Pfaffenhofen a. d. Ilm

Würzburg 2022

Submitted on: _____

Members of the Thesis Committee

Chairperson: Prof. Dr. Carmen Villmann

Primary Supervisor: Prof. Dr. Torsten Blunk

Second Supervisor: Dr. Jörg Teßmar

Third Supervisor: Dr. Rainer Detsch

Date of Public Defence: _____

Date of Receipt of Certificates: _____

Contents

Summary

Articular cartilage is a highly specialized tissue in the human body which provides a lubricated gliding surface in joints and thereby enables low-friction movement. If damaged once, for example by traumatic injury or natural wear and tear, it has a very low intrinsic healing capacity, and the formation of osteoarthritis (OA) is highly prevalent. This disease is the main cause of disability among elderly and there is still no treatment in the clinic which can stop the progression of OA and restore healthy cartilage tissue. Tissue engineering and especially 3D biofabrication presents a promising perspective in the field of articular cartilage regeneration. With this technology, cartilage defects can be filled with healthy cells embedded in bioactive ink materials. Thereby, the composition of the applied bioink is crucial for defect restoration, as it needs to have the physical properties for the fabrication process and also suitable chemical cues to provide a chondro-supportive environment for embedded cells. In the last years, ink compositions with high polymer contents and crosslink densities were frequently used to provide 3D printability, shape fidelity and construct stability. However, these dense polymeric networks were often associated with restricted bioactivity and impaired cell processes like proliferation, migration, differentiation and the distribution of newly produced extracellular matrix (ECM), which is especially important in the field of cartilage engineering. Therefore, the aim of this thesis was the development of hyaluronic acid (HA)-based bioinks with a reduced polymer content which meet the physical needs for 3D bioprinting and additionally facilitate chondrogenic differentiation of mesenchymal stromal cells (MSCs) and the homogeneous distribution of newly produced ECM.

Chapter I: In the first part of this thesis, the polymer content of HA-based bioinks was reduced from 15 % to 3 %. Further addition of 1 % unmodified high molecular weight HA (hmHA) increased ink viscosity and enabled PCL-supported 3D bioprinting. Due to the newly observed porogenic effect of hmHA, homogeneous ECM distribution was achieved, which resulted in significantly increased mechanical properties and an overall improved quality of cartilage constructs.

Chapter II: In the second part, a novel dual-stage crosslinking mechanism was developed which enabled stand-alone 3D bioprinting of HA-based bioinks with very low polymer contents (down to 2 %). By adjusting molecular weights of HA and PEG-crosslinkers, a versatile bioink platform was generated with different properties for articular cartilage regeneration and prospective applications also for other tissue engineering approaches.

Chapter III: In the last part of this thesis, the composition of one special bioink from the novel platform (Chapter II) was adjusted to enable biomimetic functionalization and covalent tethering of the chondrogenic differentiation factor TGF-β1. A detailed analysis of protein function after

3D printing was performed and cartilage constructs with superior properties and promising clinical perspectives were generated.

Taken together, this thesis presents valuable new developments in the field of HA-based biomaterials. Starting from not-printable hydrogels with high polymer contents and restricted bioactivity, distinct stepwise improvements were achieved regarding stand-alone 3D printability as well as MSC differentiation and homogeneous ECM distribution. Therefore, all newly developed inks in this thesis made a valuable contribution in the field of cartilage regeneration and represent promising approaches for potential clinical applications. The underlying mechanisms and established ink design criteria can further be applied to other biofabricated tissues, emphasizing their importance also in a more general research setting.

Zusammenfassung

Gelenkknorpel ist ein sehr spezialisiertes Gewebe im menschlichen Körper, das durch seine gleitfähige Oberfläche reibungsarme Bewegungen der Gelenke ermöglicht. Ist der Knorpel jedoch einmal geschädigt, zum Beispiel durch einen Unfall oder graduelle Abnutzung, kann er sich kaum selbst reparieren und es kommt häufig zur Entstehung von Osteoarthritis (OA) – einer Krankheit, die besonders bei alten Menschen die Hauptursache von körperlicher Behinderung darstellt und in der modernen Medizin noch nicht geheilt werden kann. Ein vielversprechender Ansatz ist die Geweberekonstruktion mittels Tissue Engineering, insbesondere der 3D Biofabrikation von Knorpeltransplantaten. Mithilfe dieser Technologie kann man Knorpeldefekte mit gesunden Zellen in bioaktiven Tintenmaterialen füllen. Hierbei ist die Zusammensetzung der Tinte besonders wichtig für die Funktionsweise des Konstruktes, da sie sowohl die physikalischen Voraussetzungen für den 3D Druck als auch die biologische Unterstützung für die Zellkultivierung mitbringen muss. In den letzten Jahren wurden häufig Tintenzusammensetzungen mit hohen Polymergehalten und Vernetzungsdichten verwendet, um 3D-Druckbarkeit, Formtreue und Konstruktstabilität zu gewährleisten. Diese dichten Polymernetzwerke verursachten jedoch häufig eine eingeschränkte Bioaktivität und die Beeinträchtigung von Zellprozessen wie Proliferation, Migration, Differenzierung und der Verteilung der neu gebildeten Extrazellulärmatrix (ECM), die insbesondere im Knorpel-Engineering von großer Bedeutung ist. Daher war das Ziel dieser Arbeit Tinten auf Hyaluronsäure (HA)-Basis mit reduziertem Polymergehalt zu entwickeln, die die physikalischen Anforderungen für den 3D-Biodruck erfüllen und zusätzlich die chondrogene Differenzierung von mesenchymalen Stromazellen (MSCs) unterstützen und eine homogene Verteilung der neu produzierten ECM ermöglichen.

Kapitel I: Im ersten Teil der Arbeit wurde der Polymergehalt von HA-basierten Tinten von 15 % auf 3 % reduziert. Die Zugabe von 1 % unmodifizierter hochmolekularer Hyaluronsäure (hmHA) hat die Viskosität der Tinten erhöht und den PCL-unterstützten 3D Druck ermöglicht. Der neu beobachtete porogene Effekt der hmHA trug außerdem zu einer homogenen ECM-Verteilung bei, die die mechanischen Eigenschaften und damit die Qualität der Konstrukte signifikant verbessert hat.

Kapitel II: Im zweiten Teil wurde ein zweistufiger Vernetzungsmechanismus entwickelt, der den freistehenden 3D Druck von Tinten mit sehr geringem Polymergehalt (bis zu 2 %) ermöglichte. Durch die Einstellung der Molekulargewichte von HA und PEG-Vernetzern konnte eine Tintenplattform mit unterschiedlichen Eigenschaften generiert werden, die für die Knorpelregeneration, aber auch für andere Ansätze im Tissue Engineering vielversprechend ist.

Kapitel III: Im letzten Teil der Arbeit wurde eine Tinte der neuen Plattform aus Kapitel II dahingehend verbessert, dass sie eine kovalente Modifikation mit dem Differenzierungsfaktor TGF-β1 ermöglichte. In dieser Studie wurde die Proteinfunktionalität nach dem Druckprozess ausführlich analysiert und es konnten Knorpelkonstrukte mit vielversprechenden Eigenschaften für eine potenzielle klinische Anwendung hergestellt werden.

Insgesamt stellt diese Arbeit wertvolle neue Entwicklungen auf dem Gebiet der HA-basierten Biomaterialien vor. Ausgehend von nicht druckbaren Hydrogelen mit hohem Polymergehalt und eingeschränkter Bioaktivität wurde eine deutliche schrittweise Verbesserung hinsichtlich 3D-Druckbarkeit sowie MSC-Differenzierung und homogener ECM-Verteilung erreicht. Daher leisten alle hier neu entwickelten Tinten einen wertvollen Beitrag auf dem Gebiet der Knorpelregeneration mit Potenzial zur klinischen Anwendung. Die zugrunde liegenden Mechanismen und etablierten Tinten-Designkriterien können weiterhin auch auf andere biofabrizierte Gewebe übertragen werden, was ihre Bedeutung auch für ein weiter gefasstes Forschungsfeld unterstreicht.

1. General Introduction

1.1. Cartilage in the human body

Human cartilage arises from the embryonal mesenchyme and can be classified as elastic, fibrous or hyaline. Each subgroup has a special composition of extracellular matrix (ECM) and differs in morphology, collagen composition and elastin content. Elastic cartilage is a flexible non-load bearing tissue with a high elastin content and can be found for example in the epiglottis, the external ear and the auditory tube. Fibrous cartilage contains mainly collagen type I and functions as the transitional tissue between tendons and hyaline cartilage, like the menisci or intervertebral discs. Hyaline cartilage is the most abundant type of cartilage in the human body. It is responsible for bone formation in the embryonal development and can be found in costal cartilages, the respiratory system and in synovial joints in the adult body.[1-4]

1.1.1. Structure and function of articular cartilage

Articular cartilage is a specialized form of hyaline cartilage and covers the articulating ends of bones. This aneural, avascular and alymphatic tissue is 2 to 4 mm thick, wear-resistant and has a high compressive strength. It is located in the synovial joints like hips or knees, where it provides a lubricated gliding surface and enables low-friction movement. Chondrocytes account only for 1 – 5 % of the total articular cartilage volume and are responsible for ECM maintenance. The dense ECM is principally composed of water, collagens and proteoglycans.[3-6] Collagen type II is predominant in articular cartilage with around 60 % of the dry weight and forms a tight fibrillar meshwork, stabilized by less abundant collagens (type I, IV, V, VI, IX and XI). Proteoglycans consist of a protein core with covalently attached glycosaminoglycans (GAG) like chondroitin sulfate, keratan sulfate or hyaluronic acid. Examples for proteoglycans are aggrecan, decorin, biglycan and fibromodulin. Aggrecan is the most abundant proteoglycan in articular cartilage and forms large aggregates with hyaluronic acid via link proteins. Negatively charged GAGs attract positively charged ions like Ca^{2+} and Na^{+} and are responsible for water absorption. GAGs and collagens form a tight network and thereby enable load-dependent and viscoelastic deformation. The tensile strength of collagen fibrils and the compressive strength of GAG aggregates provide these unique mechanical properties, which are needed to withstand high cyclic loads of articular cartilage.[4, 5, 7-9]

At a macroscopic view, articular cartilage has a highly organized structure and is composed of four zones, which differ in chondrocyte morphology and expression patterns and therefore also in ECM composition and arrangement:[3-5] (Figure 1)

1. The superficial (tangential) zone (STZ) makes up 10 – 20 % of thickness and covers articular cartilage. It is in contact with the synovial fluid, contains a comparably high

number of flattened chondrocytes and is responsible for biggest part of tensile and shear strength, due to the tangential collagen fibril arrangement.

2. The middle (transitional) zone comprises 40 – 60 % and is characterized by randomly arranged collagen fibrils and a low number of spherical chondrocytes.
3. The deep (radial) zone represents around 30 – 40 % of articular cartilage volume and shows perpendicular orientation of chondrocytes and large collagen fibrils. It contains the highest amount of GAGs and the lowest amount of cells and water and has therefore the greatest resistance to compressive forces.
4. The calcified zone (confined by the tidemark) connects articular cartilage with the underlying subchondral bone. Chondrocytes in this compartment have a low metabolic activity and express a hypertrophic phenotype (e.g., collagen type X).

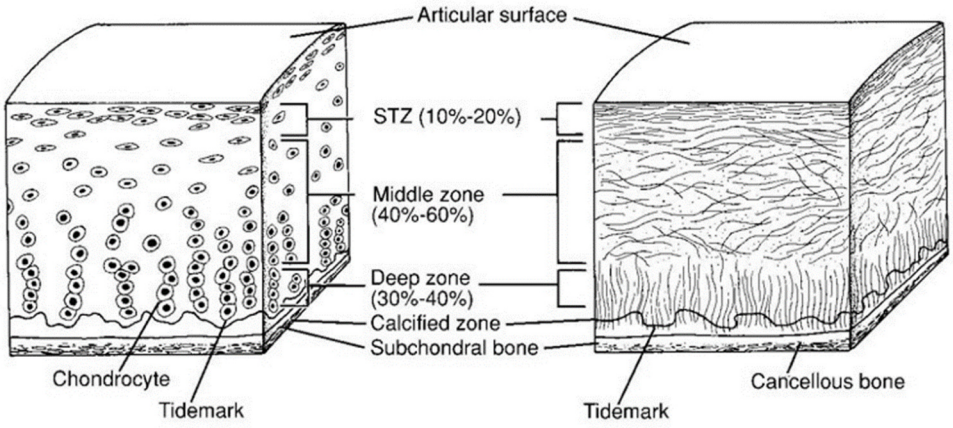

Figure 1: Structure of articular cartilage. Schematic diagram of chondrocyte (left) and collagen fiber (right) organization in the three main zones of the uncalcified cartilage (superficial, middle and deep zone) as well as the calcified zone and the subchondral bone. Reprinted by permission from Wolters Kluwer Health, Inc.: *J. Buckwalter, V. Mow and A. Ratcliffe, Journal of the American Academy of Orthopedic Surgeons*, *1994, Volume 2, Issue 4, p 192-201;*[10] License number: 5150751337150.

1.1.2. Clinical approaches for the treatment of articular cartilage defects

Focal cartilage defects are mainly caused by traumatic injuries. A direct consequence is severe pain and the impact on joint function, but the patient is furthermore predisposed to progressive degenerative changes within the tissue. In healthy cartilage, chondrocytes maintain ECM homeostasis leading to a functional tissue. But an imbalance of anabolic and catabolic mechanisms can lead to abnormal tissue remodeling, cartilage thinning and a pathologic state called osteoarthritis (OA).[11] OA is a highly prevalent disorder of the synovial joints and a main cause of disability among elderly. In 2020, approximately 654 million people of 40 years and older suffered from OA worldwide and the disease becomes more and more important with regard to the demographic change.[12] The main risk factors besides age are gender, joint injury, obesity, genetic predisposition and mechanical factors like malalignment or abnormal joint shape.[13, 14]

OA is usually graded with a assessment system developed by Collins,[15-17] which rates cartilage surface texture, lesion size, bony changes and metabolic activity of chondrocytes in an ascending severity from grade I to IV. Due to the lacking blood supply, cartilage has a very low intrinsic self-healing capacity and still, there is no clinical treatment that can prevent or stop the progression of OA. Small lesions (< 0.5 – 1 cm^2, grade I and II) are generally treated non operatively. Conventional therapies like physiotherapy, anti-inflammatory or pain-relieving drugs and diverse intra-articular joint injections can only relieve trauma or OA symptoms and frequently require joint replacement in later stages (grade III and IV).[18] Therefore, several surgical techniques are applied in the clinic, which are summarized in the following:[19-22]

- Microfracture is a marrow stimulation technique that can be applied for small osteochondral lesions (< 2 cm^2). Thereby, an arthroscopic awl is used to make multiple holes in the subchondral bone plate of full-thickness chondral defects to stimulate blood flow and release of bone marrow including MSCs. It is minimally invasive, fast and of low costs and therefore represents a frequently used first-line treatment. However, the formed blood clots mainly produce fibrocartilaginous tissue with reduced mechanical resistance than hyaline cartilage which likely results in treatment failure beyond 5 years postoperatively.[19-21, 23, 24] Commercial transplants like TruFit,[25, 26] MaioRegen[27, 28] or ChondroMimetic®[29] use endogenous stem cells indirectly via bone marrow stimulation. However, clinical evaluations show mixed results and large-scale clinical trials are needed to prove safety and effectiveness.[22, 30]
- Mosaicplasty or osteochondral autograft transfer (OAT) includes removal of an osteochondral plug from the patient's healthy cartilage tissue and the transfer to the damaged joint (< 4 cm^2). Several studies report a beneficial medium-term outcome, but donor site morbidity and long-term failure especially for older patients or defects sizes greater than 3 cm^2 are still problematic.[19, 21, 31-33]
- Another similar approach for larger defects is osteochondral allograft transfer (OCA), where allografts from a different human are used for defect filling, but availability and preservation of fresh grafts, high costs and the risk of disease transmission represent problems for this technique.[19, 20, 22, 34] Commercial cylindric allografts are for example Cartiform®[35] or Chondrofix®.[36]
- Particulate articular cartilage implantation (PACI) uses autologous or allogenic cartilage particles (1 – 2 mm) for defect filling. Examples in the clinic and on the market are CAIS,[37] DeNovo NT[38, 39] or BioCartilage®.[40] Those methods are used for small defects (< 3.5 cm^2) and are still lacking long-term follow-up data.[22]
- Autologous chondrocyte implantation (ACI) is frequently used for larger defects (> 4 cm^2) and requires two consecutive surgeries. Chondrocytes are isolated during a first arthroscopy from healthy patient tissue and expanded for several weeks *in vitro*. In a

second surgery, these chondrocytes are implanted to the defect site and covered with a periosteal flap (first generation),[41, 42] a collagen membrane (second generation)[43, 44] or cell-carrying matrices (matrix-induced autologous chondrocyte implantation – MACI; third generation, also see below).[45] Follow-up studies provided promising results especially for young patients, but long recovery times, high costs, donor-site morbidities, the need for two surgeries and the generation of mechanically inferior fibrocartilage are among the disadvantages.[19-22, 46] A commercial example of ACI is Chondrosphere® (spherox),[47, 48] which uses spheroids from autologous chondrocytes. This strategy provides a natural matrix and prevents chondrocyte loss but requires a long and complex culturing procedure at high costs.[22]

- Cell-scaffold construct strategies are the most commonly used tissue engineering techniques in the field. Commercial MACI products are for example BioSeed®-C,[49, 50] CaReS®,[51] NeoCart®[52, 53] or NOVOCART® 3D.[54, 55] MACI inevitably faces similar limitations like ACI (see above) and long-term follow-up data of clinical trials are needed to prove safety and effectiveness of these products. Further possible cell sources besides chondrocytes are mesenchymal stem cells (MSCs), embryonic stem cells (ESCs) or induced pluripotent stem cells (iPSCs).[22]

Cartilage tissue engineering is considered to be the most promising approach to regenerate hyaline cartilage. However, the optimal solution has been not found yet. Current challenges include safe and minimal-invasive cell sources, advanced biomimetic scaffold materials, better cell-scaffold binding methods for example by hydrogel loading and advanced fabrication techniques like 3D bioprinting.[22]

1.2. Cartilage tissue engineering

Tissue engineering (TE) evolved in the early 1990s and was defined by Langer and Vacanti in 1993 as “an interdisciplinary field that applies the principles of engineering and the life sciences toward the development of biological substitutes that restore, maintain, or improve tissue function.”[56] It was proposed as a promising new horizon in treatment approaches of articular cartilage defects, involving three key components: cells, signaling factors and scaffolds.[56, 57] Another, more recent, advancement in the field was 3D biofabrication which generates living tissue analogues in automated processes and in computer-generated designs. In the last decades, scientists developed a wide range of cell-material combinations for cartilage regeneration. Frequently used cell sources, signaling factors and diverse applied biomaterials for TE and 3D biofabrication with their main benefits and limitations are summarized in the following.

1.2.1. 3D biofabrication of cartilage

3D biofabrication addresses many tissue engineering challenges as it generates complex tissues with living cells using additive manufacturing techniques.[58, 59] Bioassembly and bioprinting represent the main biofabrication techniques to produce defined 2D or 3D architectures. Bioassembly uses self-assembled preformed cell-containing units, while bioprinting enables precise patterning and assembly of cells, biomaterials, and biologically active factors to build defined hierarchical constructs. Thereby, the use of synthetic or natural derived biomaterials like hydrogels allow for the spatiotemporal modulation of cell-cell and cell-ECM interactions. These hydrogels, which are processed together with cells and/or biological molecules, are termed bioinks.[60-62] Commonly applied techniques in the field of biofabrication are for example selective laser sintering, stereolithography, fused deposition modelling, solution and melt electrospinning and 3D printing or plotting.[61, 63] Cell-laden hydrogel scaffolds can be produced by laser-based, droplet-based or extrusion-based bioprinting.[58, 64] Laser-based bioprinting includes laser-induced forward transfer or laser-guided direct writing but is rarely used for cartilage TE.[65] Droplet-based bioprinting employs thermal, piezoelectric or electrostatic drop-on-demand technologies to create precise constructs, which were already applied for *in vitro* and *in vivo* cartilage regeneration approaches.[66, 67] The most frequently used bioprinting technique is extrusion-based bioprinting, as it is comparably easy to conduct, it has a high economic efficiency, and allows for a wide range of applicable materials.[58, 64] Thereby, a robotic dispensing system extrudes a bioink filament by using pneumatic or mechanical (piston or screw) driven ink transfer.[62, 68] In the last years, many researchers utilized this technique and generated promising perspectives in the field of cartilage TE.[69-72]

1.2.2. Cell sources

Autologous chondrocytes were the first cell source explored for cartilage TE as they exhibit the natural chondrocyte phenotype and no risk of immune rejection or disease transmission. However, limitations like low cell numbers, dedifferentiation, donor site morbidity or the generation of fibrocartilage shifted the focus on other possibilities.[22, 73] Stem cells are a widely used alternative cell source due to their strong proliferation and differentiation capacity. Most frequently used are pluripotent mesenchymal stem cells (MSCs)[74] which can differentiate towards the adipogenic, osteogenic and chondrogenic lineage. These cells can be isolated from the bone marrow (BMSCs),[75] adipose tissue (ASCs),[76] peripheral blood (PBMSCs),[77] umbilical cord blood (UCB-MSCs),[78] Wharton's jelly (WJ-MSCs)[79] or synovial tissue/fluid (SMSCs).[80, 81] Although these cell sources have a great potential and provide hope for cartilage regeneration, there are still problems to be solved like availability, high variability due to donor age[82] and disease status,[83] donor site morbidity from autologous cells, disease transmission and immune rejection from allogenic MSCs[84] or hypertrophic differentiation.[22, 85] Embryonic stem cells (ESCs) are

totipotent and can differentiate into any kind of cells, which makes them – in theory – the ideal seed cell for tissue engineering approaches. But ethical controversy, the risk of immune rejection, disease transmission and tumorigenicity impede their clinical potential.[86, 87] Induced pluripotent stem cells (iPSCs) can be obtained by reprogramming differentiated adult cells via OCT4, SOX2, MYC and KLF4.[88] This technique allows autologous cell transplantation with beneficial cell properties and no ethical controversy. Preclinical studies proved their application value for cartilage regeneration[89], but complicated preparation procedures, high costs, varying reprogramming efficiency and tumorigenicity are among the limitations.[90, 91]

1.2.3. Biological and environmental factors

Native articular cartilage has a complex three-dimensional (3D) ECM architecture providing cells a specialized niche to reside, proliferate and differentiate. This 3D environment is crucial especially for isolated chondrocytes, as they lose their differentiated phenotype in 2D culture.[92] Therefore, 3D cultures like pellet or micromass systems have been used for culturing chondrocytes or for promoting differentiation of MSCs.[93, 94] Other factors adopted from the native environment is the reduced oxygen tension and mechanical stimulation of TE constructs. Both biophysical stimuli were shown to increase cartilaginous ECM production.[95, 96] Apart from biophysical stimuli, biochemical stimuli like growth factors play a crucial role for cartilage engineering, especially for implantation of MSCs. Cartilage formation during embryonal development involves several growth factors, which can be utilized for chondrogenic differentiation of stem cells. Most commonly used are members of the transforming growth factor β (TGF-β) superfamily, TGF-β1 and -β3 or bone morphogenic proteins (BMPs) in combination with a chondrogenic culture medium containing insulin, transferrin, and selenous acid (ITS), dexamethasone, ascorbic acid and proline.[97, 98]

1.2.4. Scaffold materials

Scaffold materials for cartilage TE represent a major challenge in the field with high requirements regarding chemical and physical properties. They need to support cell migration, proliferation and differentiation and possess an open porous network to enable distribution of newly produced ECM. On the other hand, they should provide sufficient mechanical properties, have the potential to integrate properly with adjacent cartilage and should be biodegradable.[99] Scaffolds for cartilage engineering can be of natural or synthetic origin, or a hybrid of both. Favorable synthetic polymers are immunological inert, slowly degradable and their mechanical and structural features are easily adjustable and enable further chemical modification and processing. Widely used synthetic polymers are for example polyurethane (PU),[100-102] poly(glycolic acid) (PGA),[103-105] ply(lactic acid) (PLA),[105-107] poly(ethylene glycol) (PEG)[108-110] or poly(ε-caprolactone) (PCL).[111-113] However, synthetic polymers often enable only poor cell adhesion and can release

harmful acidic degradation products at implantation sites.[99, 114, 115] In contrast, natural polymers frequently have excellent biocompatibility, biodegradability, low immunogenicity and favorable cellular interaction properties and were therefore extensively studied in cartilage TE approaches. Frequently used natural polymers are for example hyaluronic acid,[116-118] collagen,[119-121] gelatin,[122-124] chondroitin sulfate,[125-127] chitosan,[128-130] alginate,[131-133] silk,[134-136] cellulose[137-139] or decellularized ECM (dECM).[140-142] However, natural polymers may have pathogen risks or batch to batch inconsistencies and have limited mechanical properties impeding further processing methods like 3D printing. Therefore, composite materials are also frequently utilized for cartilage TE to combine physical and chemical benefits from both sources.[143]

1.2.4.1. Hyaluronic acid

Most natural polymers used for cartilage TE are not overly specific for this tissue and lack cartilage-like ECM molecules or binding sites. In contrast, hyaluronic acid is ubiquitously expressed in all vertebrates and represents a main component of articular cartilage ECM and the synovial fluid. It is a non-sulfated GAG and a linear polysaccharide containing alternating N-acetyl-D-glucosamine and D-glucuronic acid linked via β(1-4) and β(1-3) bonds[144] and provides two recognition sites for the cell surface receptors CD44 and CD168 (or RHAMM; receptor for hyaluronan mediated motility).[145, 146] Thereby, natural HA is involved for example in cell attachment, migration, proliferation, differentiation and cartilage formation. By addition of HA to inert hydrogels, several studies proved the chondro-supportive properties of this molecule.[147, 148] HA has a great biocompatibility, inherent biodegradability and low immunogenicity, which characterizes this polysaccharide as a beneficial material for biomedical applications including cartilage TE.[118, 149-151] Furthermore, its structure is easily accessible for chemical modifications at its functional carboxyl, hydroxyl or N-acetyl groups. Thereby, HA properties regarding hydrophobicity or biological activity can be altered or chemical crosslinkers can be introduced for hydrogel network formation with other polymers.[152-154] HA-based materials normally have poor mechanical properties, but are frequently used for the regeneration of tissues with different mechanics like cartilage, bone, skin or brain. To mimic the tough mechanical properties within stiff tissues like cartilage or bone, several approaches utilized a high polymer content or crosslink density,[68, 155-157] the supplementation of inorganic materials like calcium phosphate or hydroxyapatite,[158, 159] or hybrid printing with synthetic polymers like PCL.[160-162] In the last years, many researchers focused on HA-based materials for cartilage regeneration and expanded the field of tissue engineering and 3D biofabrication with promising results.[151, 155]

1.2.4.2. Biomimetic functionalization

Although HA-based hydrogels have a great clinical potential as outlined above, they often lack biomimetic or biochemical functionalities[163-165] and effectiveness in practical applications like adhesiveness[166-168] or injectability.[169-172] Especially in the field of cartilage TE, the introduction of biomimetic peptides was frequently used to further enhance the chondro-supportive potential of the used HA-based biomaterials.[151, 173-175] Another crucial factor to drive chondrogenic differentiation of MSCs and maintain normal cartilage homeostasis is the differentiation factor TGF-β.[176] In normal cell culture approaches, this protein is continuously applied with each medium change, which impedes a transfer to clinical approaches. For this reason, several studies focused on long-lasting application methods to circumvent the need for constant protein supplementation.[177] Direct loading, encapsulation, reverse binding or covalent tethering are among the commonly used techniques to provide and control the release of TGF-β from hydrogels.[178] Improved MSC differentiation was shown *in vitro* and *in vivo* by non-covalent TGF-β loading in cast[179-181] and printed approaches.[65, 182, 183] Further enhancement of TGF-β maintenance in not-printable constructs was successfully performed via covalent protein incorporation.[184-186] Covalent TGF-β tethering to 3D printable bioinks and the examination of protein function after applied shear stresses was not described in the literature so far. Therefore, this topic was analyzed as one goal of this thesis.

1.3. Goals of the thesis

In recent years, a wide range of different therapy approaches were developed for the treatment and regeneration of damaged articular cartilage. Although many therapies improved the clinical outcome of patients, several problems like long-term failure or the formation of mechanically inferior fibrocartilage persisted.[22] Tissue engineering and especially 3D bioprinting represents a very promising alternative in the field of cartilage regeneration, as it combines living cells with chondro-supportive bioinks in personalized construct geometries via scalable automated additive manufacturing. Thereby, a great variety of bioinks may be used for construct generation, which opened a new field in this research area. Special ink requirements are for example physical properties like viscoelasticity and shape fidelity for the 3D printing process, biocompatibility and biodegradability to enable cell proliferation and differentiation, as well as a porous and loose gel network to support the distribution of newly produced ECM during construct maturation.[68] Shape fidelity and nice printability has been mainly achieved by using hydrogels with high polymer contents or high crosslink densities, resulting in limited cell proliferation, migration and differentiation.[156, 157] In contrast, low-concentrated and soft hydrogels support bioactivity, but are often too liquid for 3D fabrication processes.[187] The traditional biofabrication window represents a balance between these properties and exists for medium crosslinked hydrogels, which compromise both, biological and physical needs.[68] New strategies and novel bioink approaches

are therefore urgently needed to shift the existing biofabrication window towards constructs obtaining high shape fidelity and advanced biocompatibility.

For this reason, this thesis focused on the development of hyaluronic acid (HA)-based bioinks which should comprise both, 3D printability and the support of MSC differentiation and ECM distribution. The following chapters describe the successive improvement of HA-based bioinks, starting from not-printable hydrogels with very high polymer contents and only pericellular matrix deposition, and ending with advanced bioinks with very low polymer contents, enabling stand-alone 3D bioprinting as well as homogeneous ECM distribution and the generation of superior quality cartilage constructs with a promising potential for clinical applications.

Chapter I: In the first study a pre-existing hydrogel composition of thiol-modified hyaluronic acid (HA-SH) and allyl-modified poly(glycidol) (P(AGE-*co*-G)) was refined. The previous not-printable hydrogel supported MSC differentiation, but the newly produced ECM was deposited only pericellularly due to its high polymer content of 10 %.[147] To achieve better diffusivity and a looser hydrogel network, ink compositions with less polymer content (down to 3 %) were developed. Furthermore, unmodified high molecular weight HA (hmHA) was added to increase ink viscosity and enable PCL-supported 3D bioprinting. The printing process itself was also brought into focus and therefore one major aim in this chapter was the detailed analysis of potential impacts of shear stresses during printing on viability and chondrogenic differentiation of embedded MSCs. Therefore, all studies were performed comparatively with cast and printed constructs. For further material and construct characterizations, ink rheology, construct swelling, diffusion properties, pore size and hmHA release were investigated in addition to the classical cartilage readouts like quantitative and qualitative ECM production, chondrogenic gene expression and mechanical stiffness.

Chapter II: The second study presents a further improvement of the study presented in Chapter I regarding 3D printability. While HA-SH/P(AGE-*co*-G) hydrogels were only printable with PCL-support structures, the here presented HA-based inks all have stand-alone 3D printability in common. This was achieved by the development of a novel dual-stage crosslinking approach: The first step is a pH dependent Michael addition between a part of HA-SH thiol-groups and acryl-modified polyethylene glycol (PEG-diacryl), resulting in a highly viscous and printable ink. After fabrication, the constructs are UV irradiated and final gelation is conducted between residual HA-SH thiol-groups and allyl-modified PEG (PEG-diallyl) in the presence of the photoinitiator Irgacure I2959. The influence of HA-SH and PEG-diacryl molecular weight and concentration on 3D printability was extensively evaluated and a variable bioink platform with adjustable properties was generated. The inks were further rheologically characterized and the final constructs were analyzed regarding their pore size and diffusion properties. As a biological readout for the different inks, chondrogenic differentiation of embedded MSCs was utilized and

quantitative and qualitative ECM production, chondrogenic gene expression and mechanical stiffness was investigated.

Chapter III: Based on the bioink platform developed in Chapter II, this study improved a specific ink composition regarding its biological performance towards potential clinical applications. Chondrogenic differentiation of MSCs *in vitro* requires continuous supply of the differentiation factor TGF-β with each medium change. This complicates a transfer to *in vivo* applications and inspired the aim of this study to circumvent the need for TGF-β supplementation by covalent incorporation of the protein into the bioink. This study represents the first covalent tethering approach in a 3D printable ink with the extensive characterization of potential impacts on protein function. TGF-β1 was thiol-modified via Traut's reagent and tethered to 8-arm PEG-acryl before ink crosslinking. The potential impact of the tethering process on ink properties was analyzed by rheological measurements and comparative construct swelling studies. The chondrogenic potential of tethered vs. non-covalently incorporated TGF-β1 was extensively characterized by investigation of qualitative and quantitative ECM production, Western blot analysis, chondrogenic gene expression and mechanical measurements. Furthermore, in a comprehensive comparative analysis of cast and printed bioinks it was evaluated whether the covalently tethered TGF-β1 maintained its functionality after 3D printing.

2. Methods

All used methods and materials are described in detail in the experimental sections (3.3., 4.3., and 5.3.) of the separate chapters. No other methods were used for the presented studies.

3. Chapter I – Hyaluronic Acid-based Bioink Composition Enabling 3D Bioprinting and Improving Quality of Deposited Cartilaginous Extracellular Matrix

DOI: 10.1002/adhm.202000737[188]

Julia Hauptstein[1], Thomas Böck[2], Michael Bartolf-Kopp[2], Leonard Forster[2], Philipp Stahlhut[2], Ali Nadernezhad[2], Gina Blahetek[3], Alma Zernecke-Madsen[3], Rainer Detsch[4], Tomasz Jüngst[2], Jürgen Groll[2], Jörg Teßmar[2] and Torsten Blunk[1]

[1] Department of Trauma, Hand, Plastic and Reconstructive Surgery, University of Würzburg

[2] Chair for Functional Materials in Medicine and Dentistry and Bavarian Polymer Institute, University of Würzburg

[3] Institute of Experimental Biomedicine II, University Hospital Würzburg

[4] Institute of Biomaterials, Department of Materials Science and Engineering, University of Erlangen-Nuremberg

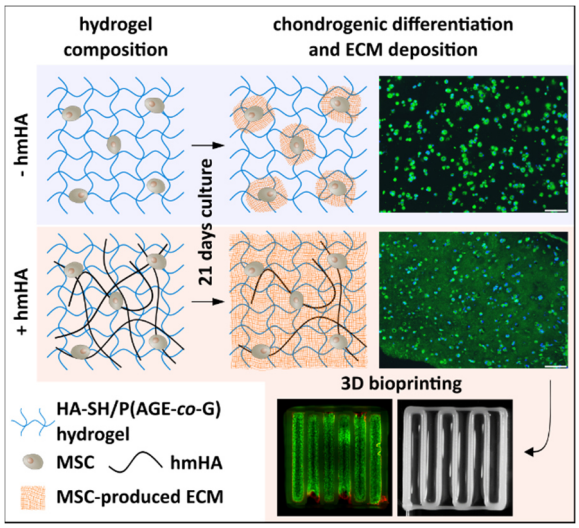

3D printable constructs for cartilage biofabrication combining sufficient construct stability with a cell-supportive environment still represent a challenge in the field. Here, hyaluronic acid-based bioink compositions are used to modulate biological properties of 3D constructs after bioprinting and chondrogenic differentiation of MSCs, focusing on ECM distribution. The study contributes to effective bioink development and presents a perspective for cartilage regeneration.

3.1. Abstract

In 3D bioprinting, bioinks with high concentrations of polymeric materials are frequently used to enable fabrication of 3D cell-hydrogel constructs with sufficient stability. However, this is often associated with restricted cell bioactivity and an inhomogeneous distribution of newly produced extracellular matrix (ECM). Therefore, this study investigates bioink compositions based on hyaluronic acid (HA), an attractive material for cartilage regeneration, which allow for reduction of polymer content. Thiolated HA and allyl-modified poly(glycidol) in varying concentrations are UV-crosslinked. To adapt bioinks to PCL-supported 3D bioprinting, the gels are further supplemented with 1 wt.% unmodified high molecular weight HA (hmHA) and chondrogenic differentiation of incorporated human mesenchymal stromal cells is assessed. Strikingly, addition of hmHA to gels with a low polymer content (3 wt.%) results in distinct increase of construct quality with a homogeneous ECM distribution throughout the constructs, independent of the printing process. Improved ECM distribution in those constructs is associated with increased construct stiffness after chondrogenic differentiation, as compared to higher concentrated constructs (10 wt.%), which only show pericellular matrix deposition. The study contributes to effective bioink development, demonstrating dual function of a supplement enabling PCL-supported bioprinting and at the same time improving biological properties of the resulting constructs.

3.2. Introduction

The research field of biofabrication has recently emerged as a powerful approach to the generation of engineered living tissues urgently needed for disease models and regenerative medicine.[61] Automated, cell-compatible fabrication methods, such as bioprinting and bioassembly, allow the precise combination and patterning of cells and biomaterials into three-dimensional (3D) constructs.[60] In this context, the development of appropriate bioinks consisting of cells and hydrogel materials for extrusion-based 3D printing is a major focus of research. In order to enable the fabrication of 3D constructs with sufficient shape fidelity and resulting stability, often high concentrations of polymeric hydrogel materials in the bioinks are employed.[68] However, this is commonly associated with a high network stiffness and density, thereby possibly restricting cell bioactivity and the homogeneous distribution of newly produced extracellular matrix (ECM).[68] Currently, various modified and unmodified biopolymers are used as basis of bioinks which are utilized in bioprinting processes, including decellularized ECM (dECM), alginate, gelatin and hyaluronic acid (HA).[71, 72, 189-191] HA represents an attractive material for cartilage regeneration, as it is a main component in human articular cartilage ECM.[71, 160] It enables attachment and migration of mesenchymal stromal cells (MSCs) via the cluster of differentiation 44 (CD44) or other cell surface receptors[146] and is highly accessible for different chemical modifications

allowing for a stable chemical crosslinking.[152, 154, 192] In previous non-printed tissue engineering approaches, the effect of limited ECM distribution depending on network density has been shown for several hydrogel-based constructs, including photo-crosslinked hyaluronic acid.[156, 157, 193-195] Therefore, different strategies to modulate mechanical properties and network density have been applied, such as modification of the macromer amount or variation of the irradiation time in UV photo-crosslinked hydrogels.[156, 157, 196]

In a recent study, we have established a bioink based on thiolated HA (HA-SH) and allyl-modified poly(glycidol) [P(AGE-*co*-G)], which were crosslinked by UV-induced thiol-ene coupling.[147] This formulation with an overall polymer concentration of 10 wt.% was further supplemented with 1 wt.% of unmodified high molecular weight HA (hmHA) to adapt it to double printing together with poly(ε-caprolactone) (PCL),[147] a biodegradable thermoplastic polymer frequently used in order to yield mechanically more robust composite hydrogel scaffolds.[160-162] While in principle 3D printability was demonstrated, chondrogenesis of MSCs was only investigated in non-printed constructs. Encapsulated MSCs showed a robust chondrogenic differentiation within this bioink, in contrast to corresponding pure poly(glycidol) hydrogels.[147, 197] However, due to the relatively high overall polymer content, the deposition of cartilage-specific ECM molecules, unfortunately, was mainly restricted to pericellular regions.[147] Thus, homogeneous ECM distribution desirable for engineered cartilaginous constructs was not achieved and still represents a major challenge for printable bioinks.[68, 71] Therefore, in this study we aimed to evaluate different bioink compositions based on the previously employed hydrogel components, with regard to chondrogenesis of embedded MSCs and in particular the resulting ECM distribution. Using equal amounts of HA-SH and P(AGE-*co*-G), initially hydrogel constructs with overall polymer concentrations ranging from 3 wt.% to 15 wt.% were analyzed, whereby decreasing polymer content yielded an improved ECM distribution. In all further experiments, constructs with 3 wt.% and 10 wt.% overall polymer content were investigated, either without or with additional unmodified hmHA (1 wt.%). Furthermore, cast and dispensed hydrogels of the same geometry were compared, employing a dispensing unit mimicking an extrusion-based printing process. Chondrogenic differentiation of MSC and construct quality was evaluated with regard to ECM distribution and content, chondrogenic gene expression, and construct stiffness. Hydrogel constructs with 3 wt.% polymer content yielded distinctly improved ECM distribution and higher stiffness after chondrogenic differentiation. Interestingly, the addition of unmodified hmHA to hydrogels with 3 wt.% polymer content led to constructs with highest quality exhibiting evenly distributed ECM components throughout both cast and printed constructs. Finally, this most favorable bioink composition was double printed with PCL in two different geometries using an extrusion-based bioprinter, again yielding homogeneous ECM distribution within the constructs after 21 days of chondrogenic culture. The study contributes to effective bioink development,

demonstrating the dual function of a supplement, hmHA, that not only enables PCL-supported bioprinting, but also improves biological properties of the resulting constructs.

3.3. Experimental section

3.3.1. Materials

Thiol-modified hyaluronic acid HA-SH (molecular weight: M_w 35.5 kDa, M_n 13.9 kDa, Đ 2.55, degree of substitution: DS 39.8 %) and allyl-modified poly(glycidol) (P(AGE-*co*-G)) (M_w 5.21 kDa, M_n 4.72 kDa, Đ 1.10, DS 9.8 %) were kindly provided by PolyVation BV (Groningen, Netherlands). High molecular weight hyaluronic acid (M_w 1,100 kDa, M_n 900 kDa, Đ 1.22) was purchased form Carbosynth (Compton, UK). All chemicals were purchased from Sigma Aldrich (St. Louis, USA) if not stated differently. 2-hydroxy-1-[4-(hydroxyethoxy)-phenyl]-2-methyl-1-propanone (I2959; BASF, Ludwigshafen, Germany), 4(dimethylamino)-benzaldehyde (DAB; Roth, Karlsruhe, Germany), basic fibroblast growth factor (bFGF; BioLegend, London, UK), DAPI mounting medium ImmunoSelect® (Dako, Hamburg, Germany), Dulbecco's Modified Eagle's Medium high glucose 4.5 g L^{-1} (DMEM; Thermo Scientific, Waltham, USA), Dulbecco's Modified Eagle's Medium/Ham's F-12 (DMEM/F12; Thermo Scientific, Waltham, USA), ethanol (EtOH; 99 %, TH Geyer, Renningen, Germany), fetal calf serum (FCS; Thermo Scientific, Waltham, USA), formaldehyde (37%, Roth, Karlsruhe, Germany), hydrocloric acid (HCl; 37 %, Merck, Darmstadt, Germany), isopropanol (VWR, Radnor, USA), ITS+ Premix (Corning, NY, USA), L-hydroxyprolin (Merck, Darmstadt, Germany), Live/Dead Cell Staining Kit (PromoKine, Heidelberg, Germany), papain suspension (Worthington, Lakewood, USA), penicillin-streptomycin (PS; 100 U mL^{-1} penicillin, 0.1 mg mL^{-1} streptomycin; Thermo Scientific, Waltham, USA), perchloric acid (60 %, Merck, Darmstadt, Germany), phosphate-buffered saline (PBS; Life Technologies, Karlsruhe, Germany), Proteinase K (Digest-All 4, Life Technologies, Karlsruhe, Germany), Tissue Tek® O.C.T. (Sakura Finetek, Tokyo, Japan), transforming growth factor β 1 (TGF-β1; BioLegend, London, UK), trypsin-EDTA (0.25 %, Life Technologies, Karlsruhe, Germany).

Primary antibodies: anti-aggrecan 969D4D11 (Thermo Scientific, Waltham, USA), anti-collagen I ab34710 (Abcam, Cambridge, UK) and anti-collagen II II-4C11 (Acris, Herford, Germany). Secondary antibodies: goat-anti-mouse Alexa 488 115-545-146 (Jackson ImmunoResearch, Cambridge, UK), goat-anti-rabbit Alexa 488 111-545-003 (Jackson ImmunoResearch, Cambridge, UK).

3.3.2. Methods

NMR analysis: ^{1}H-NMR measurements were realized at a 300 MHz Bruker Biospin spectrometer (Bruker, Billerica, MA) using D_2O as a solvent. The solvent peak was set to $\delta = 4.79$ ppm to

which all chemical shifts refer. The percentage of thiol groups per repetition unit of HA-SH were determined by the ratio of the integrals of the thiol carrying modification and the acetyl signal of the backbone. The percentage of allyl groups were calculated by dividing the sum of integrals of the allyl group signals by the integrals of the backbone signals.

GPC analysis: GPC analysis were performed on a GPC system from Malvern (Herrenberg, Germany) with two A6000M mixed-bed columns using a triple detection containing a refractive index detector, a multi angle light scattering detector and a viscometer. The columns were calibrated with PEG standards (Malvern, Herrenberg, Germany) and the eluent was made from deionized water containing 0.2 g L^{-1} NaN_3 and 8.5 g L^{-1} $NaNO_3$. The samples were dissolved over night at room temperature in the eluent and measured at 35 °C with a flow rate of 0.7 mL min^{-1}. The obtained data was processed with the software OmniSEC 5.12 (Malvern, Herrenberg, Germany).

Rheological analysis: Shear viscosity of different hydrogel precursors was determined using an Anton Paar MCR 702 rheometer (Anton Paar, Austria) with a parallel plate geometry (d = 25 mm) and the gap of 0.5 mm. A solvent trap was used to minimize solvent evaporation during the experiments. In order to eliminate the environmental noise in data acquisition, the shear rate sweeps were performed in the range of 1-100 s^{-1} for low-viscosity samples, while the experimental range of shear rates was extended to 0.1-100 s^{-1} for the samples containing high molecular weight HA as thickener. In order to obtain apparent steady-state shear data, a dynamic data acquisition method was implemented in which at each data point, the shear rate was kept constant until the variations in viscosity was smaller than 1 % over the observation period.

MSC isolation and expansion: Bone marrows were recovered, after informed consent, from the explanted femoral heads of patients undergoing elective hip arthroplasty. The procedure was approved by the local Ethics Committee of the University of Würzburg (186/18). Human bone marrow-derived mesenchymal stromal cells (MSCs) were isolated as previously described.[184] Cells were expanded in DMEM/F12 supplemented with 10 % FCS, 1 % PS and 3 ng mL^{-1} bFGF in T175 cm^2 flasks (Greiner Bio-One, Frickenhausen, Germany) at 37 °C and 5 % CO_2.

Hydrogel preparation: HA-SH and P(AGE-*co*-G) were dissolved in PBS and mixed in an equal ratio (1.5 wt.%, 2.5 wt.%, 5 wt.% or 7.5 wt.% of each component, resulting in equimolar ratios of thiol and allyl groups). 0.05 wt.% of the photo initiator Irgacure I2959 and, depending on the experiment, 1 wt.% of unmodified high molecular hyaluronic acid (hmHA, 1100 kDa) was added. The hydrogel suspension was neutralized with 5 M NaOH to a final pH of 7.4. MSCs at passage 3 - 4 were suspended in the hydrogel precursor solution (20.0 x 10^6 cells mL^{-1}). For printing simulation, the cell loaded hydrogel suspension was transferred to a cartridge, dispensed (Vieweg DC200, Kranzberg, Germany) through a 330 µm steel nozzle (Nordson EFD, East Providence, USA) at 1 bar and collected in a tube. Dispensed as well as cast hydrogel-cell suspensions were

filled in glass molds (5 mm diameter, 2 mm height with 40 µL per construct) and UV irradiated (UVL hand lamp with filter, A. Hartenstein, Würzburg, Germany) at 365 nm for 10 min. Intensity of the UV lamp was 1 mW cm^{-2}. MSC containing hydrogels were cultured for 21 days in chondrogenic differentiation medium (DMEM high glucose medium supplemented with 1 % ITS+ premix, 1 % PS, 0.1 µM dexamethasone, 50 µg mL^{-1} L-ascorbic acid 2-phosphate sequimagnesium salt hydrate, 40 µg mL^{-1} L-proline and 10 ng mL^{-1} TGF-β1) at 37 °C and 5 % CO_2. Medium was changed every two days.

3D printing of PCL-supported HA-SH/P(AGE-co-G) constructs: For the fabrication of the 3D (three dimensional) scaffolds, a 3D Discovery robotic dispensing system (RegenHU, Villaz-St-Pierre, Switzerland) was employed under sterile conditions. The G-code used for the operation of the printer was generated with the BioCAD software (RegenHU, Villaz-St-Pierre, Switzerland). To enable the simultaneous double-printing of poly(ε-caprolactone) (PCL) and the hydrogel precursor solution, two printheads were utilized: An extruder-based system with integrated heating for the printhead and the material reservoir attached to it (HM-300H) with an inner needle diameter of 250 µm was employed for printing of medical grade PCL (Plurasorb PC12, Corbion, Amsterdam, Netherlands). The second printhead operated via an electromagnetic valve (Cell friendly CN-300N) with an inner diameter of 450 µm and was used for printing the hydrogel-cell suspension. The hydrogel precursor solution was composed of 3 wt.% polymers (1.5 wt.% HA-SH and 1.5 wt.% P(AGE-*co*-G)), 0.05 wt.% I2959 and 1 wt.% unmodified high molecular weight HA (hmHA) as a thickener with 20 x 10^6 MSCs mL^{-1}. The cell-laden hydrogel precursor solution was transferred into a 3 cc printing cartridge (Nordson EFD, Ohio, USA) and inserted into the microvalve printhead. Prior to the print, the heating of the extruder-based printhead was initiated to heat the PCL reservoir to 85 °C and the printhead to 93 °C respectively. In addition, a custom-made water bath heated collector was employed and set to 32 °C. Printing parameters for PCL were adjusted to 17.5 revolutions per minute, 3 bar extrusion pressure and a collector speed of 5 mm s^{-1}. For the cell-laden hydrogel precursor solution, the microvalve printhead was set to a dosing distance of 400 µm with valve opening times of 700-900 µs and an extrusion pressure of 1 bar. Both printheads operated in the y and z planes while the collector moved along the x axis. For the fabrication of both types of constructs, the PCL scaffold was printed first, followed by the print of the hydrogel precursor solution into the designated cavities within the scaffold. Rectangular scaffolds with straight, 9 mm long trenches along with circular scaffolds with a diameter of 5 mm and an incorporated lattice structure, featuring an intersection distance of 1.5 mm, were created. While the rectangular scaffold was printed in a continuous movement of the printhead, the layers for the circular scaffold were alternatively rotated by 90 ° every layer to realize the internal lattice pattern. Layer height for the PCL scaffolds was set to 200 µm and four layers in total for a final construct height of 800 µm. The constructs were printed onto glass coverslips and consecutively crosslinked for 10 min with a UV light source (UVL hand lamp with

filter, A. Hartenstein, Würzburg, Germany) at 365 nm. The final constructs were transferred into a 6-well cell culture plate and supplemented with 2 mL of chondrogenic differentiation medium. Medium was changed every two days. Documentation of overview images was performed using a stereo microscope (SteREO Discovery.V20, Carl Zeiss, Jena, Germany).

Cell viability assay: Cell viability of hydrogel-encapsulated MSCs was analysed using a Live/Dead Assay Cell Staining Kit (PromoKine, Heidelberg, Germany) at d1 or d21 after encapsulation. Constructs were washed twice with PBS before staining solution (4 µM ethidium homodimer III (EthD-III) and 2 µM calcein acetoxymethylester (calcein-AM) in PBS) was added and incubated for 45 min at room temperature in the dark. After an additional wash step with PBS, images of the cross section of hydrogel constructs were taken at a fluorescence microscope (Olympus BX51/DP71, Olympus, Hamburg, Germany). Stitched overview images of 3D double-printed constructs were taken with an inverted fluorescence microscope (Axio Observer Z1/7, EC Plan-Neofluar 10x/0.30 Ph 1, Carl Zeiss Microscopy, Jena, Germany).

Histological and immunohistochemical analysis: MSC-laden hydrogel constructs were harvested on d1 or d21 and fixed in 3.7 % PBS buffered formaldehyde at 4°C over night. The next day, constructs were transferred to Tissue Tek® O.C.T. (Sakura Finetek, Torrance, USA) and incubated over night at room temperature in a wet chamber. After shock freezing in liquid nitrogen, constructs were either stored at -20 °C or directly sliced (8 µm per longitudinal section) using a cryostat (CM 3050S, Leica, Wetzlar, Germany) and mounted on SuperFrost® plus glass slides (R. Langenbrick, Emmendingen, Germany). Cross-sections were obtained throughout the whole constructs. For histological analysis of glycosaminoglycan (GAG) deposition, sections were stained with safranin O and fast green. Cells were counterstained with Weigert's haematoxylin.[198] For immunohistochemical analysis, proteinase K digestion for 10 min at room temperature was used for antigen retrieval. After washing in PBS, sections were blocked with 1 % BSA in PBS for 1 h at room temperature before antibody staining (anti-aggrecan 969D4D11,1:300; anti-collagen I ab34710, 1:500, anti-collagen II II-4C11, 1:500 in 1 % BSA in PBS) was performed over night at room temperature. After three washing steps in PBS, the secondary antibody (goat-anti-mouse Alexa488 115-545-146, 1:400; goat-anti-rabbit Alexa488 111-545-003, 1:400 in 1 % BSA in PBS) was incubated on the sections for 1 h at room temperature in the dark before additional washing and mounting with DAPI mounting medium ImmunoSelect®. Visualization of immunohistochemically stained ECM deposition was performed by fluorescence microscopy (Olympus BX51/DP71, Olympus, Hamburg, Germany). Quantification of stained gel areas was conducted with the particle analysis function of NIH ImageJ Fiji software (version 1.52p) using a 10 % threshold of the maximal white value for all binary images.[199] Values represent an average of four images of each condition taken randomly throughout the construct cross sections.

Biochemical analysis: Biochemical assays were performed for quantification of DNA content as well as GAG and collagen deposition in constructs and the culture supernatant.[184] For construct analysis, hydrogels were harvested on d1 and d21, washed with PBS and homogenized with a TissueLyser (Quiagen, Hilden, Germany) for 5 min at 25 Hz. Subsequently, the suspension was digested with papain (3 U mL^{-1}) at 60°C over night. For GAG and collagen quantification in the culture supernatant, medium of three replicates per condition was collected every two days and stored at -20 °C till the end of the experiment. The same amount of medium from each harvesting day was pooled within the three replicates and analyzed for GAG and collagen content. DNA quantification was performed with fluorescent DNA intercalating agent Hoechst 33258 at 340 nm and 465 nm using a spectrofluorometer (Infinite M200 Pro,Tecan, Crailsheim, Germany) and salmon sperm DNA as defined DNA standard.[200] Collagen content was quantified after acid hydrolysis with a hydroxyproline assay and L-hydroxyproline as a standard. Thereby chloramine T oxidizes hydroxyproline to pyrrols, which are visualized by 4(dimethylamino)benzaldehyde (DAB) at 550 nm (Infinite M200 Pro, Tecan, Crailsheim, Germany).[201, 202] Dimethylmethylene blue binds to sulphated glycosaminoglycanes (GAG) leading to a shift in the absorption maximum. This enables GAG quantification at 525 nm (Infinite M200 Pro, Tecan, Crailsheim, Germany) by using bovine chondroitin sulfate as standard.[203]

RNA isolation and gene expression analysis: Constructs were harvested on day 3, 7 and 21 and homogenized in TRIzol Reagent (Thermo Scientific, Waltham, USA) with a TissueLyser (Quiagen, Hilden, Germany) for 5 min at 25 Hz. Subsequently, RNA was isolated according to manufacturers instructions and cDNA was transcribed with the ImProm-II™ Reverse Transcription System (Promega, Madison, USA) after quantification of RNA yield and purity (NanoDrop, Thermo Scientific, Waltham, USA). qRT-PCR was performed with the QuantStudio 6 Flex Real-Time PCR machine (Thermo Scientific, Waltham, USA) and the corresponding PowerUp SYBR Green Master Mix (Thermo Scientific, Waltham, USA). Primer pairs were designed intron spanning. The sequences are listed in Table I.S1, 3.7. Supporting information. The expression of all genes was normalized to the housekeeping gene glyceraldehyde 3-phosphate dehydrogenase (GAPDH) and to gene expression of MSC 2D samples on d0. Relative expression was calculated with the $2^{-\Delta\Delta C_T}$ method.[204]

Mechanical analysis: MSC laden constructs were fabricated as described above and analyzed after d1 and d21 of chondrogenic culture. Mechanical properties of six hydrogels per condition and time point were measured with a dynamical mechanical testing machine from Bose (ElectroForce® 5500 test instrument, Bose, Eden Prairie, MN, USA) with a load cell of 250 g. The constructs were compressed to a final depth of 0.5 mm with a constant cross head displacement rate of 0.001 mm s^{-1}. Young's modulus was determined as the slope of the true stress-strain curve in the linear elastic range.

Swelling analysis: Swelling and shrinking behavior of hydrogels without embedded MSCs was analyzed by weight measurements. Four different hydrogel compositions (3 wt.% and 10 wt.% HA-SH/P(AGE-*co*-G) gels +/- 1 wt.% hmHA) were produced and crosslinked in small disks (5 mm diameter, 2 mm height) as described above. Those constructs were weight directly after preparation (time point 0 h) and incubated in 1 mL PBS for following time intervals: 30 min, 1 h, 2 h, 4 h, 6 h, 8 h, 24 h, 2 d, 4 d, 7 d, 10 d and 14 d. For intermediate weight measurements, gels were removed from the culture plate, carefully drained from excess PBS, weight and subsequently transferred to PBS again.

Quantitative GPC measurement: To determine the release of high molecular weight thickener (hmHA) and low molecular weight thiolated hyaluronic (HA-SH) acid from the different crosslinked hydrogels (3 wt.% and 10 wt.% gels +/-hmHA) the incubation buffer of ten hydrogel specimens (each 40 µL) was pooled and freeze-dried after different timepoints using a pilot freeze dryer (Epsilon 2-4 LSCplus, Martin Christ, Osterode/Harz, Germany). The obtained dried powder was dissolved again in 1 mL of demineralized water and filtered through a syringe filter (0.45 µm, regenerated cellulose). The obtained samples were analyzed using a Shimadzu high performance liquid chromatography system (Pump (LC-20AT) with autosampler (SIL-20AC) and a photodiode array detector (SPD-M20A)) at a fixed wavelength λ of 202 nm. For separation a GPC column set was used consisting of two Viscotek A-Columns (A6000M, Malvern) for aqueous GPC/SEC (300 mm x 8 mm, particle size = 13 µm) and a respective precolumn. A 0.05 M KH_2PO_4 buffer at pH = 7.0 was used as eluent at an elution rate of 0.7 mL min^{-1}. The obtained peaks at high and low molecular weight were quantified with a calibration curve using pure high molecular weight hyaluronic acid and the thiolated hyaluronic acid used for gel fabrication.

Analysis of FITC-labeled dextran diffusion: 3 wt.% and 10 wt.% HA-SH/P(AGE-*co*-G) hydrogels with and without additional 1 wt.% hmHA were prepared as described before (each 40 µL) and incubated for 5 days in 1 mL PBS at 37 °C to allow the release of hmHA. Afterwards, PBS was replaced by 1 mL 40 kDa FITC-dextran (1 mg mL^{-1}) or 500 kDa FITC-dextran (1 mg mL^{-1}) solution and hydrogels were incubated for 24 h at 37 °C in the dark. Before analysis, the constructs were washed in PBS and homogenized with a TissueLyser (Quiagen, Hilden, Germany) for 5 min at 25 Hz. Fluorescence intensity was analyzed with a spectrofluorometer (Infinite M200 Pro,Tecan, Crailsheim, Germany; Ex/Em 495nm/535nm) and quantification was performed in relation to a 40 kDa or 500 kDa FITC-dextran standard curve.

Pore size analysis by cryo-SEM: 3 wt.% and 10 wt.% HA-SH/P(AGE-*co*-G) hydrogels with additional 1 wt.% hmHA were analyzed for their pore size with a cryo-scanning electron microscope (cryo-SEM). Samples were rapidly frozen in slushed nitrogen at -210 °C after placing them between aluminum plates (d = 3 mm) with a 2 mm notch for sample fixation. All following transfer steps were performed at -140 °C with a EM VCT100 cryo-shuttle (Leica Microsystems).

To generate a freshly fractured hydrogel surface, one of the aluminum plates was knocked off and freeze etched for 15 min at -85 °C under high vacuum (< 1 x 10^3 mbar) in a Sputter Coater machine (ACE 400, Leica Microsystems). Afterwards, samples were sputtered with 3 nm platinum and transferred to the SEM chamber (Crossbeam 340, Zeiss). Images of the hydrogel surface morphology were taken at -140 °C using an acceleration voltage of 2 kV.

Statistical Analysis: Data is represented by mean ± standard deviation from three replicates, if not otherwise mentioned. Statistic evaluation was performed with Graphpad Prism 5 software, comparing multiple groups using oneway ANOVA with a Tukey post hoc test and multiple groups at different time points using twoway ANOVA with a Bonferroni post hoc test. Comparison of two groups was performed with a students t-test. Significant differences are marked as follows: * ($p < 0.05$), ** ($p < 0.01$) and *** ($p < 0.001$).

3.4. Results and discussion

3.4.1. Hydrogel formation

For hydrogel formation, thiol-modified hyaluronic acid (HA-SH) was crosslinked with allyl-functional poly(glycidol) (P(AGE-*co*-G)) via UV light-initiated radical thiol-ene coupling in the presence of the photoinitiator I2959, as described previously.[147] (Figure I.1a). ^{1}H-NMR and GPC

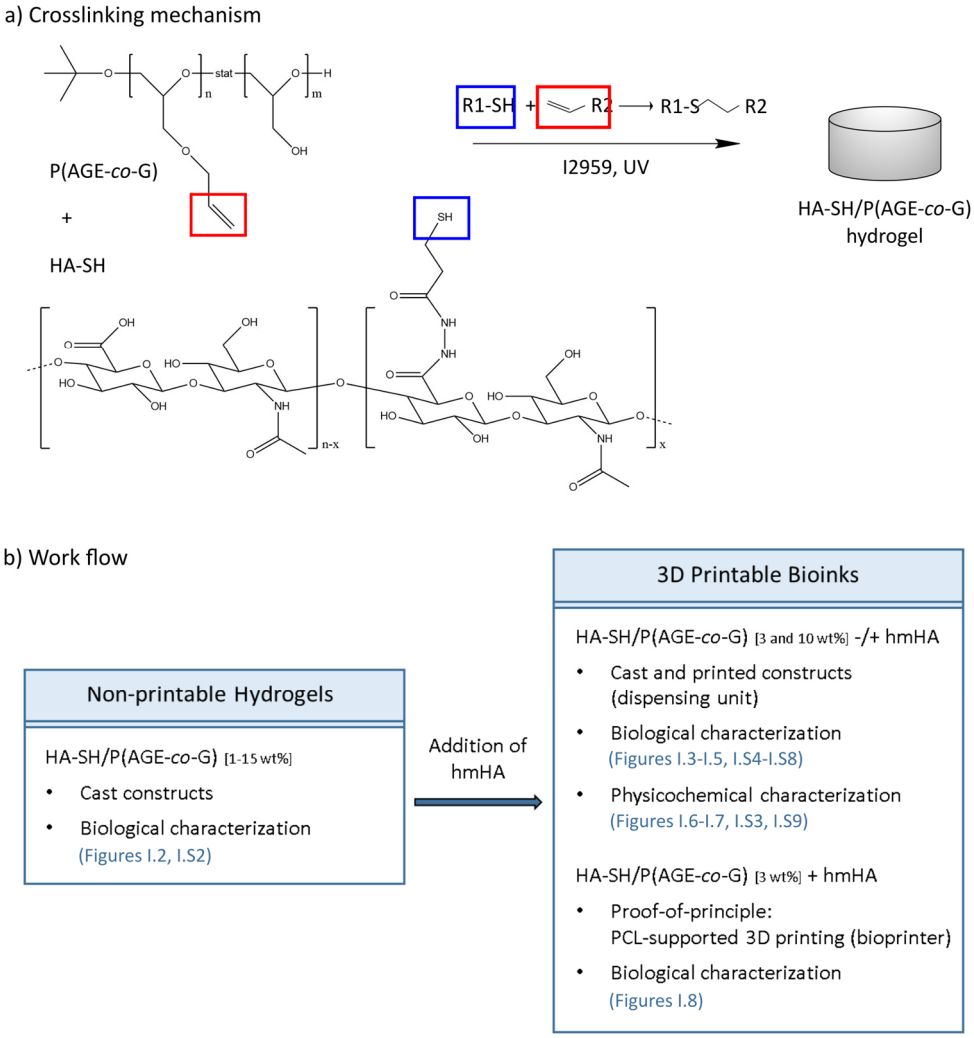

Figure I.1: Hydrogel formation and work flow of the study. a) Chemical structure and crosslinking mechanism of HA-SH and P(AGE-*co*-G). The photoinitiator Irgacure (I2959) is activated by UV-light (365 nm) and induces the covalent bond between the thiol-group of HA-SH (blue) and the allyl-group of P(AGE-*co*-G) (red). b) Overall work flow of the study. All 3D constructs were made from hydrogels seeded with MSCs, and chondrogenic differentiation was investigated after 21 days. At first, constructs made from a concentration series of HA-SH/P(AGE-*co*-G) hydrogels (1 – 15 wt.%), which are non-printable as such, were characterized biologically, mainly to verify the influence of polymer concentration on ECM distribution. In the main part of the study, HA-SH/P(AGE-*co*-G) hydrogels were supplemented with high molecular weight hyaluronic acid (hmHA), which enables PCL-supported 3D bioprinting. Hydrogels with 3 and 10 wt.% polymer concentration, either without or with hmHA (1 wt.%), were either cast or printed. Here, for printing, a dispensing unit mimicking an extrusion-based printing process was used, which facilitated the generation of constructs in the same geometry for both printed and cast groups to enable comparability. Constructs were thoroughly characterized biologically and physicochemically. Subsequently, as a proof-of-principle, the most favorable HA-SH/P(AGE-*co*-G) hydrogels (3 wt.% +hmHA; completely homogeneous ECM distribution, high stiffness) were employed in PCL-supported 3D bioprinting, and resulting constructs were biologically characterized.

confirmed the expected degree of functionalization as well as the desired molecular weight of the used polymers, to confirm an approximate 1:1 ratio of thiol and allyl groups (Figure I.S1a-d, 3.7. Supporting information). This hydrogel system was utilized as the basis for all experiments. The overall work flow of the study is depicted in Figure I.1b.

3.4.2. Effect of polymer concentration in HA-SH/P(AGE-*co*-G) gels on ECM distribution

In order to examine the impact of polymer concentration in HA-SH/P(AGE-*co*-G) hydrogels on chondrogenic differentiation of human bone marrow-derived MSCs, a concentration series was performed. In a previous study using this hydrogel system, an overall polymer concentration of 10 wt.% was employed resulting in only pericellular ECM distribution.[147] Therefore, here we used just one higher concentration for completeness, but focused on decreasing the total polymer content. Thus, the investigated concentrations ranged from a total polymer content of 1 wt.% to 15 wt.% using equal amounts of HA-SH and P(AGE-*co*-G). Compositions below a polymer content of 3 wt.% HA-SH/P(AGE-*co*-G) showed incomplete polymerization and were not usable for long-term tissue culture. For this reason, in the following experiments hydrogels with concentrations between 3 wt.% and 15 wt.% HA-SH/P(AGE-*co*-G) were employed, and MSCs were cultured for 21 days under chondrogenic differentiation conditions within these hydrogels. Live/dead staining showed good cell survival after hydrogel preparation at day 1 as well as after 21 days in chondrogenic culture with no distinct differences between the conditions (Figure I.S2a, 3.7. Supporting information). All hydrogel formulations supported the formation of cartilage-specific ECM by the encapsulated MSCs (Figure I.2). Glycosaminoglycan (GAG) staining with safranin O revealed that after 21 days of chondrogenic differentiation the produced GAGs were located intra- and mainly pericellularly around the cells in 15 wt.% and 10 wt.% gels. In contrast, with decreasing polymer content an improved GAG distribution was detected (Figure I.2a). In images at day 1, serving as controls, due to staining of hyaluronic acid itself by safranin O, increased background staining was observed with increasing polymer content; nevertheless, the pericellular staining of newly produced GAG could clearly be distinguished. Similar distribution patterns as found for GAG were also observed in the immunohistochemical (IHC) staining for aggrecan. In hydrogels with a higher polymer content, aggrecan deposition was restricted to pericellular regions, while especially in hydrogels with 3 wt.% polymer content, an improved ECM distribution was observed, although still not completely throughout the hydrogel (Figure I.2b). Another important cartilage-specific ECM component, collagen type II, was found to be located pericellularly irrespective of hydrogel concentration (Figure I.2c). Control IHC images at day 1 are shown in Figure I.S2b and C (3.7. Supporting information). These findings were in accordance with previous studies with different types of hydrogels, also demonstrating better ECM distribution in hydrogels with lower polymer content.[156, 157] Biochemical quantification of DNA, GAG and collagen content are shown in the Supporting information (3.7.,

Figure I.S2d-f). DNA quantification showed consistent slight cell proliferation in all approaches during incubation without significant differences between varying hydrogel concentrations. All constructs contained a markedly increased GAG and total collagen content at day 21 compared to day 1, confirming in principle the chondrogenic differentiation observed histologically. At day 21, the hydrogels with 3 wt.% polymer content had a slightly lower GAG content than the other formulations, while the hydrogels with higher polymer content showed a comparably lower total collagen content.

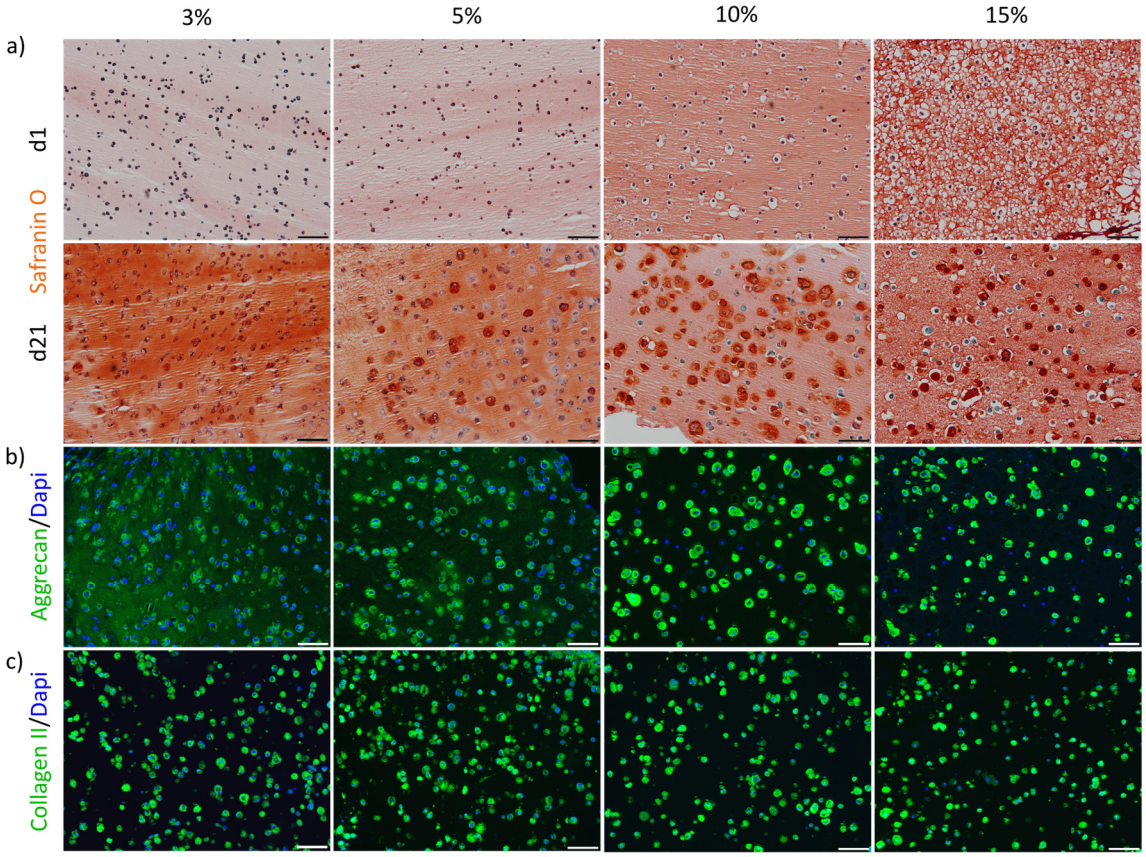

Figure I.2: Decreasing polymer concentration in HA-SH/P(AGE-*co*-G) hydrogels improved GAG and aggrecan distribution. Histological and immunohistochemical staining for deposited ECM components in 3 wt.% - 15 wt.% HA-SH/P(AGE-*co*-G) hydrogels, seeded with 20.0 x 10^6 MSCs mL^{-1}, after 21 days of chondrogenic differentiation. a) Longitudinal sections were stained for deposition of GAGs with safranin O after 21 days. (Please note: In control images at day 1, increased background staining was observed with increasing polymer content due to staining of hyaluronic acid itself by safranin O; nevertheless, the pericellular staining of newly produced GAG could clearly be distinguished.) b) Immunohistochemical staining for aggrecan (green), and c) for collagen type II (green) after 21 days. Nuclei (blue) were counterstained with DAPI. Scale bars represent 100 µm.

3.4.3. Effect of HA-based bioink composition on the quality of 3D cast and printed constructs after chondrogenic differentiation

3.4.3.1. Homogeneous ECM distribution in constructs with low polymer content and additional hmHA

In order to prepare bioinks for PCL-supported 3D bioprinting, inks were supplemented with unmodified high molecular weight hyaluronic acid (hmHA) as previously described.[147] hmHA increases the viscosity of the bioinks already at a relatively low concentration (1 wt.%), as confirmed in rheological measurements (Figure I.S3, 3.7. Supporting information). In the following, 3 wt.% gels, which were found to be beneficial for ECM distribution, and 10 wt.% gels, both with and without additional hmHA, were compared. Extrusion bioprinting may affect cell viability and function and impair the biological outcome.[205-208] Therefore, in order to assess the potential impact of the bioprinting process on chondrogenic differentiation, the different formulations were cast and printed. For printing, a dispensing unit mimicking an extrusion-based printing process was used. The bioinks (3 wt.% gels, which were found to be beneficial for ECM distribution, and 10 wt.% gels, both with and without additional hmHA) were extruded through a 330 µm nozzle at 1 bar and collected in a tube. Subsequently, bioinks were pipetted in glass molds, as it was also done with inks in the casting approaches. Thereby, final gelation was conducted in the same geometry for both printed and cast groups to enable comparability and avoid impact of nutrient and oxygen supply in differently shaped constructs.[209, 210]

All approaches showed good cell survival on day 1 as well as after 21 days of chondrogenic differentiation, irrespective of bioink processing (cast or print) or initial ink viscosity (+/- hmHA) (Figure I.S4, 3.7. Supporting information). Chondrogenic differentiation was demonstrated in all approaches after 21 days by IHC staining of the main cartilage ECM components (Figure I.3; controls at day 1 in Figure I.S5, 3.7. Supporting information). Strikingly, IHC staining of aggrecan and collagen type II revealed that, in strong contrast to all other groups, 3 wt.% gels with additional 1 wt.% hmHA exhibited completely homogeneous matrix distribution, which was observed on cross-sections throughout the whole constructs (Figure I.3a,b and Figure I.S6, 3.7. Supporting information). A similar distribution pattern could also be seen for the fibrocartilage marker collagen type I, although with decreased intensity (Figure I.3c). For 10 wt.% HA-SH/P(AGE-*co*-G) hydrogels, either without or with hmHA, IHC staining for aggrecan and collagen type II and I again showed intra- and mainly pericellular matrix deposition (Figure I.3a-c and Figure I.S6; compare Figure I.2). As observed before, 3 wt.% HA-SH/P(AGE-*co*-G) hydrogels without hmHA showed broader aggrecan distribution, although not completely throughout the hydrogel (Figure I.3a and Figure I.S6, 3.7. Supporting information). Histomorphometric analysis of aggrecan and collagen type II distribution (Figure I.3d,e) further underscored the immunohistochemical observations. 96 % of the total area in 3 wt.% +hmHA

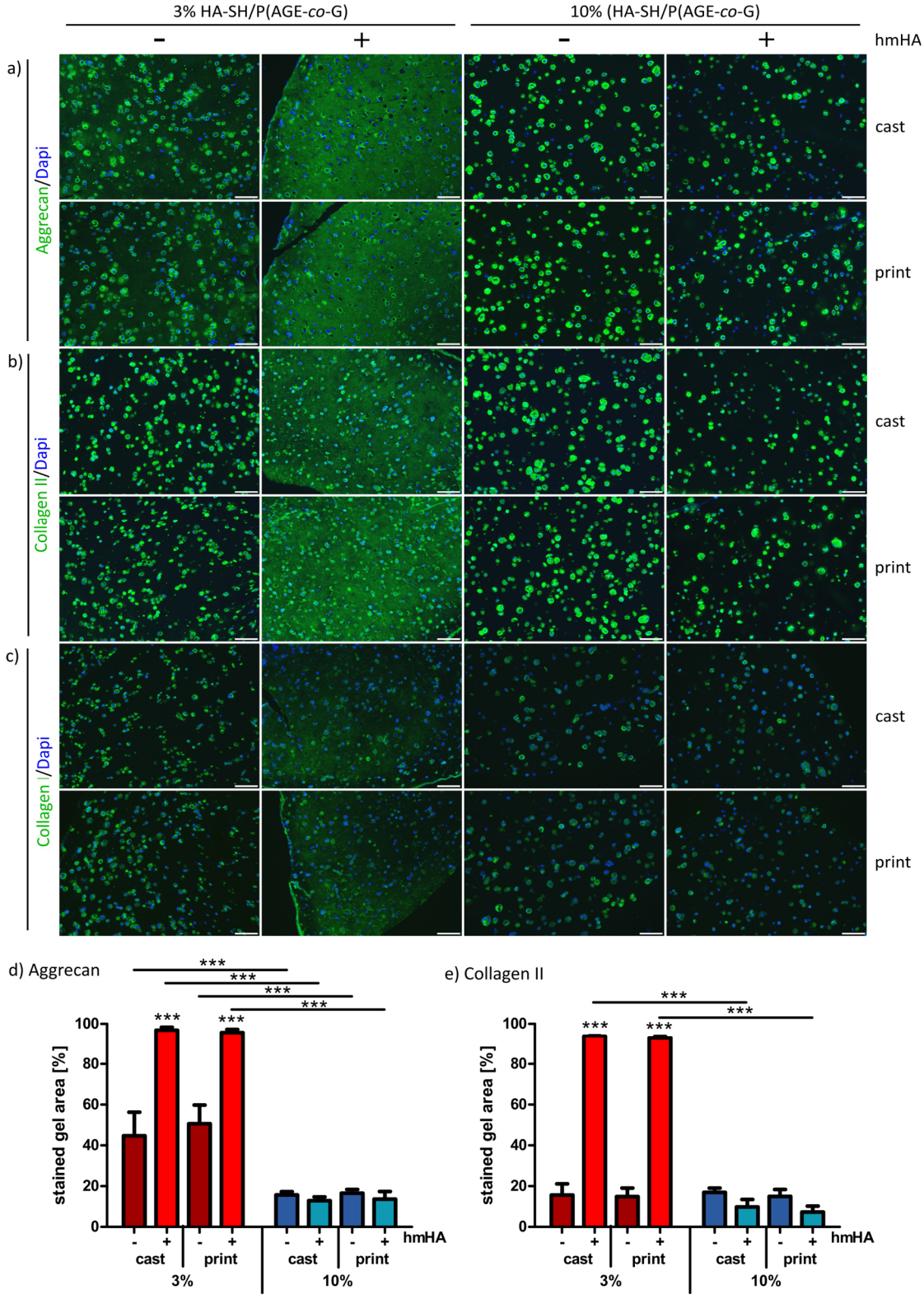

Figure I.3: Homogeneous ECM distribution in 3D constructs with low polymer content and additional hmHA. 3 wt.% and 10 wt.% HA-SH/P(AGE-*co*-G) hydrogels, either with or without additional hmHA (+/- hmHA) and seeded with MSCs, were either cast or printed. a-c) Immunohistochemical staining for ECM components deposited by incorporated MSCs after 21 days of chondrogenic differentiation; a) aggrecan, b) collagen type II, and c) collagen type I (all green). Nuclei (blue) were counterstained with DAPI. Scale bars represent 100 µm. Histomorphometric analysis of d) aggrecan and e) collagen type II distribution. Data are presented as means ± standard deviation (n = 4). Significant differences between groups are marked as follows: * ($p < 0.05$), ** ($p < 0.01$) and *** ($p < 0.001$). Stars (***) above bars of groups with additional hmHA (+) indicate significant differences to the corresponding groups without hmHA (-).

gels was stained for aggrecan and 93 % for collagen type II, while the same gel formulation without additional hmHA only showed ~50 % aggrecan and ~15 % collagen type II staining. 10 wt.% gels +hmHA enabled only pericellular ECM deposition, resulting in stained area of ~15 % and below for both aggrecan and collagen type II. Notably, the strong differences between the various hydrogel formulations with regard to ECM distribution were observed irrespective of bioink processing, i.e. either cast or print. The completely homogeneous matrix distribution within the bioinks consisting of 3 wt.% HA-SH/P(AGE-*co*-G) + hmHA was a distinct improvement compared to previous studies also employing HA-SH/P(AGE-*co*-G),[147, 211] but showing only pericellular ECM. In contrast to constructs with only pericellular matrix distribution, a homogeneous ECM distribution as observed in this study is regarded to likely improve mechanical characteristics such as stiffness and to favor the development of the constructs into a coherent tissue.[147, 157]

3.4.3.2. Biochemical quantification and gene expression analysis of ECM components

Biochemical quantification of ECM production and gene expression analysis were performed on all constructs. These experiments enabled an assessment if the observed strong improvement in ECM distribution in 3 wt.% +hmHA hydrogels was maybe due to an enhanced biological stimulus elicited by the additional hmHA. Analysis of DNA content on day 21 showed no significant differences among the different constructs (Figure I.4a). Quantitative analysis of GAG and total collagen content in the constructs confirmed chondrogenic differentiation after 21 days in all approaches (Figure I.4b,e) with distinct increase in produced matrix components compared to day 1 (Figure I.S7, 3.7. Supporting information). Interestingly, lower amounts of GAGs were detected in 3 wt.% gels compared to 10 wt.% gels, particularly 3 wt.% +hmHA gels (cast and printed) had a significantly lower GAG content than the corresponding 10 wt.% gels (Figure I.4b). To examine the total GAG production over 21 days, the culture supernatants were collected at each media change and additionally analyzed. Cumulative GAG contents in the supernatants were found to be increased in the 3 wt.% gels, as compared to the 10 wt.% gels, with highest values for the 3 wt.% +hmHA gels (Figure I.4c). Adding GAG content in constructs and respective supernatants showed no significant differences in total production between groups (Figure I.4d). These findings indicated higher GAG diffusion out of low concentrated constructs, presumably due to the reported increasing pore size with decreasing polymer content.[156, 157] Collagen quantification in constructs as well as in the culture supernatants revealed no significant differences between the conditions (Figure I.4e,f), with consequently also no differences in total production (Figure I.4g). Collagen fibers are larger than glycosaminoglycans (length of collagen: 4-12 μm vs. aggrecan: 0.5-4 μm) and have an average positive charge,[212] which were most likely the reasons for the lower release from the negatively charged HA-based gels. In general, quantification of the total production of glycosaminoglycans and collagens revealed no

statistically significant differences between the conditions. Thus, neither gel concentration, the addition of hmHA nor the bioink processing (cast or print) was observed to influence the total production of ECM components (Figure I.4d,g).

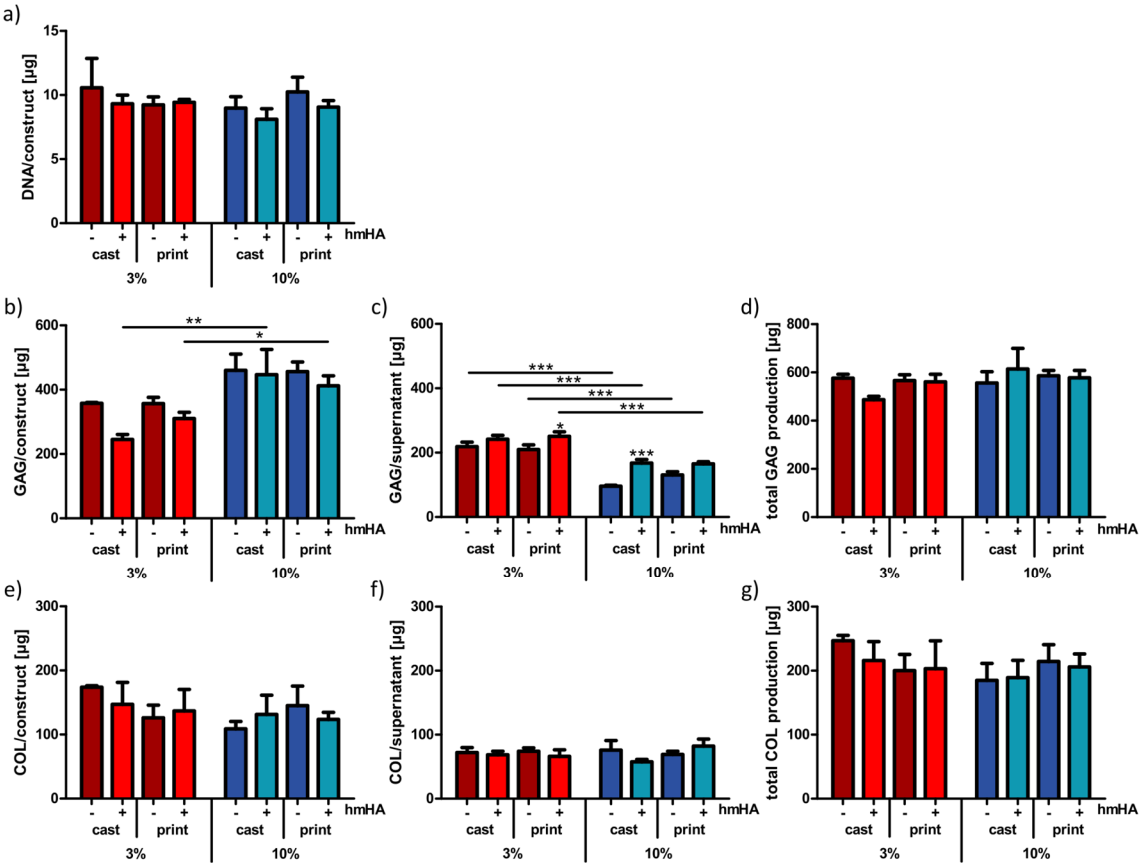

Figure I.4: GAG and collagen production of MSCs cultured in HA-SH/P(AGE-*co*-G) hydrogels. 3 wt.% and 10 wt.% HA-SH/P(AGE-*co*-G) hydrogels, either without or with additional hmHA (-/+ hmHA) and seeded with MSCs, were either cast or printed. Quantitative analysis was performed after 21 days of chondrogenic differentiation; data are presented as means ± standard deviation (n = 3). a) DNA in constructs. b) GAG content in constructs, c) cumulative GAG amount in supernatant, d) total GAG production; i.e., b+c=d. e) Collagen (COL) content in constructs, f) cumulative collagen amount in supernatant, g) total collagen production; i.e., e+f=g. Significant differences between groups are marked as follows: * ($p < 0.05$), ** ($p < 0.01$) and *** ($p < 0.001$).

Gene expression analysis by quantitative real-time PCR (qRT-PCR) was performed on d3, d7 and d21 of chondrogenic culture and normalized to gene expression of MSCs before seeding into the different hydrogels. Expression of the transcription factor SOX9, aggrecan (ACAN), collagen type II (COL2A1), collagen type IX (COL9A1), collagen type XI (COL11A1) and hyaluronan and proteoglycan link protein 1 (HAPLN1) confirmed chondrogenic differentiation under all conditions. In general, 10 wt.% gels had a higher SOX9 expression compared to 3 wt.% gels at all time points, and a higher aggrecan expression at days 7 and 21, although the differences were not always significant (Figure I.5a,b). Similarly, increased gene expression in hydrogels with higher polymer content was also observed at day 21 for collagen type IX, HAPLN1, and by trend also for collagen type XI, proteins that contribute to the generation and maintenance of ECM network stability and integrity (Figure I.S8a-c, 3.7. Supporting information). Collagen type II

expression increased strongly over time in all groups, with no clear differences between 3 wt.% gels and 10 wt.% gels (Figure I.5c). To analyze a potential ECM modulation or degradation, which may have contributed to the detected homogeneous matrix distribution, gene expression of several matrix-modulating enzymes was examined: hyaluronidases 1-3 (HYAL1, HYAL2, HYAL3), matrix metalloproteinase 2 (MMP2) and its opponents, the tissue inhibitors of metalloproteinases 1-2 (TIMP1, TIMP2) (Figure I.S8d-i. 3.7. Supporting information).

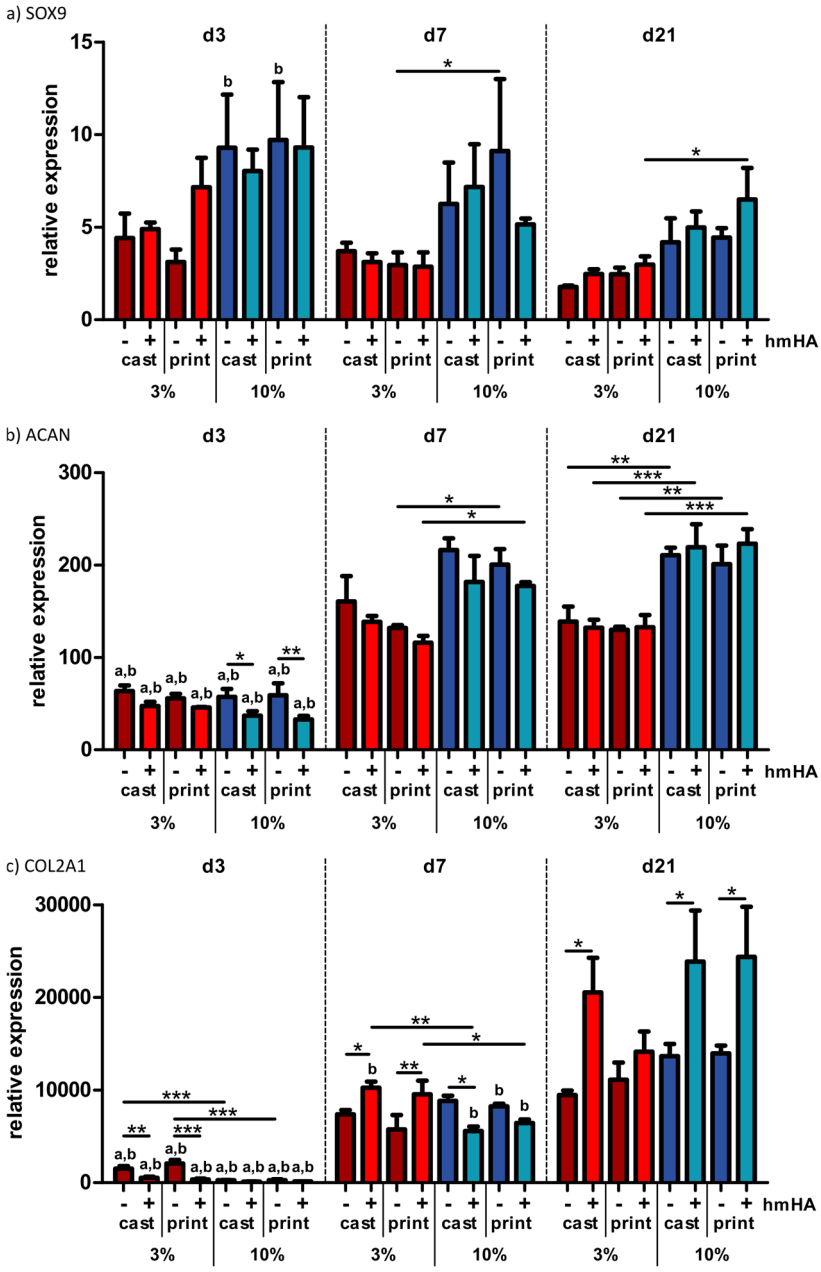

Figure I.5: Chondrogenic gene expression of MSCs in HA-SH/P(AGE-*co*-G) hydrogels. 3 wt.% and 10 wt.% HA-SH/P(AGE-*co*-G) hydrogels, either with or without additional hmHA (+/- hmHA) and seeded with MSCs, were either cast or printed. Gene expression of MSCs was determined by qRT-PCR after 3, 7, and 2 days of chondrogenic differentiation. Gene expression was normalized to GAPDH; the obtained values were further normalized to expression of MSCs before seeding into the hydrogels at day 0. Data are presented as means ± standard deviation (n = 3). Significant differences between groups are marked as follows: * ($p < 0.05$), ** ($p < 0.01$) and *** ($p < 0.001$). (a) Significantly different to corresponding value of the same group at day 7 (at least $p < 0.05$), (b) significantly different to corresponding value of the same group at day 21 (at least $p < 0.05$).

For all analyzed genes, no obvious general differences were observed when comparing respective groups without or with hmHA, or when comparing corresponding cast or printed samples. Enhanced gene expression in hydrogels with higher polymer content has been reported previously for a different series of non-printed hydrogels and several possibly contributing factors have been discussed.[157] HA is a main component of the natural cartilage ECM and incorporated MSCs can bind to HA via cell surface receptors such as CD44, which in turn can promote chondrogenic differentiation.[213-215] Hydrogels with higher HA content are, in principle, associated with a greater probability of such receptor-mediated interaction with the material. Furthermore, microenvironmental stiffness is supposed to influence the differentiation fate of MSCs.[216] In the present study, the initial Young's modulus after crosslinking of 10 wt.% HA-SH/P(AGE-*co*-G) constructs was around 40-fold higher than the Young's modulus of 3 wt.% HA-SH/P(AGE-*co*-G) constructs (Figure I.6a), which may have favored chondrogenic gene expression. Alternatively, in high concentrated hydrogels the strong ECM accumulation closely around the cells may increase cell-ECM interaction sites and may generate a chondrogenesis-supportive microenvironment.[157]

The observed enhanced expression of chondrogenic genes in hydrogels with higher polymer concentration (Figure I.5) did not correlate with the production of the main ECM components, (Figure I.4), as also reported previously.[157] With regard to the bioinks with additionally incorporated hmHA, an improved chondrogenic response may have been assumed due to possibly enhanced HA receptor-mediated interaction with the material. However, importantly, the biochemical quantitative assays and qRT-PCR analysis showed neither an enhanced ECM production (Figure I.4) nor enhanced expression of chondrogenic or ECM-related genes (Figures I.5 and I.S8, 3.7. Supporting information). Thus, they did not provide an explanation for the strikingly improved ECM distribution in the low concentrated bioinks with additional hmHA (Figures I.3 and I.S6, 3.7. Supporting information).

3.4.3.3. Correlation of ECM distribution with construct stiffness after chondrogenic differentiation

As an important mechanical feature for engineered cartilage, the Young's modulus was assessed after construct preparation as well as after 21 days of chondrogenic differentiation. 3 wt.% gels appeared very weak after preparation on day 1 (0.30 kPa for 3 wt.% without additional hmHA and 0.26 kPa for 3 wt.% + 1 wt.% hmHA) compared to 10 wt.% gels, which showed an initial Young's modulus of 10.9 kPa. After 21 days of chondrogenic differentiation, both 10 wt.% systems had a Young's modulus of around 28 kPa, while the 3 wt.% gels appeared considerably stiffer with 36.9 kPa for 3 wt.% -hmHA and 45.4 kPa for 3 wt.% +hmHA gels (Figure I.6a). This represented an increase in Young's modulus of ~123-fold for 3 wt.% -hmHA and ~175-fold for

3 wt.% +hmHA constructs, while 10 wt.% gels only increased their stiffness 2.5-fold during maturation (Figure I.6b).

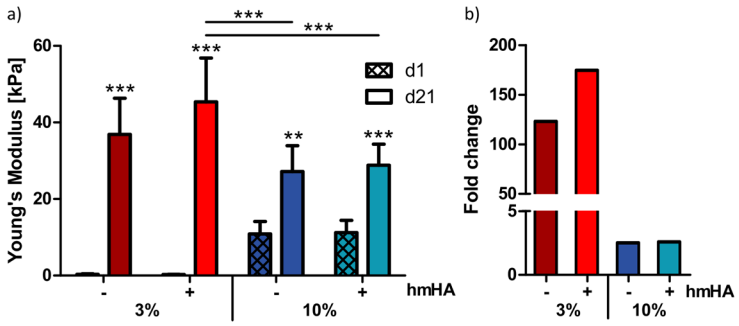

Figure I.6: Bioink composition affected construct stiffness after chondrogenic differentiation. Analysis of Young's modulus of MSC-laden 3 wt.% and 10 wt.% HA-SH/P(AGE-*co*-G) hydrogels, either with or without additional hmHA (+/- hmHA). a) Young's modulus of constructs on day 1 and after 21 days of chondrogenic differentiation, and b) the fold-change in Young's modulus over time. Data are presented as means ± standard deviation (n = 3). Significant differences are marked as follows: * ($p < 0.05$), ** ($p < 0.01$) and *** ($p < 0.001$). Stars (***) above bars of groups at day 21 indicate significant differences to the corresponding values of the same group at day 1.

Interestingly, lower GAG and similar collagen amounts were detected for the 3 wt.% gels (Figure I.4), however, the Young's modulus and especially the increase of Young's modulus after chondrogenic differentiation was distinctly higher for the 3 wt.% gels, as compared with the 10 wt.% gels (Figure I.6). Yet, this is no contradiction and very plausible when considering the distinct differences in ECM distribution between the low and high concentrated gels (Figures I.3 and I.S6, 3.7. Supporting information), and further highlights that a homogeneous ECM distribution likely is more important for higher construct stiffness.[157] 10 wt.% gels are more densely crosslinked networks with a higher initial stiffness, while 3 wt.% gels are more loosely crosslinked and initially distinctly softer due to their lower polymer content. Upon chondrogenic differentiation, pericellular ECM distribution in 10 wt.% gels only facilitated a comparably small increase in Young's modulus. In contrast, in 3 wt.% gels the more even ECM distribution throughout the constructs likely contributed to a strong increase in construct stiffness, with the most pronounced increase in 3 wt.% +hmHA gels, since the produced macromolecules can interact with and bind to each other throughout the gels, which is far less possible for ECM deposited mainly pericellularly.

3.4.3.4. Increased release of unbound hmHA from low concentrated hydrogels

The assumed different structure of the hydrogels was confirmed by cryo-scanning electron microscopy (SEM) showing larger pores in the 3 wt.% + hmHA than in the 10 wt.% +hmHA gels (Figure I.S9a, 3.7. Supporting information), likely favoring an increased diffusion throughout the hydrogels. To further examine hydrogel properties, gel swelling studies were performed with cylindrical hydrogels without cells over two weeks in PBS (Figure I.S9b, 3.7. Supporting information). 10 wt.% gels strongly swelled within the first two hours in PBS up to approx. 190 %

of the initial gel weight and reached a swelling equilibrium after two days at approx. 150 %, with slightly higher values in the composition with additional hmHA. In contrast, 3 wt.% gels showed just minor wet weight changes. The gels also reached their maximum weight after two hours at approx. 125 % and the equilibrium state after two days. Interestingly, 3 wt.% constructs with additional hmHA nearly reached volume stability with approx. 94 % of the initial gel weight in the equilibrium state. These results furthermore excluded the possibility that the different pore sizes detected by cryo-SEM might have been due to a higher swelling of the 3 wt.% gels.

The observed difference in pore size was assumed to influence also the diffusion behavior of unmodified hmHA. Therefore, 3 wt.% and 10 wt.% gels with and without additional 1 wt.% hmHA were incubated in PBS over 21 days and the collected supernatant was analyzed by quantitative gel permeation chromatography (GPC) for hmHA release (Figure I.7a).

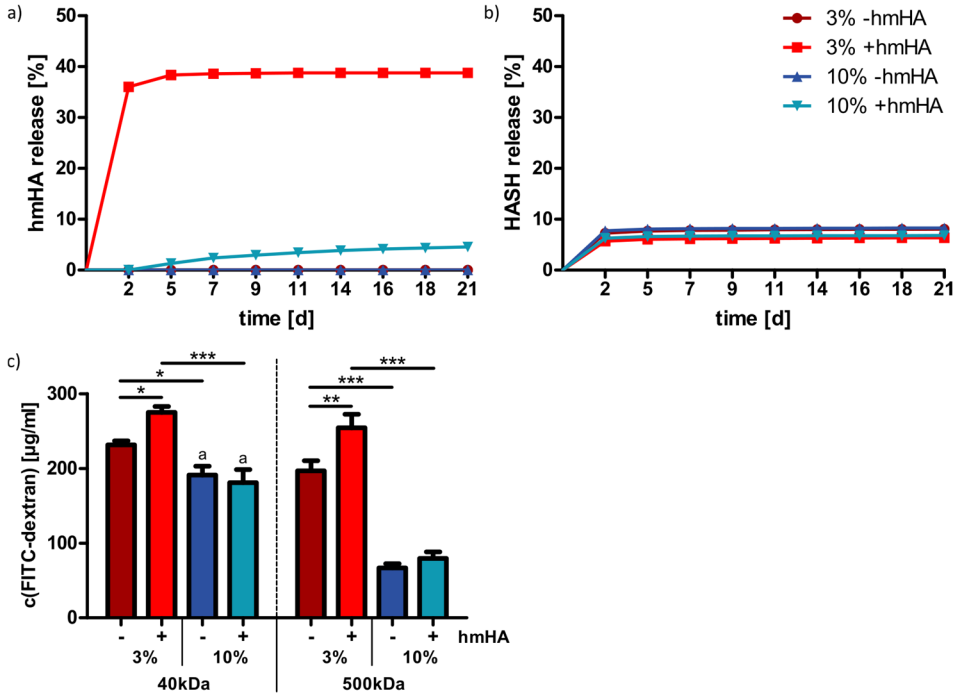

Figure I.7: Release of unmodified hmHA was dependent on overall polymer concentration. Analysis of release of a) unmodified high molecular hyaluronic acid (hmHA) and b) non-crosslinked HA-SH (= sol fraction) from 3 wt.% and 10 wt.% HA-SH/P(AGE-*co*-G) hydrogels, either with or without additional hmHA (+/- hmHA). GPC measurements of concentrated gel supernatants were performed in a HPLC machine to determine hmHA (a) and HA-SH (b) release from gels without cells incubated for 21 days in PBS. Values are depicted in percent and are related to the total amount of each component per gel. c) Diffusion in hydrogels after release of hmHA. Analysis of diffusion of FITC-labeled dextrans (40 and 500 kDa) into 3 wt.% and 10 wt.% HA-SH/P(AGE-*co*-G) hydrogels, either with or without additional hmHA (+/- hmHA). Hydrogels were incubated for 5 days in PBS before adding the FITC-dextran solution (1 mg ml^{-1} each) for 24 h. Data are presented as means ± standard deviation (n = 3). Significant differences are marked as follows: * ($p < 0.05$), ** ($p < 0.01$) and *** ($p < 0.001$). (a) Significantly different to corresponding value of the same group incubated in 500 kDa FITC-dextran solution (both with $p < 0.001$).

10 wt.% +hmHA gels allowed a cumulative release of only 4.5 % hmHA of the total quantity of 0.4 mg hmHA per construct over 21 days (i.e. 0.018 mg). In contrast, 3 wt.% +hmHA gels enabling better diffusion led to a strong burst release within the first two days and a strongly

increased total release of 39 % of the originally incorporated hmHA (i.e. 0.155 mg). Release of low molecular HA-SH, which was not covalently bound during gelation, was also analyzed from the same gel supernatants. Compared to the total amounts of HA-SH in the different gel types (0.6 mg HA-SH for 3 wt.% gels and 2 mg for 10 wt.% gels), only minor amounts were released from the gels. The study revealed consistently approx. 6.5% HA-SH release out of constructs with additional hmHA and approx. 8 % HA-SH release out of those without additional hmHA, irrespective of the overall gel concentration (Figure I.7b). These results indicated an equal extent of crosslinking in both gel concentrations. Furthermore, it could be concluded that the diffusion and release of small components like the non-crosslinked HA-SH (35.5 kDa) was not influenced by the different pore sizes. In contrast, the unmodified HA with high molecular weight (hmHA, 1100 kDa) was impaired to be released from densely crosslinked 10 wt.% gels, while 3 wt.% gels enabled a release of considerable amounts.

To further examine the diffusion through the different hydrogels after the above observed release of hmHA, fluorescein isothiocyanate (FITC)-labeled dextrans (40 and 500 kDa) were used. 3 wt.% and 10 wt.% hydrogels with and without additional 1 wt.% hmHA were incubated for 5 days in PBS, as this was the necessary time period for hmHA to be released from the low-concentrated constructs (see Figure I.7a). Subsequently, the gels were transferred to the different FITC-labeled dextran solutions (1 mg mL^{-1}) and incubated for 24 h before analysis (Figure I.7c). Quantification in the hydrogels revealed an increased amount of FITC-dextrans in the 3 wt.% gels compared to the corresponding higher concentrated gels, irrespective of dextran molecular weight. Furthermore, 3 wt.% gels +hmHA allowed for significantly more FITC-dextran penetration than 3 wt.% gels without hmHA also for both FITC-dextran solutions (Figure I.7c).

Taken together, reducing the polymer concentration in HA-SH/P(AGE-*co*-G) hydrogels improved GAG and aggrecan distribution within the constructs (Figure I.2). Most importantly, completely homogenous ECM distribution was achieved in 3 wt.% HA-SH/P(AGE-*co*-G) constructs with the addition of 1 wt.% hmHA (Figure I.3 and Figure I.S6, 3.7. Supporting information). Cryo-SEM images showed distinctly larger pores for 3 wt.% HA-SH/P(AGE-*co*-G) +hmHA as compared to corresponding higher concentrated constructs (Figure I.S9a). The substantial release of almost 40 % hmHA out of 3 wt.% HA-SH/P(AGE-*co*-G) gels within 5 days, as revealed by quantitative GPC measurement (Figure I.7a), likely created even more space in the constructs. This hypothesis was further supported by significantly increased FITC-dextran diffusion (40 kDa and 500 kDa) into the 3 wt.% +hmHA gel compared to the 3 wt.% gel without additional hmHA (Figure I.7c). Thus, increased porosity in 3 wt.% bioinks +hmHA likely contributed to the improved distribution of cartilage-specific ECM during chondrogenic differentiation, as compared to corresponding bioinks without additional hmHA.

3.4.4. 3D PCL-supported bioprinting of 3 wt.% HA-SH/P(AGE-*co*-G) + 1 wt.% hmHA as a proof of principle

So far, all differentiation studies of cast and printed gels were performed with constructs of the same cylindrical geometry to uncouple potential effects of the printing process from effects of altered medium diffusion or different surface-to-volume ratios associated with differently shaped constructs. These experiments were enabled by the use of a Vieweg DC200 dispenser, which closely simulated the printing process, and no adverse impact of the printing process on cell survival, gene expression, ECM production or distribution was detected (Figure I.3, I.4 and I.5). As a next step, in a proof-of-principle experiment, poly(ε-caprolactone) (PCL)-supported 3D constructs in two different geometries were double-printed using a 3D Discovery robotic dispensing system (RegenHU). The addition of hmHA does not render the bioinks printable into stand-alone constructs, however, the viscosity increase by hmHA (Figure I.S3, 3.7. Supporting information) enables PCL-supported 3D bioprinting, as previously described for high-concentrated (10 wt.%) bioinks,[147] and confirmed here as a proof-of-principle even for low-concentrated (3 wt.%) bioinks. This well-accepted approach combines beneficial materials for cartilage biofabrication: the bioactive hydrogel enables chondrogenic differentiation of MSCs, while PCL strands support hydrogel shape fidelity during 3D printing and additionally can increase construct stiffness, possibly beneficial for this load-bearing tissue.[147, 161, 217, 218] Here, the most favorable bioink consisting of 3 wt.% HA-SH/P(AGE-*co*-G) + 1 wt.% hmHA and 20 x 10^6 MSCs mL^{-1} was prepared and printed in the designated cavities of circular-shaped and rectangular-shaped PCL scaffolds (Figure I.8a). Live/dead staining of constructs at day 1 showed good cell survival after printing (Figure I.8b). An increase in dead cells observed at some border regions of the constructs may resulted from partial drying out during the printing process and the subsequent irradiation time. DNA content increased over 21 days of culture time (Figure I.8c), and MSCs were demonstrated to differentiate and deposit substantial amounts of cartilage-specific matrix components within the constructs (Figure I.8d,e). Importantly, as observed for the printed bioinks of the same composition in the cylindrical geometry (Figure I.3), the produced ECM after 21 days was again found to be homogeneously distributed throughout the whole constructs. This was shown for GAG staining with safranin O, and IHC staining for aggrecan, collagen type II, and, with weaker staining intensity, the fibrocartilage marker collagen type I (Figure I.8f-i).

Overall, besides enabling PCL-supported 3D printing as previously shown[147] and utilized here, the addition of 1 wt.% unmodified hmHA in 3 wt.% HA-SH/P(AGE-*co*-G) bioinks was revealed to facilitate not only substantial MSC differentiation, but strikingly a homogeneous ECM distribution throughout the constructs (Figure I.3, I.8 and I.S6), likely due to a distinctly enhanced release of hmHA from the low concentrated hydrogels (Figure I.7).

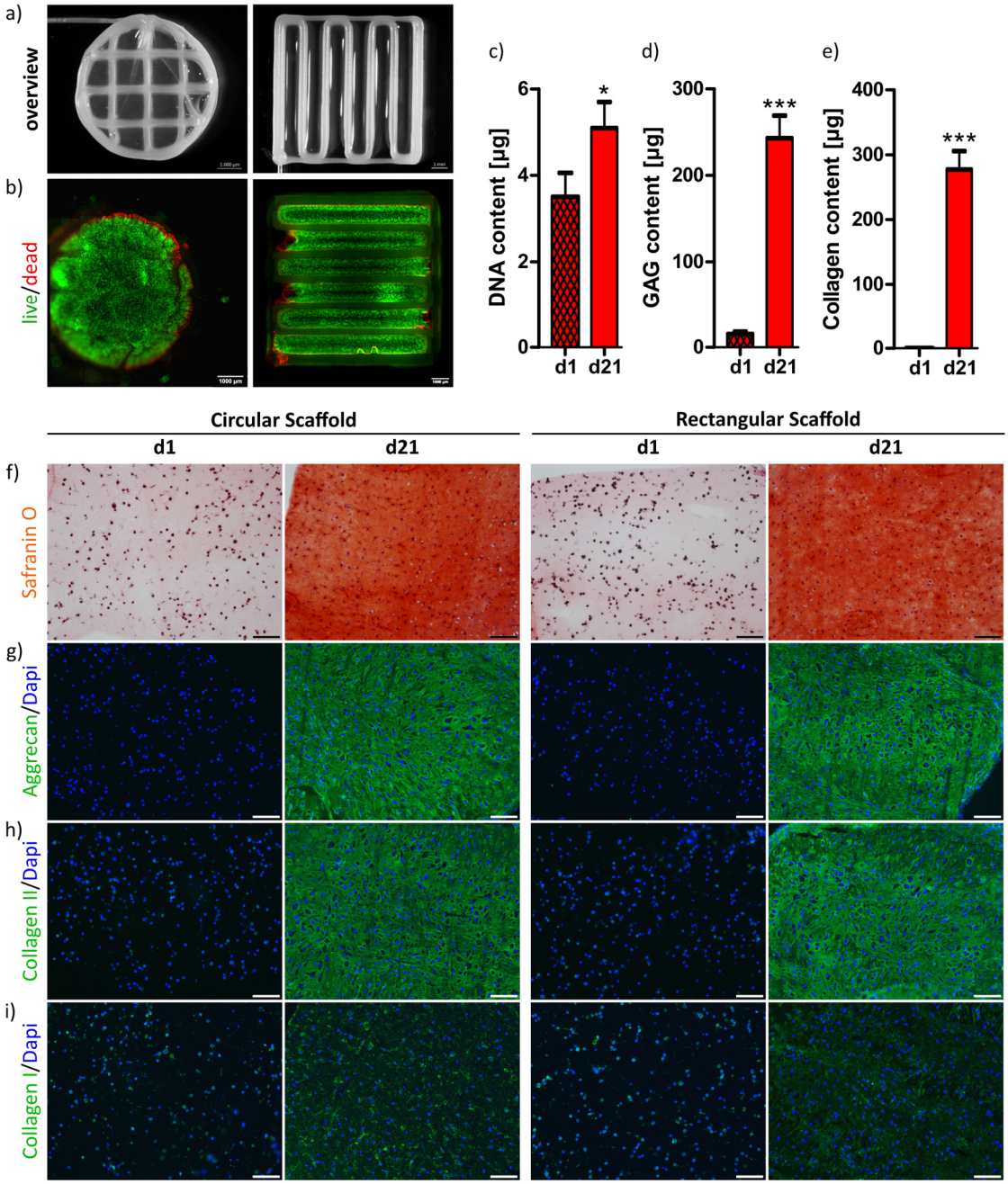

Figure I.8: Homogeneous ECM distribution in 3D bioprinted PCL-supported constructs after chondrogenic differentiation of MSCs. a) Overview and b) live/dead staining of circular and rectangular shaped PCL scaffolds with embedded cell-laden 3 wt.% HA-SH/P(AGE-*co*-G) + 1 wt.% hmHA bioink. Living cells were labeled with calcein-AM and appear in green, dead cells were stained red by EthD-III. Scale bars represent 1000 µm. Quantitative analysis of c) DNA, d) glycosaminoglycan (GAG) and e) collagen content at day 1 and day 21 of chondrogenic differentiation. Data are presented as means ± standard deviation (n = 3); (values of the rectangular scaffold are depicted but are representative for both structures). Significant differences between values at day 1 and 21 are marked as follows: * ($p < 0.05$), ** ($p < 0.01$) and *** ($p < 0.001$). f) Histological staining for deposition of GAG with safranin O after 21 days. g) Immunohistochemical staining for aggrecan (green), h) collagen type II, and i) collagen type I (green) after 21 days. Nuclei (blue) were counterstained with DAPI. Scale bars represent 100 µm.

In general, biofabrication studies using higher polymer contents and stiffer hydrogel networks for 3D printing have resulted in limited cell growth, differentiation, and ECM distribution.[68] To overcome the biological limitations and simultaneously improve mechanical properties for 3D

printing, researchers have used cellulose fibers,[219] silica nanoparticles,[220] or other thermoplastic structures as hydrogel additives.[221] Alternatively, PCL strands have been used as support structures[147, 218, 222] facilitating the use of less stiff hydrogels. A similar approach was also successfully employed in this study. Notably, the favorable outcome associated with the newly developed bioink (3 wt.% HA-SH/P(AGE-*co*-G) + 1 wt.% hmHA), including the completely homogeneous ECM distribution after 21 days of chondrogenic differentiation, could be demonstrated irrespective of the printing process or construct geometry.

3.5. Conclusion

In summary, this study demonstrated distinct modulation of 3D cell-hydrogel construct quality by HA-based bioink compositions. The distribution of cartilaginous ECM in HA-SH/P(AGE-*co*-G) bioinks with low polymer content was strongly improved by supplementation with hmHA, a component of the bioinks that was initially added to enable PCL-supported 3D bioprinting. The development of homogeneous ECM deposited by chondrogenically differentiated MSCs was demonstrated to be independent of the bioprinting process. Furthermore, the most favorable hydrogels also led to increased construct stiffness after chondrogenic culture. Taken together, these constructs combine PCL-supported 3D printability with homogeneous ECM distribution and increased stiffness after chondrogenic differentiation and, therefore, represent a promising perspective cartilage regeneration. Using the bioinks developed here, future strategies should explicitly include the evaluation of the PCL support structures with regard to further improvement of the mechanical characteristics such as construct stiffness. Moreover, in future studies the possible dual function of a bioink supplement that both enables PCL-supported bioprinting *and* improves the quality of the developing 3D constructs may be investigated also for other bioinks and additive components. Beyond PCL-supported printing, this strategy may be further explored also for printable bioinks that do not require mechanical support structures and utilized in other applications in biofabrication.

3.6. Acknowledgements

This work was funded by the Deutsche Forschungsgemeinschaft (DFG, German Research Foundation) – Project number 326998133 – TRR 225 (subproject A02, A06, B02, B06 and Z). The work was further supported by the DFG within the “State Major Instrumentation Programme”, providing funding for the SEM Crossbeam 340 (Zeiss) – funding number INST 105022/58-1 FUGG. The authors thank the Orthopedic Center for Musculoskeletal Research, University of Würzburg, for providing bone samples.

3.7. Supporting information

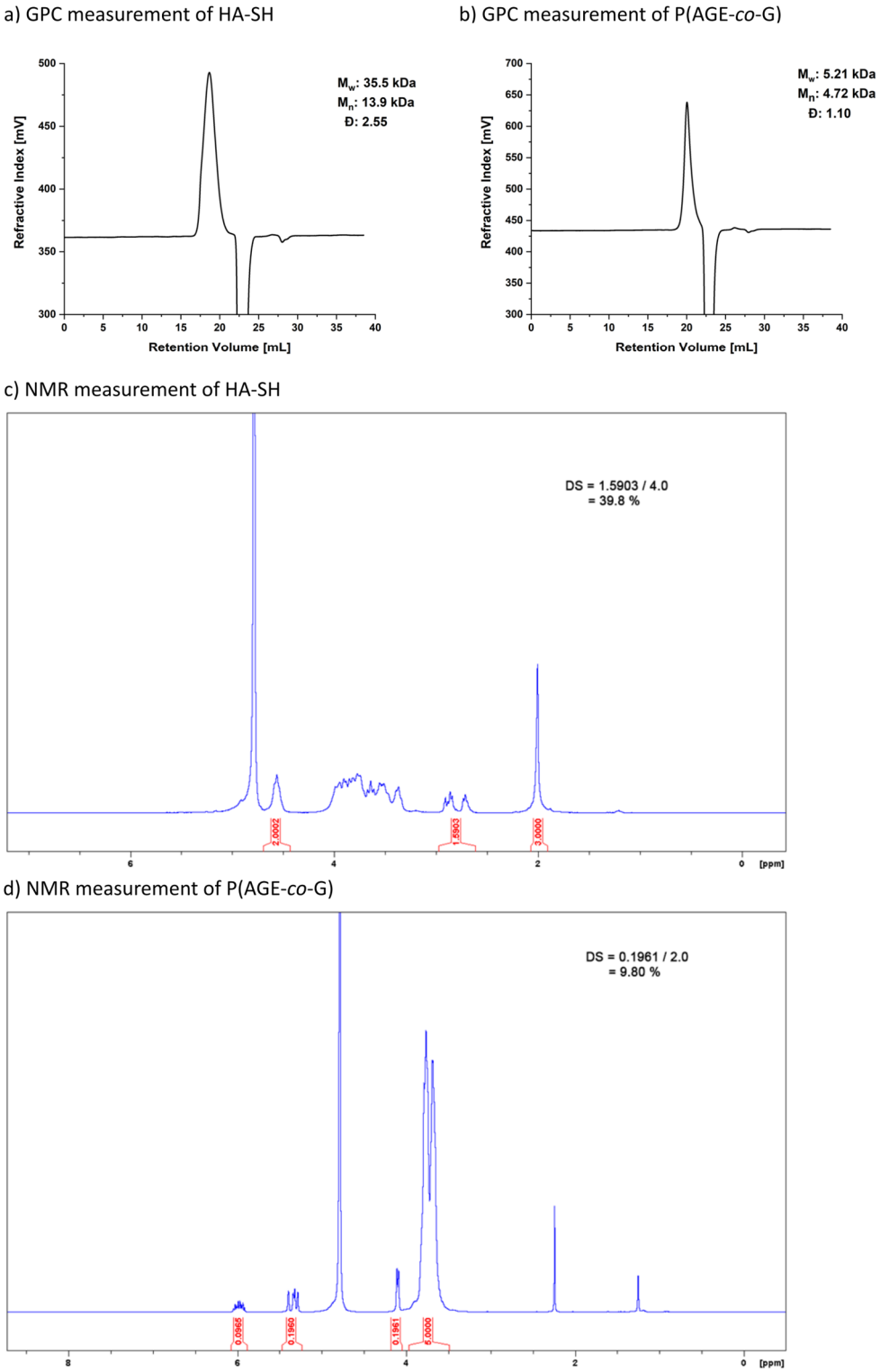

Figure I.S1: Polymer characterization of hydrogel components HA-SH and P(AGE-*co*-G). a) GPC and c) NMR analysis of HA-SH and b) GPC and d) NMR analysis of P(AGE-*co*-G) was used to confirm the exact molecular weight as well as the degree of substitution of the used polymers for covalently crosslinked hydrogels.

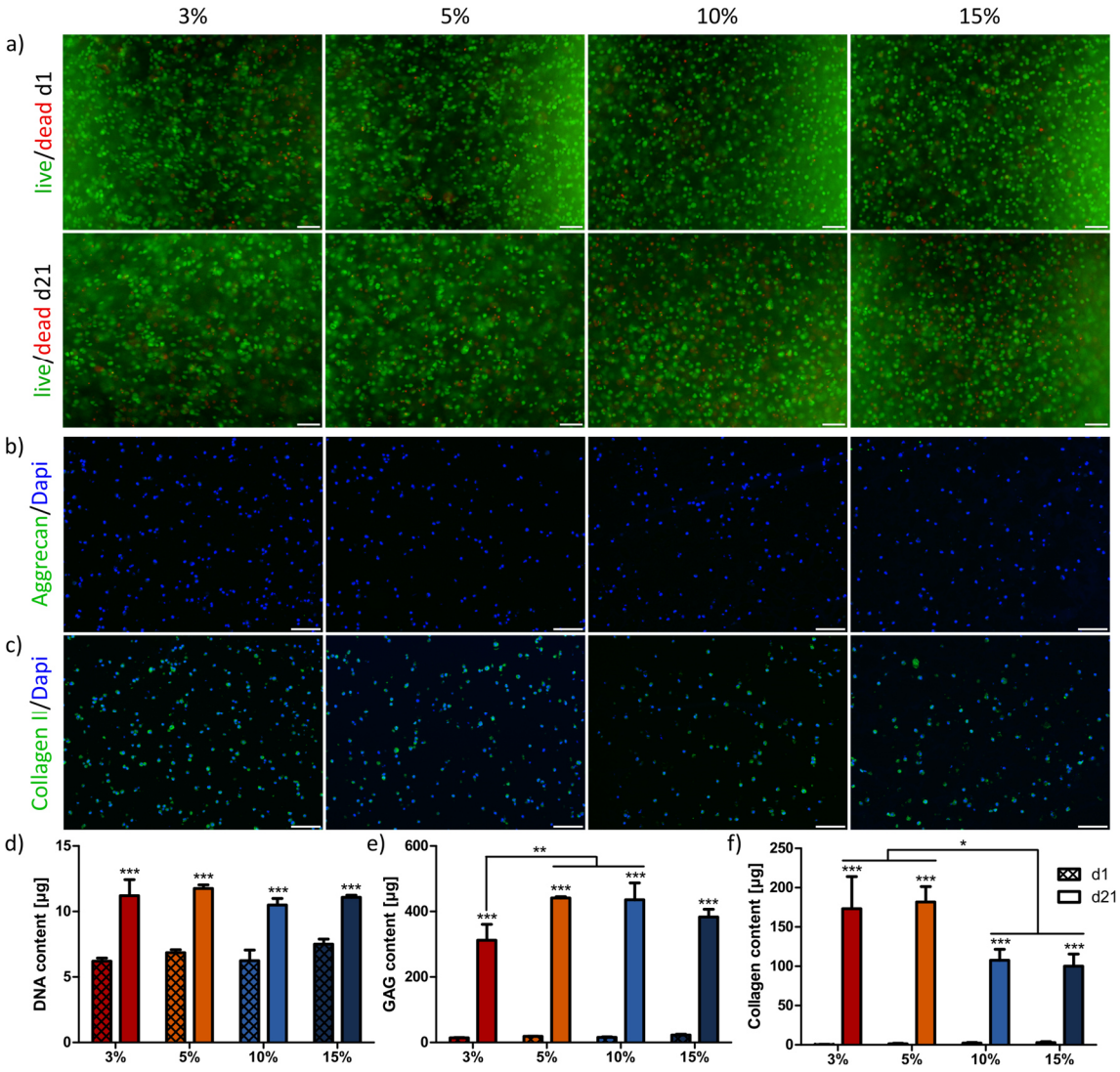

Figure I.S2: Viability and chondrogenic differentiation of MSC in differently concentrated HA-SH/P(AGE-*co*-G) hydrogels. (Complementary to Figure I.2). a) Viability of MSC was assessed in 3 wt.% - 15 wt.% HA-SH/P(AGE-*co*-G) hydrogels using a live/dead assay on day 1 and after 21 days of chondrogenic differentiation. Living cells were labeled with calcein-AM and appear in green, dead cells were stained red by EthD-III. Scale bars represent 100 µm. Immunohistochemical staining for b) aggrecan and c) collagen type II at day 1 with negligible ECM deposition served as controls for ECM deposition after chondrogenic differentiation (see Figure I.1b and c for immunohistochemical staining at day 21). Nuclei (blue) were counterstained with DAPI. Scale bars represent 100 µm. d-f) Quantitative analysis of DNA, GAG and collagen content was performed on day 1 and after 21 days of chondrogenic differentiation, data are presented as means ± standard deviation (n = 3). d) DNA, e) GAG, and f) collagen content in constructs. Significant differences between groups are marked as follows: * ($p < 0.05$), ** ($p < 0.01$) and *** ($p < 0.001$). Stars (***) above bars of groups at day 21 indicate significant differences to the corresponding values of the same group at day 1.

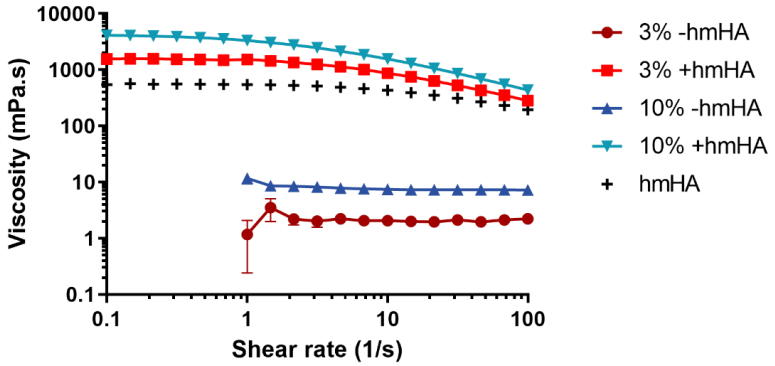

Figure I.S3: Rheological characterization of the used HA-SH/P(AGE-*co*-G) precursor solutions +/- hmHA and the hmHA. Addition of 1 wt.% hmHA to the 3 wt.% as well as 10 wt.% precursor solution increased viscosity significantly and introduced a shear-thinning behavior to allow for PCL-supported bioprinting with the used printer setup.

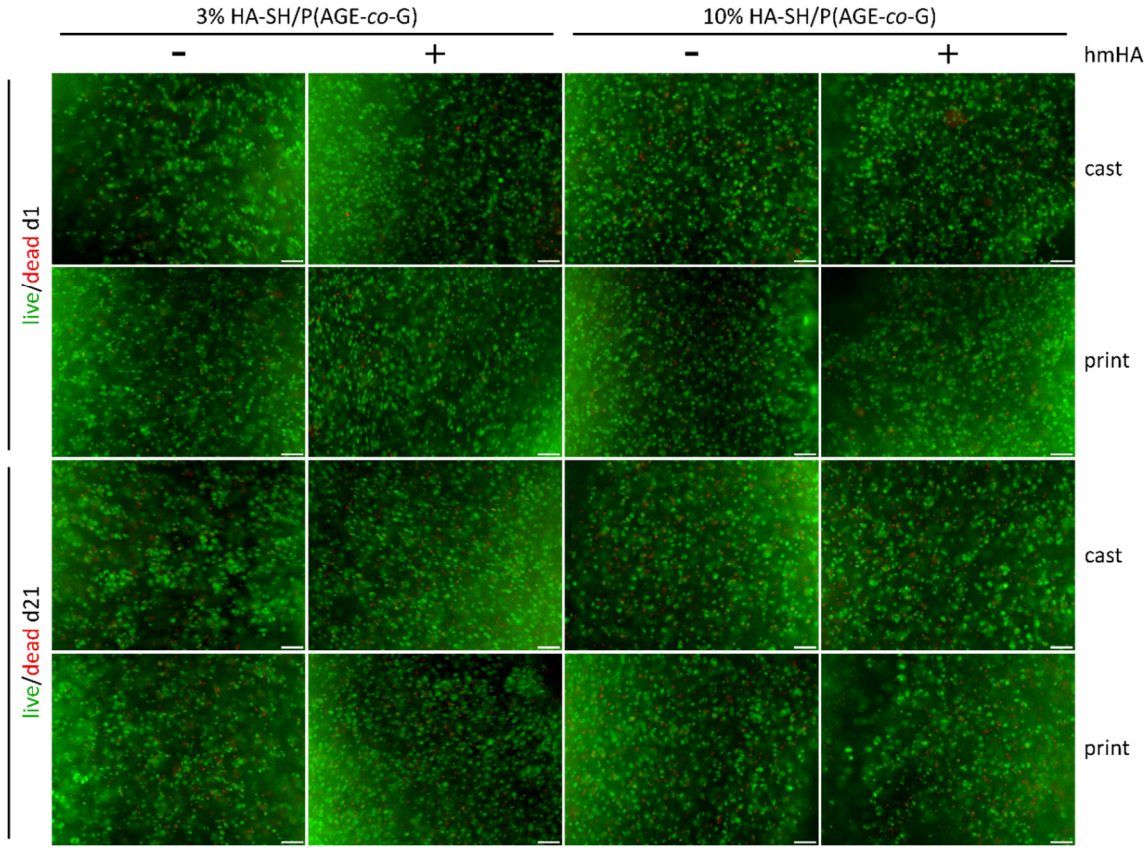

Figure I.S4: Viability of MSCs in HA-SH/P(AGE-*co*-G) hydrogels +/- hmHA. 3 wt.% and 10 wt.% HA-SH/P(AGE-*co*-G) hydrogels, either without or with additional hmHA (+/- hmHA) and seeded with MSCs, were either cast or printed. Viability was assessed using a live/dead assay on day 1 and after 21 days of chondrogenic differentiation. Living cells were labeled with calcein-AM and appear in green, dead cells were stained red by EthD-III. Scale bars represent 100 µm.

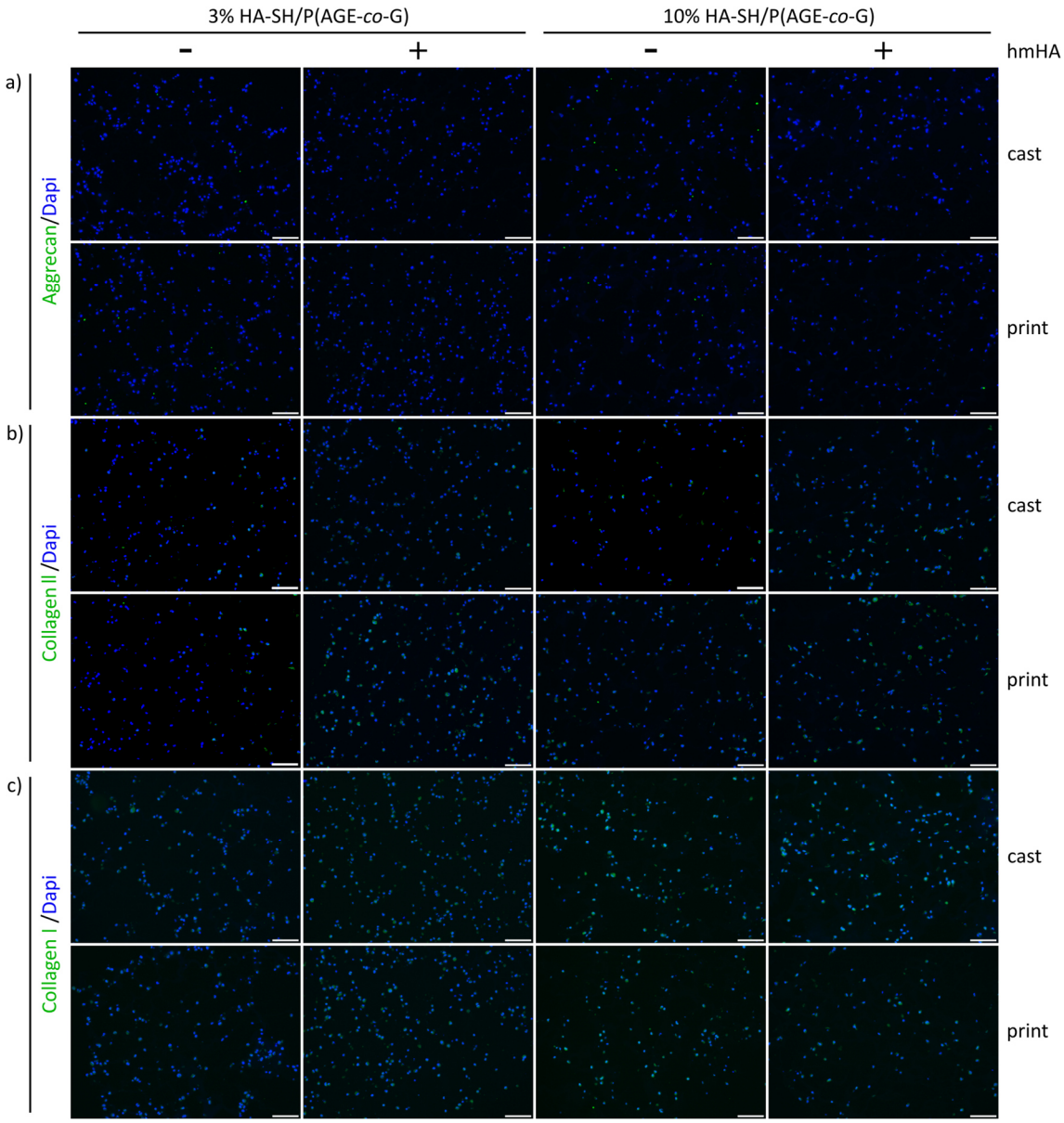

Figure I.S5: Immunohistochemical staining for ECM components at day 1 in HA-SH/P(AGE-*co*-G) hydrogels +/- hmHA. 3 wt.% and 10 wt.% HA-SH/P(AGE-*co*-G) hydrogels, either with or without additional hmHA (+/- hmHA) and seeded with MSCs, were either cast or printed. Immunohistochemical staining at day 1 with negligible ECM deposition served as controls (see Figure I.3 for immunohistochemical staining at day 21). a) aggrecan, b) collagen type II, and c) collagen type I (all green). Nuclei (blue) were counterstained with DAPI. Scale bars represent 100 µm.

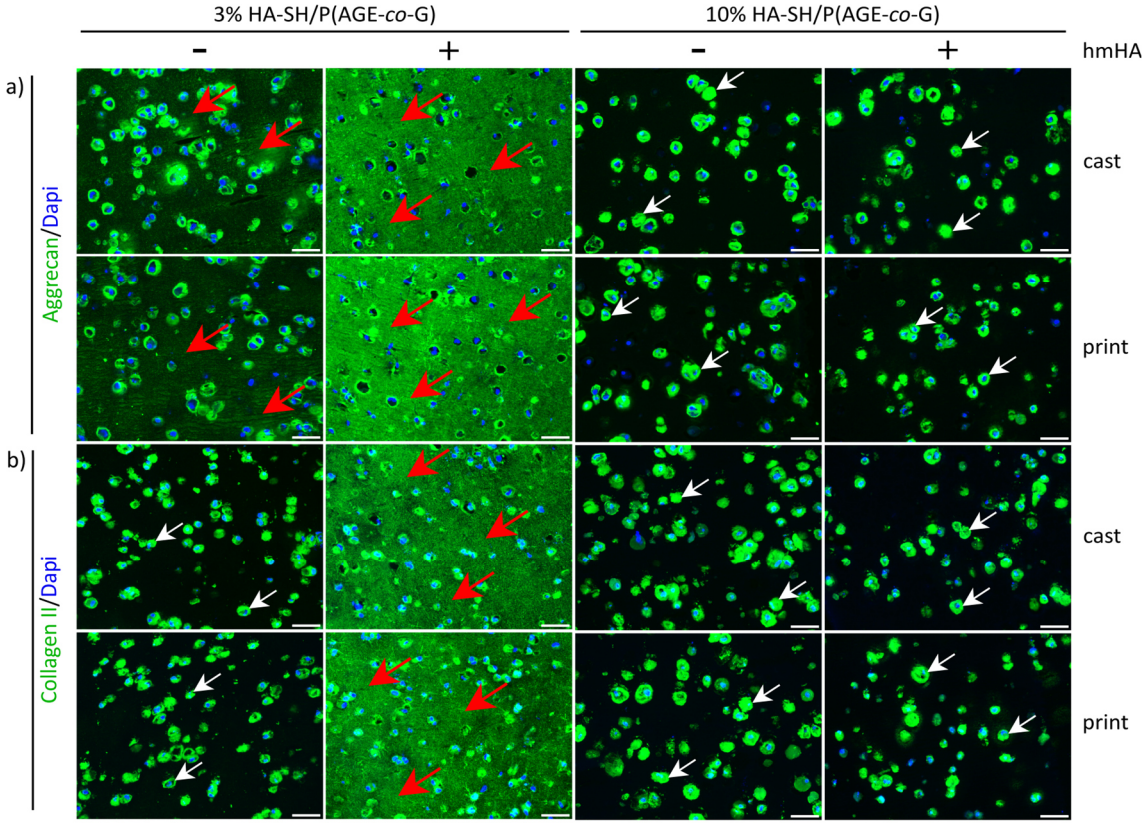

Figure I.S6: Homogeneous ECM distribution in 3D constructs with low polymer content and additional hmHA. 3 wt.% and 10 wt.% HA-SH/P(AGE-*co*-G) hydrogels, either with or without additional 1 wt.% hmHA (+/- hmHA) and seeded with MSCs, were cast or printed. ECM components a) aggrecan and b) collagen type II, which were deposited by incorporated MSCs after 21 days of chondrogenic differentiation, were immunohistochemically stained (green). White arrows exemplarily indicate ECM intra- and mainly pericellularly distributed around the cells, while red arrows mark ECM distribution within the gels. Nuclei (blue) were counterstained with DAPI. Scale bars represent 50 µm.

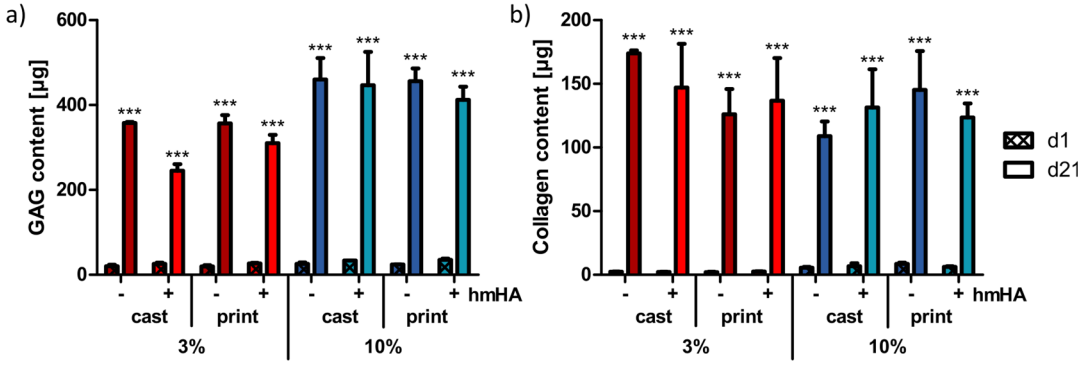

Figure I.S7: GAG and collagen content in HA-SH/P(AGE-*co*-G) hydrogels +/- hmHA. 3 wt.% and 10 wt.% HA-SH/P(AGE-*co*-G) hydrogels, either with or without additional hmHA (+/- hmHA) and seeded with MSCs, were either cast or printed. Quantitative analysis was performed on day 1 and after 21 days of chondrogenic differentiation, data are presented as means ± standard deviation (n = 3). a) GAG and b) collagen content in constructs. (Values at day 21 are also depicted in Figure I.4b and e). Significant differences of values at day 21 to values at day 1 are marked as follows: * ($p < 0.05$), ** ($p < 0.01$) and *** ($p < 0.001$).

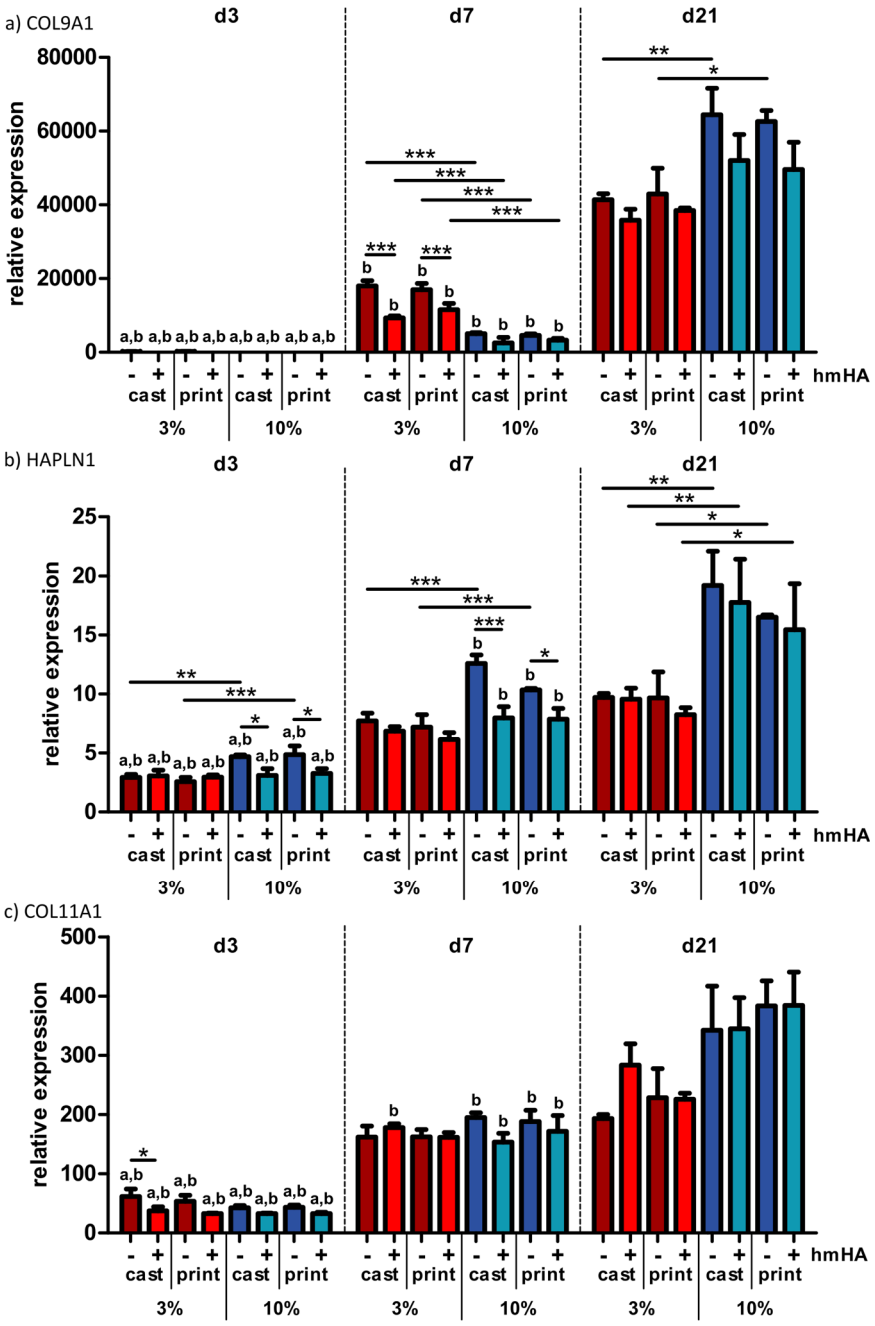
a) COL9A1
d3
d7
d21
relative expression
80000
60000
40000
20000
0
hmHA
cast
print
3%
10%
b) HAPLN1
25
20
15
10
5
c) COL11A1
500
400
300
200
100

d) HYAL1

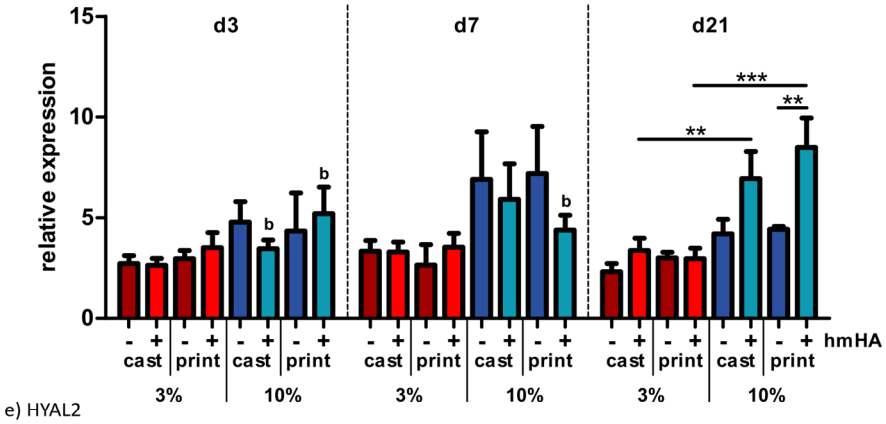

e) HYAL2

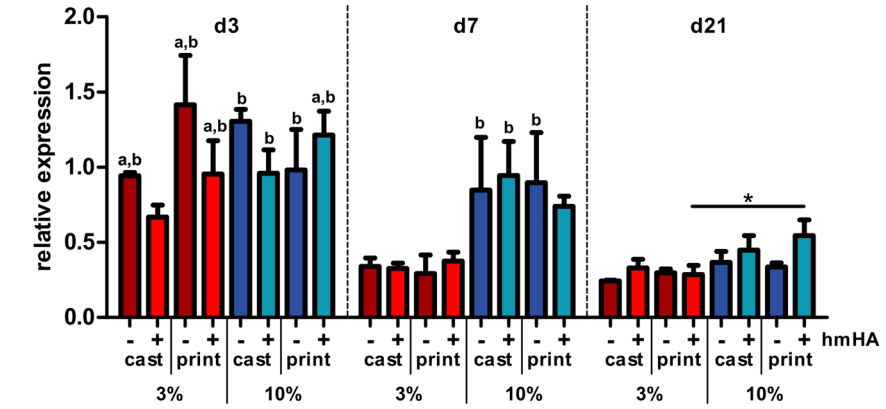

f) HYAL3

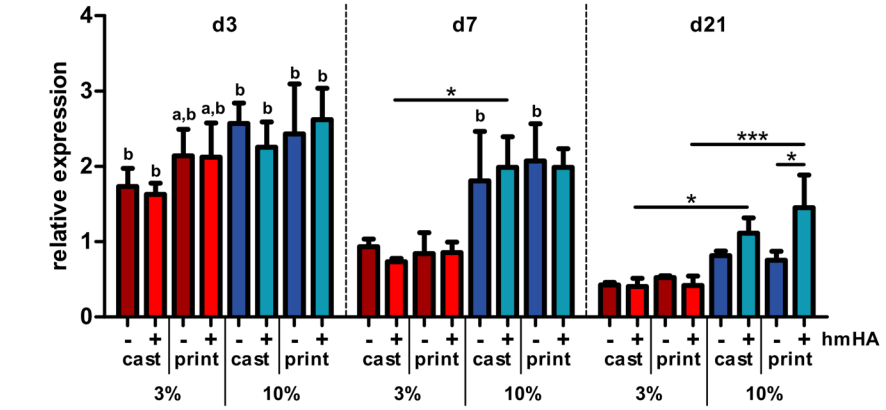

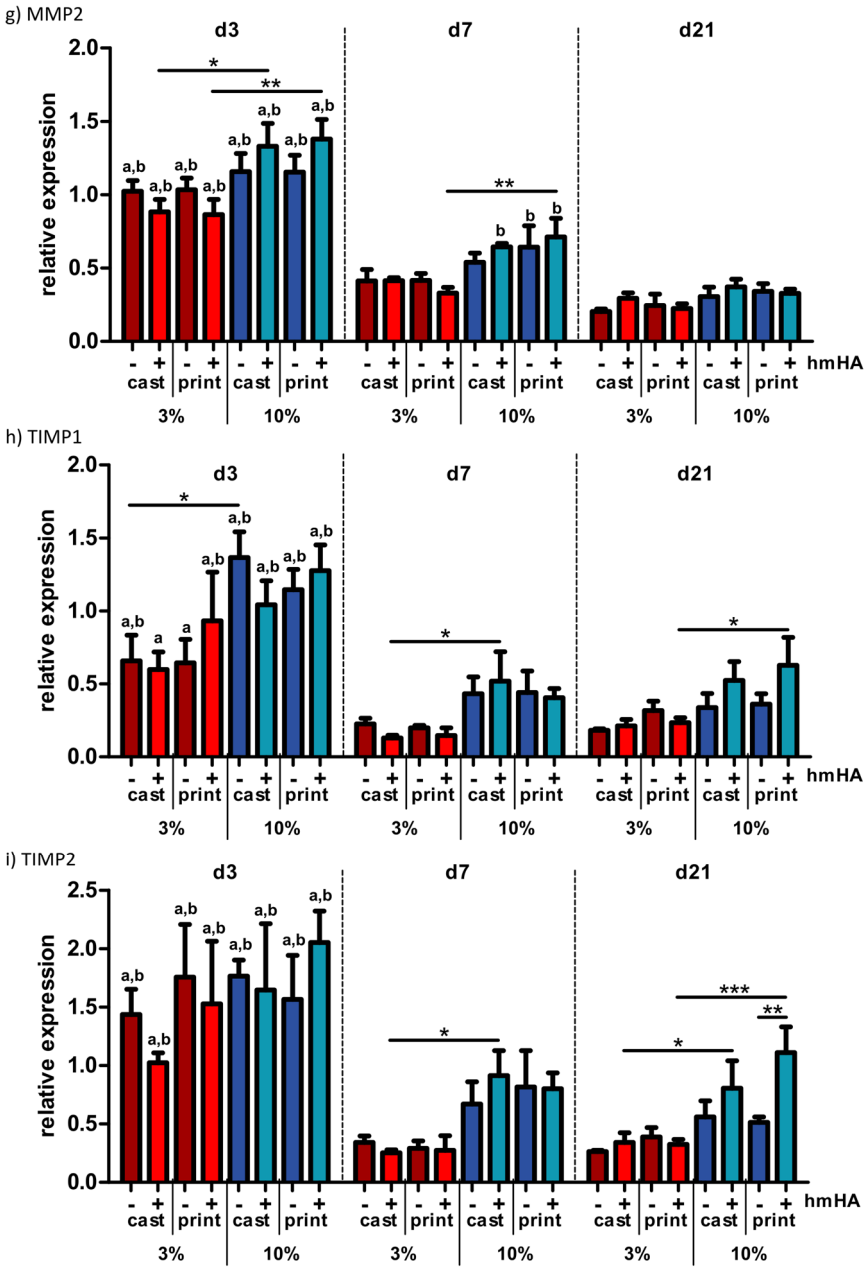

Figure I.S8. Chondrogenic gene expression of MSCs in HA-SH/P(AGE-*co*-G) hydrogels +/- hmHA. (Complementary to Figure I.5). 3 wt.% and 10 wt.% HA-SH/P(AGE-*co*-G) hydrogels, either with or without additional hmHA (+/- hmHA) and seeded with MSCs, were cast or printed. Gene expression of MSCs was determined by qRT-PCR after 3, 7, and 21 days of chondrogenic differentiation. Gene expression was normalized to GAPDH; the obtained values were further normalized to expression of MSCs before seeding into the hydrogels at day 0. Data are presented as means ± standard deviation (n = 3). Significant differences between groups are marked as follows: * ($p < 0.05$), ** ($p < 0.01$) and *** ($p < 0.001$). (a) Significantly different to corresponding value of the same group at day 7 (at least $p < 0.05$), (b) significantly different to corresponding value of the same group at day 21 (at least $p < 0.05$).

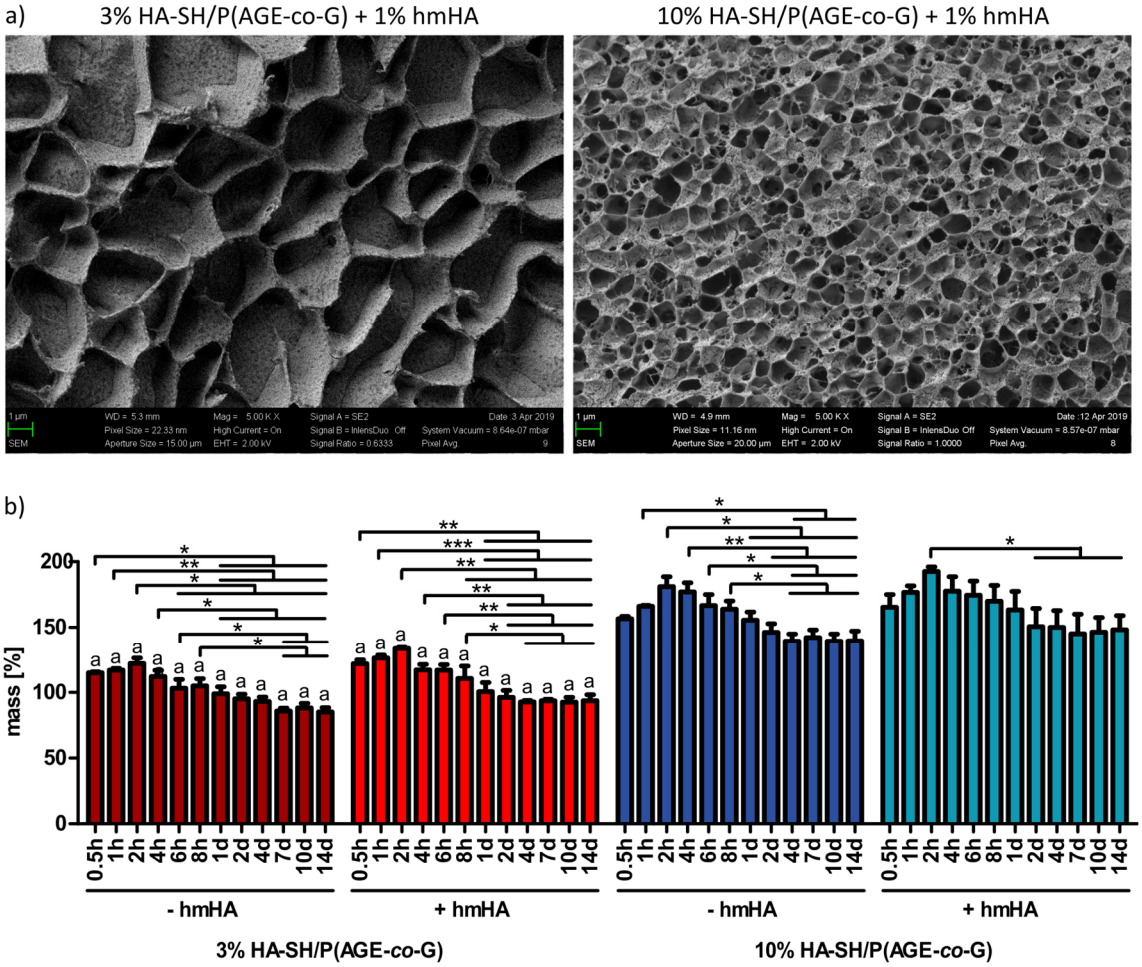

Figure I.S9: Pore structure and swelling behavior of HA-SH/P(AGE-*co*-G) hydrogels. a) Visualization of pore structure of 3 wt.% and 10 wt.% HA-SH/P(AGE-*co*-G) +1 wt.% hmHA hydrogels by cryo-SEM. Scale bars represent 1 µm. b) Swelling analysis of 3 wt.% and 10 wt.% HA-SH/P(AGE-*co*-G) +/- 1 wt.% hmHA hydrogels over 2 weeks. Bars represent deviation from the original wet weight (=100%). Data are presented as means ± standard deviation (n = 3). Significant differences between groups are marked as follows: * ($p < 0.05$), ** ($p < 0.01$) and *** ($p < 0.001$). (a) Significantly different to corresponding value of 10 wt.% hydrogel at the same time point, with $p < 0.001$.

Table I.S1: Primer sequences for qRT-PCR.

	Primer	**Sequence**
1	ACAN forward	5’-TACGACGCCATCTGCTACAC-3’
2	ACAN reverse	5’-GACGGTGATGTCCTCCTCAC-3’
3	COL2A1 forward	5’-CTGTCCTTCGGTGTCAGGG-3’
4	COL2A1 reverse	5’-CAGACACAGATCCGGCAGG-3’
5	COL9A1 forward	5’-GCTACATTGCAGGTGGCTTAC-3’
6	COL9A1 reverse	5’-GCTTCCAGTCATTCGAAACGTC-3’
7	COL11A1 forward	5’-ACACTGGAAAACCTGCCCC-3’
8	COL11A1 reverse	5’-CACAGTTTTCTTCTCCACGCTG-3’
9	GAPDH forward	5’-GGAAGGTGAAGGTCGGAGTC-3’
10	GAPDH reverse	5’-AGTTGAGGTCAATGAAGGGGTC-3’
11	HAPLN1 forward	5’-CATCCAAGCAGAAAATGGCCC-3’
12	HAPLN1 reverse	5’-GCAGTGTAACATTGCCACCTC-3’
13	HYAL1 forward	5’-GTGCTGCCCTATGTCCAGAT-3’
14	HYAL1 reverse	5’-GTATTTTCCCAGCTCACCCAGA-3’
15	HYAL2 forward	5’-CCATGCACTCCCAGTCTACG-3’
16	HYAL2 reverse	5’-CCAGAGGATGACACCAGCTG-3’
17	HYAL3 forward	5’-CCTTTGTCCGACATCGCCT-3’
18	HYAL3 reverse	5’-ACTGCACAAGGTCATCCTGG-3’
19	MMP2 forward	5’-GAAGGATGGCAAGTACGGCT-3’
20	MMP2 reverse	5’-GCGGAATGGAAACTTGCAGG-3’
21	SOX9 forward	5’-GGGCAAGCTCTGGAGACTTC-3’
22	SOX9 reverse	5’-AATCCGGGTGGTCCTTCTTG-3’
23	TIMP1 forward	5’-CATCCTGTTGTTGCTGTGGC-3’
24	TIMP1 reverse	5’-AACTTGGCCCTGATGACGAG-3’
25	TIMP2 forward	5’-TGGACGTTGGAGGAAAGAAGG-3’
26	TIMP2 reverse	5’-AGGGCACGATGAAGTCACAG-3’

4. Chapter II – Bioink Platform Utilizing Dual-stage Crosslinking of Hyaluronic Acid Tailored for Chondrogenic Differentiation of Mesenchymal Stromal Cells

DOI: 10.1002/mabi.202100331[223]

Julia Hauptstein‡[1], Leonard Forster‡[2], Ali Nadernezhad[2], Hannes Horder[1], Philipp Stahlhut[2], Jürgen Groll[2], Torsten Blunk*[1] and Jörg Teßmar*[2]

[1] Department of Trauma, Hand, Plastic and Reconstructive Surgery, University of Würzburg

[2] Chair for Functional Materials in Medicine and Dentistry and Bavarian Polymer Institute, University of Würzburg

‡ Authors contributed equally, * Corresponding authors

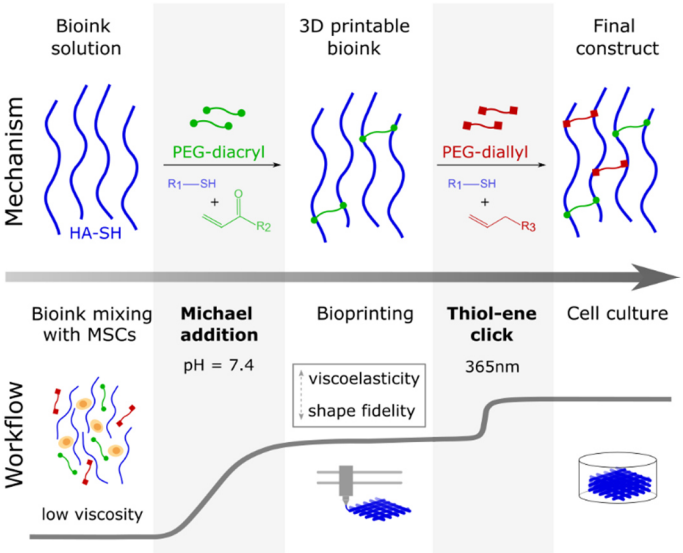

A versatile bioink platform based on hyaluronic acid is designed for cartilage biofabrication. The novel dual-stage crosslinking approach allows adjustment of bioink 3D printability and material properties of the final constructs. Selected bioink compositions are used for long-term cell culture and support differentiation of human mesenchymal stromal cells (MSCs) and the distribution of newly produced extracellular matrix (ECM).

4.1. Abstract

3D bioprinting often involves application of highly concentrated polymeric bioinks to enable fabrication of stable cell-hydrogel constructs, although poor cell survival, compromised stem cell differentiation, and an inhomogeneous distribution of newly produced extracellular matrix (ECM) is frequently observed. Therefore, this study presents a bioink platform utilizing a new versatile dual-stage crosslinking approach based on thiolated hyaluronic acid (HA-SH), which not only provides stand-alone 3D printability, but also facilitates effective chondrogenic differentiation of mesenchymal stromal cells (MSCs). A range of HA-SH with different molecular weights is synthesized and crosslinked with acrylated (PEG-diacryl) and allylated (PEG-diallyl) polyethylene glycol in a two-step reaction scheme. The initial Michael addition is used to achieve ink printability, followed by UV-mediated thiol-ene reaction to stabilize the printed bioink for long-term cell culture. Bioinks with high molecular weight HA-SH (> 200 kDa) require comparably low polymer content to facilitate bioprinting. This leads to superior quality of cartilaginous constructs which possess a coherent ECM and a strongly increased stiffness of long-term cultured constructs. The dual-stage system may serve as an example to design platforms utilizing two independent crosslinking reactions at one functional group, which allows to adjust printability as well as material and biological properties of bioinks.

4.2. Introduction

In recent years, biofabrication evolved as a promising and fast-growing field for applications in general life sciences as well as in regenerative medicine. Cell-compatible 3D fabrication methods such as bioprinting are used for precise patterning of bioinks consisting of living cells and bioactive hydrogel materials. Therefore, a special interest of the field focuses on hydrogels which combine cell-supportive properties with adequate 3D printability.[60, 224-227] To facilitate the generation of 3D printed constructs with sufficient shape fidelity, frequently highly concentrated polymeric hydrogels are used as cell supportive matrices.[68, 226] However, the resulting high network density and material stiffness can negatively affect cell bioactivity and the homogeneous distribution of newly produced extracellular matrix (ECM).[68, 226] As an alternative approach to increased shape fidelity, thermoplastic polymers such as poly(ε-caprolactone) may be used as support structures for very weak hydrogels to achieve mechanically more robust composite constructs. However, the necessity of integrating these thermoplastic materials reduces the degrees of freedom in the design of an application and can distinctly impair the development of a coherent tissue within the construct.[226] Thus, a major challenge of the field is the development of hydrogels that can be applied in low polymer concentrations providing favorable conditions for the incorporated cells, but can also be adequately 3D printed into constructs without further support structures.[68, 226]

For biofabrication of cartilage, hyaluronic acid (HA) represents an attractive basis for a suitable hydrogel since it is one of the major components of the extracellular matrix in human articular cartilage.[71, 152, 228] In previous non-printed approaches of HA hydrogels for cartilage engineering, ECM deposition with only limited spatial distribution depended mainly on hydrogel network density.[156, 157, 194-196] Reduction of the polymer concentration has led to an improved ECM distribution,[156, 157, 196] but this has yet to be transferred to printable systems. For 3D bioprinted constructs, several differently modified HA-based bioinks were utilized that were not stand-alone printable and needed an additional support structure for construct stabilization.[147, 188, 229, 230] However, flexible stand-alone HA hydrogel systems which show a high initial shape stability after printing as well as favorable conditions with regard to viability of mesenchymal stromal cells (MSC) and long-term chondrogenic differentiation are still rare. Recent publications confirmed the general interest in such HA bioinks for MSC culture and demonstrated printability. However, biological characterization mostly did not exceed visual demonstration of cell viability.[228, 231, 232] A promising approach to enable support-free bioprinting appears to be dual-stage crosslinking of HA, as it provides an extrudable ink after a first weak or reversible crosslinking step and terminal construct stability after final crosslinking. Similar approaches have already been studied also for hydrogels used for wound closure applications.[233] In previous studies attempting dual-stage crosslinking of bioinks, printability has been achieved via thermo reversible gelation,[234] reversible guest-host assembly,[235] or weak enzymatic pre-crosslinking of attached tyrosine units,[192] each followed by a final crosslinking step via UV or visible light irradiation to guarantee the required network stability for cell culture. Again, these approaches presented printable materials, but lacked extended biological characterizations, as they analyzed only short-term viability of embedded cells.

Therefore, in this study we aimed to develop a new versatile HA bioink platform based on a dual-stage crosslinking approach, which provides not only stand-alone 3D printability after the first crosslinking step, but also favorable conditions after terminal crosslinking for long-term chondrogenic differentiation of MSCs, with a focus on the distribution of newly produced ECM. A range of thiolated HA (HA-SH) with different molecular weights was synthesized and crosslinking was achieved in two stages, utilizing adjustable amounts of polyethylene glycol-diacrylate (PEG-diacryl) for pre-crosslinking and polyethylene glycol-diallyl carbamate (PEG-diallyl) for thiol-ene mediated post-crosslinking after 3D printing. In general, a distinctly lower total polymer content was needed for the more viscous high molecular weight HA-SH (> 200 kDa), to achieve an optimal 3D printability of the inks, as compared to low molecular weight HA-SH (ca. 50 kDa). In long-term cell culture over 21 days, MSCs were demonstrated to differentiate chondrogenically in all bioprinted constructs. Bioinks with 51 kDa HA-SH required a high polymer content for good printability but resulted in only pericellular ECM distribution and overall weak mechanical properties of the final constructs after chondrogenic differentiation.

In contrast, constructs made from 230 kDa and 410 kDa HA-SH, needing only a low polymer content for 3D printing, exhibited higher GAG and collagen contents, a homogeneous ECM distribution throughout the constructs and strongly improved stiffness after chondrogenic differentiation. The study contributes to effective bioink development leading to improved biological properties of bioprinted constructs.

4.3. Experimental section

4.3.1. Materials

All chemicals were purchased from Sigma Aldrich (St. Louis, MO, USA) if not stated differently. Acryloyl chloride stabilized with phenothiazine (abcr GmbH, Karlsruhe, Germany), 1-(3-dimethylaminopropyl)-3-ethylcarbodiimide HCl (EDC, Biosynth CarboSynth, Compton, UK), 1,4-dithiothreitol (DTT, Biosynth CarboSynth, Compton, UK), 2-hydroxy-1-[4-(hydroxyethoxy)-phenyl]-2-methyl-1-propanone (I2959; BASF, Ludwigshafen, Germany), 4-(dimethylamino)benzaldehyde (DAB; Carl Roth, Karlsruhe, Germany), basic fibroblast growth factor (bFGF; BioLegend, London, UK), chloroform-d^1 (Eurisotope, St-Aubin Cedex, France), DAPI mounting medium ImmunoSelect® (Dako, Hamburg, Germany), deuterium oxide (Deutero GmbH, Kastellaun, Germany), regenerated cellulose dialysis tubes MWCO 3500 Da (Carl Roth, Karlsruhe, Germany), diethylether (Chemobar University of Würzburg, Würzburg, Germany), dimethyl-3,3'-dithiodipropionate (TCI Chemical Industry Co. Ltd., Tokyo, Japan), di-potassium hydrogen phosphate (Merck KGaA, Darmstadt, Germany), di-sodium hydrogen phosphate (Merck KGaA, Darmstadt, Germany), Dulbecco's Modified Eagle's Medium high glucose 4.5 g L^{-1} (DMEM; Thermo Scientific, Waltham, MA, USA), Dulbecco's Modified Eagle's Medium/Ham's F-12 (DMEM/F12; Thermo Scientific, Waltham, MA, USA), ethanol (99 %, TH Geyer, Renningen, Germany), fetal calf serum (FCS; Thermo Scientific, Waltham, MA, USA), formaldehyde (37 %, Carl Roth, Karlsruhe, Germany), hyaluronic acid sodium salt (Mw 1 - 2 MDa; 0.2 - 0.5 MDa; 0.08 - 0.1 MDa; Biosynth CarboSynth, Compton, UK), hydrochloric acid (HCl; 32 %, 37 %, Merck KGaA, Darmstadt, Germany), isopropanol (VWR, Radnor, PA, USA), ITS+ premix (Corning, New York, NY, USA), L-hydroxyprolin (Merck KGaA, Darmstadt, Germany), live/dead cell staining kit (PromoKine, Heidelberg, Germany), methanol (Fisher Scientific, Schwerte, Germany), *N*-hydroxysuccinimide (NHS, Biosynth CarboSynth, Compton, UK), papain (Worthington, Lakewood, CA, USA), penicillin-streptomycin (PS; 100 U mL^{-1} penicillin, 0.1 mg mL^{-1} streptomycin; Thermo Scientific, Waltham, MA, USA), perchloric acid (60 %, Merck KGaA, Darmstadt, Germany), phosphate-buffered saline (PBS; Life Technologies, Carlsbad, CA, USA), potassium dihydrogen phosphate (Merck KGaA, Darmstadt, Germany), Proteinase K (Digest-All 4, Life Technologies, Carlsbad, CA, USA), sodium hydrogen carbonate (Merck KGaA, Darmstadt, Germany), sodium hydroxide (Merck KGaA, Darmstadt, Germany),

Tissue Tek® O.C.T. (Sakura Finetek, Tokyo, Japan), toluene (Fisher Scientific, Schwerte, Germany), transforming growth factor β1 (TGF-β1; BioLegend, London, UK), tris(carboxyethyl)phosphine HCl (TCEP, Biosynth CarboSynth, Compton, UK), trypsin-EDTA (0.25 %, Life Technologies, Carlsbad, CA, USA).

4.3.2. Methods

Synthesis of 3,3'-dithiobis(propanoic dihydrazide) (DTPH): The synthesis was performed according to Vercruysse et al.[236] with slight modifications. Dimethyl-3,3' dithiodipropionate (82 mL, 1 eq.) was dissolved in 1 L methanol at rt. The clear solution was cooled to 0 °C by an ice bath and an excess of hydrazine monohydrate (8.0 eq.) was added. The clear, yellowish reaction solution was stirred at 0 °C for 4 h and then stirred overnight at rt to form a shiny, yellowish suspension. Afterwards, the clear, yellow supernatant was discarded, and the precipitate was washed with methanol. Remaining methanol was removed by washing the precipitate with an excess of diethyl ether. The final product was dried in vacuo at rt to give a shiny, white solid.

Synthesis of thiolated hyaluronic acid (HA-SH): The synthesis was performed according to Stichler et al.[147] with several modifications. Hyaluronic acid (HA) of different molecular weights (3 g, 1.0 eq.) (Table II.S1, Supporting Information) was dissolved in 300 mL deionized water overnight at 37 °C to give a viscous, clear solution. NHS (4.0 eq.) and DTPH (4.0 eq.) were dissolved in 300 mL Sørensen buffer (0.2 M, pH 5.5) at rt and mixed with the HA solution. After the addition of EDC (7.5 eq.) the pH was adjusted to 4.0 with 10 % HCl and the mixture was incubated for 4 h at 37 °C. The pH of the resulting clear gel was raised to over 8.5 with 2 N NaOH and DTT (5.0 eq.) was added. The mixture was incubated overnight at 37 °C to form a clear, brownish solution. Afterwards, the pH was adjusted to 3.0 with 10 % HCl, and the mixture was dialyzed (MWCO 1 kDa) against K_2HPO_4/HCl buffer (0.3 mM, pH 5.0) with the addition of ascorbic acid/TCEP (each 1 g/15 L) for 3 days, then against K_2HPO_4/HCl buffer (0.3 mM, pH 5.0) 2 days without TCEP. The obtained clear solution was freeze-dried to give a white foamy solid.

Synthesis of polyethylene glycol-diacrylate (PEG-diacryl): The acrylation of PEG was identically performed for all three linear PEGs (6, 10, 20 kDa) according to Cruise et al.[237] First, PEG (100 g, 1.0 eq.) was molten at 110 °C and high vacuum was applied for 2 h to remove residual water. The clear melt was dissolved in 1 L of dry toluene under argon atmosphere. Dry triethylamine (3.0 eq.) was added, followed by a stepwise addition of freshly distilled acryloyl chloride (3.0 eq.). The turbid, yellow reaction solution was stirred overnight at rt to form an orange suspension. After centrifugation, the sediment was discarded and the clear, orange supernatant was cooled to 0 °C. The resulting precipitate was obtained by centrifugation and

recrystallized in ethanol until discoloration of the solid phase. The purified product was dried in vacuo at rt and a white solid was obtained.

Synthesis of polyethylene glycol-diamine: The amination of PEG was carried out according to Iijima et al.[238] with slight modifications. Linear PEG (100 g, 1.0 eq.) was dried under high vacuum at 110 °C for 2 h, cooled to rt under argon atmosphere, and dissolved in 900 mL dry dichloromethane. Triethylamine (3.0 eq.) was added, and the clear solution was cooled to 0 °C in an ice bath. After the stepwise addition of methanesulfonyl chloride (3.0 eq.), the clear, yellow reaction solution was stirred for 1 h at 0 °C and then 4 h at rt. The solvents were removed with a rotary evaporator at 50 °C and the orange solid dissolved in 100 mL deionized water. 500 mL of a 30 % ammonium hydroxide solution were added, and the clear, yellow reaction solution was stirred 3 d at 0 °C followed by 1 d at rt. Remaining ammonia was evaporated overnight in the fume hood and the clear solution was alkalified to pH 9 - 10 with 2 N NaOH. The aqueous layer was washed with diethyl ether (3 x 150 mL) and then extracted with dichloromethane (6 x 150 mL). The combined organic layer was dried over $MgSO_4$, concentrated in vacuo, and precipitated in cold diethyl ether. The sediment was dried in high vacuum to give a yellowish solid.

Synthesis of polyethylene glycol-diallyl carbamate (PEG-diallyl): Linear PEG diamine (10 g, 1.0 eq.) was dissolved in 100 mL deionized water and 8.67 mL 2 N NaOH (5.0 eq.) were added. Allyl chloroformate (1.6 eq.) was added, and the resulting two-phase system was stirred intensively for 4 h at 0 °C. After washing with diethyl ether (2 x 100 mL), the aqueous layer was extracted with dichloromethane (5 x 75 mL), the organic layers were combined, dried over $MgSO_4$, and filtered. The yellowish product solution was concentrated, precipitated in cold diethyl ether, and the sediment dried under high vacuum at rt. The purified product appeared as white solid.

NMR analysis: ^{1}H-NMR measurements of DTPH were performed at a 400 MHz Bruker Avance III HD using d_6-DMSO and ^{1}H-NMR measurements of all polymers were performed at a 300 MHz Bruker Biospin spectrometer (Bruker, Billerica, MA) using $CDCl_3$ (PEG), and D_2O (HA-SH) as solvents. The solvent peak was set to the chemical shift δ = 2.50 ppm for DMSO, 7.26 ppm for $CDCl_3$, and 4.79 ppm for D_2O to which all chemical shifts refer. The percentage of thiol groups per repetition unit of HA-SH was determined by the ratio of the integrals of the thiol-carrying modification and an internal reference, the acetyl signal together with the anomeric protons of the saccharide backbone. The quantitative PEG-modification was verified by the absence of a change in the spectra after the addition of trifluoroacetic anhydride to the NMR sample solution.

GPC analysis: A GPC system entirely made from Malvern (Herrenberg, Germany) with a triple detection containing a refractive index detector (VE 3580), a viscometer (270 dual detector) and

a multi angle light scattering detector (SEC-MALS 20) was used for the GPC analysis. Depending on the molecular weight of the sample, different column sets (Malvern, Herrenberg, Germany) were used. For HA-SH samples, two A6000M mixed-bed columns and for PEG samples, a set of A2000/A3000 columns were chosen. The eluent was made from deionized water containing 8.5 g L^{-1} $NaNO_3$ and 0.2 g L^{-1} NaN_3 and the columns were calibrated with PEG standards (Malvern, Herrenberg, Germany) with a range of 150 Da to 660 kDa using a MALS calibration. All HA-SH samples were dissolved in deionized water with 0.5 g L^{-1} TCEP over 6 h at rt and PEG samples were dissolved in deionized water over 6 h at rt.

Extrudability test: For the extrudability experiments, HA-SH/PEG-diacryl solutions were prepared in syringes with a 1:1 ratio of the functional groups in different concentrations in the range of 0.1 - 2.0 %. After 1 h incubation at 37 °C, the syringes were placed in a custom-made setup inside a Z010 universal testing machine from Zwick Roell (Ulm, Germany) with a 2.5 kN load cell. By applying a constant crosshead displacement rate of 10 mm min^{-1}, the solutions/hydrogels were extruded through a 250 µm steel needle and the required force and the obtained hydrogel strands were monitored.

Rheological analysis: Rheological properties of different hydrogel formulations were characterized using an Anton Paar MCR 702 rheometer (Anton Paar, Austria) with a 25 mm parallel plate geometry at a 0.5 mm gap. A solvent trap was used to minimize evaporation throughout the experiments. All experiments were performed by loading the freshly prepared hydrogel precursors on the measurement plate pre-heated at 37 °C. Four categories of experiments were performed to characterize different aspects of the hydrogels: Time sweep measurements with 0.5 % strain at 10 rad s^{-1} angular frequency were conducted to identify the processing window of the inks. Shear rate sweeps from 1.0 to 100 s^{-1} were performed to evaluate the shear thinning properties. Frequency sweeps from 100 - 1.0 rad s^{-1} were performed before and after exposure to UV light. Photo-crosslinking measurements were performed by exposure to UV light (bluepoint 4, Dr. Höhnle AG, Gräfelfing, Germany) for 60 s after slightly different incubation times at 37 °C, depending on the rate of Michael reaction progression in different inks (Table II.S2, Supporting Information).

MSC isolation and expansion: For isolation of mesenchymal stromal cells (MSCs), bone marrows were recovered from the explanted femoral heads of patients undergoing elective hip arthroplasty as previously described.[147] The procedure was performed after informed consent of all patients and with the approval of the local ethics committee of the University of Würzburg (186/18). Cells were expanded at 37 °C and 5 % CO_2 in DMEM/F12 supplemented with 10 % FCS, 1 % PS and 3 ng mL^{-1} bFGF.

Hydrogel preparation, 3D printing, and MSC culture: Thiol-modified hyaluronic acid (HA-SH) was dissolved in HEPES buffer (154 mM, pH = 7.6) to sustain a suitable pH of 7.4 for Michael

addition. All other hydrogel components (PEG-diacryl, PEG-diallyl, Irgacure I2959) were dissolved in PBS and mixed in a range of different concentrations for the establishment of the necessary ratio of thiol to acryl/allyl groups for pre-/final crosslinking. Printability was assessed by manual extrusion using a displacement pipette (Gilson, Middleton, WI, USA) or a Cellink+ 3D bioprinter (Cellink, Boston, MA, USA). For 3D printing, G-codes for grids and filament fusion tests were generated with the HeartWare software of the same manufacturer. Strand thickness measurements were performed with the NIH ImageJ Fiji software (version 1.52a). The CAD file of the femoral condyles of a human right leg was obtained from MakerBot Thingiverse (object 5820, created by BME_Sundevil) and sliced with the HeartWare software. Hydrogel solutions were mixed with or without MSCs (passage 3 – 4, 20 x 10^6 cells mL^{-1}) and transferred to 3 cc printing cartridges (Nordson EFD, Westlake, OH, USA), pre-crosslinked for 1 h at 37 °C, and extruded through a 330 µm steel nozzle at a printing pressure of 40 - 200 kPa, depending on the ink formulation. Constructs were finally crosslinked for 10 min at 365 nm (1 mW cm^{-2}, UV hand lamp with filter, A. Hartenstein, Würzburg, Germany). MSC-laden constructs prepared with 51 kDa, 230 kDa, and 410 kDa HA-SH bioinks were incubated for 21 days at 37 °C and 5 % CO_2 in differentiation medium (DMEM high glucose medium supplemented with 1 % ITS+ premix, 1 % PS, 0.1 x 10^{-6} M dexamethasone, 50 µg mL^{-1} L-ascorbic acid 2-phosphate sesquimagnesium salt hydrate, 40 µg mL^{-1} L-proline and 10 ng mL^{-1} TGF-β1).

Swelling analysis: 51 kDa, 230 kDa and 410 kDa HA-SH gels were prepared in a defined cylindrical geometry (diameter: 5 mm, volume: 40 µL) and weighed directly after preparation (d0). Samples were transferred to PBS and incubated for 21 days at 37 °C. Weight measurements were performed after excessive PBS was removed carefully from the hydrogel surface using a filter paper. At each time point (1, 3, 5, 7, 9, 12, 14 and 21 days), wet weight deviation compared to the weight directly after preparation was calculated.

Analysis of FITC-labeled dextran diffusion: 51k Da, 230 kDa and 410 kDa HA-SH gels were prepared in a defined cylindrical geometry (diameter: 5 mm, volume: 40 µL) to ensure comparable diffusion parameters. All constructs were equilibrated in PBS overnight before replacing the buffer with FITC-dextran solutions (40 kDa, 500 kDa or 2000 kDa at 1 mg mL^{-1}). Diffusion was performed for 24 h at 37 °C in the dark. Afterwards, constructs were briefly washed in PBS and homogenized with a TissueLyser (Quiagen, Hilden, Germany) for 5 min at 25 Hz. Fluorescence intensity was measured with a spectrofluorometer (Infinite M200 Pro, Tecan, Crailsheim, Germany; Ex/Em 495 nm/535 nm). Quantification was performed using a 40 kDa, 500 kDa, or 2000 kDa FITC-dextran standard curve.

Pore size analysis via cryo-SEM: 51 kDa, 230 kDa and 410 kDa HA-SH gels were prepared as described above and directly used for cryo-scanning electron microscopy (cryo-SEM) analysis. Samples were fixed in a sandwich of 3 mm aluminum plates in a 2 mm notch and slushed nitrogen

at -210 °C was used for rapid freezing. A EM VCT100 cryo-shuttle (Leica Microsystems) at -140 °C was utilized for all following transfer steps. One aluminum plate was knocked off to generate a freshly fractured hydrogel surface and samples were freeze edged in a ACE400 sputter coater machine (Leica Microsystems) under high vacuum (< 1 x 10^3 mbar) for 15 min at -85 °C. Afterwards, samples were sputtered with 2.5 nm platinum before placing them into the SEM chamber (Crossbeam 340, Zeiss). Imaging was performed at -140 °C at an acceleration voltage of 8 kV.

Cell viability analysis: 3D constructs with encapsulated MSCs were washed with PBS before adding the live/dead staining solution (4 x 10^{-6} M ethidium homodimer III (EthD-III) and 2 x 10^{-6} M calcein acetoxymethylester (calcein-AM) in PBS; PromoKine, Heidelberg, Germany). After incubation for 45 min at rt in the dark, constructs were washed again with PBS and images were taken at a fluorescence microscope (Olympus BX51/DP71, Olympus, Hamburg, Germany). For quantification, three constructs per condition were imaged and living and dead cells were counted manually on at least 12 images per condition with the cell counter plugin of the NIH ImageJ Fiji software (version 1.52a).

Histological and immunohistochemical analysis: Histology and immunohistochemistry of MSC laden 3D constructs were performed as previously described.[188] In brief, for all histological methods, sections with 8 µm thickness were mounted on SuperFrost plus glass slides (R. Langenbrick, Emmendingen, Germany). Collagen was stained with picrosirius red (0.1 % direct red 80 in a saturated solution of picric acid), cells were counterstained with Weigert's haematoxylin. For staining of glycosaminoglycans (GAG), 0.1 % safranin O was utilized, and cells were counterstained with 0.02 % fast green. For immunohistochemistry the following primary antibodies were used: anti-aggrecan 969D4D11 (1:200; Thermo Scientific, Waltham, MA, USA); anti-collagen type I ab34710 (1:200; Abcam, Cambridge, UK); anti-collagen type II clone II-4C11 (1:1000; Abnova, Taipei, Taiwan); and as a secondary antibody: goat-anti-mouse Alexa488 111-545-003 (1:400; Jackson ImmunoResearch, Cambridge, UK); all diluted in 1 % BSA/PBS. Sections were mounted with DAPI mounting medium and analyzed with a fluorescence microscope. For quantification of the stained gel areas, cross-sections from all areas of the construct were used. The values represent the average staining area of 10 randomly taken images of each condition. All microscopic images were transformed to binary images and analyzed with the particle analysis function of the NIH ImageJ Fiji software (version 1.52p) using a 10 % threshold of the maximal white value.[199]

Biochemical analysis: MSC-laden 3D printed constructs, harvested on day 1 or 21, were homogenized for 5 min at 25 Hz before digesting the suspension with 3 U mL^{-1} papain for 20 h at 60 °C. Quantification of DNA,[200] GAG[203] and collagen content[201, 202] was performed after established protocols, with slight alterations as previously described.[188] Additionally, for

quantification of total GAG and collagen production, culture supernatants of three replicates per condition were harvested every two days during culture and analyzed with the same protocols.

RNA isolation and gene expression analysis: RNA was isolated from 3D constructs with encapsulated MSCs on day 1, 7, and 21 using TRIzol reagent (Life Technologies, Carlsbad, CA, USA) according to the manufacturer's instructions. Yield and purity of resulting RNA samples were assessed with a NanoDrop (Thermo Scientific, Waltham, MA, USA) and cDNA was transcribed with the High-Capacity cDNA Reverse Transcription Kit (Applied Biosystems, Foster City, CA, USA). For qRT-PCR, a CFX96 Real-Time System (Bio-Rad, Hercules, CA, USA) and MESA GREEN qPCR Mastermix Plus for SYBR® Assay (Eurogentec, Liège, Belgium) was used. Sequences of self-designed primer pairs for SOX9, ACAN, COL1A1, COL2A1, and GAPDH expression analysis are listed in the Supporting Information (Table II.S3). Relative expression was calculated using the $2^{-\Delta\Delta CT}$ method[204] and all samples were normalized to the housekeeping gene GAPDH and to gene expression of MSC 2D samples on d0.

Mechanical analysis: Constructs were prepared in a defined cylindrical geometry (diameter: 5 mm, volume: 40 µL) and six constructs per condition were analyzed at day 1 and 21 of chondrogenic differentiation with a dynamical mechanical testing machine (ElectroForce 5500 test instrument, Bose, Eden Prairie, MN, USA) with a load cell of 250 g. Compression of the constructs was performed with a constant crosshead displacement rate of 0.001 mm s^{-1} to a final depth of 0.5 mm and the Young's modulus was determined as the slope of the true stress-strain curve in the linear elastic range.

Statistical analysis: Data is represented as mean ± standard deviation of at least three replicates and statistical analysis was performed with GraphPad Prism 5 software. One-way ANOVA with a Bonferroni posthoc test was performed when comparing multiple groups at one time point. For comparing multiple groups at different time points, two-way ANOVA with Bonferroni posthoc test was utilized. Significant differences were marked as follows: * ($p < 0.05$), ** ($p < 0.01$) and *** ($p < 0.001$).

4.4. Results and discussion

This study presents a new category of hyaluronic acid-based bioinks for 3D printing utilizing a novel dual-stage crosslinking mechanism (Figure II.1), based on thiol-modified hyaluronic acid (HA-SH) and the crosslinkers PEG-diacryl and PEG-diallyl. The cells are suspended in the ink precursor solution containing HA-SH and both crosslinkers. The first crosslinking step (pre-crosslinking) is a spontaneous Michael addition at pH = 7.4, where HA-SH is partially crosslinked with PEG-diacryl at 37 °C to a shear thinning and 3D printable ink (Figure II.1). The viscoelastic properties of the ink and the shape fidelity of the printed constructs can be adjusted by altering the molecular weights of HA-SH and PEG-diacryl or by shifting the HA-SH/PEG-diacryl ratio. Depending on the ink composition, the 3D printing process can be started after one hour of pre-crosslinking and conducted within a processing window of around 2 h. After printing, the second crosslinking step is induced in presence of the photoinitiator Irgacure I2959 by using UV light at 365 nm. This initiates the thiol-ene click reaction of remaining HA-SH thiol groups and PEG-diallyl, resulting in stably crosslinked constructs (Figure II.1).

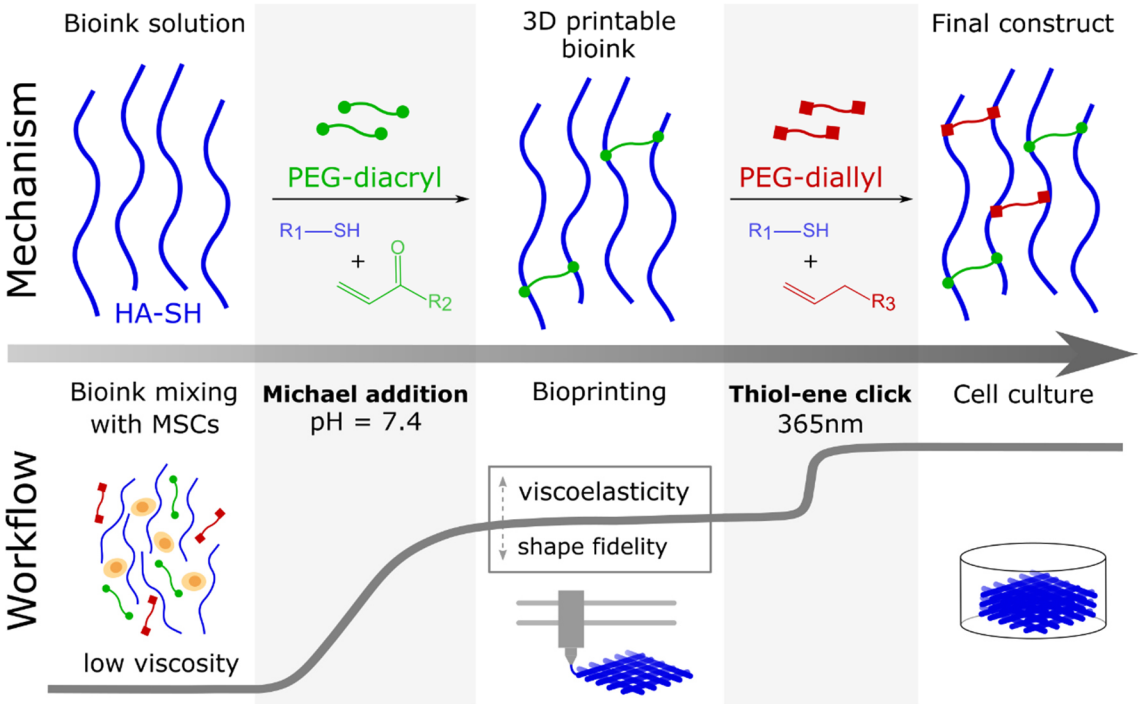

Figure II.1: Dual-stage crosslinking of the hyaluronic acid-based bioinks. *Mechanism:* HA-SH (blue) pre-crosslinks with PEG-diacryl (green) in a spontaneous Michael addition at neutral pH to a 3D printable ink. Final crosslinking of the printed constructs is performed by UV-induced thiol-ene click chemistry between the remaining HA-SH thiol groups and PEG-diallyl (red) in the presence of the photoinitiator Irgacure (I2959). *Workflow:* All bioink components are mixed with MSCs in a low viscosity suspension. After appropriate pre-crosslinking, the viscoelastic bioink can be printed with improved shape fidelity. Final crosslinking is achieved via UV initiated thiol-ene click reaction leading to stable constructs, which subsequently can be subjected to cell culture.

4.4.1. Synthesis and characterization

4.4.1.1. Synthesis of 3,3'-dithiobis(propanoic dihydrazide) (DTPH)

DTPH, required for subsequent modification of hyaluronic acid, could be synthesized in 100 gram scales according to literature, with only minor changes in the purification steps as described before.[236] NMR analysis was performed in d_6-DMSO and confirmed successful synthesis and purification (Figure II.S1b, 4.7. Supporting information).

4.4.1.2. Synthesis of thiolated hyaluronic acid (HA-SH)

Educts used in the literature for HA-SH synthesis are almost exclusively of low molecular weight nature (< 100 kDa), with a high solubility and low viscosity in concentrations below 1.5 %, and have mostly resulted in substituted HA-SHs of < 50 kDa.[147, 239] To facilitate the generation of hydrogels with comparably low polymer content, HA-SH of larger molecular weights were synthesized (Figure II.S1a and c, 4.7. Supporting information). Therefore, transfer of the published reaction conditions[147, 239] to starting materials with up to 1.4 MDa and the associated very high viscosity of 1 % solutions had to be adapted to yield appropriate thiol modification and high product quality. Educts and products used in this study are listed in Table II.S1 (4.7. Supporting information). Product quality was substantially improved by addition of *N*-hydroxy succinimide (NHS) which prevents formation of an *N*-acylureate. This byproduct would inhibit accurate determination of the degree of substitution (DS) via NMR (Figure II.S1d and e, 4.7. Supporting information), and has unknown effects on hydrogel formation and cell biology.[153] Constant reaction parameters (pH, temperature, mixing) and thus reproducibility were achieved by using a Sørensen buffer system and a thermostated incubator.

4.4.1.3. Synthesis of polyethylene glycol-diacrylate (PEG-diacryl)

The acrylation of linear PEG and its purification was carried out as described in literature[237] (Figure II.S2a, 4.7. Supporting information). Complete acrylation was possible, but contrary to the described purification, precipitation in diethyl ether was ineffective. Instead, recrystallization in ethanol led to the desired pure product and was suited to remove the organic salts formed during synthesis. Successful acrylation was demonstrated by the absence of TFA ester signals in ^{1}H-NMR (Figure II.S2c, 4.7. Supporting information). Molecular weights of the obtained products reflected well the used educts and showed only slight polymerization during recrystallization (Figure II.S2b, 4.7. Supporting information).

4.4.1.4. Synthesis of polyethylene glycol-diamine (PEG-NH_2)

The conversion of PEG-OH to PEG-NH_2 was straightforward with respect to the literature[238] (see Figure II.S3a-c, 4.7. Supporting information). Higher yields were achieved by omitting the purification of the mesylate intermediate and by processing under constant cooling.

4.4.1.5. Synthesis of polyethylene glycol-diallyl carbamate (PEG-diallyl)

For the synthesis of PEG-diallyl derivative, the reaction conditions for the alloc-protection of amino groups in peptide synthesis were applied to the previously prepared linear PEG-diamine (Figure II.S3a, 4.7. Supporting information).[240] The obtained products exhibited a narrow molecular weight distribution and high purity due to volatile byproducts (Figure II.S3b-c, 4.7. Supporting information). Quantitative conversion was demonstrated by ^{1}H-NMR using the same analysis as for PEG-diacryl (Figure II.S3d, 4.7. Supporting information).

4.4.2. Ink development

4.4.2.1. Influence of HA-SH and PEG-diacryl properties on 3D printability

As a first step of bioink development, the pre-crosslinking mechanism via Michael addition (Figure II.1) was established for HA-SH batches of different molecular weights with 6 kDa PEG-diacryl. The aim was to get stably printable inks after a cell-compatible crosslinking time. Therefore, HA-SH and PEG-diacryl were mixed in varying concentrations, and the solutions were examined for their viscosity over time in handling experiments by pipetting or extrusion at a bioprinter, revealing an optimal printability when mixing HA-SH and PEG-diacryl in similar weight percentages. These results were further supported with extrudability experiments at the Z010 universal testing machine. Here, several hydrogel formulations were extruded after 1 h of pre-crosslinking at a constant feed rate and the required force as well as the obtained strands were recorded. In the following, all polymer concentrations are labeled as % and indicate weight percent. For extrudability experiments, the HA-SH (230 kDa) content was kept constant at 0.5 % and the PEG-diacryl (6 kDa) concentration was varied between 0.1 - 2.0 % (Figure II.2).

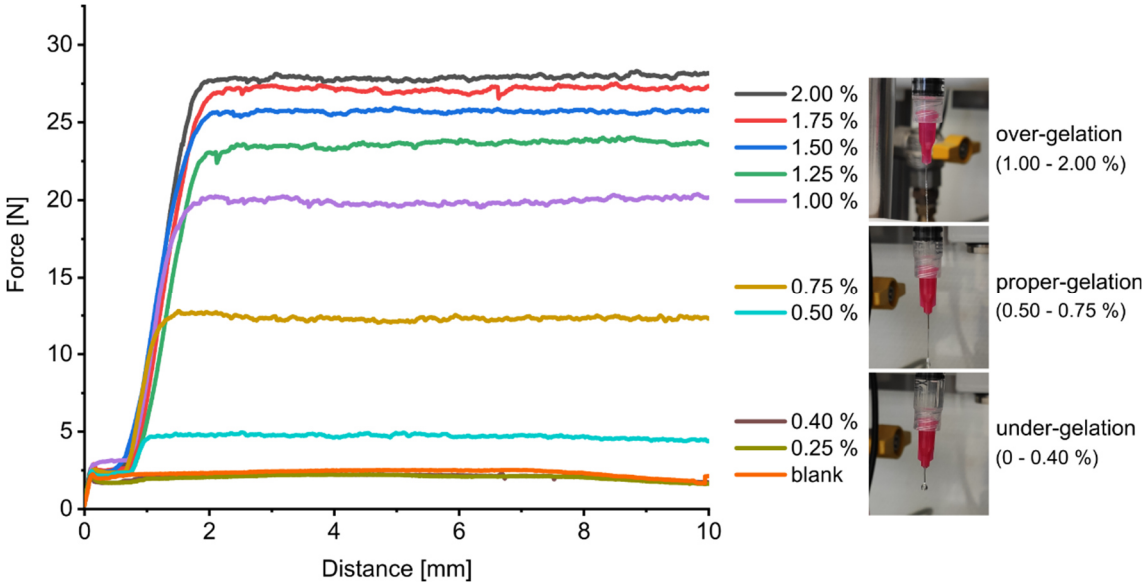

Figure II.2: Force-distance-diagram for an extrudability test of 230 kDa HA-SH (0.5 %) hydrogels formulations with different 6 kDa PEG-diacryl contents after 1 hour of incubation. Pictures indicate different strand examples for each gelation state.

Ink formulations with 0.4 % PEG-diacryl and below showed no increase in viscosity, but 0.5 % or more resulted in hydrogels with increased viscosity. Thereby, the correlation between acrylate content and hydrogel viscosity was not of linear nature. Instead, the stiffness increased rapidly between 0.5 and 1.0 % and then converged towards an upper limit at 2.0 %, which corresponds to the quantitative saturation of the present thiols. Within the range of hydrogel forming formulations, only hydrogels with 0.5 and 0.75 % PEG-diacryl were found to be proper-gelled and thus suitable for printing, whereas the hydrogel formulations with higher acrylate content were already over-gelled and resulted in strands of visibly sheared microgel particles. Since a lower polymer content was expected to be more beneficial for the cell performance, the formulation with a 1:1 ratio (0.5 % HA-SH + 0.5 % PEG-diacryl) was used in further experiments. This corresponded to a HA-SH thiol saturation of around 30 %. In the following, an extended series of formulations was investigated with a constant 1:1 ratio but different polymer contents (0.1 % - 3.25 % each), based on six differently sized HA-SH batches (M_W = 51 kDa – 410 kDa) and 6 kDa PEG-diacryl, in which the components were mixed, and the viscosity was assessed over time. Figure II.3a represents a summarized overview of the investigated formulations with different HA-SH/PEG-diacryl concentrations and the suitability for 3D printing. Each line of the graph represents 16 different pre-crosslinking approaches, which were analyzed separately over 5 h, and all formulations resulting in sufficient strand formation already after a cell-compatible pre-crosslinking time of 1 h were defined as printable. An exemplary more detailed analysis table is presented in the Supporting information, showing the relevant HA-SH/PEG-diacryl concentrations tested with the 410 kDa HA-SH batch (Figure II.S4, 4.7. Supporting information). The dependence of the processing window on the polymer content was also similarly found for all other tested HA-SH batches. Summarizing Figure II.3a, a clear trend was observed: With increasing molecular weight of the HA-SH component (top to bottom), a decreasing total polymer content was necessary for optimal 3D printability of the inks. HA-SH batches with the lowest molecular weight (around 50 kDa) required a total polymer content of at least 4.5 % (2.25 % HA-SH + 2.25 % PEG-diacryl), whereas those with molecular weights over 200 kDa required a significantly lower total polymer content to be printable after 1 h of pre-crosslinking. This was in line with observations in the literature in which the effect of the M_W of unmodified hyaluronic acid on the viscosity in aqueous solutions has been investigated.[241] Interestingly, no further reduction of polymer content was possible when increasing the M_w from 230 kDa to the highest achieved M_w of 410 kDa.

As a next step, the impact of PEG-diacryl molecular weight on ink printability was assessed. Therefore, three HA-SH batches (51 kDa, 230 kDa, 410 kDa) were selected. The HA-SH concentration was fixed while concentrations of 6 kDa, 10 kDa, and 20 kDa PEG-diacryl were varied. Figure II.3b shows exemplarily the results for the 410 kDa HA-SH batch. The PEG content needed for adequate 3D printability increased with the molecular weight of PEG-diacryl.

The same trend was also observed for the 51 kDa and 230 kDa HA-SH batches (Figure II.S5, 4.7. Supporting information). These observations can be explained by the fact that PEG-diacryl with increased molecular weight requires a higher concentration to provide the same amount of acrylate groups. Accordingly, stoichiometric calculations revealed again around 30 % HA-SH thiol saturation for all printable formulations.

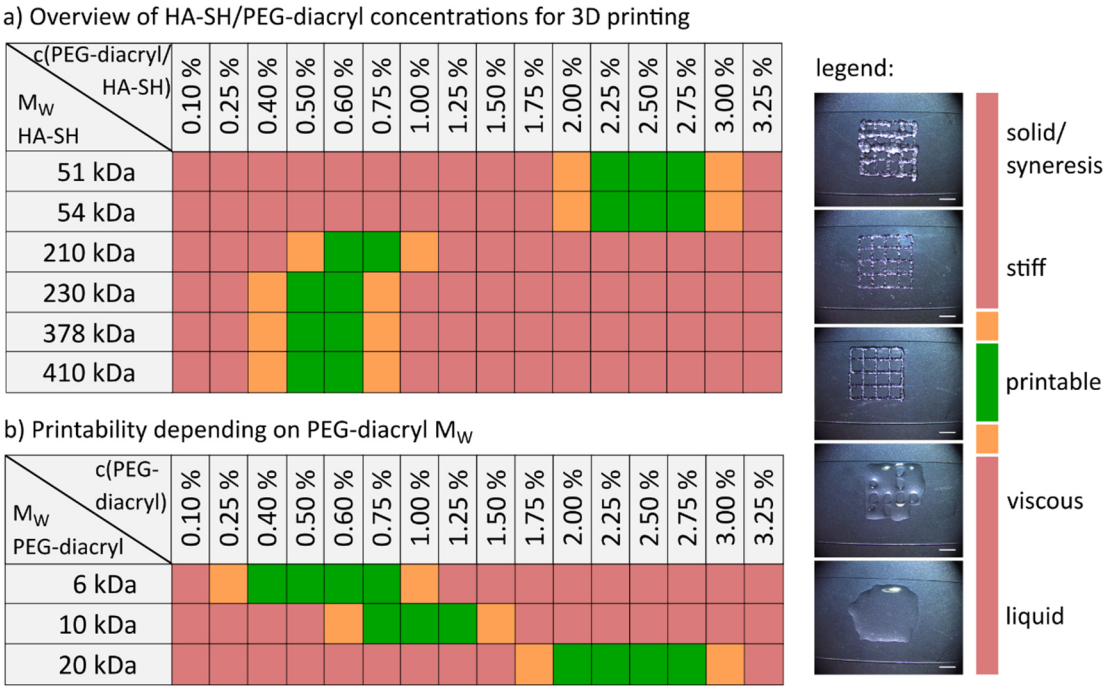

Figure II.3: Processing-windows of different HASH/PEG-diacryl molecular weights and concentrations. All mixtures resulting in sufficient strand formation after a cell-compatible pre-crosslinking time of 1 h are defined as printable. The general printability is visualized by a color code (green = printable, red = not printable (either too liquid, viscous, stiff or too solid) and yellow marks the transition region). The legend depicts exemplary printed grids for each condition. Scale bars represent 5 mm. a) 6 different HA-SH batches (MW = 51 kDa – 410 kDa) were tested with PEG-diacryl (6 kDa) in 1:1 ratios (0.1 % - 3.25 % each) and printability of the resulting polymer solutions was analyzed over 5 h. b) Influence of PEG-diacryl molecular weight on ink printability. 0.5 % HA-SH (410 kDa) was mixed in different ratios with PEG-diacryl (6 kDa, 10 kDa and 20 kDa) and printability of the resulting solutions was analyzed over 5 h.

4.4.2.2. Thiol-ene crosslinking of the printed bioink using PEG-diallyl

The final crosslinking of printable ink formulations (Figure II.1, second viscosity increase) was conducted with 6 kDa PEG-diallyl in the presence of the photoinitiator Irgacure (I2959) at 365 nm. The concentrations of PEG-diallyl were determined by stoichiometric calculations to achieve a complete thiol saturation for the different HA-SH batches. For the following detailed physicochemical and biological characterizations, three inks with different HA-SH batches (51 kDa, 230 kDa and 410 kDa) were produced. Each HA-SH was pre-crosslinked with 6 kDa PEG-diacryl and finally gelated with 6 kDa PEG-diallyl. The exact ink compositions were in accordance with the printability studies shown in Figure II.3 and are listed in Table II.1. In the following, these inks are termed as 51 kDa, 230 kDa, and 410 kDa HA-SH inks. In order to evaluate potential effects of each crosslinking process, MSC cell viability was analyzed after pre-

crosslinking as well as after final UV irradiation. Quantification revealed 95 – 98 % cell survival for both crosslinking steps in all three bioinks without significant differences between the conditions (Figure II.S6, 4.7. Supporting information), demonstrating no detrimental influence of the crosslinking processes.

Table II.1: Compositions of inks used in all further experiments. All values are represented as % (wt/V).

HA-SH batch	c(HA-SH)	c(PEG-diacryl)	c(PEG-diallyl)	c(Irgacure)
51 kDa	2.5 %	2.5 %	5.0 %	0.05 %
230 kDa	0.5 %	0.5 %	1.0 %	0.05 %
410 kDa	0.5 %	0.5 %	1.0 %	0.05 %

4.4.2.3. Rheological characterization of the dual-stage crosslinking

Rheological properties of the inks play a significant role in their applicability to extrusion-based bioprinting. In this context, viscoelastic features of the hydrogels are highly dependent on the molecular weight as well as polymer content of the ink formulations. Moreover, progression of crosslinking reactions and kinetics of gel formation depend on chain mobility and availability of functional groups. A series of rheological experiments was performed to investigate the kinetics of the gelation in different ink formulations and to evaluate the processing window for application of such inks (Figure II.4). Pre-crosslinking via Michael addition at 37 °C for the three different inks, 51 kDa, 230 kDa, and 410 kDa HA-SH led to increased storage and loss moduli after an initial induction period (Figure II.4a). The molecular weight of HA-SH as well as the polymer content played a significant role in the reaction kinetics. Decreasing the molecular weight at the same concentration (410 kDa vs. 230 kDa, Table II.1) resulted in slower crosslinking kinetics. This could be explained by the availability of functional groups per polymer chain, considering that the degree of substitution in both ink formulations was nearly identical (Table II.S1, 4.7. Supporting information). Thus, decreasing the molecular weight of the polymer caused smaller number of available thiols per polymer chain for the Michael addition, which in turn formed less long-range entanglement of chains due to lower probability of network formation. On the other hand, increasing the concentration, and consequently the number of available functional groups, resulted in faster kinetics of network formation in 51 kDa HA-SH, despite having a significantly shorter chain length. In comparison to experimental observations that all inks were printable after only 1 hour of incubation, obtained time sweeps showed slightly different gelation points and thus possible printability. This was explained by obvious differences in hydrogel formation. While rheological studies were performed under almost stationary conditions, in extrudability experiments the hydrogel formulations were frequently mixed during incubation and thus, had a higher probability of network formation. For all tested bioinks, a steady slow increase

in G' was observed after the initial steep rise, which was attributed to the formation of additional disulfide bonds from unsaturated thiols. Disulfide formation is a spontaneous process in systems based on thiol chemistry that is much slower than Michael addition between free thiols and acrylates of PEG-diacryl.[242] Furthermore, the growing noise in G" after 3 hours of incubation could be related to such disulfide formation resulting in hydrogel shrinkage during the measurements. Hydrogel precursor solutions showed only very weak dependency of the viscosity on applied shear, which is a characteristic of diluted polymer solutions (Figure II.4b). The shear-thinning indices of pre-gel solutions were 0.88, 0.96, and 0.86 for formulations based on 51 kDa, 230 kDa, and 410 kDa HA-SH, respectively. The shear dependent viscosity behavior of formulations after the first stage of crosslinking was more evident, as all the formulations showed strong pseudoplastic behavior with flow indices of 0.33, 0.38, and 0.58 for formulations based on 51 kDa, 230 kDa, and 410 kDa HA-SH, respectively. This behavior confirmed the shear rate dependency of the viscosity of the bioinks after the first stage of crosslinking, which would facilitate an appropriate extrusion through a fine nozzle with a sufficient shape fidelity.

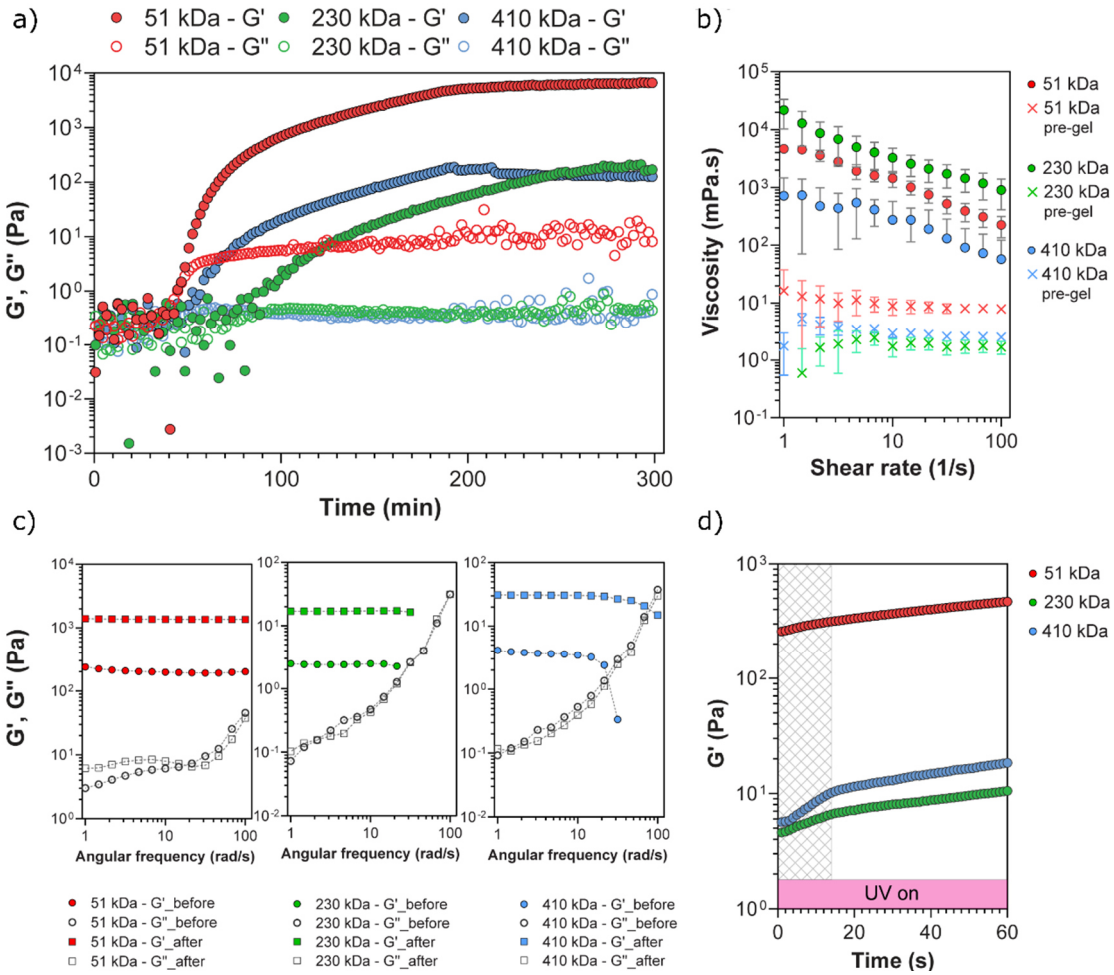

Figure II.4: Rheological characterization of the different HA-SH bioinks. a) Time sweep measurements to identify the kinetics of the Michael addition and identification of the processing window of the bioinks. b) Shear rate dependence of the viscosity of HA-SH formulations before and after pre-crosslinking via Michael addition. c) Frequency sweeps of the different inks before (circle) and after (square) exposure of UV light. d) Close-up of the change in storage modulus during the 60 s UV exposure period. Dashed region indicates the initial rapid rise in elastic properties of the formed networks during photo-crosslinking.

For the second crosslinking stage, involving a thiol-ene click reaction, the network viscoelasticity before, after, and during the photo-crosslinking by UV light was monitored (Figure II.4c and d). The frequency sweeps prior to and after the photo-crosslinking stage showed a distinct increase of the storage modulus, i.e. an enhancement in viscoelastic properties of inks, through development of longer interaction ranges, as well as shifting of the relaxation time of the network to higher frequency values (Figure II.4c). Two distinguishable regions within the period of UV light exposure were identified (Figure II.4d). The increase in storage modulus within the first 15 s of exposure was higher compared to the remaining exposure period, and the difference was greater for inks with longer HA-SH chains. The initially differing growth rates for the different inks converged in the second region, resulting in a steady increase of the storage modulus until the end of UV exposure. This corresponds to the quantitative thiol saturation via thiol-ene reaction and thus to the intended terminal plateau of viscoelasticity in the workflow of ink processing (Figure II.1). The higher increase rate for G' of longer polymer chains in Figure II.4d was attributed to a higher number of available thiol groups per polymer chain, which resulted in more efficient polymer immobilization and consequently, entanglement and formation of long-range interactions.

4.4.3. Printability assessment

In the following, a detailed printability characterization of the platform bioinks was performed. At first, the strand intersection diagonal of grid constructs printed with a viscous, printable, stiff, and solid ink composition – corresponding to the color code in Figure II.3 – was analyzed and quantified (Figure II.5a and b). 3D printing of viscous and solid inks was characterized by a large and inconsistent intersection diagonal, while printable and stiff inks yielded uniform constructs with an intersection diagonal of around 1.3 mm. The printable compositions of 51 kDa, 230 kDa and 410 kDa HA-SH inks (see Table II.1) were furthermore printed in a filament fusion test, with narrowing strand distances of 2, 1.5, 1, 0.75 and 0.5 mm (Figure II.5c). Only the smallest distance of 0.5 mm led to strand fusion. All other distances were well printable using a 330 µm nozzle. The same inks were also printed in grid structures (Figure II.5d) and the resulting strand thickness was quantified (Figure II.5e). No significant differences between the different inks were detected. All printed strands yielded an average thickness between 630 and 730 µm. Finally, a large construct with 21 layers was printed with the 410 kDa HA-SH ink as a proof-of-principle experiment resembling human femoral condyles (Figure II.5f).

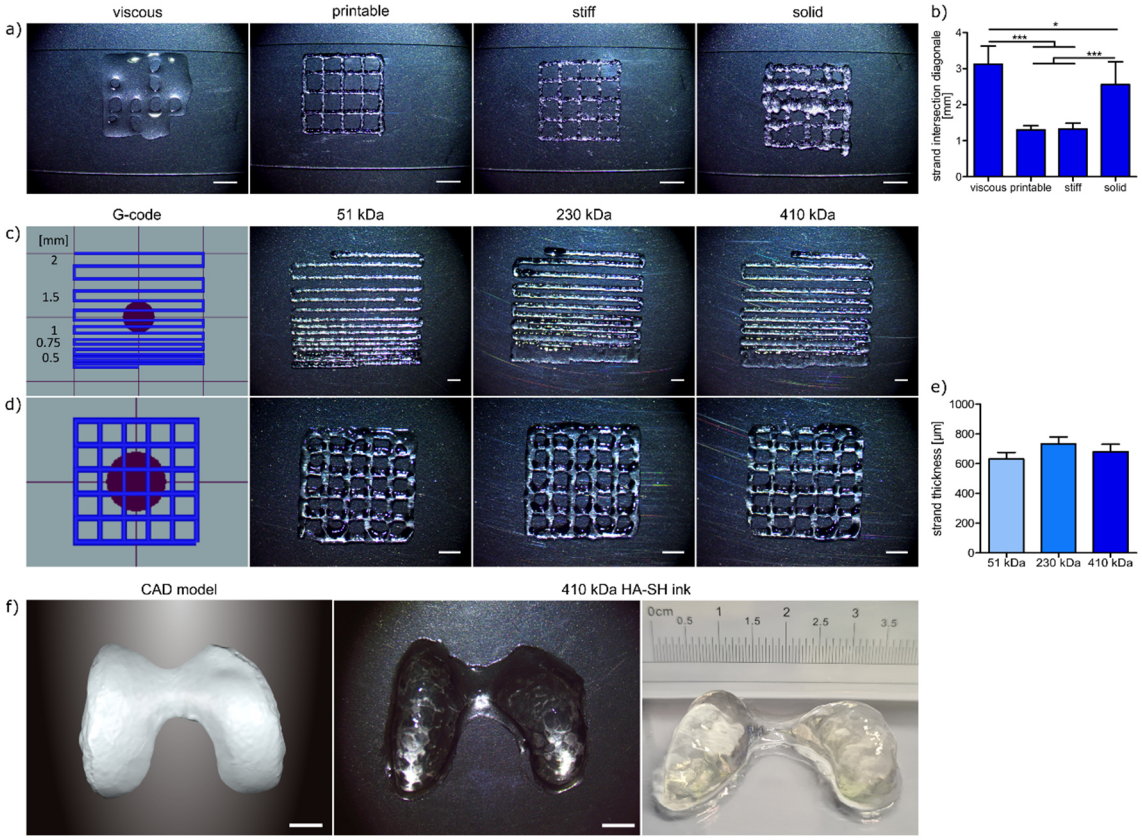

Figure II.5: Shape fidelity of 3D printed HA-SH inks. a) 3D printed grids with different HA-SH ink compositions, leading to viscous, printable, stiff, and solid inks, respectively (images were also used in the legend of Figure 3). Scale bars represent 5 mm. b) Quantification of the strand intersection diagonal of printed grids in (a). c) G-code and filament fusion tests of 51 kDa, 230 kDa and 410 kDa HA-SH inks. Scale bars represent 2 mm. Strand distance of the printed filament is indicated next to the G-code. d) G-code and printed grids of the same inks. Scale bars represent 2 mm. e) Quantification of the strand thickness. f) CAD model of the human right femur condyles (left) and the real construct exemplarily printed with 410 kDa HA-SH in 21 layers (middle: top view, right: side view). Scale bars represent 5 mm.

4.4.4. Impact of ink formulation on construct stability, pore structure and diffusion

Construct stability of 51 kDa, 230 kDa and 410 kDa HA-SH inks was determined in a swelling study. Therefore, constructs were prepared as described above and incubated for 21 days in PBS. Weight measurements were performed, and the wet weight deviation at a specific time point compared to the weight directly after preparation was calculated (Figure II.S7, 4.7. Supporting information). After an initial swelling due to PBS inflow, all constructs decreased in wet weight again and reached an equilibrium weight at day 3 (~145 % for 51 kDa and ~100 % for 230 kDa and 410 kDa). In general, all constructs maintained a constant wet weight between 3 and 21 days, indicating a stable network without degradation. The polymer content and network density can distinctly impact macromolecular diffusion within hydrogels, which in turn may modulate nutrient supply and decisively influence the ECM distribution, newly produced by incorporated cells.[156, 157, 188] To assess the pore structure of 51 kDa, 230 kDa and 410 kDa HA-SH inks, cryo-scanning electron microscopy (cryo-SEM) images were taken directly after gel preparation (Figure II.6a). The high concentrated 51 kDa ink has distinctly smaller pores than the low

concentrated 230 kDa and 410 kDa HA-SH inks. Furthermore, the impact of polymer content on diffusivity in these inks was analyzed with fluorescein isothiocyanate (FITC)-labeled dextrans of different sizes (Figure II.6b). Hydrogel cylinders were incubated in three different FITC-labeled dextran solutions (40 kDa, on the order of growth factors; 500 kDa and 2000 kDa, on the order of ECM molecules and aggregates), and diffusion into the constructs was analyzed after 24 h. Quantification in the constructs revealed unimpaired diffusion of 40 kDa and 500 kDa FITC-labeled dextrans into the constructs with low polymer content (230 kDa and 410 kDa HA-SH), while diffusion into the constructs with high polymer content (51 kDa HA-SH) was slightly reduced for the 40 kDa and strongly impaired for the 500 kDa FITC-labeled dextrans. The 2000 kDa dextran diffusion was reduced in all ink compositions, but again a significantly higher diffusion into the 230 kDa and 410 kDa HA-SH constructs was detected. These results were well in agreement with the cryo-SEM images indicating a looser network with increased diffusivity in constructs with low polymer content (230 kDa and 410 kDa).

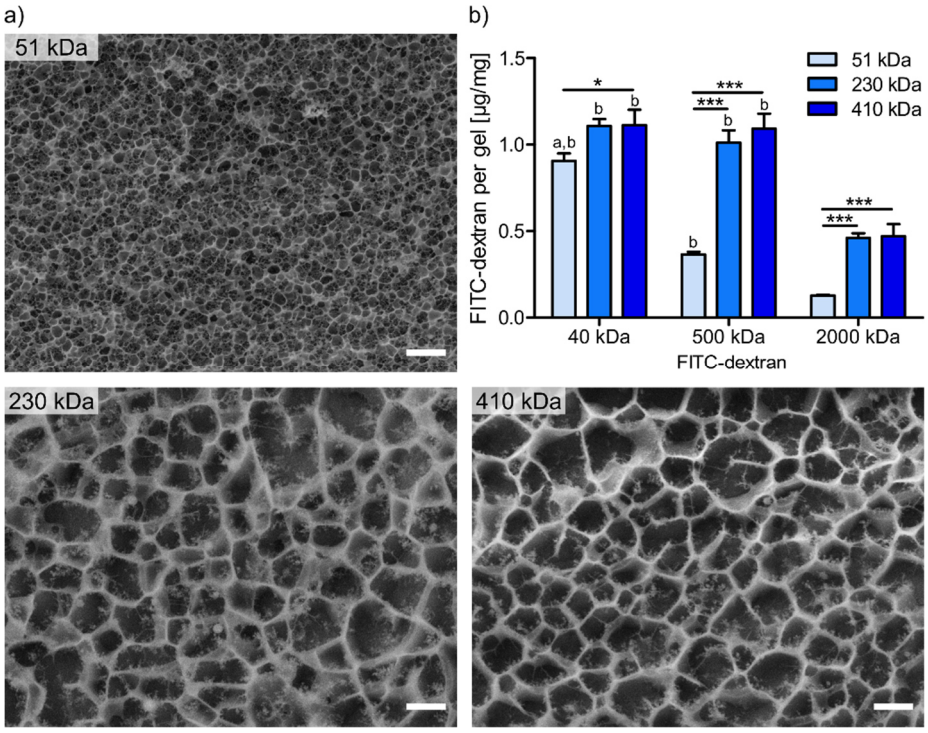

a) Pore structure visualization selected inks by cryo-SEM imaging. Scale bars represent 2 µm. b) Analysis of diffusion of FITC-labeled dextrans (40 kDa, 500 kDa, and 2000 kDa) into the HA-SH constructs. Data are represented as mean ± standard deviation (n = 3). Significant differences are marked as follows: * ($p < 0.05$), ** ($p < 0.01$), and *** ($p < 0.001$). (a) Significantly different to the corresponding group incubated in 500 kDa FITC-dextran solution, (b) significantly different to the corresponding group incubated in 2000 kDa FITC-dextran solution (at least $p < 0.05$).

4.4.5. Differential chondrogenic differentiation of MSCs in platform bioinks

4.4.5.1. Histological and immunohistochemical analysis

The three selected ink compositions were examined regarding chondrogenic differentiation of MSC. Constructs made from 51 kDa, 230 kDa, or 410 kDa HA-SH bioinks showed good cell

survival on day 1 as well as after 21 days of chondrogenic differentiation, with no distinct differences between the conditions (Figure II.S8, 4.7. Supporting information). The production of cartilaginous extracellular matrix (ECM) was supported by all constructs, which was visualized by histology and immunohistochemistry after 21 days (Figure II.7a-d; compare images at day 1, Figure II.S9, 4.7. Supporting information,). Safranin O staining of glycosaminoglycans and

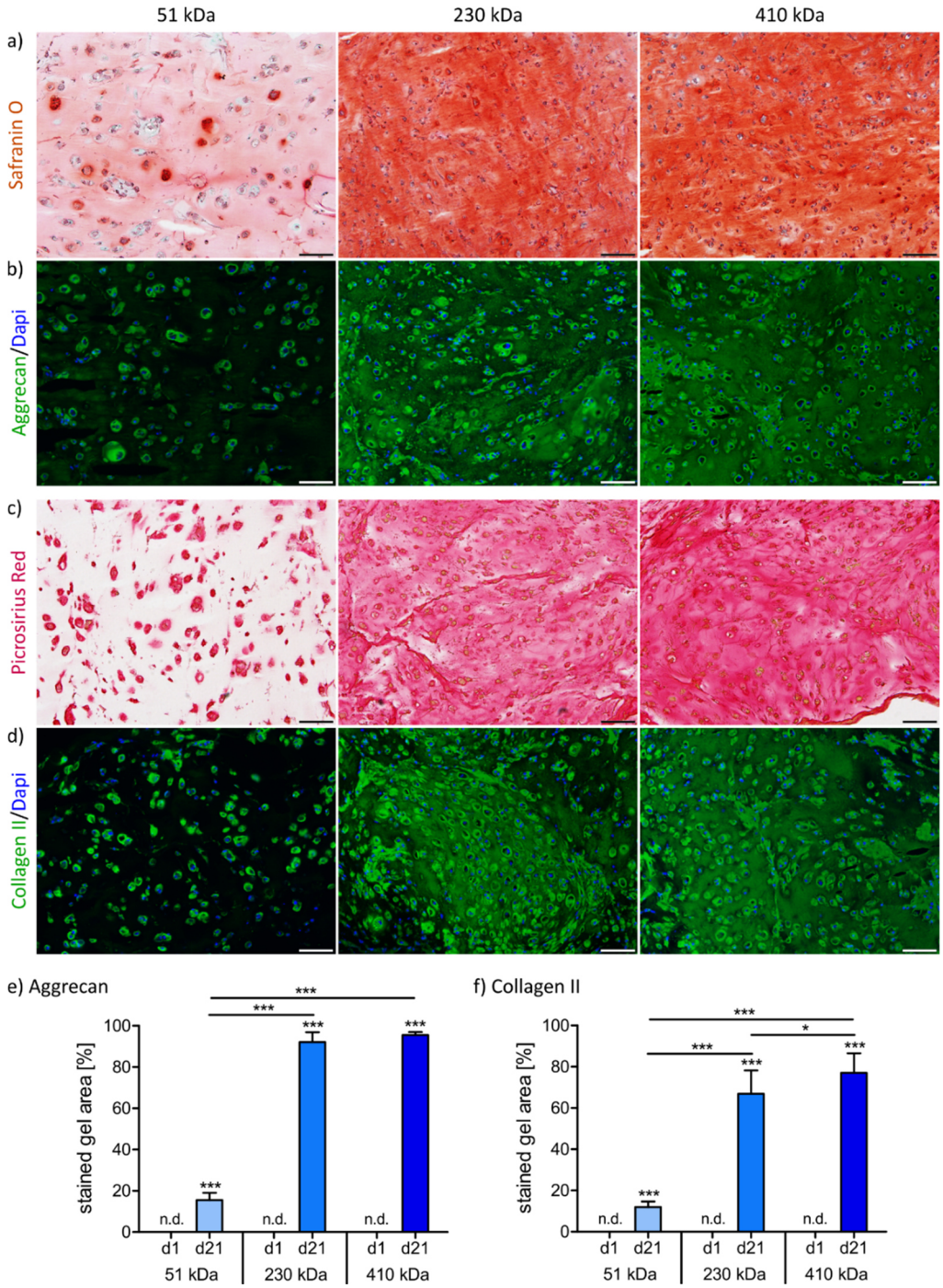

Figure II.7: Histological and immunohistochemical (IHC) staining of ECM components produced by MSCs during 21 days of chondrogenic culture in 3D printed 51 kDa, 230 kDa, and 410 kDa HA-SH constructs. a) Safranin O staining of total glycosaminoglycans and b) IHC staining of aggrecan. c) Picrosirius red staining of total collagens and IHC staining of d) collagen type II. Nuclei were counterstained with DAPI (blue). Scale bars represent 100 µm. Histomorphometric analysis of e) aggrecan and f) collagen type II distribution at day 1 and 21. Data are represented as mean ± standard deviation (n = 10). Significant differences are marked as follows: * ($p < 0.05$), ** ($p < 0.01$) and *** ($p < 0.001$).

picrosirius red staining of collagens revealed mainly intra- and pericellular ECM deposition in the 51 kDa HA-SH gels, while the 230 kDa and 410 kDa HA-SH constructs presented a homogeneous matrix distribution. Immunohistochemistry of the specific ECM components aggrecan and collagen type II showed similar results, and immunohistomorphometric quantification of aggrecan and collagen type II staining verified the visual observations (Figure II.7e and f). Only 15 % of the total area was stained for aggrecan in 51 kDa HA-SH constructs, but homogeneous distribution was observed in 230 kDa and 410 kDa HA-SH gels (92 % and 95 %). A similar trend was detected for collagen type II, with 12 % distribution in 51 kDa, 67 % in 230 kDa, and 77 % in 410 kDa HA-SH gels. The fibrocartilage marker collagen type I was also produced, albeit to a low extent (Figure II.S10, 4.7. Supporting information). In general, the strongly improved distribution of large ECM components in bioinks with low polymer content (230 kDa and 410 kDa HA-SH) was well in accordance with the increased diffusion and the analyzed pore structure of these gels (Figure II.6), as compared to constructs with high polymer content (51 kDa HA-SH). The small differences between aggrecan and collagen type II distribution can be explained by different sizes of the ECM components (length of collagen: 4-12 µm versus aggrecan: 0.5-4 µm) and the positive charge of collagens,[212] which might impact the free diffusion in the negatively charged HA-SH gels.

4.4.5.2. Biochemical quantification and gene expression analysis of ECM components

The main cartilage ECM components were quantified in printed hydrogels in biochemical assays. Substantial amounts of glycosaminoglycans (GAG) and collagens (COL) were detected in all constructs after 21 days of chondrogenic culture, but significantly more in the 230 kDa and 410 kDa gels, as compared with the 51 kDa HA-SH gels (Figure II.8a and c). When normalized to DNA content, also distinctly higher GAG and COL amounts were detected for the 230 kDa and 410 kDa bioinks (Figure II.8b and d). Thus, quantification of ECM components well reflected the histological observations.

Furthermore, gene expression analysis of MSCs in 3D printed 51 kDa, 230 kDa, and 410 kDa HA-SH gels was performed on days 1, 7 and 21 of chondrogenic culture. The expression of the transcription factor SOX9, the genes of the main ECM components aggrecan (ACAN) and collagen type II (COL2A1) as well as the fibrocartilage marker collagen type I (COL1A1) were assessed by quantitative real-time PCR (qRT-PCR) and confirmed chondrogenic differentiation under all conditions (Figure II.8e-h). In general, increased expression over culture time was detected for all genes and in all constructs, showing the proceeding MSC differentiation. Comparison of the constructs with low polymer content (230 kDa vs. 410 kDa HA-SH gels) revealed no significant differences for all analyzed genes. SOX9 and ACAN expression on day 7 and 21, as well as COL1A1 expression on day 7, was higher in the 51 kDa HA-SH gels compared to the 230 kDa and 410 kDa constructs. This may be attributed to the HA content in the gels, as

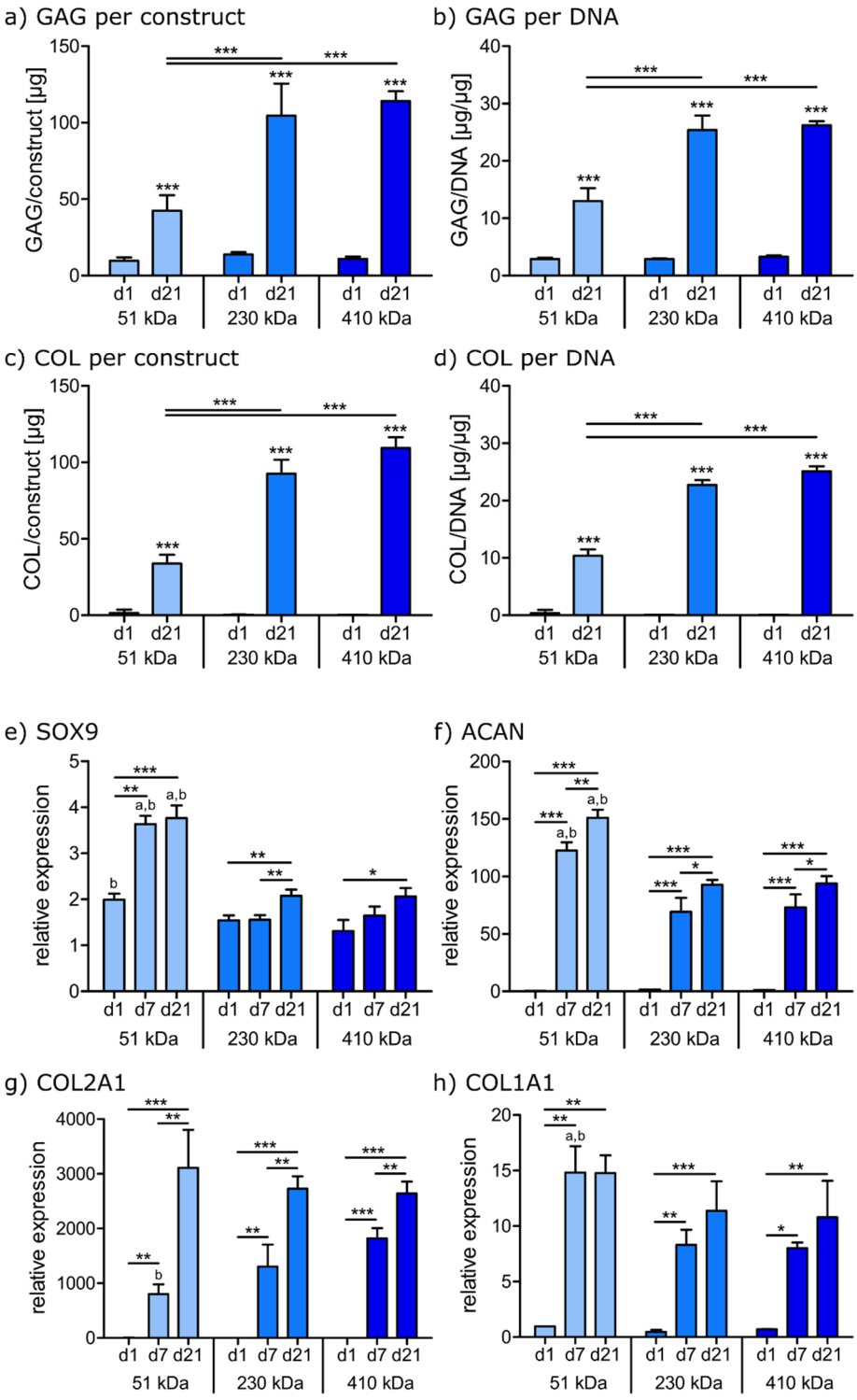

Figure II.8: Quantification of glycosaminoglycan (GAG) and collagen (COL) production of MSCs cultured in 3D printed 51 kDa, 230 kDa, and 410 kDa HA-SH constructs at day 1 and after 21 days. GAG content was quantified a) in the constructs and b) per DNA. Likewise, COL production was quantified c) in the constructs and d) per DNA. Chondrogenic gene expression of MSCs in the same constructs determined by qRT-PCR. Samples at day 1, 7 and 21 were analyzed for e) SOX9, f) ACAN, g) COL2A1 and h) COL1A1 gene expression and normalized to the housekeeping gene GAPDH and to gene expression of 2D MSCs at day 0. (a) indicates significant differences to 230 kDa HA-SH gels at the same day, and (b) indicates significant differences to 410 kDa HA-SH gels at the same day (at least $p < 0.05$). Data for both studies are represented as mean ± standard deviation ($n = 3$). Significant differences are marked as follows: * ($p < 0.05$), ** ($p < 0.01$) and *** ($p < 0.001$).

51 kDa HA-SH constructs contained 2.5 % hyaluronic acid, while 230 kDa and 410 kDa gels only contained 0.5 %. MSC can bind to HA, e.g. via CD44 and CD168 receptors, and a higher HA concentration may increase the probability of receptor binding and thereby may promote chondrogenic gene expression.[157, 214, 215, 243] Initially, the gels with high polymer content (51 kDa HA-SH) were significantly stiffer than the low concentrated ones (Figure II.9), which also may have an impact on MSC differentiation.[156, 216] Nevertheless, increased gene expression in constructs with higher polymer content did not result in increased GAG and collagen production (Figure II.8a-d), which has also been reported previously in other studies for non-printed hydrogels[157] and printed constructs with thermoplastic support structure.[188]

4.4.6. Construct stiffness in the context of ECM distribution

Another important feature of engineered cartilage is the construct stiffness of this load-bearing tissue. For this reason, the Young's moduli of printed 51 kDa, 230 kDa, and 410 kDa HA-SH constructs with embedded MSCs were analyzed on day 1 and 21 of chondrogenic differentiation. Exemplary stress-strain curves of constructs on day 21 are shown in Figure II.9a and the calculated average Young's moduli on day 1 and 21 in Figure II.9b. The initial Young's modulus of the gels with high polymer content (51 kDa HA-SH) was 5.1 kPa and significantly higher than that of both gels with low polymer content (0.7 kPa for 230 kDa and 410 kDa HA-SH). However, after 21 days of chondrogenic culture, the 230 kDa and 410 kDa HA-SH gels exhibited a strong increase of the Young's modulus to 52.6 kPa and 54.6 kPa, respectively, while the 51 kDa HA-SH gels were markedly weaker (4.2 kPa). This corresponded to a 0.8-fold decreased 51 kDa HA-SH construct stiffness, but a significantly increased constructs stiffness of around 73- and 74-fold over 21 days of culture time for the 230 kDa and 410 kDa HA-SH gels (Figure II.9c).

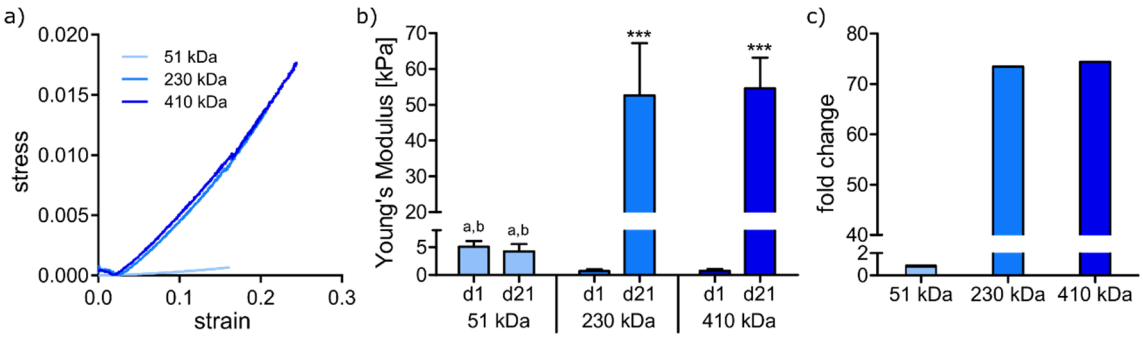

Figure II.9: a) Representative stress-strain curves at day 21 and b) Young's modulus of 3D printed 51 kDa, 230 kDa, and 410 kDa HA-SH constructs with embedded MSCs on day 1 and after 21 days of chondrogenic culture. Data are represented as mean ± standard deviation (n = 7). Significant differences are marked as follows: Stars (***) above bars of groups at day 21 indicate significant differences to the corresponding values of the same group at day 1, ($p < 0.001$). (a) indicates significant differences to 230 kDa HA-SH gels at the same day, and (b) indicates significant differences to 410 kDa HA-SH gels at the same day (at least $p < 0.05$). c) Fold-change in Young's modulus during 21 days of chondrogenic differentiation.

The initially higher stiffness of the 51 kDa HA-SH gels was attributed to the higher polymer content (10 %) (Table II.1) and the resulting high crosslink density, whereas the gels with low polymer content (2 %) with their loosely crosslinked networks appeared softer. Within 21 days of chondrogenic differentiation, MSCs produced considerable amounts of cartilaginous ECM under all conditions, but significantly more in 230 kDa and 410 kDa HA-SH gels (Figures II.7 and II.8a-d). Even more importantly, a homogeneous ECM distribution was observed in 230 kDa and 410 kDa HASH gels (Figure II.7), facilitated by a looser hydrogel network and an enhanced diffusivity (Figure II.6). This allowed for increased interaction of the produced macromolecules which is considered a likely explanation for the strong increase in construct stiffness, as shown previously.[157, 188] In contrast, ECM deposition in 51 kDa HA-SH gels appeared only pericellularly (Figure II.7) due to the high polymer content, which resulted in a tight network and low diffusivity (Figure II.6). This prevented the distribution of ECM molecules and an increase of the Young's modulus over time. The results underscored the correlation between diffusivity, distribution of cartilaginous ECM, and construct stiffness, which has also been demonstrated in a recent study that indicated a homogeneous distribution to be even more important for construct stiffness than the bare amounts of produced ECM components.[188]

4.5. Conclusion

In this study, we established a flexible platform of hyaluronic acid-based bioinks for 3D printing of hMSCs which facilitated a distinct modulation of the quality of cartilaginous constructs. The bioink platform utilizes a novel dual-stage crosslinking mechanism based on a single type of modified hyaluronic acid (HA-SH) with two independent polymeric PEG crosslinkers for Michael addition (pre-crosslinking) and thiol-ene click chemistry (final crosslinking). In contrast to formulations with low molecular weight HA-SH, bioinks prepared with high molecular weight HA-SH yielded low concentrated hydrogels with a loose porous network and allowed for enhanced macromolecular diffusion. This led to a homogeneous distribution of key ECM components aggrecan and collagen type II throughout the constructs and, thereby, resulted in a marked increase of Young's modulus over time. The principle that HA hydrogels with low polymer content allow for an improved ECM distribution compared to gels with high polymer content has been previously shown for non-printed hydrogels[156, 157] and for constructs printed with an additional PCL support structure.[188] The current study transferred this to 3D constructs that are printable without the requirement of an additional thermoplastic support, which is regarded as a distinct extension of the biofabrication window.[68, 226]

Taken together, these platform bioinks combine 3D printability with chondrogenic differentiation of MSC, characterized by homogeneous ECM distribution and distinctly increased construct stiffness, and therefore represent a promising perspective for cartilage regeneration. Based on the established bioink platform, future studies may include investigation of the effects of different

PEG-acryl geometries or other acrylated polymers on 3D printability, and different molecular weights or geometries (e.g. 4-arm or 8-arm PEG-allyl) or other allylated polymers to fine-tune the resulting hydrogel stiffness after irradiation. Overall, the developed dual-stage system may serve as an example to design bioink platforms utilizing two independent crosslinking reactions at one functional group, which allows to adjust 3D printability as well as material and biological properties of the printed bioinks in a wide range. Here, the presented platform based on thiolated HA was tailored for cartilage engineering but may provide a high flexibility also for other applications in biofabrication.

4.6. Acknowledgements

Julia Hauptstein and Leonard Forster contributed equally to this work, which was funded by the Deutsche Forschungsgemeinschaft (DFG, German Research Foundation) – Project number 326998133 – TRR 225 (subprojects A02, A06, B02, and C02). The work was further supported by the DFG within the "State Major Instrumentation Programme", providing funding for the SEM Crossbeam 340 (Zeiss) – funding number INST 105022/58-1 FUGG. The authors thank the Orthopedic Centre for Musculoskeletal Research, University of Würzburg, for providing bone samples, Jan Weichhold, Chair for Functional Materials in Medicine and Dentistry and Bavarian Polymer Institute, University of Würzburg, for designing the extrudability test setup, Malte Mildner, Institute of Organic Chemistry, University of Würzburg, for 400 MHz NMR measurements, and Jonas Hazur, Institute of Biomaterials, Friedrich-Alexander-University Erlangen-Nürnberg, for grid and filament fusion test G-codes.

4.7. Supporting information

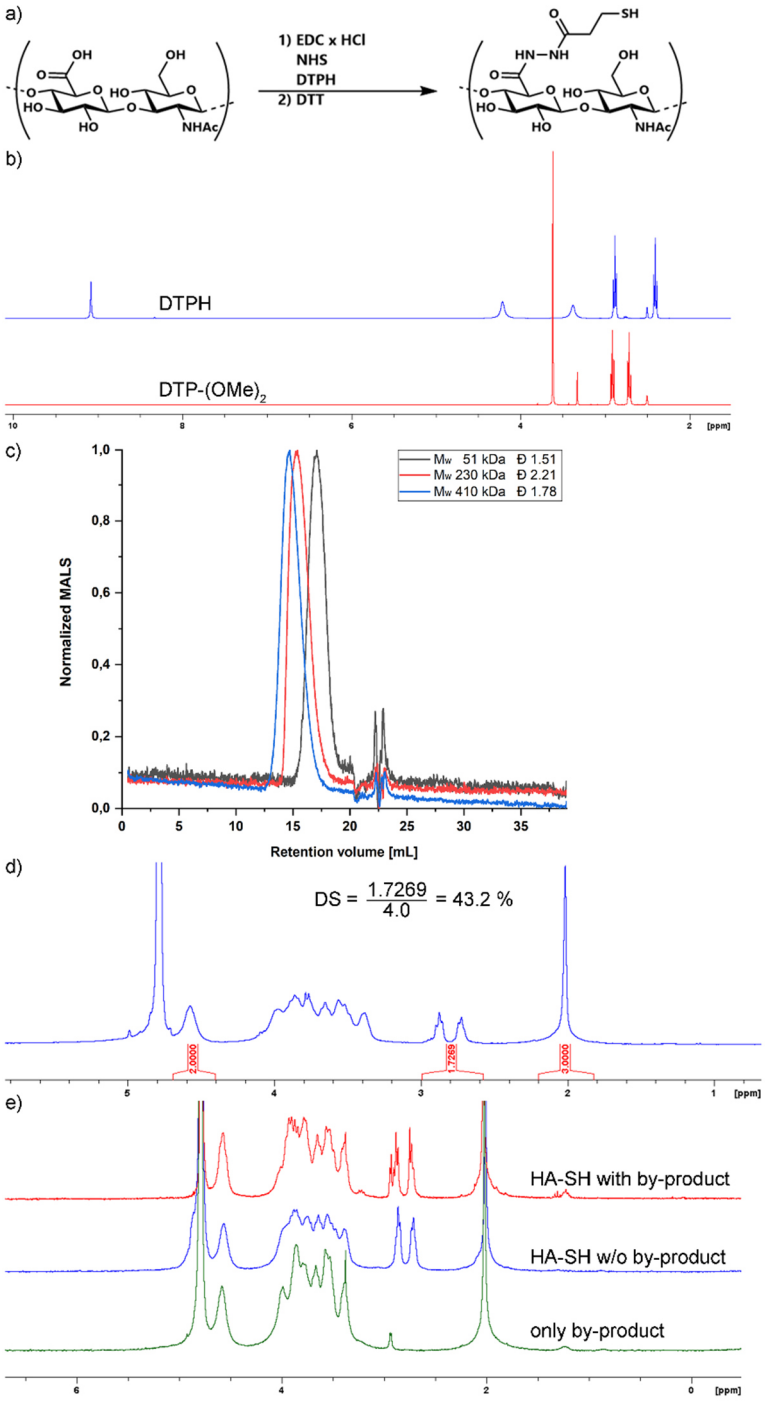

Figure II.S1: a) Reaction scheme of HA-SH synthesis. b) ^{1}H-NMR spectra overlay plot proving quantitative conversion from DTP-$(OMe)_2$ to DTPH by the absence of methyl ester signal: (400 MHz, d_6-DMSO) δ (ppm) = 2.67-2.76 (t, 2 H, -CH_2-$COOCH_3$), 2.85-2.95 (t, 2 H, -CH_2-S), 3.54-3.65 (s, 3 H, -COOCH_3) for DTP-$(OMe)_2$ and (400 MHz, d_6-DMSO) δ (ppm) = 2.36-2.45 (t, 2 H, -CH_2-CONH-NH_2), 2.83-2.93 (t, 2 H, -CH_2-S-), 4.08-4.34 (s, 2 H, -CONH-NH_2), 8.99-9.18 (s, 2 H, -CONH-NH_2) for DTP, both with water residues around 3.3 ppm. c) GPC elugram overlay plot of the three used HA-SH batches including their molecular weight and dispersity d) ^{1}H-NMR spectra of HA-SH showing exemplary determination of degree of substitution (DS) by internal references: (300 MHz, D_2O) δ (ppm) = 1.82-2.20 (s, 3 H, *N*-Acetyl), 2.57-3.00 (m, thiol-modification), 3.20-4.20 (m, 10 H, HA-backbone), 4.40-4.70 (s, 2 H, anomeric protons) e) ^{1}H-NMR spectra overlay plot demonstrating the influence of NHS addition on *N*-acylurea by-product formation and DS determination. Byproduct signals are inseparable from those of the thiol-bearing modification of HA-SH. Byproduct signals: (300 MHz, D_2O) δ (ppm) = 1.15-1.36 (m, -N(CH_2-CH_3), 2.72-2.92 (m, -N(CH_2)$_3$N-), 3.38 (m, -N(CH_3)$_2$).

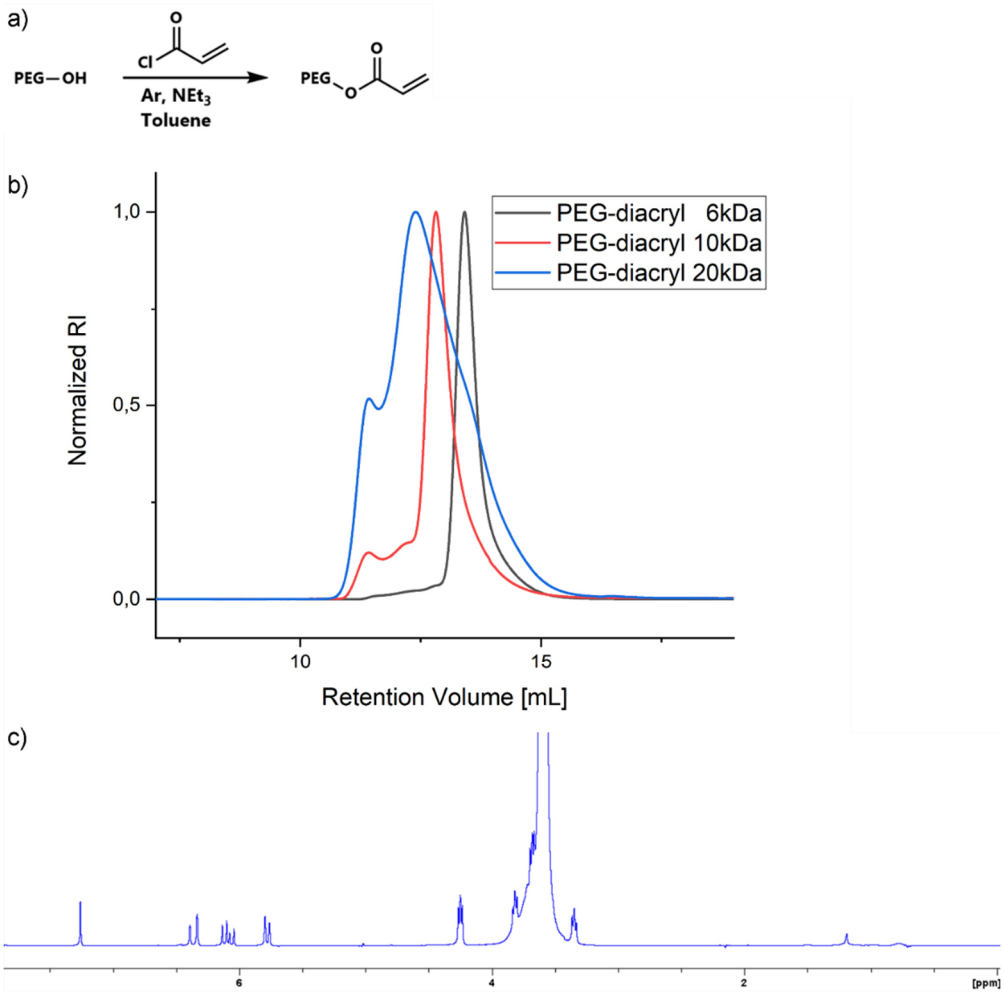

Figure II.S2: a) Reaction scheme of PEG-diacryl synthesis. b) GPC elugram overlay plot of the three PEG-diacryl batches including their molecular weight. c) ^{1}H-NMR spectra of PEG-diacryl 6 kDa (300 MHz, $CDCl_3$) δ (ppm) = 3.25-3.95 (m, PEG-backbone and satellites), 4.19-4.30 (t, 2 H, PEG-O-CH_2-C*H*$_2$-O-acryl) 5.72-6.44 (d/dd, C*H*=C*H*$_2$) after addition of TFAA to reveal unreacted PEG-OH groups by shifting neighboring CH_2-signals to 4.48 ppm.

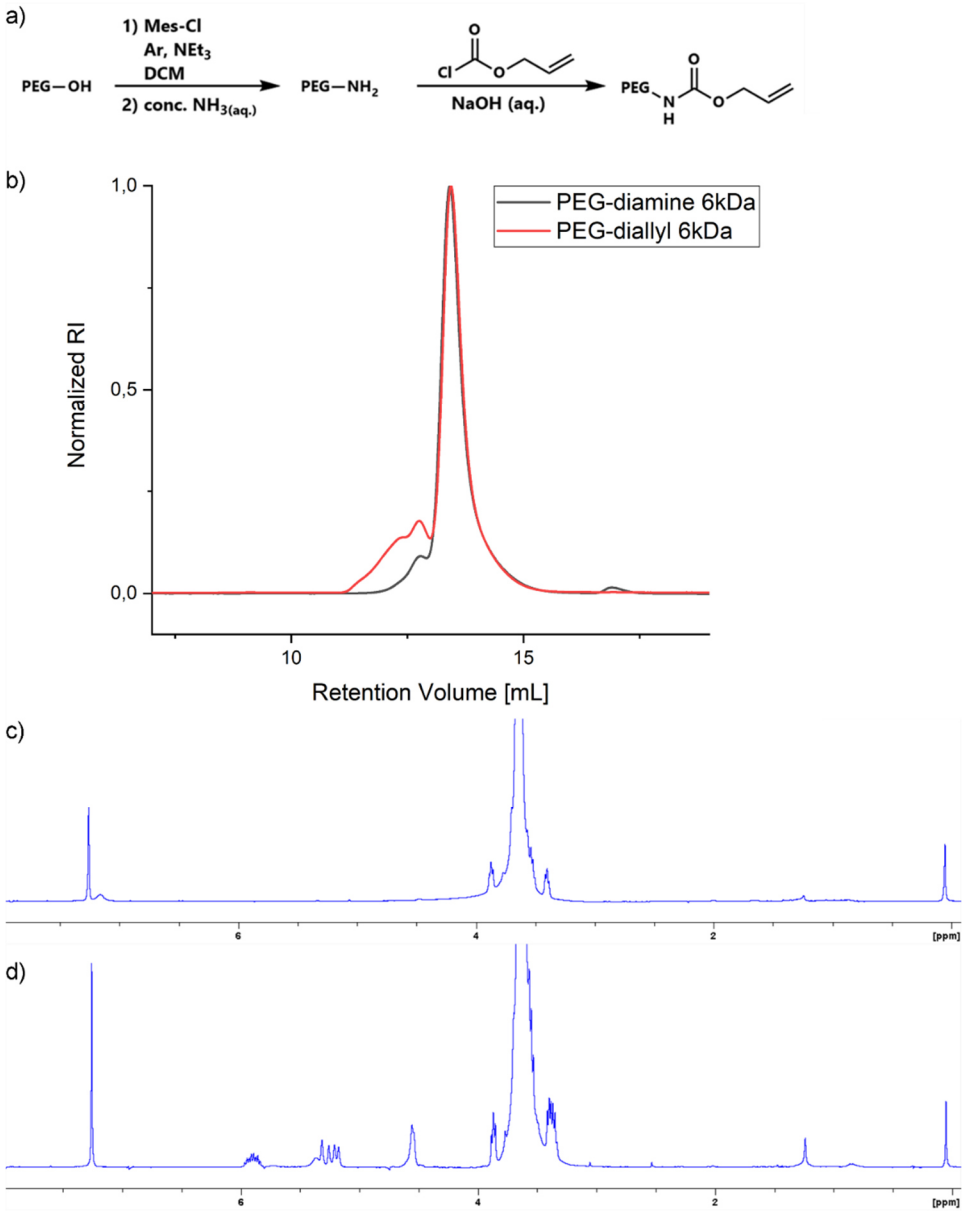

Figure II.S3: a) Reaction scheme of PEG-diallyl synthesis via PEG-diamine. b) GPC elugram overlay plot of the PEG-diamine and PEG-diallyl 6 kDa. c) ^{1}H-NMR spectra of PEG-diamine 6 kDa after TFAA addition (300 MHz, $CDCl_3$) δ (ppm) = 3.25-3.95 (m, PEG-backbone and satellites), 7.18 (s, -N*H*-C(=O)CF_3) with traces of grease (0.10) and acetone (2.17). d) ^{1}H-NMR spectra of PEG-diallyl 6 kDa after TFAA addition (300 MHz, $CDCl_3$) δ (ppm) = 3.25-3.95 (m, PEG-backbone and satellites), 4.50-4.66 (m, PEG-O-CH_2-C*H*$_2$-N-), 5.13-6.00 (d/d/m, O-C*H*$_2$-C*H*=C*H*$_2$), 5.37 (s, -N*H*-C(=O)-O-) with traces of grease (0.10) and acetone (2.17).

c \ t	10 min	20 min	30 min	45 min	1 h	1.5 h	2 h	3 h	4 h	5 h
0.40 %	liquid	liquid	liquid	liquid	viscous	viscous/ printable	printable	printable	printable*	printable/ stiff*
0.50 %	liquid	liquid	liquid	viscous	printable	printable	printable	printable*	printable/ stiff*	printable/ stiff*
0.60 %	liquid	liquid	viscous	viscous/ printable	printable	printable	printable	printable*	printable/ stiff*	printable/ stiff*
0.75 %	liquid	viscous/ printable	printable	printable	printable	printable/ stiff	printable/ stiff	solid	solid*	solid*
1.00 %	liquid	printable	printable	printable/ stiff	printable/ stiff	solid	solid	solid	solid*	solid*

Figure II.S4: Printability assessment of HASH/PEG-diacryl concentration series using the 410 kDa HA-SH batch as an example. Polymers were used in 1:1 ratios (0.4 % – 1 %) and the resulting hydrogel solutions were analyzed over time (10 min, 20 min, 30 min, 45 min, 1 h, 1.5 h, 2 h, 3 h, 4 h and 5 h). 0.5 % and 0.6 % HA-SH/PEG-diacryl formulation were conveniently printable in the timeframe from 1 h to 3 h after the start of crosslinking. Decreasing the polymer concentrations (0.4 %) resulted in a delayed printability, which was regarded unsuitable for cell compatibility. In contrast, increasing the polymer concentrations (0.75 %, 1.0 %) accelerated the Michael addition dramatically and resulted in shorter processing-windows. Printability assessment is visualized by a color code: green = printable, red = not printable (liquid, viscous or solid) and yellow presents the transition phase (viscous/printable or printable/stiff). Syneresis (marked with *) was seen in all tested approaches after at 3 – 4 h of pre-crosslinking.

a) Ink printability with 0.5 % HA-SH (230 kDa) depending on PEG-diacryl M_W

M_W PEG-diacryl \ c(PEG-diacryl)	0.10 %	0.25 %	0.40 %	0.50 %	0.60 %	0.75 %	1.00 %	1.25 %	1.50 %	1.75 %	2.00 %	2.25 %	2.50 %	2.75 %	3.00 %	3.25 %
6 kDa																
10 kDa																
20 kDa																

b) Ink printability with 2.5 % HA-SH (51 kDa) depending on PEG-diacryl M_W

M_W PEG-diacryl \ c(PEG-diacryl)	0.50 %	1.00 %	1.50 %	2.00 %	2.50 %	3.00 %	3.50 %	4.00 %	4.50 %	5.00 %	5.50 %	6.00 %	7.00 %	8.00 %	9.00 %	10.0 %
6 kDa																
10 kDa																

Figure II.S5: Influence of PEG-diacryl molecular weight on ink printability. a) 0.5 % HA-SH (230 kDa) or b) 2.5 % HA-SH (51 kDa) were mixed with different concentrations of PEG-diacryl (6 kDa, 10 kDa and 20 kDa) and printability of the resulting solutions was analyzed over 5 h.

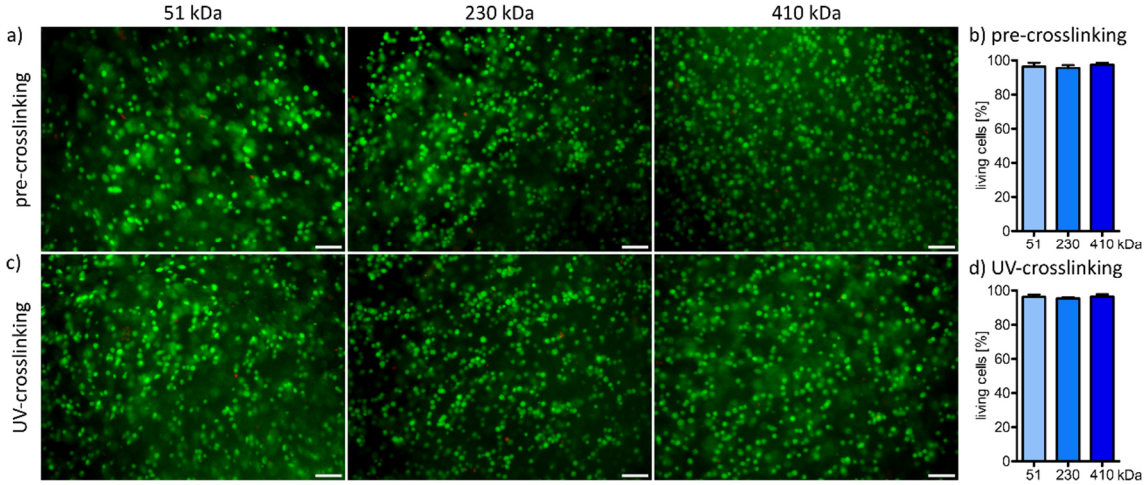

Figure II.S6: Live/dead staining of MSCs in a) pre-crosslinked and c) final UV-crosslinked 51 kDa, 230 kDa, and 410 kDa HA-SH constructs. Quantification of living cells after b) pre-crosslinking and d) final UV-crosslinking.

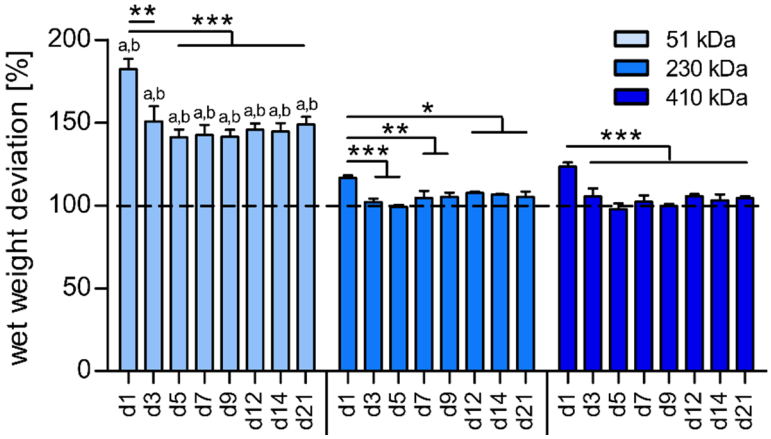

Figure II.S7: Swelling analysis of 51 kDa, 230 kDa and 410 kDa HA-SH constructs over 21 days. Bars represent the deviation from the original wet weight (= 100 %, dotted line) and represent the mean ± standard deviation (n = 3). (a) Significantly different to the corresponding time point of 230 kDa HA-SH, (b) significantly different to the corresponding time points of 410 kDa HA-SH (at least $p < 0.05$).

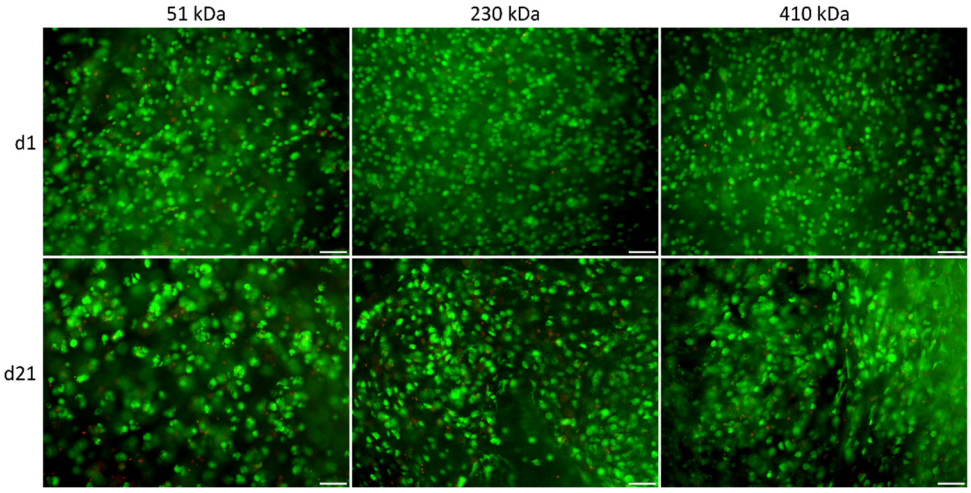

Figure II.S8: Live/dead staining of MSCs in 3D printed 51 kDa, 230 kDa, and 410 kDa HA-SH constructs after 1 and 21 days of chondrogenic culture. Living cells were stained with calcein-AM and appear in green, dead cells were stained in red with EthD-III. Scale bars represent 100 µm.

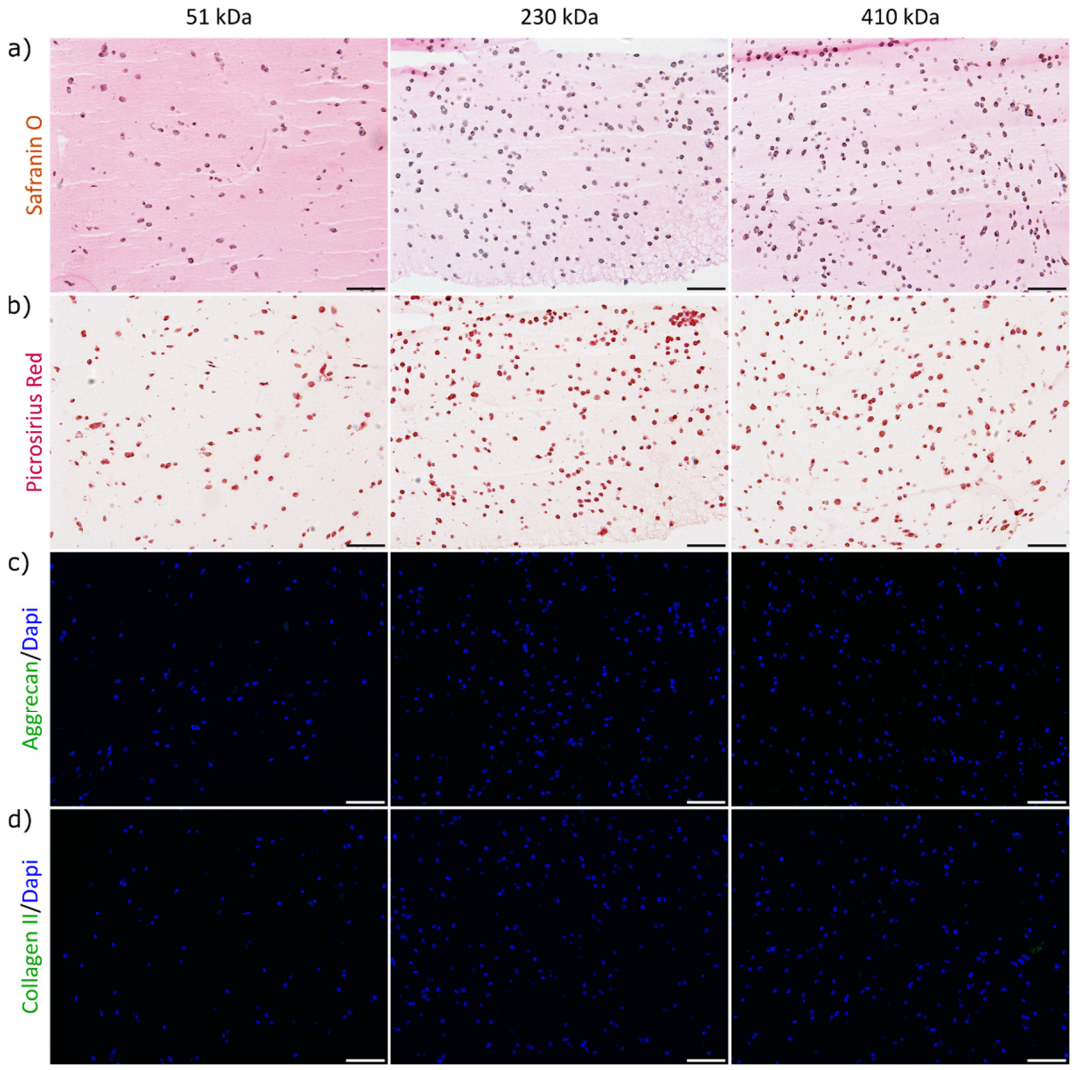

Figure II.S9: Histological and immunohistochemical (IHC) staining of ECM components at day 1 in 3D printed 51 kDa, 230 kDa, and 410 kDa HA-SH constructs. a) Safranin O staining of glycosaminoglycans. b) Picrosirius red staining of collagens. IHC staining of c) aggrecan and d) collagen type II, both depicted in green. Nuclei were counterstained with DAPI (blue). Scale bars represent 100 µm.

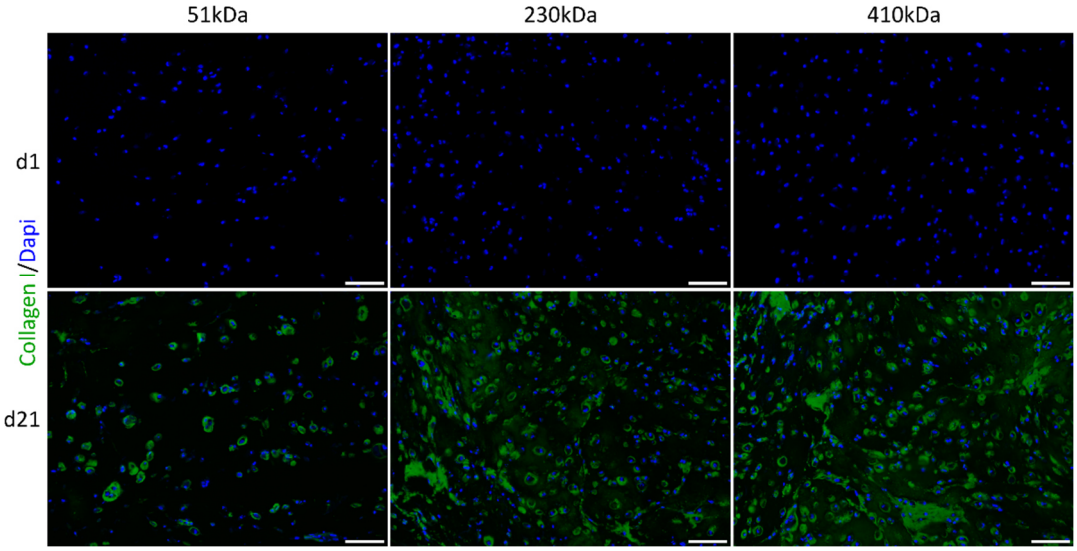

Figure II.S10: Immunohistochemical staining of the fibrocartilage marker collagen type I (green) after 1 and 21 days of chondrogenic culture of 3D printed 51 kDa, 230 kDa, and 410 kDa HA-SH constructs with embedded MSCs. Nuclei were counterstained with DAPI (blue). Scale bars represent 100 µm.

Table II.S1: Educts and products of the HA-SH syntheses.

Educts						Products		
Initial HA		EDC	NHS	DTPH	DTT	HA-SH		
Mw [kDa]	weight [g]	weight [g]	weight [g]	weight [g]	weight [g]	Mw [kDa]	DS [%]	yield [g]
1014	3.0	10.7	3.44	7.13	5.77	**410**	44	2.7
765						398	40	2.7
389						**230**	43	2.7
389						210	38	2.7
60.5						54	45	2.4
60.5						**51**	45	2.4

Table II.S2: Incubation periods for different bioinks prior frequency sweep, UV exposure and shear rate sweeps. (FS: frequency sweep)

Ink	polymer content (HA-SH, PEG-diacryl) [%]	Before initial FS [min]	After UV exposure (prior second FS) [min]	Before shear rate sweep [min]
HA-SH 51 kDa	2.5 + 2.5	40	30	40
HA-SH 230 kDa	0.5 + 0.5	110	30	110
HA-SH 410 kDa	0.5 + 0.5	70	30	70

Table II.S3: Primer sequences for qRT-PCR.

	Primer	**Sequence**
1	ACAN forward	5'-TACGACGCCATCTGCTACAC-3'
2	ACAN reverse	5'-GACGGTGATGTCCTCCTCAC-3'
3	COL1A1 forward	5'- TTCAGCTTTGTGGACCTCCG-3'
4	COL1A1 reverse	5'- TGGGATGTCTTCGTCTTGGC-3'
5	COL2A1 forward	5'-CTGTCCTTCGGTGTCAGGG-3'
6	COL2A1 reverse	5'-CAGACACAGATCCGGCAGG-3'
7	GAPDH forward	5'-GGAAGGTGAAGGTCGGAGTC-3'
8	GAPDH reverse	5'-AGTTGAGGTCAATGAAGGGGTC-3'
9	SOX9 forward	5'-GGGCAAGCTCTGGAGACTTC-3'
10	SOX9 reverse	5'-AATCCGGGTGGTCCTTCTTG-3'

5. Chapter III – Tethered TGF-β1 in a Hyaluronic Acid-Based Bioink for Bioprinting Cartilaginous Tissues

DOI: 10.3390/ijms23020924[244]

Julia Hauptstein[1], Leonard Forster[2], Ali Nadernezhad[2], Jürgen Groll[2], Jörg Teßmar[2] and Torsten Blunk[1]

[1] Department of Trauma, Hand, Plastic and Reconstructive Surgery, University of Würzburg

[2] Department for Functional Materials in Medicine and Dentistry, Bavarian Polymer Institute (BPI), University of Würzburg

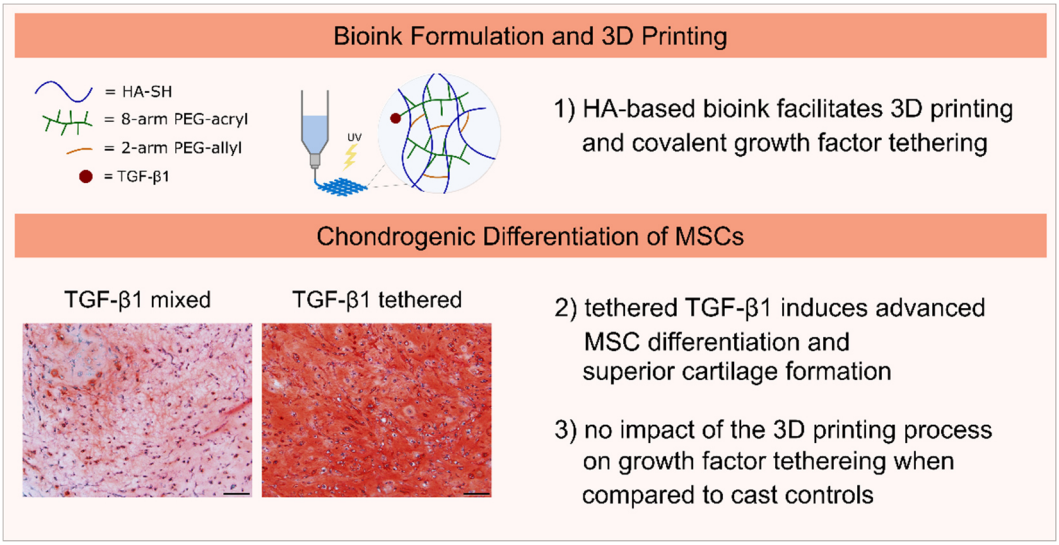

5.1. Abstract

In 3D bioprinting for cartilage regeneration, bioinks that support chondrogenic development are of key importance. Growth factors covalently bound in non-printable hydrogels have been shown to effectively promote chondrogenesis. However, studies that investigate the functionality of tethered growth factors within 3D printable bioinks are still lacking. Therefore, in this study, we established a dual-stage crosslinked hyaluronic acid-based bioink that enabled covalent tethering of transforming growth factor-beta 1 (TGF-β1). Bone marrow-derived mesenchymal stromal cells (MSCs) were cultured over three weeks *in vitro*, and chondrogenic differentiation of MSCs within bioink constructs with tethered TGF-β1 was markedly enhanced, as compared to constructs with non-covalently incorporated TGF-β1. This was substantiated with regard to early TGF-β1 signaling, chondrogenic gene expression, qualitative and quantitative ECM deposition and distribution, and resulting construct stiffness. Furthermore, it was successfully demonstrated, in a comparative analysis of cast and printed bioinks, that covalently tethered TGF-β1 maintained its functionality after 3D printing. Taken together, the presented ink composition enabled the generation of high-quality cartilaginous tissues without the need for continuous exogenous growth factor supply and, thus, bears great potential for future investigation towards cartilage regeneration. Furthermore, growth factor tethering within bioinks, potentially leading to superior tissue development may also be explored for other biofabrication applications.

5.2. Introduction

In recent years, 3D biofabrication including bioprinting has evolved as a fast-growing research field in regenerative medicine and for the development of disease models.[60, 61, 226] 3D bioprinting enables precise patterning of cells and hydrogel materials, i.e. bioinks, and is investigated as a promising alternative approach for treatment of cartilage defects in trauma and degenerative diseases. To obtain functional cartilage transplants, bioinks that support chondrogenic development are of key importance.[58, 62, 71, 72]

Hyaluronic acid represents a promising and attractive material for cartilage regeneration, as it is a main component of the natural cartilage extracellular matrix (ECM), and it enables diverse chemical modifications for crosslinking reactions with other bioink components.[71, 152, 154, 228] Frequently applied functionalizations are, for example, thiol,[147] methacrylate,[245] glycidyl methacrylate,[246] tyramine,[247] or norbornene[248] among several others. Nevertheless, studies that show flexible hyaluronic acid inks with a high initial shape stability after printing as well as convincing long-term development of cartilaginous constructs are still rare.[223, 228]

Apart from a suitable ink material, the growth factor TGF-β is crucial for chondrogenic differentiation of mesenchymal stromal cells (MSCs) and cartilage homeostasis. It stimulates ECM production and can enhance cartilage repair, while its absence results in osteoarthritis

(OA)-like changes.[249, 250] However, application of TGF-β to the synovial tissue of the joint, for example via injections, results in a short half-life[251] and can induce fibrosis and osteophyte formation in adjacent tissues.[252, 253] Therefore, a precise local supplementation and dose control appears desirable. TGF-β immobilization within hydrogel scaffolds could be achieved, e.g., by direct loading, encapsulation into particulate carriers which are incorporated into the scaffold, reverse binding, for example via electrostatic interactions, or covalent tethering.[177, 221] Especially the covalent approach holds great promise for functional cartilage transplants with respect to prolonged availability for embedded MSCs and low release rates into the surrounding tissue.[184-186] With regard to 3D bioprinting, covalent incorporation into the used bioink may avert the necessity for repeated injections *in vivo*, likely enhancing the clinical potential of the inks for cartilage regeneration. Over the last couple of years, the impact of shear stresses during 3D printing on cell survival and differentiation has been extensively studied.[205, 254-256] Furthermore, it is known that shear stresses can also strongly impact protein structure and function.[257, 258] However, surprisingly, studies that investigate whether the 3D printing process may have an impact on the functionality of covalently tethered growth factors are still lacking. For this reason, this study focused on the protein function of soluble and covalently tethered TGF-β1 in a comparative analysis of cast and printed bioinks.

In a recent study, we established a novel hyaluronic acid-based bioink platform for cartilage 3D biofabrication.[223] Within this platform, we identified bioinks which enabled high shape fidelity during and after printing, but still had a very low polymer content of 2 % and a highly porous network. This facilitated effective chondrogenic differentiation of MSCs, a homogeneous distribution of newly produced extracellular matrix (ECM) and thereby a superior quality of resulting cartilaginous constructs. However, these novel bioinks were not suitable for growth factor binding and TGF-β1 had to be supplemented with each medium change.

Therefore, in this study, we investigated a new hyaluronic acid-based bioink which maintained the beneficial properties of the established bioink platform and further enabled covalent TGF-β1 tethering. Specifically, TGF-β1 was thiol-modified with Traut's reagent and covalently tethered to a newly integrated crosslinker, polyethylene glycol-octaacrylate (8-arm PEG-acryl), via Michael addition. In the first step of hydrogel formation, the remaining acryl groups of 8-arm PEG-acryl reacted via Michael addition with thiol-modified hyaluronic acid (HA-SH), resulting in a highly viscous and 3D printable ink. After fabrication, a UV-induced thiol-ene click reaction between polyethylene glycol-diallyl carbamate (2-arm PEG-allyl) and the residual thiol groups of HA-SH ensured final crosslinking. We characterized the inks with regard to rheological properties, swelling behavior, and TGF-β1 release. MSC chondrogenesis was assessed in cast constructs with varying amounts of covalently or non-covalently incorporated TGF-β1, with distinct advantages achieved by TGF-β1 tethering. Subsequently, constructs with 150 nM TGF-β1, either tethered or non-covalently incorporated, were cast or 3D bioprinted.

Chondrogenic differentiation of MSCs was extensively evaluated regarding early TGF-β1 signaling, gene expression, qualitative and quantitative ECM deposition and distribution, and resulting construct stiffness. The presented HA-based bioink with tethered TGF-β1 yielded superior chondrogenic differentiation, as compared to constructs with non-covalently incorporated TGF-β1. Furthermore, it was successfully demonstrated in the comparative analysis of cast and printed bioinks that covalently tethered TGF-β1 maintained its functionality after 3D printing.

5.3. Experimental section

5.3.1. Materials

All chemicals were purchased from Sigma Aldrich (St. Louis, MO, USA) if not stated differently. Acryloyl chloride stabilized with phenothiazine (abcr GmbH, Karlsruhe, Germany), 1-(3-dimethylaminopropyl)-3-ethylcarbodiimide HCl (EDC, Biosynth CarboSynth, Compton, UK), 1,4-dithiothreitol (DTT, Biosynth CarboSynth, Compton, UK), 2-hydroxy-1-[4-(hydroxyethoxy)-phenyl]-2-methyl-1-propanone (I2959; BASF, Ludwigshafen, Germany), 4-(dimethylamino)benzaldehyde (DAB; Carl Roth, Karlsruhe, Germany), basic fibroblast growth factor (bFGF; BioLegend, London, UK), chloroform-d^1 (Eurisotope, St-Aubin Cedex, France), DAPI mounting medium ImmunoSelect® (Dako, Hamburg, Germany), deuterium oxide (Deutero GmbH, Kastellaun, Germany), regenerated cellulose dialysis tubes MWCO 3500 Da (Carl Roth, Karlsruhe, Germany), diethylether (Chemobar University of Würzburg, Würzburg, Germany), dimethyl-3,3'-dithiodipropionate (TCI Chemical Industry Co. Ltd., Tokyo, Japan), di-potassium hydrogen phosphate (Merck KGaA, Darmstadt, Germany), di-sodium hydrogen phosphate (Merck KGaA, Darmstadt, Germany), Dulbecco's Modified Eagle's Medium high glucose 4.5 g L^{-1} (DMEM; Thermo Scientific, Waltham, MA, USA), Dulbecco's Modified Eagle's Medium/Ham's F-12 (DMEM/F12; Thermo Scientific, Waltham, MA, USA), ethanol (99 %, TH Geyer, Renningen, Germany), fetal calf serum (FCS; Thermo Scientific, Waltham, MA, USA), formaldehyde (37 %, Carl Roth, Karlsruhe, Germany), hyaluronic acid sodium salt (Mw 1 - 2 MDa; Biosynth CarboSynth, Compton, UK), hydrochloric acid (HCl; 32 %, 37 %, Merck KGaA, Darmstadt, Germany), isopropanol (VWR, Radnor, PA, USA), ITS+ premix (Corning, New York, NY, USA), L-hydroxyprolin (Merck KGaA, Darmstadt, Germany), live/dead cell staining kit (PromoKine, Heidelberg, Germany), methanol (Fisher Scientific, Schwerte, Germany), *N*-hydroxysuccinimide (NHS, Biosynth CarboSynth, Compton, UK), papain (Worthington, Lakewood, CA, USA), penicillin-streptomycin (PS; 100 U mL^{-1} penicillin, 0.1 mg mL^{-1} streptomycin; Thermo Scientific, Waltham, MA, USA), perchloric acid (60 %, Merck KGaA, Darmstadt, Germany), phosphate-buffered saline (PBS; Life Technologies, Carlsbad, CA, USA), polyethylene glycol (2-arm PEG, 6 kDa: Sigma Aldrich, St. Louis, MO, USA; 8-arm PEG, 10 kDa: JenKem® Technologies USA, Plano, TX, USA), potassium dihydrogen phosphate (Merck KGaA, Darmstadt, Germany), Proteinase K (Digest-All 4, Life Technologies, Carlsbad, CA, USA), sodium hydrogen carbonate (Merck KGaA, Darmstadt, Germany), sodium hydroxide (Merck KGaA, Darmstadt, Germany), Tissue Tek® O.C.T. (Sakura Finetek, Tokyo, Japan), toluene (Fisher Scientific, Schwerte, Germany), transforming growth factor β1 (TGF-β1; Novoprotein Inc., CA59, Summit, NJ, USA, purchased from PELOBIOTECH GmbH, Munich, Germany), tris(carboxyethyl)phosphine HCl (TCEP, Biosynth CarboSynth, Compton, UK), trypsin-EDTA (0.25 %, Life Technologies, Carlsbad, CA, USA).

5.3.2. Methods

Synthesis of the different bioink components: The synthesis of the different components of the previously established hyaluronic acid-based bioink (3,3'-dithiobis(propanoic dihydrazide) (DTPH), thiolated hyaluronic acid (HA-SH), polyethylene glycol-diamine, and polyethylene glycol-diallyl carbamate (2-arm PEG-allyl)) was performed as previously published.[223] Synthetical details are given in the Supporting information (5.7.).

Synthesis of polyethylene glycol octaacrylate (8-arm PEG-acryl): The synthesis of the branched PEG-acrylate necessary for growth factor immobilization was performed using enzyme catalyzed transesterification.[259, 260] In brief, 8-arm PEG (5.0 g, 1.0 eq.) was dried in vacuo at 100 °C for 1 h, cooled to 60 °C under argon atmosphere and dissolved in dry toluene (50 mL). Vinyl acrylate (3.0 eq.) and Novozyme 435 (50.0 mg) were added, the suspension was incubated for 3 days at 50 °C and subsequently filtered. After precipitation and washing with diethyl ether, the product was dried in vacuo to form a bulky white solid.

NMR analysis: ^{1}H-NMR measurements were performed at a 300 MHz Bruker Biospin spectrometer (Bruker, Billerica, MA) using $CDCl_3$ (PEG), d^6-DMSO (DTP) and D_2O (HA-SH) as solvents. The solvent peak was set to $\delta = 7.26$ ppm for $CDCl_3$, 2.50 ppm for DMSO and 4.79 ppm for D_2O to which all chemical shifts refer. The degree of substitution of HA-SH was determined by the ratio of the integrals of the thiol carrying substituent and the acetyl amide signal in combination with the anomeric protons of the saccharide backbone. The quantitative PEG-modification was verified by the absence of alterations in the spectra after the addition of trifluoroacetic anhydride to the NMR sample solution.

GPC analysis: A GPC system from Malvern (Herrenberg, Germany) with a triple detection containing a refractive index detector (VE 3580), a viscometer (270 dual detector) and a multi angle light scattering detector (SEC-MALS 20) was used for GPC analysis. Depending on the molecular weight, different column sets (Malvern, Herrenberg, Germany) were used. For HA-SH samples, two A6000M mixed-bed columns and for PEG samples, a set of A2000/A3000 columns were chosen. The eluent was prepared using deionized water containing 8.5 g L^{-1} $NaNO_3$ and 0.2 g L^{-1} NaN_3 and the columns were calibrated with PEG standards (Malvern, Herrenberg, Germany). HA-SH samples were dissolved in deionized water with 0.5 g L^{-1} TCEP over 6 h at rt and PEG samples were dissolved in deionized water over 6 h at rt. The obtained data was processed with OmniSEC 5.12 (Malvern, Herrenberg, Germany).

Ink preparation, TGF-β1 tethering and 3D printing: Final composition of the used ink is: 0.5 % HA-SH (465 kDa), 0.5 % 8-arm PEG-acryl (10 kDa), 0.4 % 2-arm PEG-allyl (6 kDa) and 0.05 % Irgacure (I2959); all concentrations are indicated as (w/V). For ink preparation, HA-SH was dissolved in HEPES buffer (pH 7.6, 154 mM), all other components were dissolved in PBS. Three

different experimental conditions were prepared: constructs without TGF-β1, constructs with non-covalently bound TGF-β1 (10 nM, 50 nM, 100 nM and 150 nM) and constructs with covalently tethered TGF-β1 (10 nM, 50 nM, 100 nM and 150 nM). For TGF-β1 tethered hydrogels, Traut's reagent was used for thiol-modification of the protein (4:1 molar excess of Traut's reagent, 1 h incubation at rt). Subsequently, different amounts of thiolated TGF-β1 were tethered to 8-arm PEG-acryl via Michael addition (1 h at 37 °C). For control constructs with mixed TGF-β1 (no tethering) the same procedure was performed without the addition of Traut's reagent. Afterwards, all ink components were mixed with or without MSCs (20 x 10^6 cells mL^{-1}, passage 4), transferred to a 3 cc printing cartridge (Nordson EFD, OH, USA) and incubated for 30 min at 37 °C to achieve the necessary viscosity for 3D printing via Michael addition. 3D bioprinting as well as printing simulation was performed with an Inkredible+ 3D bioprinter (Cellink, Boston, MA, USA) at 50 kPa through a 330 µm steel nozzle (Nordson EFD, OH, USA). G-codes for 3D printed grids and filament fusion tests were generated with the HeartWare software (Cellink, Boston, MA, USA). The NIH ImageJ Fiji software (version 1.52a) was utilized for strand thickness measurements. The CAD file source of the human femoral condyles was MakerBot Thingiverse (object 5820, created by BME_sundevil). The CAD file was sliced with the Heartware software and printed with a BioX 3D bioprinter (Cellink, Boston, MA, USA). For the printing simulation, bioink was extruded at the same printing conditions used for 3D printing and collected in a tube, subsequently filled in glass molds (5 mm diameter, 2 mm height, 40 µL volume per construct) and irradiated for 10 min at 365 nm (UVL hand lamp with white light filter, 1 mW cm^{-2}, A. Hartenstein, Würzburg, Germany). Control constructs were cast and irradiated in the same way. MSC-laden constructs were cultured in a chondrogenic differentiation medium (DMEM high glucose medium supplemented with 1 % ITS+ premix, 1 % PS, 0.1 x 10^{-6} M dexamethasone, 50 µg mL^{-1} L-ascorbic acid 2-phosphate sesquimagnesium salt hydrate and 40 µg mL^{-1} L-proline) at 37 °C and 5 % CO_2. Only constructs of the "medium" control were cultured in chondrogenic differentiation medium supplemented with 10 ng mL^{-1} TGF-β1. The medium was changed thrice per week.

Rheological analysis: Rheological properties of the hydrogel formulations were characterized using Anton Paar MCR 702 rheometer (Anton Paar, Austria). A parallel plate geometry with a diameter of 25 mm at a 0.5 mm gap was used. A solvent trap was used to minimize evaporation during the experiment. All the experiments were performed with freshly prepared ink solutions in the dark on a pre-heated plate at 37 °C. Time sweep measurements were performed by setting the oscillatory strain amplitude and angular frequency at 0.3 % and 10 rad s^{-1}, respectively. The viscoelastic properties of the formed network were characterized by an oscillatory frequency sweep between 100 – 1 rad s^{-1} at 0.3 % strain.

Swelling analysis: Gel wet weight measurements were performed to analyze the swelling and shrinking behavior of constructs without MSCs. Therefore, constructs with 150 nM tethered TGF-β1 or without the growth factor were prepared as described above and incubated in 1 mL PBS for 21 days. Intermediate weight measurements were performed after 30 min, 1 h, 2 h, 4 h, 6 h, 12 h, 1 d, 2 d, 3 d, 5 d, 7 d, 14 d and 21 d and wet weight deviations were calculated in relation to construct weights directly after preparation (0 h).

TGF-β1 release analysis: 3D constructs with 150 nM mixed or tethered TGF-β1 were prepared as described above and incubated for 21 days, each in 1 mL 1 % BSA in PBS. 5 µL samples were taken at 1, 3, 5, 7, 9, 12, 14, 16, 19 and 21 days and subsequently frozen in liquid nitrogen. Quantification of TGF-β1 concentration was performed with a DuoSet ELISA (DY240-05, R&D Systems, Minneapolis, MN, USA).

MSC isolation and expansion: Isolation of human bone-marrow derived mesenchymal stromal cells (MSCs) was performed as described previously[147] after informed consent of all patients and with approval of the local ethics committee of the University of Würzburg (186/18). Cells were expanded in DMEM/F12 supplemented with 10 % FCS, 1 % PS and 3 ng mL^{-1} bFGF at 37 °C and 5 % CO_2.

Cell viability analysis and quantification: Viability of encapsulated MSCs in 3D printed or cast constructs was performed with a live/dead assay cell staining kit (PromoKine, Heidelberg, Germany). Constructs were harvested on d1 or d21, washed in PBS and incubated in the staining solution (4 µM ethidium homodimer III (EthD-III) and 2 µM calcein acetoxymethylester (calcein-AM) in PBS) for 45 min at rt in the dark. After an additional washing step in PBS, cross sections of the constructs were imaged at a fluorescence microscope (Olympus BX51/DP71, Olympus, Hamburg, Germany). For quantification, high magnification images of three printed constructs (three pictures per construct) were analyzed with the Cell Counter plugin of the NIH Image J Fiji Software (version 1.52a), counting green and red cells.

Histological and immunohistochemical analysis: MSC-laden constructs were harvested on d1 and d21 and fixed in 3.7 % PBS-buffered formaldehyde over night at 4 °C. TissueTek® O.C.T. (Sakura Finetek, Torrance, USA) was used for embedding and 8 µm cryo-sections were performed at a cryostat (CM 3050S, Leica, Wetzlar, Germany). GAG deposition was visualized with safranin O (counterstain: Weigert's hematoxylin and fast green), and collagen deposition with picrosirius red (counterstain: Weigert's hematoxylin).[198, 261] Immunohistochemical stainings were performed as previously described.[188] Used antibodies were: anti-aggrecan, 1:300, 969D4D11, Thermo Scientific, Waltham, MA, USA; anti-collagen I, 1:200, ab34710, Abcam, Cambridge, UK; anti-collagen II, 1:1000, II-4C11, Abnova, Taipei, Taiwan; and goat-anti-mouse Alexa488, 1:400, 111-545-003, Jackson ImmunoResearch, Cambridge, UK); all in

1% BSA in PBS. Cells were counterstained with DAPI during mounting (Dako, Hamburg, Germany).

Biochemical analysis: MSC-laden constructs were homogenized at 25 Hz for 5 min (TissueLyser II, Quiagen, Hilden, Germany) before digesting the suspension with 3 U mL^{-1} papain (Worthington, Lakewood, NJ, USA) for 20 h at 60 °C. Quantification of DNA content was performed with Hoechst 33258 (340 nm and 465 nm) and salmon sperm DNA as standard.[200] Dimethylmethyleneblue (DMMB) was used to quantify sulfated glycosaminoglycans (GAG) with chondroitin sulfate as standard at 525 nm.[203] After hydrolysis with hydrochloric acid at 95 °C for 20 h, hydroxyprolines were visualized with 4-(dimethylamino)benzaldehyde at 550 nm. Collagen content was quantified with L-hydroxyproline as standard.[201, 202] For calculation of total GAG and collagen content, culture supernatants of MSC-laden constructs were collected at every medium change and also analyzed with the methods described above.

RNA isolation and gene expression analysis: 3D constructs were homogenized for 5 min at 25 Hz before isolating RNA with TRIzol reagent (Invitrogen, Waltham, MA, USA) according to manufacturer's instructions. cDNA was synthesized with the High-Capacity cDNA reverse transcription kit (Applied Biosystems, Foster City, CA, USA) and real-time qRT-PCR was performed with the MESA GREEN qPCR Mastermix Plus for SYBR® Assay (Eurogentec, Liège, Belgium) in a CFX96 real-time system (Bio-Rad, Hercules, CA, USA). Relative gene expression of all samples was normalized to the eukaryotic translation initiation factor 1α1 (EEF1A1) and to gene expression of MSC 2D samples on d0, all analyzed with the $2^{-\Delta\Delta CT}$ method.[204] A table with self-designed primer sequences can be found in the Supporting information (5.7., Table III.S1).

Protein separation and Western blot analysis: 3D constructs were homogenized for 5 min at 25 Hz in RIPA lysis and extraction buffer (Thermo Scientific, Waltham, MA, USA) supplemented with Pierce protease and phosphatase inhibitor (Thermo Scientific, Waltham, MA, USA). Protein isolation was performed by repeated freeze-thaw cycles before protein concentration was analyzed with the Pierce™ BCA protein assay kit (Thermo Scientific, Waltham, MA, USA) according to manufacturer's instructions. Protein separation was performed at 80 V by tris-glycine SDS-PAGE under reducing conditions using a 10 % polyacrylamide gel. For Western blotting, proteins were transferred to a Immobilon-FL PVDF membrane (0.45 µm; Merck KGaA, Darmstadt, Germany) at 100 V for 90 min on ice before blocking with 1 x ROTI® Block (Carl Roth, Karlsruhe, Germany) in tris-buffered saline supplemented with 0.1 % tween-20 (TBST) for 1 h at rt. Primary antibodies against Smad2/3 (Cell Signaling, 3102, rabbit, 1:1000), Phospho-Smad3 (Abcam, ab52903, rabbit, 1:1000) and GAPDH (Merck, MAB374, mouse, 1:5000) were diluted in 0.5 x ROTI® Block/TBS and incubated over night at 4 °C under agitation. After washing in TBST, secondary antibodies (Goat-anti-Rabbit 800CW IRDye, 926-32211, 1:15,000, and Goat-anti-Mouse 680CW IRDye, 925-68070, 1:15,000; LI-COR, Bad Homburg,

Germany) were incubated for 1 h at rt under agitation in the dark. Subsequently, membranes were washed in TBST before protein detection was performed at a LI-COR Odyssey® Fc imaging system.

Mechanical analysis: MSC-laden constructs were analyzed with a load cell of 250 g at a dynamical mechanical testing machine (ElectroForce 5500, Bose, Eden Prairie, MN, USA) on d1 and d21. A constant cross head displacement rate of 0.001 mm s^{-1} was used to compress the constructs to a final depth of 0.5 mm. The Young's modulus was determined as the slope of the true stress-strain curve in the linear elastic range.

Statistical analysis: Data is represented as mean ± standard deviation of at least three replicates per condition. Significant differences were marked as follows: * ($p < 0.05$), ** ($p < 0.01$) and *** ($p < 0.001$) and were calculated with GraphPad Prism 5 software. For comparison of multiple groups at one time point, a one-way ANOVA with Bonferroni posthoc test was used. A two-way ANOVA with Bonferroni posthoc test was performed for comparison of multiple groups at different time points.

5.4. Results and discussion

5.4.1. Bioink composition and dual-stage crosslinking

This study presents a novel 3D printable hyaluronic acid-based bioink that allows for biofunctionalization with tethered TGF-β1 to generate advanced cartilaginous 3D constructs without the need for an exogenous supply of the differentiation factor during long-term culture. Previously, TGF-β1 has been bound to hydrogels via Traut's reagent and other covalent approaches to induce differentiation and ECM production of embedded MSCs or chondrocytes, however, only in non-printable hydrogels.[184-186, 262-264] The HA-based ink presented here utilized a recently established dual-stage crosslinking mechanism,[223] with adapted composition in order to facilitate TGF-β1 tethering. Ink components encompassed thiol-modified hyaluronic acid (HA-SH, 465 kDa), acryl-modified polyethylene glycol (8-arm PEG-acryl, 10 kDa), and allyl-modified PEG (2-arm PEG-allyl, 6 kDa). Successful synthesis of all ink components was verified via GPC and ^{1}H-NMR (Figure III.S1, 5.7. Supporting information). For the newly established 8-arm PEG-acrylate it could be demonstrated that the acrylation was successful and quantitative using the enzymatic catalysis and no oligomers were obtained during modification (Figure III.S1b, 5.7. Supporting information).

Figure III.1 shows the detailed functionalization and crosslinking mechanism of the used ink composition. At first, free lysine residues of TGF-β1 were thiol-modified using Traut's reagent in a 4:1 molar excess of Traut to TGF-β1, as described previously.[184-186] Subsequently, 8-arm PEG-acryl was added to react with thiol-modified TGF-β1 in a spontaneous Michael addition at pH 7.4 (Figure III.1a). In the next step of bioink formulation, all other ink components (HA-SH, 2-arm PEG-allyl, I2959) as well as human MSCs (20 x 10^{6} mL^{-1}) were mixed with the TGF-β1-functionalized PEG-acryl solution. Within 30 minutes of incubation at 37 °C, free acryl groups of PEG-acryl reacted in a Michael addition at pH 7.4 with the main fraction of HA-SH thiol groups to generate a highly viscous and printable bioink (Figure III.1b). After 3D printing, constructs were UV-irradiated at 365 nm to finally crosslink the residual HA-SH thiol groups with allyl groups of PEG-allyl via thiol-ene click chemistry in the presence of the photoinitiator Irgacure I2959 (Figure III.1c). Figure III.1d presents a schematic graphical overview to visualize the ink composition with its two different crosslinking processes. The used ink had an overall polymer content of 1.4 % (0.5 % HA-SH, 0.5 % 8-arm PEG-acryl, 0.4 % 2-arm PEG-allyl and 0.05 % I2959; all w/V), and still enabled stand-alone printability. Such low polymer content has previously been shown to be favorable with regard to diffusion properties and penetrability of cellularly produced ECM in non-printed[156, 157] and printed constructs.[188, 223]

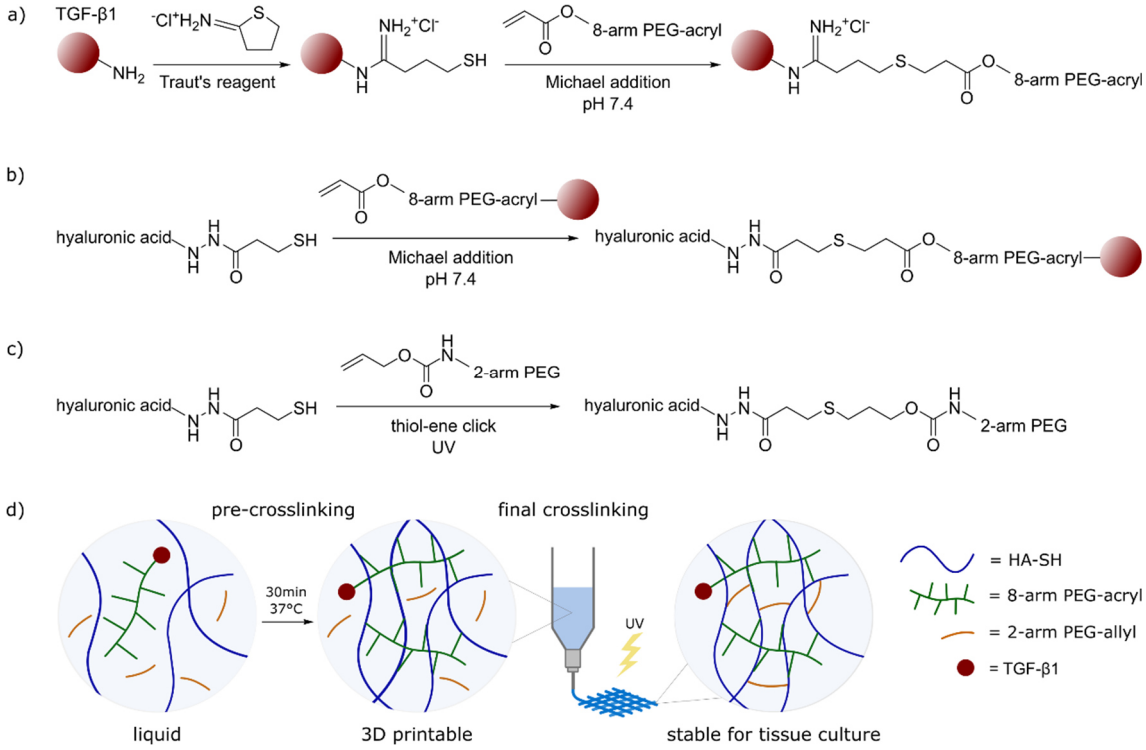

Figure III.1: Ink crosslinking mechanism and functionalization with TGF-β1. a) Thiol-functionalization of TGF-β1 with Traut's reagent and Michael addition with 8-arm PEG-acryl. b) Michael addition of TGF-β1-modified PEG-acryl with HA-SH (pre-crosslinking), resulting in a 3D printable ink. c) UV-induced final crosslinking of residual HA-SH thiol-groups with 2-arm PEG-allyl in the presence of Irgacure I2959 at 365 nm. d) Graphical overview of the dual-stage crosslinking mechanism and workflow of TGF-β1 tethered construct generation for chondrogenic tissue culture.

5.4.2. 3D printing and ink characterization

We have previously characterized printability of dual-stage crosslinked platform bi-oinks in detail.[223] In order to prove printability of the adapted ink with the new component 8-arm PEG-acrylate presented in this study, filament fusion tests and strand thickness evaluations were performed accordingly (Figure III.S2a and b, 5.7. Supporting information). Filaments fused at the smallest distance of 0.5 mm and partially at 0.75 mm, strand thickness measurements yielded the average strand thickness of 650 µm and a strand intersection diagonal of around 1.1 mm, which was well in accordance with the previously reported results of the printable platform inks.[223] Additionally, as a proof-of-principle, a large construct with 21 layers was 3D printed, resembling human femoral condyles (Figure III.S2c, 5.7. Supporting information).

Furthermore, we analyzed biocompatibility of the bioink and possible physical impacts of TGF-β1 tethering on bioink and construct properties. Therefore, the bioink was prepared as described above and printed in 2-layered constructs to enable imaging with a low background signal and quantification of single cells. Figure III.2a shows an overview of the printed grid structures and survival of MSCs directly after printing. To visualize living and dead cells separately, the split channels of a representative image with higher magnification is shown in the second row. Quantification of overall cell survival yielded around 98 % living cells and only 2 %

dead cells after printing. This proved well-adapted printing conditions and confirmed the bioink as a suitable cell carrier.

To assess the potential influence of covalent TGF-β1 tethering to 8-arm PEG-acryl on the gelation and, eventually, viscoelastic properties of the ink, we evaluated the kinetics of the first stage of crosslinking (i.e., the Michael addition). Rheological characterization of time and frequency sweeps were performed on samples without the protein or with 150 nM tethered TGF-β1 (Figure III.2b and c). Time sweep measurements revealed a drastic increase in ink viscosity after 15 minutes and almost complete Michael addition after 30 minutes. This corresponded to empirically defined pre-crosslinking times of this ink in 3D printing experiments for cell culture. Furthermore, covalent incorporation of TGF-β1 did not affect the mobility and reactivity of 8-arm PEG-acryl, and the kinetics of progression of Michael addition was almost identical in both formulations (i.e., without or with tethered TGF-β1). Moreover, the results of frequency sweep experiments showed that after the same incubation time at 37 °C, the formed covalent bonds during Michael addition yielded a similar state of long-range interactions between polymer chains. These results demonstrated that the presence of covalently bound TGF-β1 did not compromise gelation during the first stage of crosslinking.

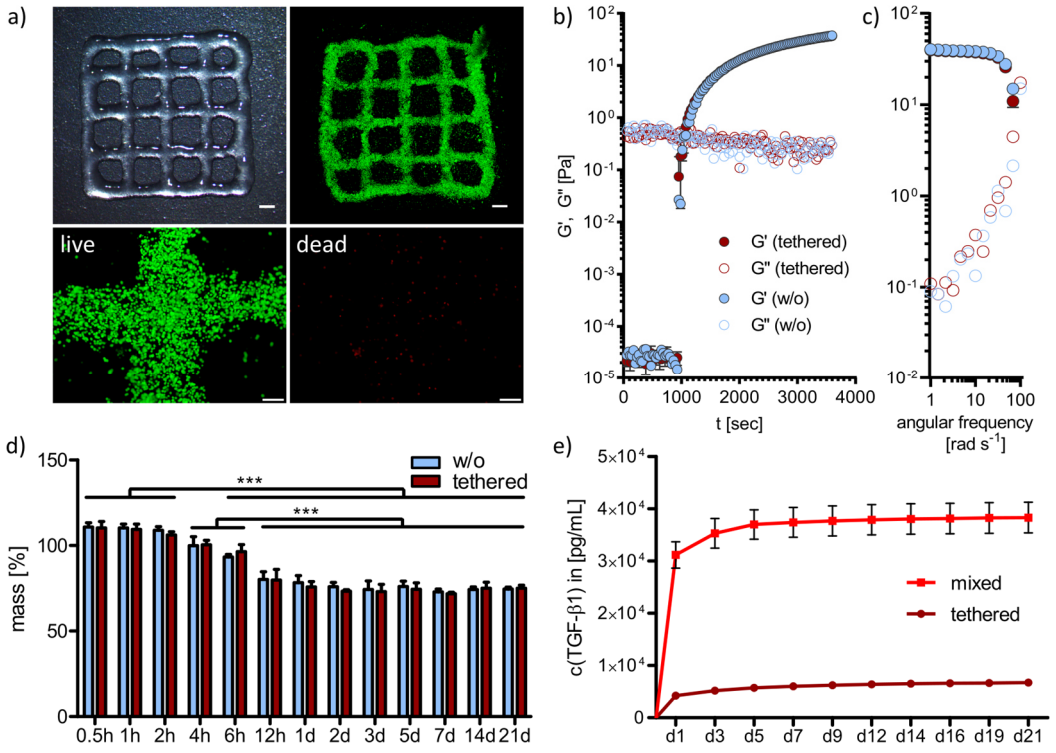

Figure III.2: 3D printing and ink characterization. a) Overview of 3D printed grids and survival of MSCs after printing. Living cells are labeled with calcein-AM (green) and dead cells with EthD-III (red). Scale Bars of overview images represent 2 mm, scale bars of split channel images at higher magnification represent 200 µm. b) Time sweep and c) frequency sweep measurements of the pre-crosslinking reaction (Michael addition) showing the progression and gelation state of inks with 150 nM tethered TGF-β1 or without the protein. d) Swelling analysis of constructs without or with 150 nM tethered TGF-β1 over three weeks. Data are represented as the percentage deviation from the original wet weight (= 100 %) as mean ± standard deviation (n = 3). Significant differences are marked with *** ($p < 0.001$). e) TGF-β1 release from constructs with 150 nM tethered or mixed TGF-β1 over 3 weeks analyzed by ELISA (n = 3). Tested conditions are significantly different at all time points with $p < 0.001$.

For further construct characterization, we examined gel stability after final crosslinking for constructs without or with 150 nM tethered TGF-β1 (Figure III.2d). Therefore, ink was prepared without cells, cast in a defined cylindrical geometry (5 mm diameter, 40 µL volume), and incubated in PBS over three weeks. No significant differences between the constructs with or without tethered TGF-β1 could be detected at all time points (0.5, 1, 2, 4, 6, 12 h, 1, 2, 3, 5, 7, 14, 21 d). Both gel systems initially swelled slightly to 110 % within the first two hours and then started to shrink to around 80 %, reaching their equilibrium state at 12 h after preparation. The swelling process was due to initial water inflow into the hydrogel system and shrinkage may be explained by formation of disulfide bonds between unreacted HA-SH thiol groups. Statistically, all thiol groups should be saturated by PEG-acryl or PEG-allyl crosslinking, but it could not be excluded that some functional groups were not in close proximity to react with each other and accordingly thiols remained available for disulfide formation.

In general, no significant impact of TGF-β1 tethering was detected on ink viscosity or the stability of the crosslinked constructs. Calculations of present equivalents of the reacting compounds during covalent tethering of 150 nM TGF-β1 to the used bioink revealed that one modified TGF-β1 molecule was facing 3.3 x 10^3 PEG-acryl molecules. As the used PEG-acryl crosslinker has eight functional groups per molecule, this means that only approximately every 400^{th} acryl group of the PEG crosslinkers was functionalized with TGF-β1. Accordingly, no impact on ink crosslinking mechanisms and resulting construct stability was expected, even for the highest growth factor concentration investigated.

To further characterize protein tethering within the bioink, we analyzed TGF-β1 release from constructs with 150 nM tethered TGF-β1 (with Traut's reagent) and non-covalently bound TGF-β1 (mixed without Traut's reagent). Therefore, gels without cells were incubated in 1 % BSA/PBS over 21 days and TGF-β1 concentration in the medium was examined via ELISA (Figure III.2e). A burst release was detected for non-covalently bound TGF-β1 (mixed) within the first day and a cumulative release of 3.8 x 10^4 pg mL^{-1} after three weeks. In contrast, only 6.7 x 10^3 pg mL^{-1} diffused out of the constructs with covalently tethered TGF-β1 within the same time. This corresponded to 25.6 % (mixed) and 4.5 % (tethered) of initially applied protein, respectively. Hyaluronic acid contains many hydrophilic groups that can interact via electrostatic forces with positively charged amino acid residues on growth factors,[179, 265-267] which might be the reason for the relatively low protein release of 25.6 % in the mixed group. However, significantly lower TGF-β1 release of 4.5 % was observed in the tethered group confirming effective growth factor thiol-functionalization with Traut's reagent and PEG-acryl tethering via Michael addition.

5.4.3. Impact of TGF-β1 concentration and administration on MSC differentiation

After successful material characterization, we analyzed the chondrogenic potential of the biofunctionalized ink. To examine the optimal growth factor concentration for chondrogenic differentiation of human MSCs, constructs were prepared and cast as described above with either covalently tethered or only mixed TGF-β1, i.e., with or without Traut's reagent, in different concentrations (10 nM, 50 nM, 100 nM and 150 nM) and cultured in TGF-β1-free differentiation medium for 21 days. As a control, constructs without incorporated TGF-β1 were cultured in differentiation medium supplemented with 10 ng mL^{-1} TGF-β1 at each medium change, or without the supplementation as negative control. Cell survival was very good under all conditions after construct preparation on day 1 as well as after 21 days in the respective culture conditions (Figure III.S3, 5.7. Supporting information). Glycosaminoglycans (GAG) and collagens, as the main components of natural cartilage ECM, were analyzed in the MSC-laden constructs after 21 days (Figure III.3).

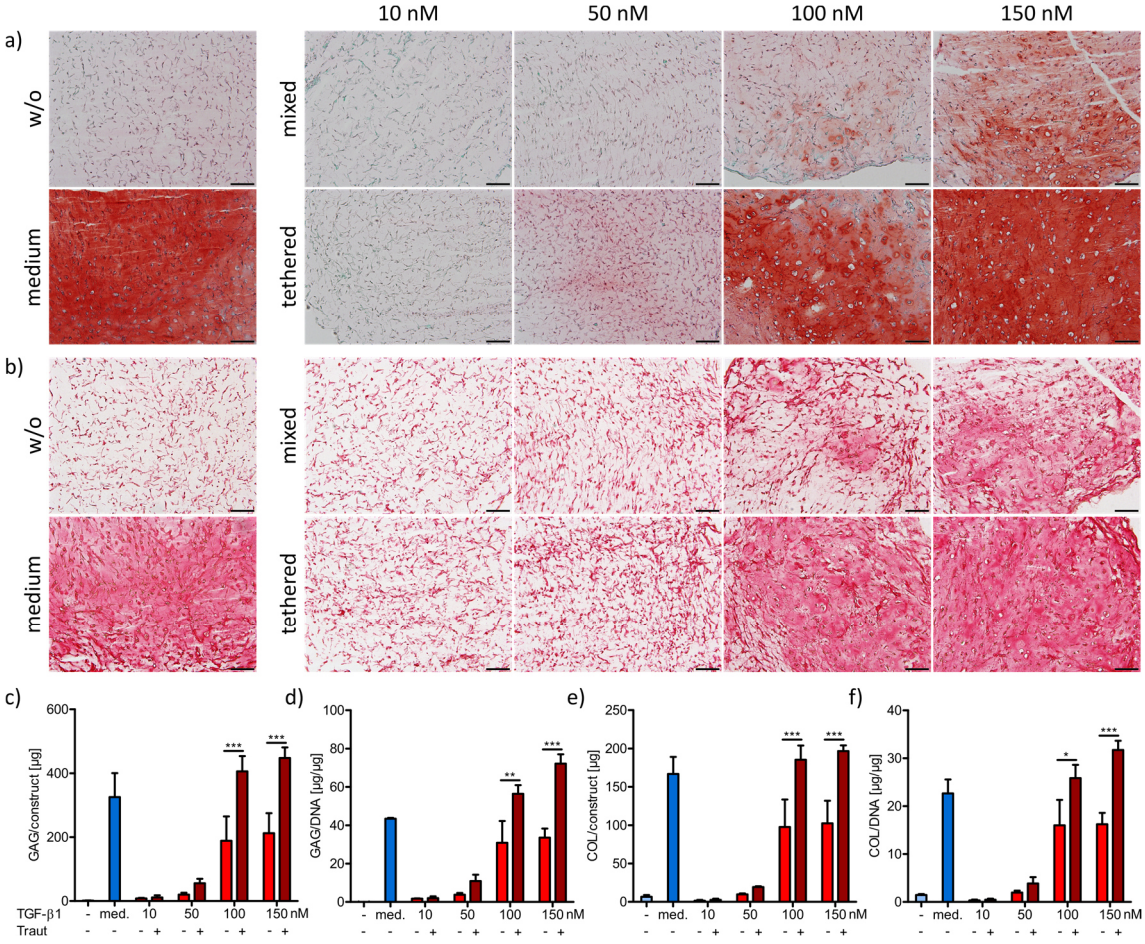

Figure III.3: Histological staining and quantification of ECM components in cast constructs after 21 days. a) Staining for GAG (safranin O) and b) collagen (picrosirius red) in constructs with 10, 50, 100 or 150 nM mixed (- Traut) or tethered (+ Traut) TGF-β1, as well as control groups cultured without (w/o, -) or with TGF-β1 (med.) as medium supplement. Scale bars represent 100 µm. c) Quantification of glycosaminoglycan (GAG) content in the constructs and d) normalized to DNA. e) Quantification of collagen (COL) content in the constructs and f) normalized to DNA. Data are represented as mean ± standard deviation (n = 3). Significant differences are marked with * ($p < 0.05$), ** ($p < 0.01$) and *** ($p < 0.001$).

Constructs without TGF-β1 supplementation showed no GAG (Figure III.3a) and collagen (Figure III.3b) production, while control constructs in medium supplemented with TGF-β1 showed strong differentiation. In the constructs with incorporated TGF-β1, the production of both GAG and collagen increased with increasing growth factor concentrations (10 – 150 nM), and importantly, tethered TGF-β1 induced markedly higher ECM production compared to the corresponding mixed conditions. These results were observed in histological stainings (Figure III.3a and b), and further confirmed by quantification of total GAG and collagen amounts in the constructs (Figure III.3c and e) as well as amounts normalized to DNA content (Figure III.3d and f). The concentrations of 10 nM and 50 nM TGF-β1 (tethered (+ Traut) and mixed (- Traut)) were not sufficient to induce adequate chondrogenic differentiation of MSCs. The concentrations of 100 nM and 150 nM tethered TGF-β1 allowed for high amounts of newly produced GAG and collagen, while non-tethered (mixed) TGF-β1 at 100 nM and 150 nM resulted in significantly reduced differentiation capacity.

In general, TGF-β1 concentration of 150 nM exhibited the best results regarding ECM production and distribution. Therefore, this concentration was used in the following printing studies. Constructs with 150 nM tethered TGF-β1 and control constructs in medium supplemented with TGF-β1 demonstrated that a homogeneous ECM distribution was achievable. This was likely due to the low overall polymer content of the used hydrogel composition (1.4 %) and validated this ink as a beneficial cell carrier for cartilage biofabrication.[68, 156, 157] Concentration dependence of MSC or chondrocyte differentiation induced by TGF-β1 tethered via Traut's reagent has been previously analyzed in not-printable hydrogels.[184-186] Only one study compared tethered with mixed TGF-β1 incorporation and detected very similar differences as those found in this study.[184] All presented results clearly indicated the superior effect of covalently tethered TGF-β1 into the ink compared to non-covalently incorporated growth factor (mixed). This can be partially explained by the differences in TGF-β1 release profiles between the conditions (Figure III.2e). A further explanation might be that free TGF-β1 can undergo endocytosis and degradation when bound to the cell surface receptor on MSCs, thus reducing the available protein concentration.[268, 269] In contrast, covalently tethered protein might trigger prolonged signaling without potential internalization.

5.4.4. Investigation of TGF-β1 functionality after bioprinting

Extrusion based bioprinting enables precise patterning of cells and biomaterials in a desired 3D structure, but still, incorporated cells and proteins can suffer from shear stresses during the printing process.[205, 257, 258, 270, 271] Therefore, we examined TGF-β1 functionality in cast and printed bioinks with 150 nM covalently tethered TGF-β1 as well as non-covalently incorporated protein (mixed). Chondrogenic differentiation of incorporated MSCs was used as a reliable readout for protein function. As a control, we used cast and printed constructs fabricated without

TGF-β1 and subsequently cultured in differentiation medium either without the protein or supplemented with 10 ng mL^{-1} soluble TGF-β1 at every medium change. To examine the influence of the printing process, bioinks were either pipetted in disk form (5 mm diameter, 40 µL volume) (cast) or first extruded at the same printing conditions used for grid printing (Figure III.2a) and afterwards pipetted in the same geometry (print). This procedure enabled final gelation in the same construct geometry to facilitate comparability and avoid the potential impact of different nutrient and oxygen supply in differently shaped constructs.[188, 209, 210] Cell survival was very good in all conditions on day 1 and after 21 days, without differences between cast and printed approaches (Figure III.S4, 5.7. Supporting information).

5.4.4.1. TGF-β1 signaling and chondrogenic gene expression

TGF-β1 induces the canonical Smad-dependent signaling cascade through binding to the cell surface receptors of MSCs. Upon receptor binding, Smad2/3 is phosphorylated and translocates to the nucleus where it is involved in chondrogenic target gene expression.[272-274] To detect the possible impact of the printing process on TGF-β1 functionality, Smad phosphorylation was analyzed via Western blotting (Figure III.4).

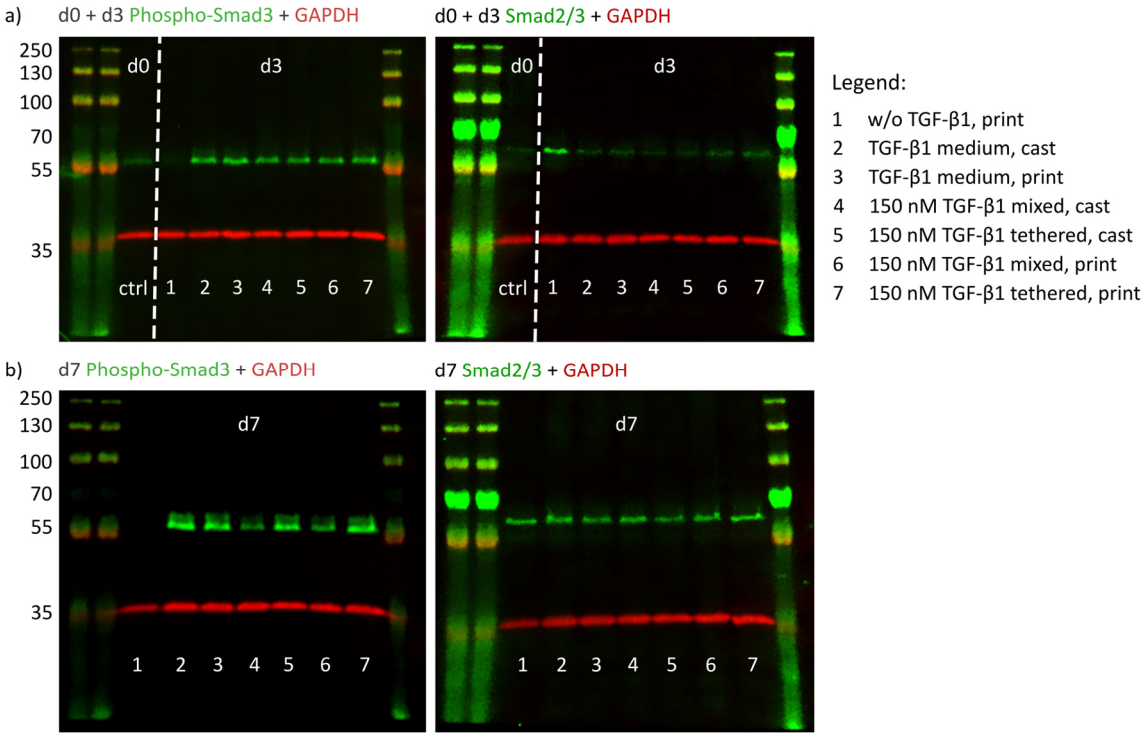

Figure III.4: Western blot analysis of TGF-β1/Smad signaling in cast and printed constructs. Cast and printed constructs with 150 nM mixed (- Traut) or tethered (+ Traut) TGF-β1 were analyzed for their protein expression. Constructs cultured without or with TGF-β1 as medium supplement served as controls. Samples were analyzed directly after fabrication (d0, ctrl) and all test conditions after a) 3 and b) 7 days. TGF-β1-induced active Smad signaling is shown by staining of phosphorylated Smad3 (P-Smad3) and can be compared with the unphosphorylated levels of the transcription factor (Smad2/3) (expected M_W 52 kDa). GAPDH served as loading control (expected M_W 38 kDa). The protein ladder is labeled on the left (protein M_W 35 – 250 kDa).

As a first response to TGF-β1 binding, Smad2/3 phosphorylation was expected early during culture. Furthermore, the initial burst release of unbound TGF-β1 was determined during the first three days (Figure III.2e). For these reasons, we analyzed cast and printed constructs with 150 nM covalently tethered or mixed TGF-β1 for activated phospho-Smad3 (P-Smad3) proteins after 3 and 7 days of culture. As a control, constructs without TGF-β1 were harvested directly after preparation, i.e. before incubation in culture medium (d0). After 3 days, activated P-Smad3 was found in all constructs which had contact to TGF-β1, independent of application (lanes 2 – 7). Only the constructs without TGF-β1 (lane 1) lacked P-Smad3. Basal levels of unphosphorylated Smad2/3 were detected in all constructs, although to a distinctly lesser extent in the conditions with TGF-β1 (Figure III.4a). After 7 days, medium controls (lanes 2 and 3), as well as the constructs with 150 nM covalently tethered TGF-β1 (lanes 5 and 7) contained high levels of P-Smad3, while constructs with 150 nM mixed TGF-β1 (lanes 4 and 6) showed distinctly lower concentrations. Constructs without TGF-β1 (lane 1) completely lacked the activated P-Smad3 protein. Unphosphorylated Smad2/3 protein was detected evenly in all conditions (Figure III.4b). Importantly, no obvious differences in Smad phosphorylation could be determined between cast and printed constructs.

As a further step in the signaling cascade, expression of the chondrogenic genes aggrecan and collagen type II, main components of natural cartilage ECM, was evaluated. Cast and printed constructs with 150 nM tethered or mixed TGF-β1 were analyzed after 3, 7, 14 and 21 days and compared to control constructs cultured without or with the protein as medium supplement (Figure III.5). In general, all constructs with MSCs subjected to TGF-β1 showed strongly elevated expression levels compared to MSCs in constructs cultured without TGF-β1. Aggrecan (ACAN) and collagen type II (COL2A1) expression during the first week of culture revealed no significant differences between the TGF-β1 conditions, however, after 14 and 21 days, constructs with tethered TGF-β1 exhibited increased ACAN and COL2A1 expression, as compared to the constructs with mixed TGF-β1 (Figure III.5a and b). Furthermore, no impact of the printing process was observed for both genes in all conditions.

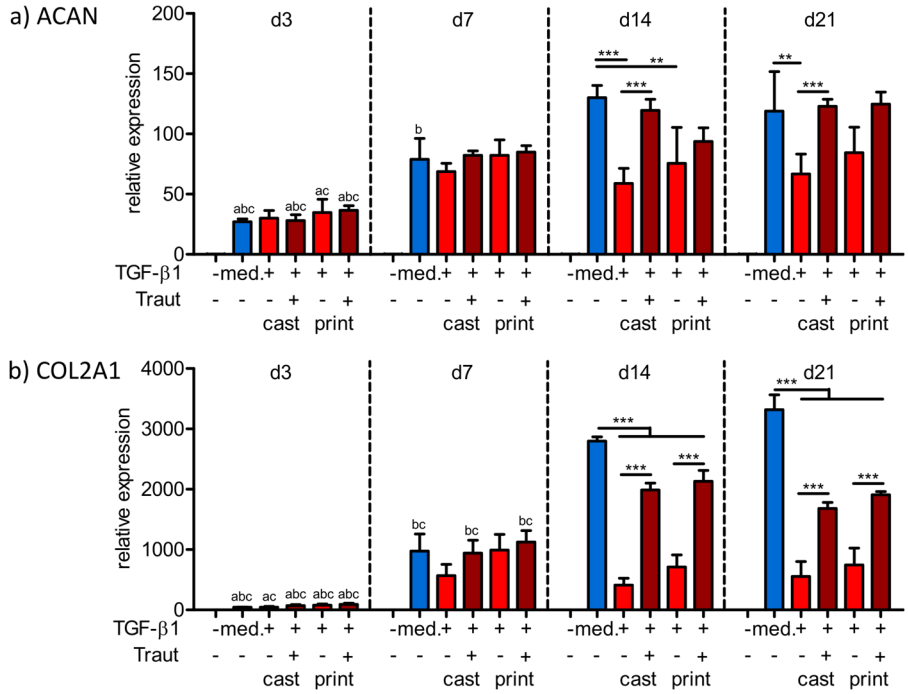

Figure III.5: Gene expression analysis of cast and printed constructs. qRT-PCR was performed on gene expression of MSCs in cast and printed constructs with 150 nM mixed (- Traut) or tethered (+ Traut) TGF-β1. Printed constructs cultured without or with TGF-β1 as medium supplement served as controls. Expression of a) aggrecan (ACAN) and b) collagen type II (COL2A1) was determined after 3, 7, 14 and 21 days and normalized to EEF1A1 and MSCs in 2D on day 0. Data are presented as mean ± standard deviation (n = 3). Significant differences between groups are marked with ** ($p < 0.01$) and *** ($p < 0.001$). *Legend:* (a) Significantly different to corresponding value of the same group at day 7 (at least $p < 0.05$), (b) significantly different to corresponding value of the same group at day 14 (at least $p < 0.05$), (c) significantly different to corresponding value of the same group at day 21 (at least $p < 0.05$).

5.4.4.2. ECM production and distribution

An important feature of bioinks for cartilage engineering is the support of MSC differentiation and the necessary porosity for ECM distribution. Figure III.6 shows histological and immunohistochemical stainings of cartilage-specific ECM components produced by embedded MSCs during 21 days.

Control images of day 1 are presented in the Supporting information (5.7., Figure III.S5). MSCs cultured in constructs without TGF-β1 were not able to differentiate and produced hardly any ECM components, while constructs in medium supplemented with TGF-β1 showed marked differentiation (Figure III.6, left). A concentration of 150 nM tethered TGF-β1 yielded strong ECM production and a homogeneous distribution comparable to the medium control, while the same protein concentration without covalent binding (mixed) was distinctly less effective (Figure III.6, right). This observation was valid for all stained ECM components, i.e. total GAG and collagen stained by safranin O and picrosirius red (Figure III.6a and c), and specific IHC staining of aggrecan and collagen type II (Figure III.6b and d). The fibrocartilage marker collagen type I was produced to a low extent in all groups receiving TGF-β1 (Figure III.S6, 5.7. Supporting

information). Importantly, no difference between cast and printed constructs were determined in any condition.

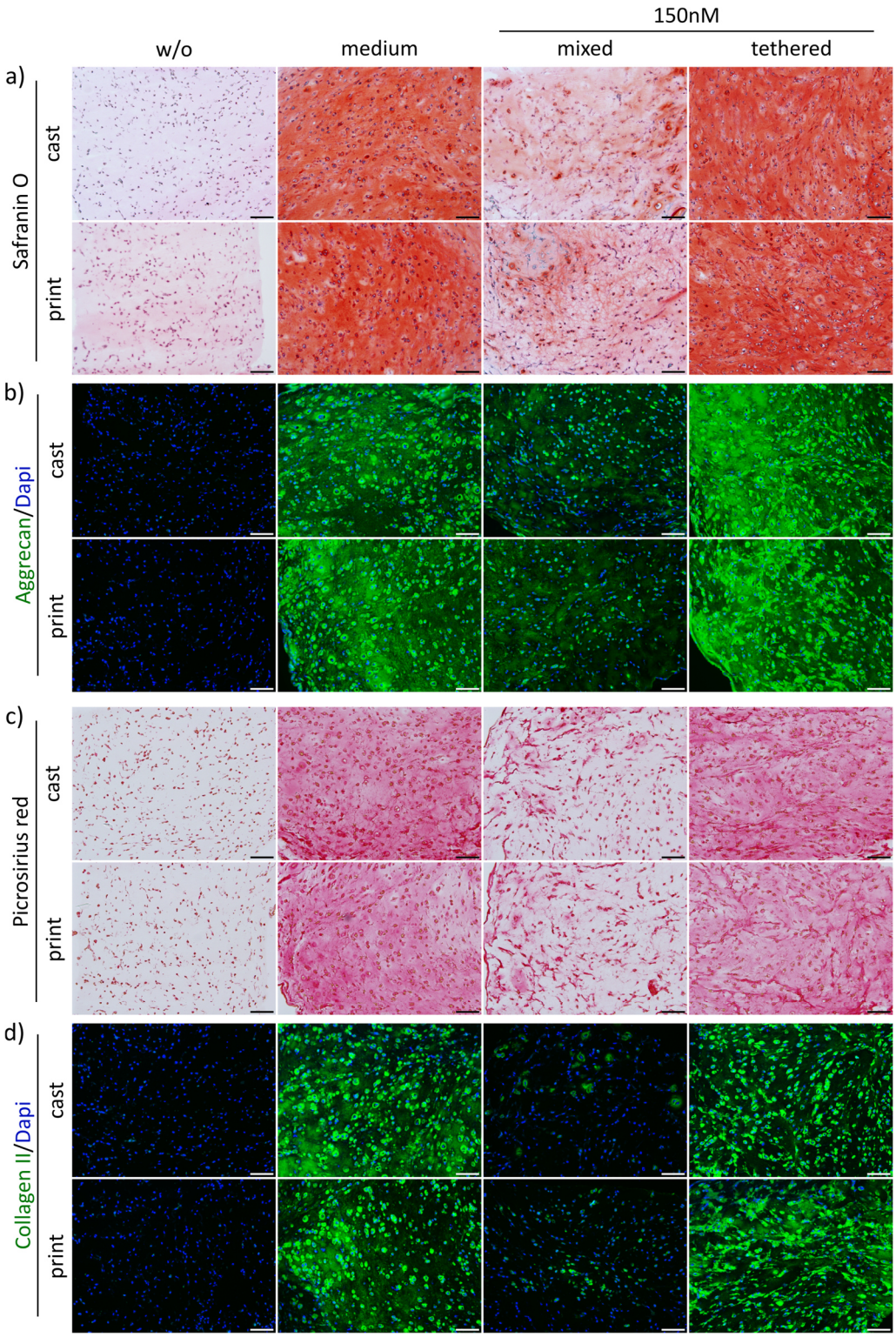

Figure III.6: Histological and immunohistochemical (IHC) staining of MSC-derived ECM components in cast and printed constructs. Cast and printed constructs with 150 nM mixed (- Traut) or tethered (+ Traut) TGF-β1 were analyzed after 21 days. Constructs cultured without (w/o) or with TGF-β1 as medium supplement (medium) served as controls. GAG production and distribution is depicted by a) safranin O staining and b) IHC staining of aggrecan. Collagen production and distribution is visualized by c) picrosirius red staining and d) IHC staining of collagen type II. Nuclei were counterstained with DAPI. Scale bars represent 100 µm.

To further validate the visual observations, we quantified GAG and collagen contents of all cast and printed constructs after 21 days with biochemical assays (Figure III.7). The analysis revealed very low GAG and collagen deposition in constructs cultured without TGF-β1, while constructs with continuous TGF-β1 medium supplementation produced high ECM amounts (Figure III.7a and d, blue bars). GAG and collagen contents in constructs with 150 nM tethered TGF-β1 were comparable to the positive control (medium), although no additional growth factor was added during the three weeks of cell culture. MSCs in constructs with 150 nM mixed TGF-β1 produced significantly lower amounts of ECM components compared to constructs in which the same protein concentration was covalently bound (Figure III.7a and d, red bars). The same significant differences were detected when GAG and collagen contents were normalized to the DNA content (Figure III.7b and e) as well as when total production was compared, i.e. the combined ECM contents in the construct and the supernatant collected during culture time (Figure III.7c and f). All initial values at day 1 as well as the analyzed DNA contents can be found in the Supporting information (5.7., Figure III.S7). In general, the quantitative results well confirmed the histological findings and again, there was no difference detected between cast and printed approaches.

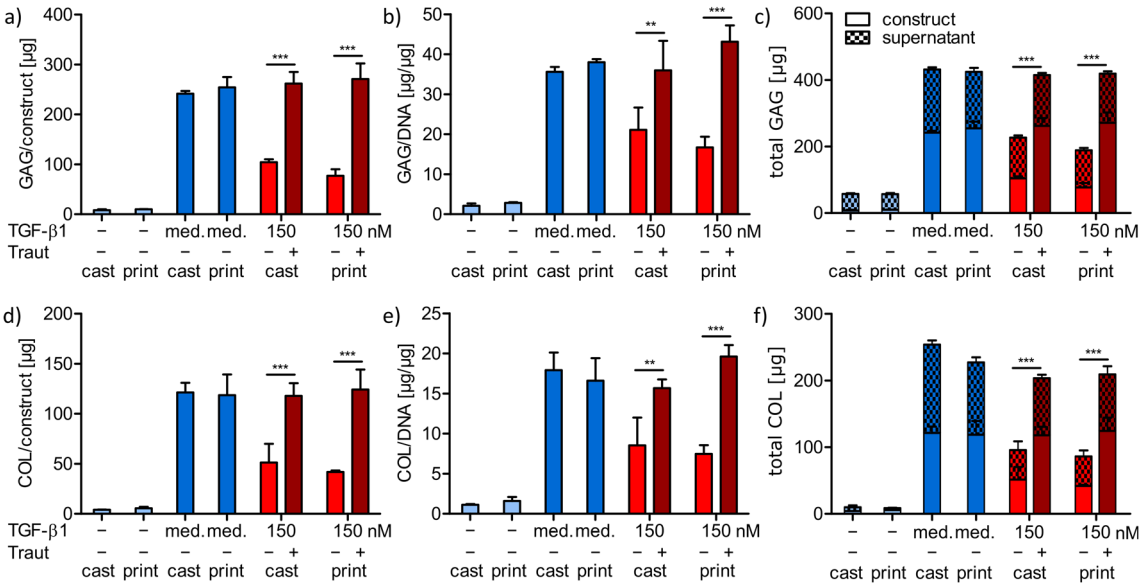

Figure III.7: Quantification of MSC-derived ECM components in cast and printed constructs. Cast and printed constructs with 150 nM mixed (- Traut) or tethered (+ Traut) TGF-β1 were analyzed after 21 days. Constructs cultured without (-) or with TGF-β1 as medium supplement (med.) served as controls. GAG content is shown for a) the constructs and b) normalized to DNA. c) Total GAG production was quantified by adding the content of the constructs and the collective culture supernatant. Collagen content is shown for d) the constructs and e) normalized to DNA. f) Total collagen production was quantified by adding the content of the constructs and the collective culture supernatant. Data are represented as mean ± standard deviation (n = 3). Significant differences are marked with ** ($p < 0.01$) and *** ($p < 0.001$).

5.4.4.3. Correlation of ECM production and construct stiffness

As an important mechanical feature of engineered cartilage, we analyzed the Young's modulus of cast and printed constructs with 150 nM tethered or mixed TGF-β1 after construct preparation at day 1 as well as after 21 days of chondrogenic differentiation. Constructs cultured without TGF-β1 or with the soluble protein as continuous medium supplementation served as controls (Figure III.8). Initially, all constructs appeared very weak and without significant differences between the conditions (all around 2.5 – 5.0 kPa at day 1). Constructs cultured without TGF-β1 maintained their weak appearance or even decreased in stiffness within 21 days to around 1.6 kPa. MSCs in constructs with TGF-β1 addition in the culture medium differentiated well and produced high amounts of ECM. This correlated with a significant increase in Young's modulus to 73.2 kPa for cast and 76.0 kPa for printed constructs (Figure III.8, blue bars). Covalently tethered TGF-β1 also induced a significant increase in stiffness to 105.5 kPa for cast and 112.1 kPa for printed constructs after 21 days, while the mixed condition only resulted in 35.6 kPa and 38.2 kPa, respectively (Figure III.8, red bars).

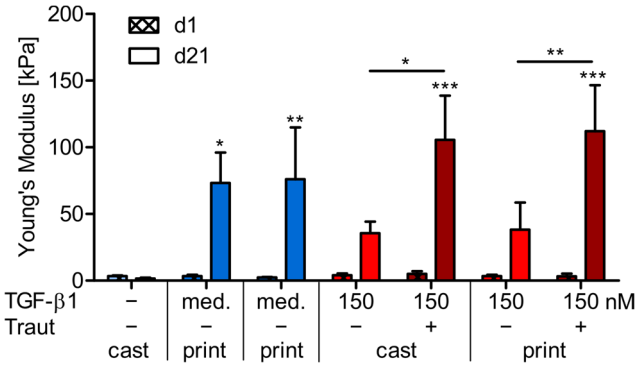

Figure III.8: Mechanical characterization of cast and printed constructs. Young's modulus of cast and printed constructs with 150 nM mixed (- Traut) or tethered (+ Traut) TGF-β1 after 1 and 21 days. Constructs cultured without (-) or with TGF-β1 as medium supplement (med.) served as controls. Data are presented as mean ± standard deviation (n = 6). Significant differences between groups are marked with * ($p < 0.05$), ** ($p < 0.01$) and *** ($p < 0.001$). Stars above bars on day 21 indicate significant differences to the corresponding value of the same group on day 1.

In general, bioinks with high polymer contents result in initially stiffer hydrogel networks with good 3D printability, but are often associated with limited cell growth, differentiation and ECM distribution.[68] In a previous study of our group, we demonstrated that the distribution of newly produced ECM molecules was significantly improved in bioinks with a low polymer content which was associated with an increased construct stiffness after chondrogenic differentiation.[188] This was shown for bioinks with 3 % polymer content which needed PCL-support structures for 3D printability. The dual-stage crosslinked bioink presented here is stand-alone 3D printable and still allows for an even lower polymer content of 1.4 %. Although it exhibited a comparably weak network in the beginning, this bioink enabled homogenous ECM distribution and thereby

significantly increased construct stiffness after three weeks in constructs with strong MSC differentiation (tethered TGF-β1 and medium control). Compared to constructs with non-covalently incorporated TGF-β1, MSCs in constructs with tethered TGF-β1 expressed distinctly higher amounts of cartilaginous ECM with a more homogeneous distribution throughout the constructs (Figure III.6 and III.7), which correlated well with a markedly higher construct stiffness (Figure III.8). This was again independent of bioink processing, i.e. no differences between cast and printed constructs were observed.

5.5. Conclusion

In this study, we established a dual-stage crosslinked hyaluronic acid-based bioink which is 3D printable and enables covalent tethering of TGF-β1. In previous reports, other printable materials were also described for growth factor administration in chondrogenic or osteogenic regeneration approaches, however, proteins were only mixed within the bioinks or administered via nanospheres but not covalently tethered.[65, 182, 275-277] In our study, it was shown that both processes, tethering and 3D printing, did not affect protein functionality or bioink properties. Covalent TGF-β1 tethering enabled prolonged availability for embedded MSCs and markedly enhanced chondrogenic differentiation, as compared to the growth factor non-covalently incorporated in the ink. Furthermore, the low polymer content of the presented ink composition facilitated a penetrable network with chondro-supportive properties and allowed for homogenous ECM distribution and a distinct increase of construct stiffness during chondrogenic differentiation of embedded MSCs. Taken together, this ink composition enabled the generation of high-quality cartilaginous tissues without the need for continuous exogenous supply and, thus, bears great potential for future investigation towards cartilage regeneration. Moreover, the observation that a tethered growth factor within a printed bioink can lead to superior tissue development may also be explored in other applications in biofabrication.

5.6. Acknowledgements

This research was funded by the Deutsche Forschungsgemeinschaft (DFG, German Research Foundation) – Project number 326998133 – TRR 225 (subprojects A02, A06 and B02). The publication was supported by the Open Access Publication Fund of the University of Würzburg. The authors thank the Orthopedic Centre for Musculoskeletal Research, University of Würzburg, for providing bone samples for MSC isolation.

5.7. Supporting information

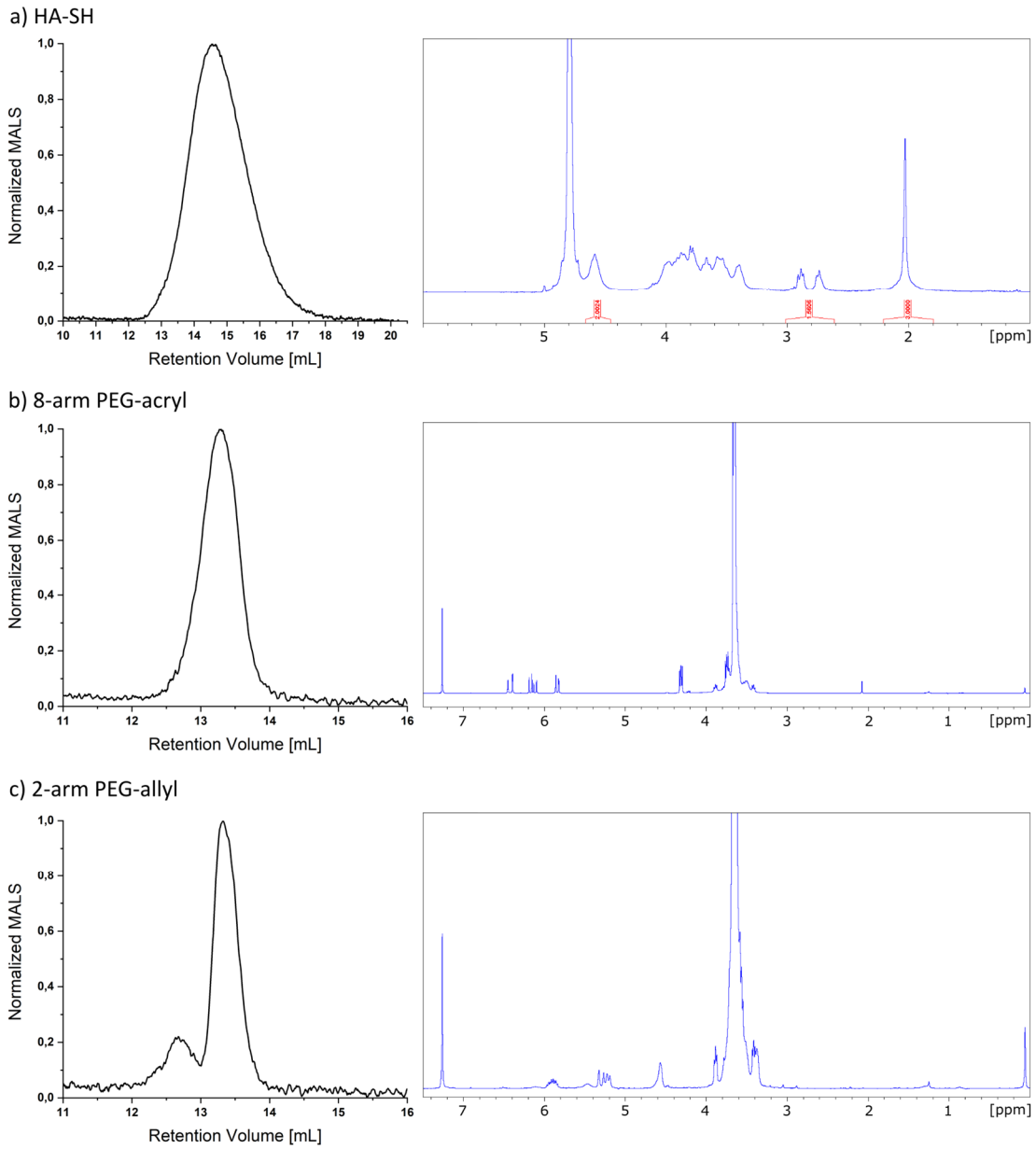

Figure III.S1: Characterization of bioink components. GPC elugrams (left) and ^{1}H-NMR spectra (right) of a) HA-SH (300-MHz, D_2O) δ (ppm) = 1.82-2.20 (s, 3 H, *N*-acetyl), 2.57-3.00 (m, thiol-modification), 3.20-4.20 (m, 10 H, HA-backbone), 4.40-4.70 (s, 2 H, anomeric protons); b) 8-arm PEG-acryl (300 MHz, $CDCl_3$) δ (ppm) = 3.33-3.99 (m, PEG-backbone and satellites), 4.18-4.38 (t, 2 H, PEG-O-CH_2-C*H*$_2$-O-acryl) 5.76-6.50 (d/dd, *CH*=*CH*$_2$) after TFAA addition; and c) 2-arm PEG-allyl (300 MHz, $CDCl_3$) δ (ppm) = 3.15-4.09 (m, PEG-backbone and satellites), 4.43-4.76 (m, PEG-O-CH_2-C*H*$_2$-N-), 5.11-6.07 (d/d/m, O-C*H*$_2$-C*H*=C*H*$_2$), 5.38 (s, -N*H*-C(=O)-O-) after TFAA addition.

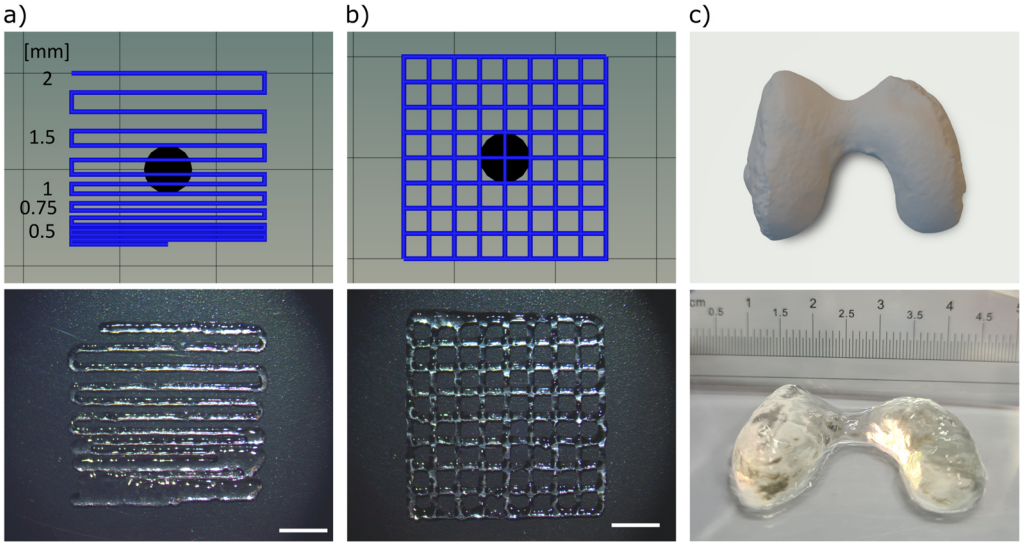

Figure III.S2: 3D printability assessment. a) Filament fusion test (strand distance indicated next to the G-code) and b) 2-layered grid structure used for strand thickness and intersection diagonal measurements. G-codes are represented in the upper row, printed constructs in the lower row. Scale bars represent 5 mm. c) CAD model of human femoral condyles (top) and the corresponding 3D printed 21-layered construct (bottom).

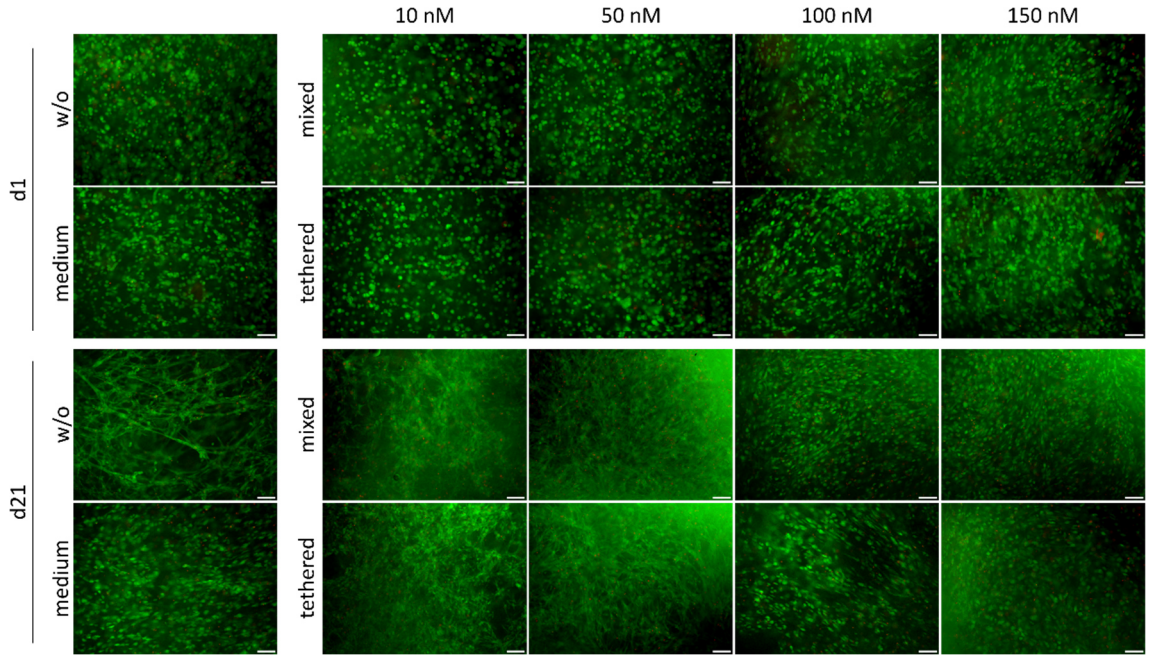

Figure III.S3: Cell survival of MSCs in cast constructs. Survival was analyzed on day 1 and 21 in constructs with 10, 50, 100 or 150 nM mixed or tethered TGF-β1, as well as control groups cultured without (w/o) or with TGF-β1 as medium supplement (medium). Living cells are stained with calcein-AM and appear in green, dead cells are stained with EthD-III and appear red. Scale bars represent 100 µm.

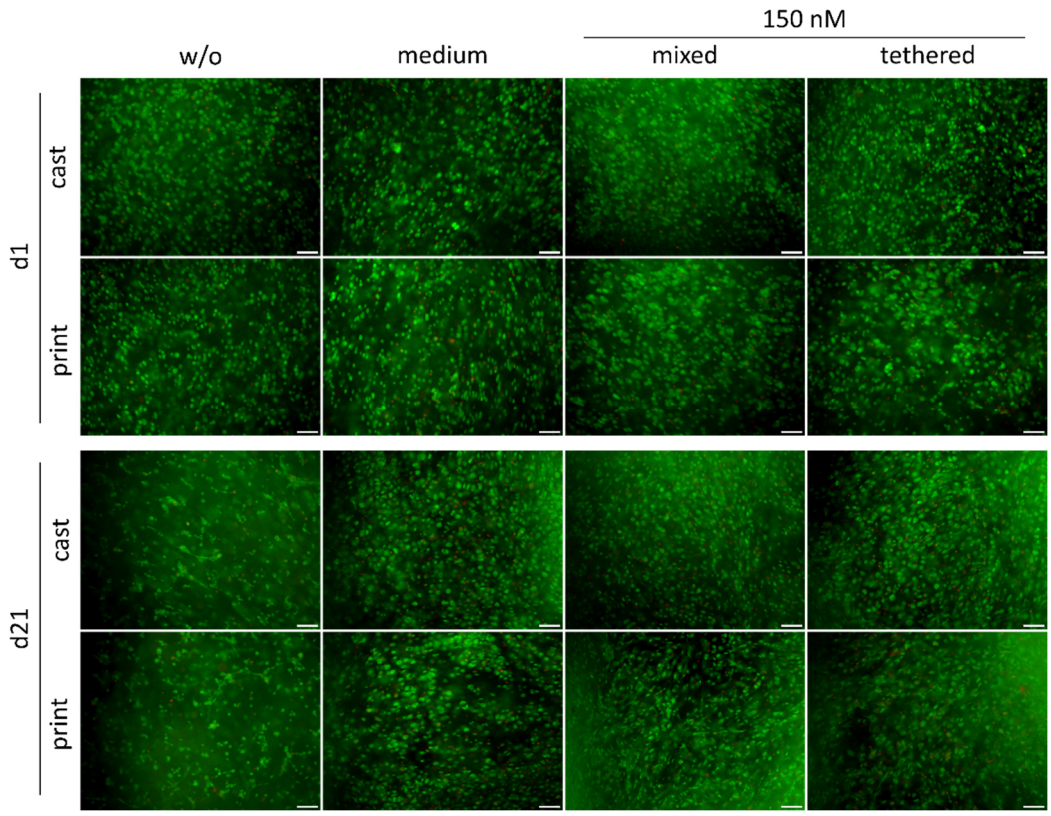

Figure III.S4: Cell survival of MSCs in cast and printed constructs. Cell survival was analyzed after 1 and 21 days in cast and printed constructs with 150 nM mixed (- Traut) or tethered (+ Traut) TGF-β1. Constructs cultured without (w/o) or with TGF-β1 as medium supplement (medium) served as control. Living cells are stained with calcein-AM and appear in green, dead cells are stained with EthD-III and appear red. Scale bars represent 100 µm.

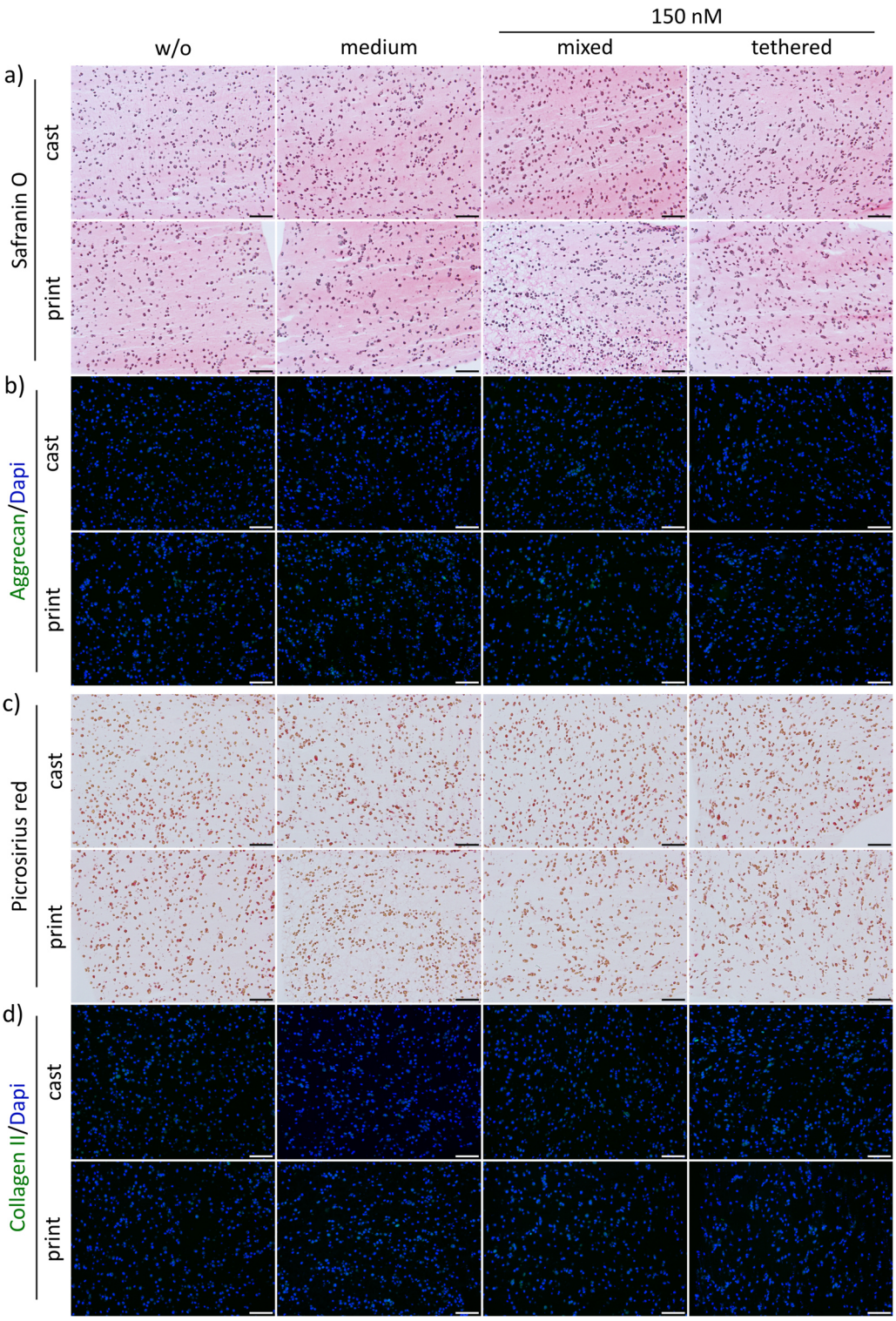

Figure III.S5: Histological and immunohistochemical (IHC) staining of ECM components in cast and printed constructs after 1 day. Cast and printed constructs were stained for a) GAG (safranin O) b) aggrecan, c) collagen (picrosirius red) and d) collagen type II. Nuclei were counterstained with DAPI. Scale bars represent 100 µm.

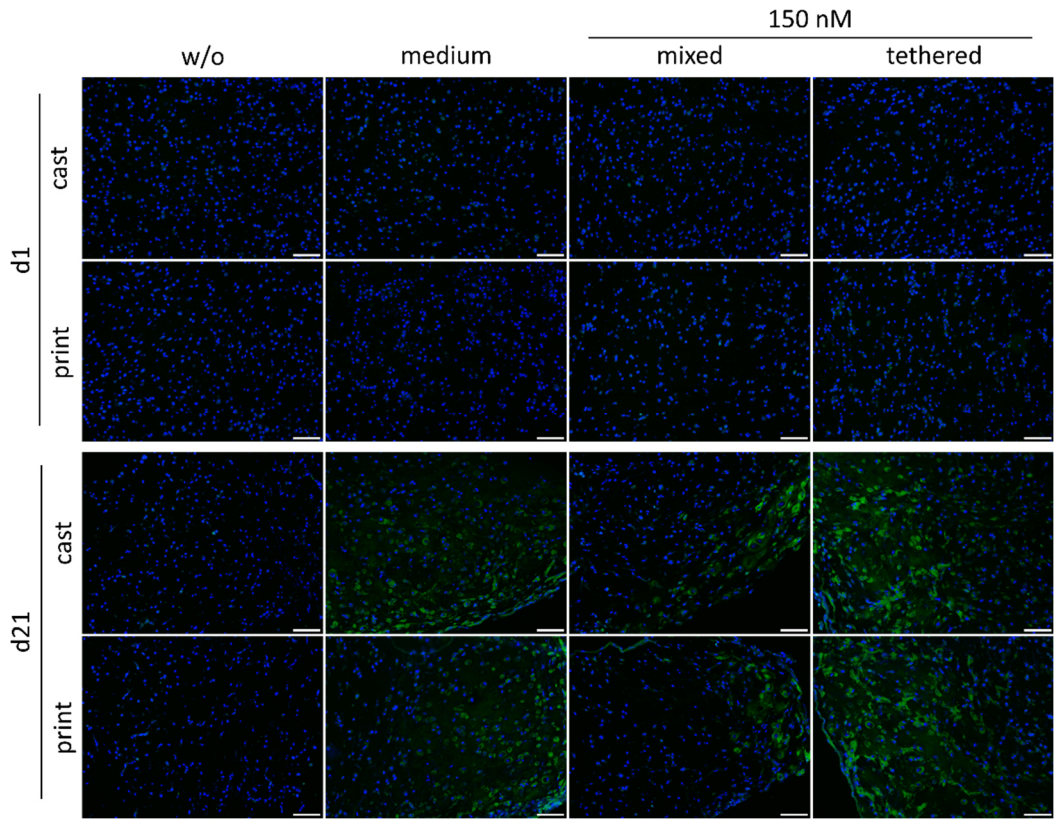

Figure III.S6: Immunohistochemical (IHC) staining of collagen type I in cast and printed constructs. Collagen type I was stained after 1 and 21 days in cast and printed constructs with 150 nM mixed (- Traut) or tethered (+ Traut) TGF-β1. Constructs cultured without or with TGF-β1 as medium supplement served as control. Nuclei were counterstained with DAPI. Scale bars represent 100 µm.

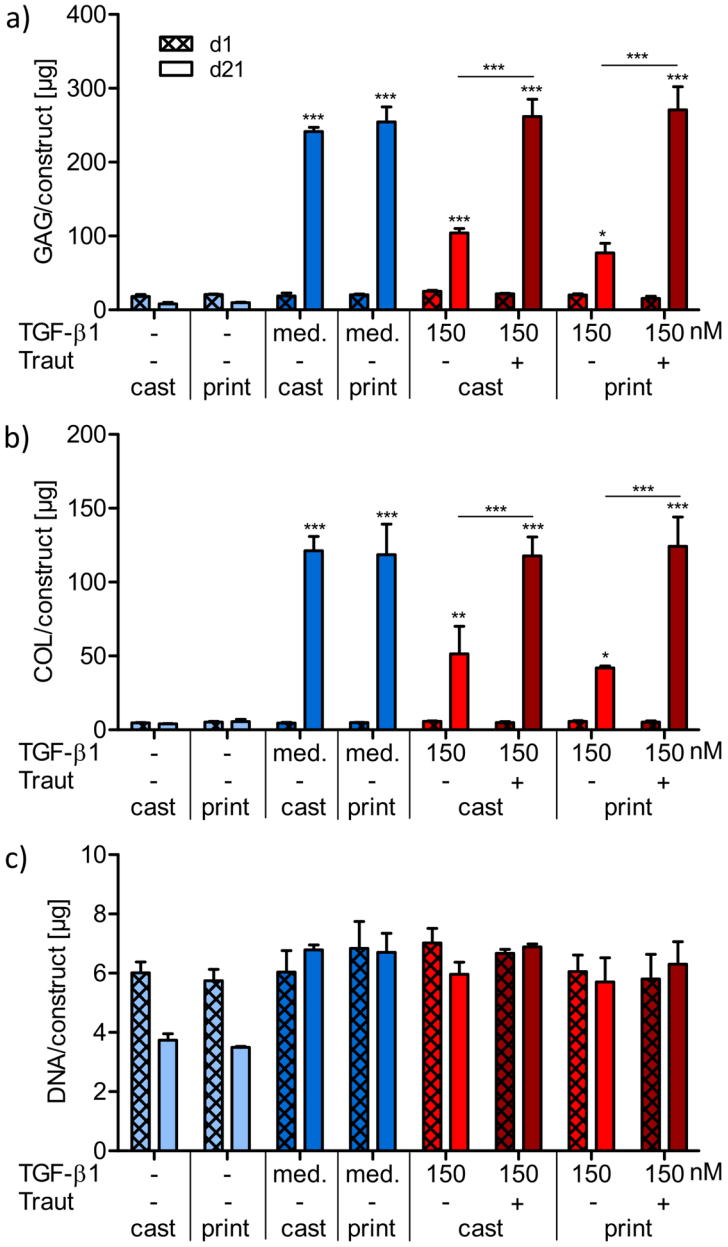

Figure III.S7: Quantification of ECM components at day 1 and 21 in cast and printed constructs. Quantification of a) GAG, b) collagen and c) DNA content in constructs with 150 nM mixed (- Traut) or tethered (+ Traut) TGF-β1. Constructs cultured without (-) or with TGF-β1 as medium supplement (med.) served as control. Data are represented as mean ± standard deviation (n = 3). Significant differences are marked with * ($p < 0.05$), ** ($p < 0.01$) and *** ($p < 0.001$). Stars above bars on day 21 indicate significant differences to the corresponding value of the same group on day 1.

Table III.S1: qRT-PCR primer sequences.

	Primer	**Sequence**
1	ACAN forward	5'- TACGACGCCATCTGCTACAC-3'
2	ACAN reverse	5'- GACGGTGATGTCCTCCTCAC-3'
3	COL2A1 forward	5'- CTGTCCTTCGGTGTCAGGG-3'
4	COL2A1 reverse	5'- CAGACACAGATCCGGCAGG-3'
5	EEF1A1 forward	5'- GCCCATGTGTGTTGAGAGC-3'
6	EEF1A1 reverse	5'- CCGCAACTGTCTGTCTCATATC-3'

Synthesis of the different ink components

Synthesis of 3,3'-dithiobis(propanoic dihydrazide) (DTPH): The synthesis was performed according to Vercruysse et al.[236] with slight modifications. In brief, dimethyl 3,3'-dithiodipropionate (1 eq.) was dissolved in methanol, cooled to 0 °C and an excess of hydrazine monohydrate (8.0 eq.) was added. The reaction solution was stirred at 0 °C for 4 h following another 16 h at rt. The supernatant of the resulting suspension was discarded, the sediment was washed with methanol and subsequently with diethyl ether. The final product was dried in vacuo to form a white, shiny solid.

Synthesis of thiolated hyaluronic acid (HA-SH): The synthesis was performed according to Stichler et al.[147] with slight modifications. Hyaluronic acid (HA) (3.0 g, 1.0 eq.) was dissolved in 300 mL MilliQ overnight at 37 °C. NHS (4.0 eq.) and DTPH (4.0 eq.) were dissolved in 300 mL Sørensen buffer (0.2 M, pH 5.5) at rt, both solutions were combined and mixed. EDC (7.5 eq.) was added, the pH was lowered to 4.0 with 10 % HCl and the mixture was incubated for 4 h at 37 °C. After a pH adjustment to over 8.5 with 2 N NaOH, DTT (5.0 eq.) was added, and the mixture was incubated overnight at 37 °C to form a clear, brownish solution. The pH was set to 3.0 with 10 % HCl following a dialysis (MWCO 1 kDa, RC) against K_2HPO_4/HCl buffer (0.3 mM, pH 5.0) with ascorbic acid/TCEP (each 1 g/15 L) for 3 days and then against K_2HPO_4/HCl buffer (0.3 mM, pH 5.0) for 2 days. The resulting clear solution was freeze dried to give a foamy white solid.

Synthesis of polyethylene glycol-diamine: The amination of PEG was carried out according to Iijima et al.[238] with modifications. Linear PEG (100 g, 1.0 eq.) was dried in vacuo at 110 °C for 2 h, cooled to rt under argon atmosphere and dissolved in dry dichloromethane (900 mL). Triethylamine (3.0 eq.) was added, the mixture cooled to 0 °C and methanesulfonyl chloride (3.0 eq.) added stepwise. The reaction solution was stirred for 1 h at 0 °C and then 4 h at rt after which the solvents were removed with a rotary evaporator at 50 °C and the orange solid dissolved in MilliQ (100 mL). 30 % ammonium hydroxide solution (500 mL) were added, the reaction solution was stirred for 3 days at rt and the remaining ammonia was allowed to evaporate overnight in the fume hood. After a pH adjustment to 9 – 10 with 2 N NaOH and washing the aqueous layer with diethyl ether (3 x 150 mL), the product was extracted with dichloromethane (6 x 150 mL), concentrated in vacuo, and precipitated in cold diethyl ether. The sediment was dried in high vacuum to give a bulky yellowish solid.

Synthesis of polyethylene glycol-diallyl carbamate (2-arm PEG-allyl): Linear PEG-diamine (10 g, 1.0 eq.) was dissolved in MilliQ (100 mL), 2 N NaOH (5.0 eq.) was added and the solution cooled to 0 °C. After the addition of allyl chloroformate (1.6 eq.), the mixture was stirred for 4 h at 0 °C and the aqueous layer was washed with diethyl ether (2 x 100 mL). Extraction was

conducted with dichloromethane (5 x 75 mL), the combined organic layers were dried over $MgSO_4$, and filtered. The obtained product solution was concentrated, precipitated in cold diethyl ether, and the sediment dried in vacuo at rt to form white solid.

6. General Discussion and Conclusion

6.1. Summary of the newly developed bioinks

This thesis presents valuable improvements and new developments in the field of HA-based biomaterials for cartilage biofabrication. The first study (Chapter I) significantly improved an already existing bioink composition regarding physical as well as biological properties. The addition of unmodified high molecular weight HA (hmHA) introduced further shear thinning properties and increased ink viscosity which enabled PCL-supported 3D bioprinting. Reduction of the overall polymer content in combination with the addition of a porogen (hmHA) facilitated homogeneous ECM distribution and superior cartilaginous quality of the maturated constructs. This work provides new insights into the field of bioink development, as it presents and extensively characterizes the impact of a natural bioink additive with two beneficial functions. These findings can be also transferred to other bioinks or other porogenic supplements and therefore provide desirable design criteria for other approaches in the field of biofabrication.

The second study (Chapter II) aimed for further improvement of HA-based bioinks regarding stand-alone 3D printability. A novel dual-stage crosslinking mechanism based on HA-SH was developed, which enabled 3D printability after the first crosslinking step and stable constructs for long-term tissue culture after the second final gelation. The impact of ink components on 3D printability, regarding their molecular weights and applied concentrations, was empirically characterized and the findings contributed to the development of a versatile bioink platform. These platform bioinks were exemplarily analyzed for their potential in the field of cartilage biofabrication and very promising results were obtained in inks with high molecular weight HA-SH (> 200 kDa) and very low polymer content of 2 %. But as the ink properties are freely adjustable by changing molecular weight, concentration or geometry of the used ink components, this platform presents also promising ink compositions for biofabrication approaches of other tissues besides cartilage. The newly developed crosslinking mechanism might be also transferrable to other polymers and ink components, which further increases the application potential in the field of biofabrication.

The third study (Chapter III) further modified and improved one platform ink composition via covalent tethering of the chondrogenic differentiation factor TGF-β1 to increase the biomimetic potential. This study presented the first detailed comparative analysis of protein function regarding the impacts of ink processing (tethering and 3D printing). Furthermore, cartilaginous constructs with superior quality were obtained, which made an exogenous protein supply redundant and thereby paved the way towards potential clinical applications.

6.2. Considerations for effective bioink design

The hyaluronic acid-based bioinks for cartilage biofabrication presented in this thesis bear already a great potential for further investigations and *in vivo* applications. However, there is still room for improvement considering the aim to develop transplants with native-like cartilaginous properties. In this section, several ideas for follow-up studies are discussed regarding physical and biochemical ink properties as well as advanced 3D models for closer simulation of native cartilage structure.

6.2.1. Physical properties

6.2.1.1. Shear stress and shear thinning during fabrication

It has been shown before that the extrusion of cells through a fine nozzle can cause membrane rupture and severe cell damage leading to reduced cell viability. The applied shear stresses can also affect cell morphology, cytoskeletal organization and gene and protein expression patterns.[205, 207, 256, 278, 279] For this reason, one focus of this thesis was the comparative examination of cell survival and differentiation in cast versus printed constructs to characterize the newly developed bioinks for further biological applications (Chapter I and III). MSC cell survival was very high (> 90 %) in all presented studies, independent of the printing process. Also, no shear-induced impact on MSC differentiation, the amount or distribution of newly produced ECM, and gene or protein expression patterns were detected. These favorable results are most likely explainable by the relatively low printing pressure and the shear thinning behavior of HA.[188, 223, 235, 280, 281] When a material passes a thin needle at a constant pressure, an increase in resistance and shear forces is detected, especially at the syringe walls.[256] In contrast, a shear thinning material decreases its viscosity with increasing shear rates at the nozzle wall, thereby acting as a lubricating layer which enables smooth extrusion of the residual ink plug in the middle.[282] Therefore, this shear thinning behavior shields cells from mechanical stresses and maintains cell survival and unaffected behavior after 3D printing.[283] This property further validates HA-based bioinks as suitable and promising material for cartilage biofabrication approaches.

6.2.1.2. Dual-stage crosslinking

Especially dual-stage crosslinked materials are a promising approach to generate stable filaments for 3D fabrication while protecting the cells within the plug-flow during printing, as outlined above. Thereby, the first crosslinking step determines the rheological behavior during printing and the resulting ink facilitates cell viability and distribution without sedimentation. The second crosslinking step yields stable constructs for long-term tissue culture and determines the final mechanical properties of the constructs.[283] Prominent examples in the literature are guest-host interactions, physical entanglements, peptide-peptide interactions and dynamic or weak covalent

strategies for the first crosslinking step and UV light-induced crosslinking, pH mediated gelation, enzymatic crosslinking, thermal gelation, or small molecule covalent crosslinkers for the second final gelation.[192, 284-290] The newly developed dual-stage crosslinking mechanism in this thesis (Chapter II, and further used in Chapter III) utilizes two covalent crosslinking approaches to achieve suitable properties of HA-based bioinks. The biological performance of MSCs in these inks was outstanding, especially in the low-concentrated ones (with HA-SH > 200 kDa), while 3D printability and shape fidelity of extruded strands was fine for the presented approach, but still improvable. To further increase the shear thinning behavior for the fabrication process, a first reversible physical crosslinking mechanism might be beneficial. But the bigger issue with this new platform bioinks was strand fusion and thereby the impediment of complex structures in the z-axis. Hyaluronic acid has the natural function to provide lubricated and slippery surfaces, which likely contributes to strand fusion and the reduction of construct height compared to the calculated CAD model. It might be a promising approach to crosslink already during printing or use hybrid materials, for example, by mixing hyaluronic acid with collagen or gelatin. This might reduce the HA-intrinsic strand fusion and could further improve the cellular environment by closer simulation of the natural cartilage ECM and the introduction of further cell adhesive motifs.

6.2.1.3. Physical ink properties after fabrication

Besides physical properties during printing, the ink properties post-fabrication are also of great importance for embedded cells. It was frequently observed that cells sense the mechanical properties of their surrounding matrix, which can regulate cell spreading, migration, proliferation, gene expression and differentiation.[291-294] And it was proposed, that bioprinted scaffolds should resemble the stiffness of the native tissue to avoid mechanical mismatches.[283, 295] In the here presented studies, we also detected higher chondrogenic gene expression patterns in MSCs embedded in stiffer bioinks with a high polymer content (see Chapter I, 3.4.3.2. and Chapter II, 4.4.5.2. for a detailed discussion). But interestingly, the enhanced gene expression did not correlate with the quantitative and qualitative ECM production. ECM quantification was at a level comparable to the mechanically weaker ink in the first study (Chapter I) and even significantly lower in the second study (Chapter II). Taken together with the fact that the mechanically weaker polymeric networks also facilitated significantly improved ECM distribution and thereby distinctly enhanced mechanical stiffness and overall quality of the resulting maturated constructs after differentiation, the initial mechanical bioink properties might at least partially lose their importance in this context.

Besides stiffness, recent studies evaluated the impact of viscoelastic properties of hydrogels on cellular behavior. In contrast to purely elastic materials, viscoelastic materials like the physiological ECM exhibit stress relaxation.[283] It has been shown that the cells apply force or strain by binding the surrounding matrix, which can be actively remodeled by crosslink

degradation or rearrangement.[296] For example, fast stress relaxation over time was discovered to drive osteogenic differentiation of MSCs.[297, 298] The developed inks in this thesis likely have different physical properties regarding yield stress, shear moduli or viscoelasticity, which may have contributed to the detected quantitative differences in ECM production between the presented studies in Chapter I and II. For a better understanding and validation of this hypothesis, these bioinks should be further characterized regarding their mechanical properties including their stress relaxation rates. And it might be a promising design criterion to include and tune these properties for follow-up studies or further ink developments.

6.2.1.4. Biophysical stimuli to improve cartilaginous construct quality

Native cartilage is an avascular tissue, and the supply of oxygen and nutrients is only conducted via passive diffusion from the synovial fluid. Therefore, this tissue experiences low and varying oxygen tensions between 1 and 7 %.[299, 300] Hypoxia was shown to increase ECM synthesis in chondrocyte cultures[95] and induce chondrogenic differentiation of MSCs.[301] Thereby, hypoxia inducible factors 1α and 2α (HIF-1α/-2α) are stabilized under hypoxic conditions and heterodimerize with HIF-1β to initiate the transcription of specific hypoxia responsive genes.[302, 303] Growth arrest and survival of chondrocytes and maintenance of the human articular chondrocyte phenotype was demonstrated to depend on the actions of HIF-1α and -2α.[304, 305] Furthermore, hypoxia might prevent the potential calcification of engineered cartilage by inhibiting the expression of collagen type X, the main hypertrophy marker.[300, 306]

Another major environmental factor in native cartilage is mechanical stimulation via hydrostatic pressure and compressive or shear forces during movement. The special ECM arrangement provides thereby the necessary biomechanical properties to withstand tensile and compressive forces (as discussed in section 1.1.1.).[307, 308] Also in the field of cartilage TE, mechanical stimulation was shown to be important for maintaining cartilage integrity and varying loads resulted in different structural ECM organizations.[96, 309] For this reason, mechanical stimulation and specific physicochemical parameters like fluid flow were integrated in bioreactor systems to improve tissue maturation.[300, 310]

In general, these biophysical stimuli were demonstrated to improve MSC differentiation and the maintenance of a chondrogenic phenotype. For this reason, it might be a promising approach for future investigations of the here presented newly developed bioinks, to expose the constructs to varying oxygen tensions and mechanical stimulations. This might further increase the quantitative and qualitative ECM production and the resulting mechanical construct stiffness after maturation for potential clinical applications.

6.2.2. Biochemical properties

The chondrogenic differentiation potential of stem cells can be modified via biochemical properties of their surrounding biomaterial. Especially synthetic hydrogels have frequently been modified to increase their adhesiveness or bioactivity, but also natural derived biomaterials with inherent binding sites can be further optimized regarding their chondrogenic potential.[311] Adhesive peptide motifs of fibronectin (RGD), laminin (IKVAV and YIGSR) or N-cadherin (HAVDI) were used to functionalize hydrogels individually or in combination with other biochemical cues, and enhanced MSC chondrogenesis.[312-317] The decorin-derived collagen type II binding sequence KLER was shown to direct fibrillogenesis of collagen molecules, thereby stabilizes and organizes cartilage ECM, and improves matrix deposition of embedded MSCs.[318, 319] These are only a few examples from the literature which should underline the potential of biomimetic functionalizations. As shown in Chapter III, utilization of 8-arm PEG-acryl opens the possibility for ink modifications without impacting the pre-crosslinking process. One promising approach could be the addition of further biochemical cues like the mentioned adhesive peptides. For further introduction of modifiable moieties, 8-arm PEG-allyl could be utilized for final gelation.

Retention and sustained release of growth factors like TGF-β was also extensively studied in cartilage TE (also discussed in Chapter III). Thereby loaded nanosheets[320] or nanospheres,[65] as well as protein adsorption,[263] direct hydrogel loading[179] or covalent tethering[185] have been frequently applied. Especially covalent TGF-β incorporation significantly enhanced protein retention and differentiation of embedded MSCs,[184] which was transferred to printable bioinks and further validated in this thesis (Chapter III).

Besides incorporation of whole proteins, functional peptide motifs with chondroinductive properties were successfully applied *in vitro* and *in vivo* like the TGF-β mimetic peptides SPPEPS[321] or cytomodulin-2.[322] Another possibility of simultaneous and sequential factor delivery, without the need of whole intact proteins, can be utilized by gene activated bioinks. Thereby nucleic acids, encoding for key signaling factors, are delivered in the bioinks and induce transgene expression and enhanced biological activity in neighboring cells. This technique could contribute to tunable and precisely controllable gradient constructs in the future.[323-327]

As also shown in this thesis, deposition and distribution of newly produced ECM is very important in the field of cartilage TE. Incorporation of cleavable peptides can further increase hydrogel biodegradability to create more space for coherent ECM formation. This was for example analyzed for MSC-derived matrix metalloproteinase 7 (MMP7) and aggrecanase (ADAMTS4) activities, which correlated with ECM deposition and therefore increased constructs stiffness after maturation.[328]

6.2.3. Advanced 3D structures

The 3D environment is crucial for the behavior and fate of embedded cells (also discussed in section 1.2.3.). This knowledge yielded several approaches which aimed for a close simulation of human native cartilage organization. One promising example are zonal or multilayered constructs, which mimic the defined regions of articular cartilage.[329] This can be achieved by utilizing different cell sources and their special ECM expression profiles. Examples in the literature are combinations of middle-zone and deep-zone chondrocytes,[330] chondrocytes and MSCs,[331] or chondroprogenitor cells (ACPCs) and MSCs.[332, 333] With respect to clinical applications, a further benefit of different cell sources is the minimized need for long *in vitro* expansions to generate large cell numbers.[334] Another possibility to facilitate zone-specific cartilaginous or osteochondral tissue formation is to stimulate different ECM expression profiles in one cell source via biomaterial properties.[335-338] Other studies printed cell-free multilayered constructs with changing mechanical properties, which were afterwards seeded with cells and successfully applied for *in vitro* and *in vivo* applications for cartilage or osteochondral tissue repair.[183, 339, 340] Aiming for the treatment of OA affecting the entire joint, whole joint resurfacing was also applied by several studies which printed complex zonal constructs of the femoral head.[341-343] The anisotropic structure of osteochondral tissue still challenges the field of biofabrication, although new fabrication techniques and the ongoing development and improvement of biomaterials present promising future perspectives. Biochemical gradients of implemented proteins (BMP-2 and IGF-1 or BMP-2 and TGF-β1) were shown to direct localized osteogenic and chondrogenic differentiation of MSCs, and TGF-β gradients can lead to the development of heterogeneous cartilage tissue.[324, 344-346] The combination of biochemical and mechanical properties in a zonal orientation was also successfully applied.[345, 347, 348] As a further application advancement of the TGF-β1 tethered bioink presented in Chapter III of this thesis, preliminary work on TGF-β1 gradient development was conducted. A microfluidic chip was designed to enable gradual mixture of inks with or without tethered TGF-β1 and first-line cell culture experiments were performed within the master thesis of Franz Moser, University of Würzburg (2021). This work paved the way for in-depth follow-up studies and opened a perspective in this relatively new field of 3D biofabrication.

6.3. Conclusion

Bioinks for 3D biofabrication bear a great potential in the field of cartilage tissue engineering and offer variable and adjustable properties which have been extensively characterized in the last years. The presented inks in this thesis are a promising example for effective bioink development for cartilage biofabrication approaches and invite for future follow-up studies with great potential. These advanced bioinks should support cells in all stages of the fabrication and maturation

process. Physical properties like the shear thinning behavior protect the cells during printing, and adjustable mechanical ink properties can guide and promote the fate of embedded cells after printing. Further lineage commitment can be optimized by incorporation of diverse biochemical cues, simulation of the spatial layer organization or adjusted culturing techniques during construct maturation, like oxygen partial pressure or mechanical stimulation. Together, these future variations of the developed already promising inks can further advance the field on the way to clinical applications and effective cartilage regeneration.

7. Bibliography

[1] L. Wachsmuth, S. Söder, Z. Fan, F. Finger, T. Aigner, *Histol Histopathol* **2006**, *21*, 477.
[2] J. C. Y. Hu, K. A. Athanasiou, "Structure and Function of Articular Cartilage", in *Handbook of Histology Methods for Bone and Cartilage*, Y.H. An and K.L. Martin, Eds., Humana Press, Totowa, NJ, 2003, p. 73.
[3] A. M. Bhosale, J. B. Richardson, *Br Med Bull* **2008**, *87*, 77.
[4] C. B. Carballo, Y. Nakagawa, I. Sekiya, S. A. Rodeo, *Clin Sports Med* **2017**, *36*, 413.
[5] A. J. Sophia Fox, A. Bedi, S. A. Rodeo, *Sports Health* **2009**, *1*, 461.
[6] S. L.-Y. Woo, J. A. Buckwalter, *J Orthop Res* **1988**, *6*, 907.
[7] J. A. Buckwalter, H. J. Mankin, *Instr Course Lect* **1998**, *47*, 477.
[8] W. M. Lai, J. S. Hou, V. C. Mow, *J Biomech Eng* **1991**, *113*, 245.
[9] V. C. Mow, M. H. Holmes, W. M. Lai, *J Biomech* **1984**, *17*, 377.
[10] J. A. Buckwalter, V. C. Mow, A. Ratcliffe, *J Am Acad Orthop Surg* **1994**, *2*, 192.
[11] J. Sanchez-Adams, H. A. Leddy, A. L. McNulty, C. J. O'Conor, F. Guilak, *Curr Rheum Rep* **2014**, *16*, 451.
[12] A. Cui, H. Li, D. Wang, J. Zhong, Y. Chen, H. Lu, *EClinicalMedicine* **2020**, *29*.
[13] D. T. Felson, R. C. Lawrence, P. A. Dieppe, R. Hirsch, C. G. Helmick, J. M. Jordan, R. S. Kington, N. E. Lane, M. C. Nevitt, Y. Zhang, M. Sowers, T. McAlindon, T. D. Spector, A. R. Poole, S. Z. Yanovski, G. Ateshian, L. Sharma, J. A. Buckwalter, K. D. Brandt, J. F. Fries, *Ann Intern Med* **2000**, *133*, 635.
[14] M. Blagojevic, C. Jinks, A. Jeffery, K. P. Jordan, *Osteoarthritis Cartilage* **2010**, *18*, 24.
[15] D. H. Collins, "*The pathology of articular and spinal diseases"*, Edward Arnold, 1949.
[16] D. H. Collins, *Br J Rheumatol* **1939**, *1*, e62.
[17] D. Collins, T. McElligott, *Ann Rheum Dis* **1960**, *19*, 318.
[18] M. Kloppenburg, F. Berenbaum, *Osteoarthritis Cartilage* **2020**, *28*, 242.
[19] D. L. Richter, R. C. Schenck, D. C. Wascher, G. Treme, *Sports Health* **2016**, *8*, 153.
[20] E. A. Makris, A. H. Gomoll, K. N. Malizos, J. C. Hu, K. A. Athanasiou, *Nat Rev Rheumatol* **2015**, *11*, 21.
[21] B. J. Cole, C. Pascual-Garrido, R. C. Grumet, *JBJS* **2009**, *91*, 1778.
[22] S. Jiang, W. Guo, G. Tian, X. Luo, L. Peng, S. Liu, X. Sui, Q. Guo, X. Li, *Stem Cells Int* **2020**, *2020*, 5690252.
[23] J. R. Steadman, W. G. Rodkey, S. B. Singleton, K. K. Briggs, *Oper Tech Orthop* **1997**, *7*, 300.
[24] D. Goyal, S. Keyhani, E. H. Lee, J. H. P. Hui, *Arthrosc – J Arthrosc Relat Surg* **2013**, *29*, 1579.
[25] A. Azam, M. Forster, A. Robertson, *J Orthop* **2018**, *15*, 47.
[26] E. Di Cave, P. Versari, F. Sciarretta, D. Luzon, L. Marcellini, *Foot (Edinb)* **2017**, *33*, 48.
[27] R. D'Ambrosi, F. Valli, P. De Luca, N. Ursino, F. G. Usuelli, *J Clin Med* **2019**, *8*.
[28] M. Berruto, M. Delcogliano, F. de Caro, G. Carimati, F. Uboldi, P. Ferrua, G. Ziveri, C. F. De Biase, *Am J Sports Med* **2014**, *42*, 1607.
[29] A. Berta, M. S. Shive, A. K. Lynn, A. Getgood, S. Totterman, G. Busby, J. Hollenstein, G. Vásárhelyi, I. Kéki, L. Hangody, *Appl Sci* **2020**, *10*, 5642.
[30] W. Wei, H. Dai, *Bioact Mater* **2021**, *6*, 4830.
[31] L. Hangody, P. Füles, *JBJS* **2003**, *85*, 25.
[32] E. Solheim, J. Hegna, J. Øyen, T. Harlem, T. Strand, *The Knee* **2013**, *20*, 287.
[33] L. C. Biant, G. Bentley, S. Vijayan, J. A. Skinner, R. W. J. Carrington, *Am J Sports Med* **2014**, *42*, 2178.
[34] D. B. Haber, C. A. Logan, C. P. Murphy, A. Sanchez, R. F. LaPrade, M. T. Provencher, *Int J Sports Phys Ther* **2019**, *14*, 487.
[35] C. Wang, S. Akhavan, "The Use of Cartiform in the Knee for Osteochondral Defects", in *Biologic and Nanoarthroscopic Approaches in Sports Medicine*, C. Lavender, Ed., Springer International Publishing, Cham, 2021, p. 67.
[36] A. S. Gudeman, B. B. Hinckel, L. Oladeji, T. E. Ray, W. Gersoff, J. Farr, S. L. Sherman, *Am J Sports Med* **2021**, *0*, 03635465211037233.
[37] B. J. Cole, J. Farr, C. S. Winalski, T. Hosea, J. Richmond, B. Mandelbaum, P. G. De Deyne, *Am J Sports Med* **2011**, *39*, 1170.
[38] J. Farr, S. K. Tabet, E. Margerrison, B. J. Cole, *Am J Sports Med* **2014**, *42*, 1417.

[39] M. Tompkins, J. C. Hamann, D. R. Diduch, K. F. Bonner, J. M. Hart, F. W. Gwathmey, M. D. Milewski, C. M. Gaskin, *Arthrosc* **2013**, *29*, 1661.
[40] J. M. Woodmass, H. P. Melugin, I. T. Wu, D. B. F. Saris, M. J. Stuart, A. J. Krych, *Arthrosc Tech* **2017**, *6*, e1661.
[41] M. Brittberg, A. Lindahl, A. Nilsson, C. Ohlsson, O. Isaksson, L. Peterson, *N Engl J Med* **1994**, *331*, 889.
[42] L. Peterson, M. Brittberg, I. Kiviranta, E. L. Akerlund, A. Lindahl, *Am J Sports Med* **2002**, *30*, 2.
[43] J. D. Harris, R. A. Siston, R. H. Brophy, C. Lattermann, J. L. Carey, D. C. Flanigan, *Osteoarthritis Cartilage* **2011**, *19*, 779.
[44] M. Steinwachs, P. C. Kreuz, *Arthrosc* **2007**, *23*, 381.
[45] D. Goyal, A. Goyal, S. Keyhani, E. H. Lee, J. H. Hui, *Arthrosc* **2013**, *29*, 1872.
[46] O. A. Behery, J. D. Harris, J. M. Karnes, R. A. Siston, D. C. Flanigan, *J Knee Surg* **2013**, *26*, 203.
[47] C. Becher, V. Laute, S. Fickert, W. Zinser, P. Niemeyer, T. John, P. Diehl, T. Kolombe, R. Siebold, J. Fay, *J Orthop Surg Res* **2017**, *12*, 71.
[48] X. Armoiry, E. Cummins, M. Connock, A. Metcalfe, P. Royle, R. Johnston, J. Rodrigues, N. Waugh, H. Mistry, *Pharmacoeconomics* **2019**, *37*, 879.
[49] B. J. Huang, J. C. Hu, K. A. Athanasiou, *Biomaterials* **2016**, *98*, 1.
[50] P. C. Kreuz, S. Müller, U. Freymann, C. Erggelet, P. Niemeyer, C. Kaps, A. Hirschmüller, *Am J Sports Med* **2011**, *39*, 1697.
[51] U. Schneider, L. Rackwitz, S. Andereya, S. Siebenlist, F. Fensky, J. Reichert, I. Löer, T. Barthel, M. Rudert, U. Nöth, *Am J Sports Med* **2011**, *39*, 2558.
[52] D. C. Crawford, T. M. DeBerardino, R. J. Williams, 3rd, *J Bone Joint Surg Am* **2012**, *94*, 979.
[53] D. E. Anderson, R. J. Williams, 3rd, T. M. DeBerardino, D. C. Taylor, C. B. Ma, M. S. Kane, D. C. Crawford, *Am J Sports Med* **2017**, *45*, 875.
[54] P. E. Müller, D. Gallik, F. Hammerschmid, A. Baur-Melnyk, M. F. Pietschmann, A. Zhang, T. R. Niethammer, *Knee Surg Sports Traumatol Arthrosc* **2020**, *28*, 470.
[55] T. R. Niethammer, M. Holzgruber, M. F. Gülecyüz, P. Weber, M. F. Pietschmann, P. E. Müller, *Int Orthop* **2017**, *41*, 343.
[56] R. Langer, J. P. Vacanti, *Science* **1993**, *260*, 920.
[57] E. A. Makris, A. H. Gomoll, K. N. Malizos, J. C. Hu, K. A. Athanasiou, *Nat Rev Rheumatol* **2015**, *11*, 21.
[58] Y. Wu, P. Kennedy, N. Bonazza, Y. Yu, A. Dhawan, I. Ozbolat, *CARTILAGE* **2021**, *12*, 76.
[59] T. Stampoultzis, P. Karami, D. P. Pioletti, *Curr Res Transl Med* **2021**, *69*, 103299.
[60] J. Groll, T. Boland, T. Blunk, J. A. Burdick, D. W. Cho, P. D. Dalton, B. Derby, G. Forgacs, Q. Li, V. A. Mironov, L. Moroni, M. Nakamura, W. Shu, S. Takeuchi, G. Vozzi, T. B. Woodfield, T. Xu, J. J. Yoo, J. Malda, *Biofabrication* **2016**, *8*, 013001.
[61] L. Moroni, T. Boland, J. A. Burdick, C. De Maria, B. Derby, G. Forgacs, J. Groll, Q. Li, J. Malda, V. A. Mironov, C. Mota, M. Nakamura, W. Shu, S. Takeuchi, T. B. F. Woodfield, T. Xu, J. J. Yoo, G. Vozzi, *Trends Biotechnol* **2018**, *36*, 384.
[62] L. Moroni, J. A. Burdick, C. Highley, S. J. Lee, Y. Morimoto, S. Takeuchi, J. J. Yoo, *Nat Rev Mater* **2018**, *3*, 21.
[63] S. M. Peltola, F. P. Melchels, D. W. Grijpma, M. Kellomäki, *Ann Med* **2008**, *40*, 268.
[64] P. Datta, A. Barui, Y. Wu, V. Ozbolat, K. K. Moncal, I. T. Ozbolat, *Biotechnol Adv* **2018**, *36*, 1481.
[65] W. Zhu, H. Cui, B. Boualam, F. Masood, E. Flynn, R. D. Rao, Z. Y. Zhang, L. G. Zhang, *Nanotechnology* **2018**, *29*, 185101.
[66] G. Gao, T. Yonezawa, K. Hubbell, G. Dai, X. Cui, *Biotechnol J* **2015**, *10*, 1568.
[67] G. Gao, X. F. Zhang, K. Hubbell, X. Cui, *Biotechnol Bioeng* **2017**, *114*, 208.
[68] J. Malda, J. Visser, F. P. Melchels, T. Jüngst, W. E. Hennink, W. J. Dhert, J. Groll, D. W. Hutmacher, *Adv Mater* **2013**, *25*, 5011.
[69] M. Costantini, J. Idaszek, K. Szöke, J. Jaroszewicz, M. Dentini, A. Barbetta, J. E. Brinchmann, W. Święszkowski, *Biofabrication* **2016**, *8*, 035002.
[70] V. H. Mouser, F. P. Melchels, J. Visser, W. J. Dhert, D. Gawlitta, J. Malda, *Biofabrication* **2016**, *8*, 035003.
[71] V. H. M. Mouser, R. Levato, L. J. Bonassar, D. D. D'Lima, D. A. Grande, T. J. Klein, D. B. F. Saris, M. Zenobi-Wong, D. Gawlitta, J. Malda, *Cartilage* **2017**, *8*, 327.
[72] C. Onofrillo, S. Duchi, C. D. O'Connell, R. Blanchard, A. J. O'Connor, M. Scott, G. G. Wallace, P. F. M. Choong, C. Di Bella, *Biofabrication* **2018**, *10*, 045006.
[73] V. Graceffa, C. Vinatier, J. Guicheux, M. Stoddart, M. Alini, D. I. Zeugolis, *Biomaterials* **2019**, *192*, 199.
[74] R. E. B. Fitzsimmons, M. S. Mazurek, A. Soos, C. A. Simmons, *Stem Cells Int* **2018**, *2018*, 8031718.

[75] R. Buda, F. Vannini, M. Cavallo, B. Grigolo, A. Cenacchi, S. Giannini, *J Bone Joint Surg Am* **2010**, *92 Suppl 2*, 2.
[76] J. L. Dragoo, G. Carlson, F. McCormick, H. Khan-Farooqi, M. Zhu, P. A. Zuk, P. Benhaim, *Tissue Eng* **2007**, *13*, 1615.
[77] K. Y. Saw, A. Anz, C. Siew-Yoke Jee, S. Merican, R. Ching-Soong Ng, S. A. Roohi, K. Ragavanaidu, *Arthrosc* **2013**, *29*, 684.
[78] Y. B. Park, C. W. Ha, C. H. Lee, Y. C. Yoon, Y. G. Park, *Stem Cells Transl Med* **2017**, *6*, 613.
[79] B. Sadlik, G. Jaroslawski, M. Puszkarz, A. Blasiak, T. Oldak, D. Gladysz, G. P. Whyte, *Arthrosc Tech* **2018**, *7*, e57.
[80] M. Pei, F. He, B. M. Boyce, V. L. Kish, *Osteoarthritis Cartilage* **2009**, *17*, 714.
[81] Y. Sakaguchi, I. Sekiya, K. Yagishita, T. Muneta, *Arthritis Rheum* **2005**, *52*, 2521.
[82] A. Stolzing, E. Jones, D. McGonagle, A. Scutt, *Mech Ageing Dev* **2008**, *129*, 163.
[83] J. M. Murphy, K. Dixon, S. Beck, D. Fabian, A. Feldman, F. Barry, *Arthritis Rheum* **2002**, *46*, 704.
[84] A. Arshi, F. A. Petrigliano, R. J. Williams, K. J. Jones, *Curr Rev Musculoskelet Med* **2020**, *13*, 20.
[85] M. B. Mueller, R. S. Tuan, *Arthritis Rheum* **2008**, *58*, 1377.
[86] M. Dattena, S. Pilichi, S. Rocca, L. Mara, S. Casu, G. Masala, L. Manunta, A. Manunta, E. S. Passino, R. R. Pool, P. Cappai, *J Tissue Eng Regen Med* **2009**, *3*, 175.
[87] S. Wakitani, H. Aoki, Y. Harada, M. Sonobe, Y. Morita, Y. Mu, N. Tomita, Y. Nakamura, S. Takeda, T. K. Watanabe, A. Tanigami, *Cell Transplant* **2004**, *13*, 331.
[88] K. Takahashi, S. Yamanaka, *Cell* **2006**, *126*, 663.
[89] A. M. Craft, J. S. Rockel, Y. Nartiss, R. A. Kandel, B. A. Alman, G. M. Keller, *Nat Biotechnol* **2015**, *33*, 638.
[90] T. Saito, F. Yano, D. Mori, M. Kawata, K. Hoshi, T. Takato, H. Masaki, M. Otsu, K. Eto, H. Nakauchi, U. I. Chung, S. Tanaka, *Biomed Res* **2015**, *36*, 179.
[91] S. A. Lietman, *World J Orthop* **2016**, *7*, 149.
[92] E. M. Darling, K. A. Athanasiou, *J Orthop Res* **2005**, *23*, 425.
[93] B. Johnstone, T. M. Hering, A. I. Caplan, V. M. Goldberg, J. U. Yoo, *Exp Cell Res* **1998**, *238*, 265.
[94] A. E. Denker, S. B. Nicoll, R. S. Tuan, *Differentiation* **1995**, *59*, 25.
[95] C. Domm, M. Schünke, K. Christesen, B. Kurz, *Osteoarthritis Cartilage* **2002**, *10*, 13.
[96] A. J. Grodzinsky, M. E. Levenston, M. Jin, E. H. Frank, *Annu Rev Biomed Eng* **2000**, *2*, 691.
[97] O. S. Beane, E. M. Darling, *Ann Biomed Eng* **2012**, *40*, 2079.
[98] J. L. Puetzer, J. N. Petitte, E. G. Loboa, *Tissue Eng Part B Rev* **2010**, *16*, 435.
[99] X. Zhao, D. A. Hu, D. Wu, F. He, H. Wang, L. Huang, D. Shi, Q. Liu, N. Ni, M. Pakvasa, Y. Zhang, K. Fu, K. H. Qin, A. J. Li, O. Hagag, E. J. Wang, M. Sabharwal, W. Wagstaff, R. R. Reid, M. J. Lee, J. M. Wolf, M. El Dafrawy, K. Hynes, J. Strelzow, S. H. Ho, T.-C. He, A. Athiviraham, *Front Bioeng Biotechnol* **2021**, *9*.
[100] H. Janik, M. Marzec, *Mater Sci Eng C* **2015**, *48*, 586.
[101] S. Grad, L. Kupcsik, K. Gorna, S. Gogolewski, M. Alini, *Biomaterials* **2003**, *24*, 5163.
[102] C. R. Lee, S. Grad, K. Gorna, S. Gogolewski, A. Goessl, M. Alini, *Tissue Eng* **2005**, *11*, 1562.
[103] A. M. Klein, V. L. Graham, Y. Gulleth, D. Lafreniere, *Laryngoscope* **2005**, *115*, 583.
[104] H. Nakao, R. D. Jacquet, M. Shasti, N. Isogai, A. S. Murthy, W. J. Landis, *Plast Reconstr Surg* **2017**, *139*.
[105] J. Zwingmann, A. T. Mehlhorn, N. Südkamp, B. Stark, M. Dauner, H. Schmal, *Tissue Eng* **2007**, *13*, 2335.
[106] W. J. Li, J. A. Cooper, Jr., R. L. Mauck, R. S. Tuan, *Acta Biomater* **2006**, *2*, 377.
[107] K. Marycz, A. Smieszek, S. Targonska, S. A. Walsh, K. Szustakiewicz, R. J. Wiglusz, *Mater Sci Eng C Mater Biol Appl* **2020**, *110*, 110634.
[108] J. Z. Wang, M. L. You, Z. Q. Ding, W. B. Ye, *Mater Sci Eng C Mater Biol Appl* **2019**, *97*, 1021.
[109] Y. Hwang, N. Sangaj, S. Varghese, *Tissue Eng Part A* **2010**, *16*, 3033.
[110] C. Fan, D.-A. Wang, *Europ Polym J* **2015**, *72*, 651.
[111] P. H. Ousema, F. T. Moutos, B. T. Estes, A. I. Caplan, D. P. Lennon, F. Guilak, J. B. Weinberg, *Biomaterials* **2012**, *33*, 8967.
[112] I. Sousa, A. Mendes, R. F. Pereira, P. J. Bártolo, *Mater Lett* **2014**, *134*, 263.
[113] K. Theodoridis, E. Aggelidou, M. Manthou, E. Demiri, A. Bakopoulou, A. Kritis, *Colloids Surf B Biointerfaces* **2019**, *183*, 110403.
[114] S. H. Lee, H. Shin, *Adv Drug Deliv Rev* **2007**, *59*, 339.
[115] S. Camarero-Espinosa, B. Rothen-Rutishauser, E. J. Foster, C. Weder, *Biomater Sci* **2016**, *4*, 734.
[116] M. N. Collins, C. Birkinshaw, *Carbohydr Polym* **2013**, *92*, 1262.
[117] R. C. Gupta, R. Lall, A. Srivastava, A. Sinha, *Front Vet Sci* **2019**, *6*, 192.
[118] I. L. Kim, R. L. Mauck, J. A. Burdick, *Biomaterials* **2011**, *32*, 8771.
[119] C. H. Lee, A. Singla, Y. Lee, *Int J Pharm* **2001**, *221*, 1.

[120] R. Kuroda, K. Ishida, T. Matsumoto, T. Akisue, H. Fujioka, K. Mizuno, H. Ohgushi, S. Wakitani, M. Kurosaka, *Osteoarthritis Cartilage* **2007**, *15*, 226.
[121] C. F. Marques, G. S. Diogo, S. Pina, J. M. Oliveira, T. H. Silva, R. L. Reis, *J Mater Sci Mater Med* **2019**, *30*, 32.
[122] Q. Feng, K. Wei, S. Lin, Z. Xu, Y. Sun, P. Shi, G. Li, L. Bian, *Biomaterials* **2016**, *101*, 217.
[123] S. Bang, U. W. Jung, I. Noh, *Tissue Eng Regen Med* **2018**, *15*, 25.
[124] M. C. Echave, R. Hernáez-Moya, L. Iturriaga, J. L. Pedraz, R. Lakshminarayanan, A. Dolatshahi-Pirouz, N. Taebnia, G. Orive, *Expert Opin Biol Ther* **2019**, *19*, 773.
[125] R. A. Muzzarelli, F. Greco, A. Busilacchi, V. Sollazzo, A. Gigante, *Carbohydr Polym* **2012**, *89*, 723.
[126] T. Li, X. Song, C. Weng, X. Wang, L. Sun, X. Gong, L. Yang, C. Chen, *Appl Mater Today* **2018**, *10*, 173.
[127] J. Yang, M. Shen, H. Wen, Y. Luo, R. Huang, L. Rong, J. Xie, *Carbohydr Polym* **2020**, *230*, 115650.
[128] L. Keller, A. Regiel-Futyra, M. Gimeno, S. Eap, G. Mendoza, V. Andreu, Q. Wagner, A. Kyzioł, V. Sebastian, G. Stochel, M. Arruebo, N. Benkirane-Jessel, *Nanomedicine* **2017**, *13*, 2231.
[129] B. Sultankulov, D. Berillo, K. Sultankulova, T. Tokay, A. Saparov, *Biomolecules* **2019**, *9*.
[130] J. K. Suh, H. W. Matthew, *Biomaterials* **2000**, *21*, 2589.
[131] S. H. Cho, S. M. Lim, D. K. Han, S. H. Yuk, G. I. Im, J. H. Lee, *J Biomater Sci Polym Ed* **2009**, *20*, 863.
[132] H. Park, K. Y. Lee, *J Biomed Mater Res A* **2014**, *102*, 4519.
[133] G. Filardo, F. Perdisa, M. Gelinsky, F. Despang, M. Fini, M. Marcacci, A. P. Parrilli, A. Roffi, F. Salamanna, M. Sartori, *J Mater Sci Mater Med* **2018**, *29*, 1.
[134] Y. Zhang, H. Yang, H. Shao, X. Hu, *J Biomed Biotechnol* **2010**, *2010*, 683962.
[135] D. Ma, Y. Wang, W. Dai, *Mater Sci Eng C Mater Biol Appl* **2018**, *89*, 456.
[136] S. Salehi, K. Koeck, T. Scheibel, *Molecules* **2020**, *25*.
[137] N. Isobe, T. Komamiya, S. Kimura, U. J. Kim, M. Wada, *Int J Biol Macromol* **2018**, *117*, 625.
[138] S. D. Dutta, D. K. Patel, K.-T. Lim, *J Biol Eng* **2019**, *13*, 1.
[139] M. L. Chinta, A. Velidandi, N. P. P. Pabbathi, S. Dahariya, S. R. Parcha, *Int J Biol Macromol* **2021**, *175*, 495.
[140] Y. S. Kim, M. Majid, A. J. Melchiorri, A. G. Mikos, *Bioeng Transl Med* **2019**, *4*, 83.
[141] Y. Sun, L. Yan, S. Chen, M. Pei, *Acta Biomater* **2018**, *74*, 56.
[142] Q. Yang, J. Peng, Q. Guo, J. Huang, L. Zhang, J. Yao, F. Yang, S. Wang, W. Xu, A. Wang, S. Lu, *Biomaterials* **2008**, *29*, 2378.
[143] X. Wu, J. Su, J. Wei, N. Jiang, X. Ge, *Stem Cells Int* **2021**, *2021*, 9477332.
[144] T. C. Laurent, U. B. Laurent, J. R. Fraser, *Immunol Cell Biol* **1996**, *74*, A1.
[145] C. Hardwick, K. Hoare, R. Owens, H. P. Hohn, M. Hook, D. Moore, V. Cripps, L. Austen, D. M. Nance, E. A. Turley, *J Cell Biol* **1992**, *117*, 1343.
[146] H. Zhu, N. Mitsuhashi, A. Klein, L. W. Barsky, K. Weinberg, M. L. Barr, A. Demetriou, G. D. Wu, *Stem Cells* **2006**, *24*, 928.
[147] S. Stichler, T. Böck, N. Paxton, S. Bertlein, R. Levato, V. Schill, W. Smolan, J. Malda, J. Teßmar, T. Blunk, J. Groll, *Biofabrication* **2017**, *9*, 044108.
[148] S.-C. Wu, P.-Y. Huang, C.-H. Chen, B. Teong, J.-W. Chen, C.-W. Wu, J.-K. Chang, M.-L. Ho, *Int J Biol Macromol* **2018**, *119*, 726.
[149] C. B. Knudson, *Birth Defects Res C Embryo Today* **2003**, *69*, 174.
[150] L. Astachov, R. Vago, M. Aviv, Z. Nevo, *Front Biosci* **2011**, *16*, 261.
[151] S. An, S. Choi, S. Min, S.-W. Cho, *Biotechnol Bioprocess Eng* **2021**, 1.
[152] J. A. Burdick, G. D. Prestwich, *Adv Mater* **2011**, *23*, H41.
[153] J. Kuo, G. Prestwich, *Comprehensive Biomaterials; Ducheyne, P., Healy, K., Hutmacher, D., Kirkpatrick, J., Eds* **2010**.
[154] C. B. Highley, G. D. Prestwich, J. A. Burdick, *Curr Opin Biotechnol* **2016**, *40*, 35.
[155] H. Li, Z. Qi, S. Zheng, Y. Chang, W. Kong, C. Fu, Z. Yu, X. Yang, S. Pan, *Adv Mater Sci Eng* **2019**, *2019*.
[156] L. Bian, C. Hou, E. Tous, R. Rai, R. L. Mauck, J. A. Burdick, *Biomaterials* **2013**, *34*, 413.
[157] I. E. Erickson, A. H. Huang, S. Sengupta, S. Kestle, J. A. Burdick, R. L. Mauck, *Osteoarthritis Cartilage* **2009**, *17*, 1639.
[158] B. Kaczmarek, A. Sionkowska, J. Kozlowska, A. Osyczka, *Int J Biol Macromol* **2018**, *107*, 247.
[159] S. Choi, J. S. Lee, J. Shin, M. S. Lee, D. Kang, N. S. Hwang, H. Lee, H. S. Yang, S.-W. Cho, *J Control Release* **2020**, *327*, 571.
[160] S. Shen, M. Chen, W. Guo, H. Li, X. Li, S. Huang, X. Luo, Z. Wang, Y. Wen, Z. Yuan, B. Zhang, L. Peng, C. Gao, Q. Guo, S. Liu, N. Zhuo, *Tissue Eng Part B Rev* **2019**, *25*, 187.

[161] W. Schuurman, V. Khristov, M. W. Pot, P. R. van Weeren, W. J. Dhert, J. Malda, *Biofabrication* **2011**, *3*, 021001.
[162] J. R. Porter, A. Henson, K. C. Popat, *Biomaterials* **2009**, *30*, 780.
[163] S. An, E. J. Jeon, J. Jeon, S.-W. Cho, *Mater Horiz* **2019**, *6*, 1169.
[164] Y. Duan, K. Li, H. Wang, T. Wu, Y. Zhao, H. Li, H. Tang, W. Yang, *Carbohydr Polym* **2020**, *238*, 116195.
[165] Y. Liu, J. Yang, Z. Luo, D. Li, J. Lu, Q. Wang, Y. Xiao, X. Zhang, *J Mater Chem B* **2019**, *7*, 2845.
[166] J. Shin, J. S. Lee, C. Lee, H. J. Park, K. Yang, Y. Jin, J. H. Ryu, K. S. Hong, S. H. Moon, H. M. Chung, *Adv Funct Mater* **2015**, *25*, 3814.
[167] Y. Zhou, L. Kang, Z. Yue, X. Liu, G. G. Wallace, *ACS Appl Bio Mater* **2019**, *3*, 628.
[168] J. Shin, S. Choi, J. H. Kim, J. H. Cho, Y. Jin, S. Kim, S. Min, S. K. Kim, D. Choi, S. W. Cho, *Adv Funct Mater* **2019**, *29*, 1903863.
[169] M. Liu, X. Zeng, C. Ma, H. Yi, Z. Ali, X. Mou, S. Li, Y. Deng, N. He, *Bone Res* **2017**, *5*, 1.
[170] N. Holten-Andersen, M. J. Harrington, H. Birkedal, B. P. Lee, P. B. Messersmith, K. Y. C. Lee, J. H. Waite, *PNAS* **2011**, *108*, 2651.
[171] M. Shin, J. H. Galarraga, M. Y. Kwon, H. Lee, J. A. Burdick, *Acta Biomater* **2019**, *95*, 165.
[172] T. P. T. Nguyen, F. Li, S. Shrestha, R. S. Tuan, H. Thissen, J. S. Forsythe, J. E. Frith, *Biomaterials* **2021**, 121214.
[173] Y. Ren, H. Zhang, W. Qin, B. Du, L. Liu, J. Yang, *Mater Sci Eng C* **2020**, *108*, 110276.
[174] B. D. Cosgrove, K. L. Mui, T. P. Driscoll, S. R. Caliari, K. D. Mehta, R. K. Assoian, J. A. Burdick, R. L. Mauck, *Nat Mater* **2016**, *15*, 1297.
[175] H. J. Lee, C. Yu, T. Chansakul, N. S. Hwang, S. Varghese, S. M. Yu, J. H. Elisseeff, *Tissue Eng Part A* **2008**, *14*, 1843.
[176] J. L. Puetzer, J. N. Petitte, E. G. Loboa, *Tissue Eng Part B* **2010**, *16*, 435.
[177] H. Madry, A. Rey-Rico, J. K. Venkatesan, B. Johnstone, M. Cucchiarini, *Tissue Eng Part B* **2014**, *20*, 106.
[178] J. Zhu, R. E. Marchant, *Expert Rev Med Devices* **2011**, *8*, 607.
[179] Y. Deng, A. X. Sun, K. J. Overholt, G. Z. Yu, M. R. Fritch, P. G. Alexander, H. Shen, R. S. Tuan, H. Lin, *Acta Biomater* **2019**, *83*, 167.
[180] C. Levinson, M. Lee, L. A. Applegate, M. Zenobi-Wong, *Acta Biomater* **2019**, *99*, 168.
[181] Q. Feng, S. Lin, K. Zhang, C. Dong, T. Wu, H. Huang, X. Yan, L. Zhang, G. Li, L. Bian, *Acta Biomater* **2017**, *53*, 329.
[182] B. Wang, P. J. Díaz-Payno, D. C. Browe, F. E. Freeman, J. Nulty, R. Burdis, D. J. Kelly, *Acta Biomater* **2021**, *128*, 130.
[183] C. Wang, H. Yue, W. Huang, X. Lin, X. Xie, Z. He, X. He, S. Liu, L. Bai, B. Lu, Y. Wei, M. Wang, *Biofabrication* **2020**, *12*, 025030.
[184] T. Böck, V. Schill, M. Krähnke, A. F. Steinert, J. Tessmar, T. Blunk, J. Groll, *Macromol Biosci* **2018**, *18*, e1700390.
[185] B. V. Sridhar, N. R. Doyle, M. A. Randolph, K. S. Anseth, *J Biomed Mater Res A* **2014**, *102*, 4464.
[186] J. D. McCall, J. E. Luoma, K. S. Anseth, *Drug Deliv Transl Res* **2012**, *2*, 305.
[187] C. A. DeForest, K. S. Anseth, *Annu Rev Chem Biomol Eng* **2012**, *3*, 421.
[188] J. Hauptstein, T. Böck, M. Bartolf-Kopp, L. Forster, P. Stahlhut, A. Nadernezhad, G. Blahetek, A. Zernecke-Madsen, R. Detsch, T. Jüngst, J. Groll, J. Teßmar, T. Blunk, *Adv Healthc Mater* **2020**, *9*, e2000737.
[189] S. Bertlein, G. Brown, K. S. Lim, T. Jungst, T. Boeck, T. Blunk, J. Tessmar, G. J. Hooper, T. B. F. Woodfield, J. Groll, *Adv Mater* **2017**, *29*.
[190] A. C. Daly, S. E. Critchley, E. M. Rencsok, D. J. Kelly, *Biofabrication* **2016**, *8*, 045002.
[191] F. Pati, J. Jang, D. H. Ha, S. Won Kim, J. W. Rhie, J. H. Shim, D. H. Kim, D. W. Cho, *Nat Commun* **2014**, *5*, 3935.
[192] D. Petta, A. R. Armiento, D. Grijpma, M. Alini, D. Eglin, M. D'Este, *Biofabrication* **2018**, *10*, 044104.
[193] S. J. Bryant, T. T. Chowdhury, D. A. Lee, D. L. Bader, K. S. Anseth, *Ann Biomed Eng* **2004**, *32*, 407.
[194] B. M. Richardson, D. G. Wilcox, M. A. Randolph, K. S. Anseth, *Acta Biomater* **2019**, *83*, 71.
[195] M. L. Vainieri, A. Lolli, N. Kops, D. D'Atri, D. Eglin, A. Yayon, M. Alini, S. Grad, K. Sivasubramaniyan, G. van Osch, *Acta Biomater* **2020**, *101*, 293.
[196] S. J. Bryant, K. S. Anseth, D. A. Lee, D. L. Bader, *J Orthop Res* **2004**, *22*, 1143.
[197] S. Stichler, T. Jungst, M. Schamel, I. Zilkowski, M. Kuhlmann, T. Böck, T. Blunk, J. Teßmar, J. Groll, *Ann Biomed Eng* **2017**, *45*, 273.
[198] I. Martin, B. Obradovic, L. E. Freed, G. Vunjak-Novakovic, *Ann Biomed Eng* **1999**, *27*, 656.
[199] E. C. Jensen, *Anat Rec (Hoboken)* **2013**, *296*, 378.

[200] Y. J. Kim, R. L. Sah, J. Y. Doong, A. J. Grodzinsky, *Anal Biochem* **1988**, *174*, 168.
[201] J. F. Woessner, Jr., *Arch Biochem Biophys* **1961**, *93*, 440.
[202] A. P. Hollander, T. F. Heathfield, C. Webber, Y. Iwata, R. Bourne, C. Rorabeck, A. R. Poole, *J Clin Invest* **1994**, *93*, 1722.
[203] R. W. Farndale, D. J. Buttle, A. J. Barrett, *Biochim Biophys Acta* **1986**, *883*, 173.
[204] K. J. Livak, T. D. Schmittgen, *Methods* **2001**, *25*, 402.
[205] A. Blaeser, D. F. Duarte Campos, U. Puster, W. Richtering, M. M. Stevens, H. Fischer, *Adv Healthc Mater* **2016**, *5*, 326.
[206] A. Tirella, A. Ahluwalia, *Biotechnol Prog* **2012**, *28*, 1315.
[207] K. Nair, M. Gandhi, S. Khalil, K. C. Yan, M. Marcolongo, K. Barbee, W. Sun, *Biotechnol J* **2009**, *4*, 1168.
[208] R. Chang, J. Nam, W. Sun, *Tissue Eng Part A* **2008**, *14*, 41.
[209] R. J. McMurtrey, *Stem Cells Dev* **2017**, *26*, 1293.
[210] R. J. McMurtrey, *Tissue Eng Part C* **2016**, *22*, 221.
[211] I. A. D. Mancini, S. Schmidt, H. Brommer, B. Pouran, S. Schäfer, J. Tessmar, A. Mensinga, M. H. P. van Rijen, J. Groll, T. Blunk, R. Levato, J. Malda, P. R. van Weeren, *Biofabrication* **2020**, *12*, 035028.
[212] P. Mesquida, D. Kohl, O. G. Andriotis, P. J. Thurner, M. Duer, S. Bansode, G. Schitter, *Sci Rep* **2018**, *8*, 10126.
[213] A. A. Hegewald, J. Ringe, J. Bartel, I. Krüger, M. Notter, D. Barnewitz, C. Kaps, M. Sittinger, *Tissue Cell* **2004**, *36*, 431.
[214] C. Chung, J. A. Burdick, *Tissue Eng Part A* **2009**, *15*, 243.
[215] C. B. Knudson, W. Knudson, *Clin Orthop Relat Res* **2004**, S152.
[216] A. J. Engler, S. Sen, H. L. Sweeney, D. E. Discher, *Cell* **2006**, *126*, 677.
[217] J. Kundu, J. H. Shim, J. Jang, S. W. Kim, D. W. Cho, *J Tissue Eng Regen Med* **2015**, *9*, 1286.
[218] J. H. Shim, K. M. Jang, S. K. Hahn, J. Y. Park, H. Jung, K. Oh, K. M. Park, J. Yeom, S. H. Park, S. W. Kim, J. H. Wang, K. Kim, D. W. Cho, *Biofabrication* **2016**, *8*, 014102.
[219] L. Trachsel, C. Johnbosco, T. Lang, E. M. Benetti, M. Zenobi-Wong, *Biomacromolecules* **2019**, *20*, 4502.
[220] M. Lee, K. Bae, P. Guillon, J. Chang, Ø. Arlov, M. Zenobi-Wong, *ACS Appl Mater Interfaces* **2018**, *10*, 37820.
[221] J. Zhu, R. E. Marchant, *Expert Rev Med Devices* **2011**, *8*, 607.
[222] J. H. Shim, J. Y. Kim, M. Park, J. Park, D. W. Cho, *Biofabrication* **2011**, *3*, 034102.
[223] J. Hauptstein, L. Forster, A. Nadernezhad, H. Horder, P. Stahlhut, J. Groll, T. Blunk, J. Teßmar, *Macromol Biosci* **2021**, e2100331.
[224] J. Groll, J. A. Burdick, D. W. Cho, B. Derby, M. Gelinsky, S. C. Heilshorn, T. Jüngst, J. Malda, V. A. Mironov, K. Nakayama, A. Ovsianikov, W. Sun, S. Takeuchi, J. J. Yoo, T. B. F. Woodfield, *Biofabrication* **2018**, *11*, 013001.
[225] W. Sun, B. Starly, A. C. Daly, J. A. Burdick, J. Groll, G. Skeldon, W. Shu, Y. Sakai, M. Shinohara, M. Nishikawa, J. Jang, D.-W. Cho, M. Nie, S. Takeuchi, S. Ostrovidov, A. Khademhosseini, R. D. Kamm, V. Mironov, L. Moroni, I. T. Ozbolat, *Biofabrication* **2020**, *12*, 022002.
[226] R. Levato, T. Jungst, R. G. Scheuring, T. Blunk, J. Groll, J. Malda, *Adv Mater* **2020**, *32*, e1906423.
[227] B. S. Kim, S. Das, J. Jang, D. W. Cho, *Chem Rev* **2020**, *120*, 10608.
[228] D. Petta, U. D'Amora, L. Ambrosio, D. W. Grijpma, D. Eglin, M. D'Este, *Biofabrication* **2020**, *12*, 032001.
[229] C. Antich, J. de Vicente, G. Jiménez, C. Chocarro, E. Carrillo, E. Montañez, P. Gálvez-Martín, J. A. Marchal, *Acta Biomater* **2020**, *106*, 114.
[230] E. Liao, M. Yaszemski, P. Krebsbach, S. Hollister, *Tissue Eng* **2007**, *13*, 537.
[231] E. A. Kiyotake, A. W. Douglas, E. E. Thomas, S. L. Nimmo, M. S. Detamore, *Acta Biomater* **2019**, *95*, 176.
[232] J. Lee, S. H. Lee, B. S. Kim, Y. S. Cho, Y. Park, *Tissue Eng Regen Med* **2018**, *15*, 761.
[233] Q. Xu, S. A, P. McMichael, J. Creagh-Flynn, D. Zhou, Y. Gao, X. Li, X. Wang, W. Wang, *ACS Macro Lett* **2018**, *7*, 509.
[234] M. Kesti, M. Müller, J. Becher, M. Schnabelrauch, M. D'Este, D. Eglin, M. Zenobi-Wong, *Acta Biomater* **2015**, *11*, 162.
[235] L. Ouyang, C. B. Highley, C. B. Rodell, W. Sun, J. A. Burdick, *ACS Biomater Sci Eng* **2016**, *2*, 1743.
[236] K. P. Vercruysse, D. M. Marecak, J. F. Marecek, G. D. Prestwich, *Bioconjug Chem* **1997**, *8*, 686.
[237] G. M. Cruise, D. S. Scharp, J. A. Hubbell, *Biomaterials* **1998**, *19*, 1287.
[238] M. Iijima, D. Ulkoski, S. Sakuma, D. Matsukuma, N. Nishiyama, H. Otsuka, C. Scholz, *Polym Int* **2016**, *65*, 1132.

[239] X. Z. Shu, Y. Liu, Y. Luo, M. C. Roberts, G. D. Prestwich, *Biomacromolecules* **2002**, *3*, 1304.
[240] B. L. Barthel, D. L. Rudnicki, T. P. Kirby, S. M. Colvin, D. J. Burkhart, T. H. Koch, *J Med Chem* **2012**, *55*, 6595.
[241] L. Ambrosio, A. Borzacchiello, P. A. Netti, L. Nicolais, *J Macromol Sci A* **1999**, *36*, 991.
[242] M. P. Lutolf, N. Tirelli, S. Cerritelli, L. Cavalli, J. A. Hubbell, *Bioconjug Chem* **2001**, *12*, 1051.
[243] C. G. Pfeifer, A. Berner, M. Koch, W. Krutsch, R. Kujat, P. Angele, M. Nerlich, J. Zellner, *Materials (Basel)* **2016**, *9*.
[244] J. Hauptstein, L. Forster, A. Nadernezhad, J. Groll, J. Teßmar, T. Blunk, *Int J Mol Sci* **2022**, *23*, 924.
[245] M. T. Poldervaart, B. Goversen, M. de Ruijter, A. Abbadessa, F. P. W. Melchels, F. C. Öner, W. J. A. Dhert, T. Vermonden, J. Alblas, *PLoS One* **2017**, *12*, e0177628.
[246] H. M. Pan, S. Chen, T.-S. Jang, W. T. Han, H.-d. Jung, Y. Li, J. Song, *Biofabrication* **2019**, *11*, 025008.
[247] D. Petta, D. W. Grijpma, M. Alini, D. Eglin, M. D'Este, *ACS Biomater Sci Eng* **2018**, *4*, 3088.
[248] J. H. Galarraga, R. C. Locke, C. E. Witherel, B. D. Stoeckl, M. Castilho, R. L. Mauck, J. Malda, R. Levato, J. A. Burdick, *Biofabrication* **2021**, *14*.
[249] F. Redini, M. Daireaux, A. Mauviel, P. Galera, G. Loyau, J. P. Pujol, *Biochim Biophys Acta* **1991**, *1093*, 196.
[250] E. N. Blaney Davidson, E. L. Vitters, P. M. van der Kraan, W. B. van den Berg, *Ann Rheum Dis* **2006**, *65*, 1414.
[251] S. J. Lee, *Yonsei Med J* **2000**, *41*, 704.
[252] H. M. van Beuningen, P. M. van der Kraan, O. J. Arntz, W. B. van den Berg, *Lab Invest* **1994**, *71*, 279.
[253] E. N. Blaney Davidson, P. M. van der Kraan, W. B. van den Berg, *Osteoarthritis Cartilage* **2007**, *15*, 597.
[254] E. Lepowsky, M. Muradoglu, S. Tasoglu, *Bioprinting* **2018**, *11*, e00034.
[255] A. D. C. Blaeser, D. F.; Puster, U.; Fischer, H., *BioNanoMaterials* **2015**, *16*, 81.
[256] S. J. Müller, E. Mirzahossein, E. N. Iftekhar, C. Bächer, S. Schrüfer, D. W. Schubert, B. Fabry, S. Gekle, *PLoS One* **2020**, *15*, e0236371.
[257] I. B. Bekard, P. Asimakis, J. Bertolini, D. E. Dunstan, *Biopolymers* **2011**, *95*, 733.
[258] C. R. Thomas, D. Geer, *Biotechnol Lett* **2011**, *33*, 443.
[259] S. Warwel, G. Steinke, M. R. g. Klaas, *Biotechnol Tech* **1996**, *10*, 283.
[260] A. Heeres, K. Vanbroekhoven, W. Van Hecke, *Biochem Eng J* **2019**, *142*, 162.
[261] N. Schmitz, S. Laverty, V. B. Kraus, T. Aigner, *Osteoarthritis Cartilage* **2010**, *18 Suppl 3*, S113.
[262] M. C. Schneider, S. Chu, M. A. Randolph, S. J. Bryant, *Acta Biomater* **2019**, *93*, 97.
[263] P. W. Kopesky, E. J. Vanderploeg, J. D. Kisiday, D. D. Frisbie, J. D. Sandy, A. J. Grodzinsky, *Tissue Eng Part A* **2011**, *17*, 83.
[264] B. Choi, S. Kim, J. Fan, T. Kowalski, F. Petrigliano, D. Evseenko, M. Lee, *Biomater Sci* **2015**, *3*, 742.
[265] J. Lam, N. F. Truong, T. Segura, *Acta Biomater* **2014**, *10*, 1571.
[266] H. D. Kim, R. F. Valentini, *J Biomed Mater Res* **2002**, *59*, 573.
[267] S. Cai, Y. Liu, X. Zheng Shu, G. D. Prestwich, *Biomaterials* **2005**, *26*, 6054.
[268] K. Tzavlaki, A. Moustakas, *Biomolecules* **2020**, *10*, 487.
[269] F. Huang, Y.-G. Chen, *Cell Biosci* **2012**, *2*, 9.
[270] L. Lucas, A. Aravind, P. Emma, M. Christophe, C. Edwin-Joffrey, *Bioprinting* **2021**, *21*.
[271] M. Askari, M. A. Naniz, M. Kouhi, A. Saberi, A. Zolfagharian, M. Bodaghi, *Biomater Sci* **2020**.
[272] A. Weiss, L. Attisano, *Wiley Interdiscip Rev Dev Biol* **2013**, *2*, 47.
[273] B. Song, K. D. Estrada, K. M. Lyons, *Cytokine Growth Factor Rev* **2009**, *20*, 379.
[274] W. Wang, D. Rigueur, K. M. Lyons, *Birth Defects Res C Embryo Today* **2014**, *102*, 37.
[275] X. Zhang, Y. Liu, C. Luo, C. Zhai, Z. Li, Y. Zhang, T. Yuan, S. Dong, J. Zhang, W. Fan, *Mater Sci Eng C Mater Biol Appl* **2021**, *118*, 111388.
[276] M. Du, B. Chen, Q. Meng, S. Liu, X. Zheng, C. Zhang, H. Wang, H. Li, N. Wang, J. Dai, *Biofabrication* **2015**, *7*, 044104.
[277] J. H. Park, G. J. Gillispie, J. S. Copus, W. Zhang, A. Atala, J. J. Yoo, P. C. Yelick, S. J. Lee, *Biofabrication* **2020**, *12*, 035029.
[278] D. Chimene, R. Kaunas, A. K. Gaharwar, *Adv Mater* **2020**, *32*, 1902026.
[279] C. T. Wong Po Foo, J. S. Lee, W. Mulyasasmita, A. Parisi-Amon, S. C. Heilshorn, *PNAS* **2009**, *106*, 22067.
[280] Z. Cai, H. Zhang, Y. Wei, M. Wu, A. Fu, *Biomater Sci* **2019**, *7*, 3143.
[281] D. E. Soranno, L. Kirkbride-Romeo, D. Han, C. Altmann, C. B. Rodell, *J Biomed Mater Res Part A* **2021**.

[282] B. D. Olsen, J. A. Kornfield, D. A. Tirrell, *Macromolecules* **2010**, *43*, 9094.
[283] S. M. Hull, L. G. Brunel, S. C. Heilshorn, *Adv Mater* **2021**, 2103691.
[284] K. Zhu, N. Chen, X. Liu, X. Mu, W. Zhang, C. Wang, Y. S. Zhang, *Macromol Biosci* **2018**, *18*, 1800127.
[285] K. Dubbin, Y. Hori, K. K. Lewis, S. C. Heilshorn, *Adv Healthc Mater* **2016**, *5*, 2488.
[286] T. Hu, X. Cui, M. Zhu, M. Wu, Y. Tian, B. Yao, W. Song, Z. Niu, S. Huang, X. Fu, *Bioact Mater* **2020**, *5*, 808.
[287] A. L. Rutz, K. E. Hyland, A. E. Jakus, W. R. Burghardt, R. N. Shah, *Adv Mater* **2015**, *27*, 1607.
[288] C. B. Highley, C. B. Rodell, J. A. Burdick, *Adv Mater* **2015**, *27*, 5075.
[289] H. D. Lu, D. E. Soranno, C. B. Rodell, I. L. Kim, J. A. Burdick, *Adv Healthc Mater* **2013**, *2*, 1028.
[290] J. Y. Shin, Y. H. Yeo, J. E. Jeong, S. A. Park, W. H. Park, *Carbohydr Polym* **2020**, *238*, 116192.
[291] T. Iskratsch, H. Wolfenson, M. P. Sheetz, *Nat Rev Mol Cell Biol* **2014**, *15*, 825.
[292] C. M. Lo, H. B. Wang, M. Dembo, Y. L. Wang, *Biophys J* **2000**, *79*, 144.
[293] T. Yeung, P. C. Georges, L. A. Flanagan, B. Marg, M. Ortiz, M. Funaki, N. Zahir, W. Ming, V. Weaver, P. A. Janmey, *Cell Motil Cytoskeleton* **2005**, *60*, 24.
[294] E. Hadjipanayi, V. Mudera, R. A. Brown, *J Tissue Eng Regen Med* **2009**, *3*, 77.
[295] K. C. Spencer, J. C. Sy, K. B. Ramadi, A. M. Graybiel, R. Langer, M. J. Cima, *Sci Rep* **2017**, *7*, 1952.
[296] B. Wehrle-Haller, *Curr Opin Cell Biol* **2012**, *24*, 569.
[297] O. Chaudhuri, J. Cooper-White, P. A. Janmey, D. J. Mooney, V. B. Shenoy, *Nature* **2020**, *584*, 535.
[298] O. Chaudhuri, L. Gu, D. Klumpers, M. Darnell, S. A. Bencherif, J. C. Weaver, N. Huebsch, H. P. Lee, E. Lippens, G. N. Duda, D. J. Mooney, *Nat Mater* **2016**, *15*, 326.
[299] J. Malda, D. E. Martens, J. Tramper, C. A. van Blitterswijk, J. Riesle, *Crit Rev Biotechnol* **2003**, *23*, 175.
[300] C. Vinatier, D. Mrugala, C. Jorgensen, J. Guicheux, D. Noël, *Trends Biotechnol* **2009**, *27*, 307.
[301] J. C. Robins, N. Akeno, A. Mukherjee, R. R. Dalal, B. J. Aronow, P. Koopman, T. L. Clemens, *Bone* **2005**, *37*, 313.
[302] B. L. Thoms, K. A. Dudek, J. E. Lafont, C. L. Murphy, *Arthritis Rheum* **2013**, *65*, 1302.
[303] K. Guillemin, M. A. Krasnow, *Cell* **1997**, *89*, 9.
[304] E. Schipani, H. E. Ryan, S. Didrickson, T. Kobayashi, M. Knight, R. S. Johnson, *Genes Dev* **2001**, *15*, 2865.
[305] J. E. Lafont, S. Talma, C. L. Murphy, *Arthritis Rheumatol* **2007**, *56*, 3297.
[306] H. Betre, S. R. Ong, F. Guilak, A. Chilkoti, B. Fermor, L. A. Setton, *Biomaterials* **2006**, *27*, 91.
[307] L. A. McMahon, F. J. O'Brien, P. J. Prendergast, *Regen Med* **2008**, *3*, 743.
[308] C. Correia, A. L. Pereira, A. R. Duarte, A. M. Frias, A. J. Pedro, J. T. Oliveira, R. A. Sousa, R. L. Reis, *Tissue Eng Part A* **2012**, *18*, 1979.
[309] J. P. A. Arokoski, J. S. Jurvelin, U. Väätäinen, H. J. Helminen, *Scand J Med Sci Sports* **2000**, *10*, 186.
[310] R. M. Schulz, A. Bader, *Eur Biophys J* **2007**, *36*, 539.
[311] M. Walker, J. Luo, E. W. Pringle, M. Cantini, *Mater Sci Eng C* **2021**, *121*, 111822.
[312] P. A. Parmar, J.-P. St-Pierre, L. W. Chow, C. D. Spicer, V. Stoichevska, Y. Y. Peng, J. A. Werkmeister, J. A. M. Ramshaw, M. M. Stevens, *Acta Biomater* **2017**, *51*, 75.
[313] A. K. Kudva, F. P. Luyten, J. Patterson, *J Biomed Mater Res A* **2018**, *106*, 33.
[314] S. L. Vega, M. Y. Kwon, K. H. Song, C. Wang, R. L. Mauck, L. Han, J. A. Burdick, *Nat Commun* **2018**, *9*, 614.
[315] L. Bian, M. Guvendiren, R. L. Mauck, J. A. Burdick, *PNAS* **2013**, *110*, 10117.
[316] S. L. Vega, M. Kwon, R. L. Mauck, J. A. Burdick, *Ann Biomed Eng* **2016**, *44*, 1921.
[317] J. E. Frith, R. J. Mills, J. E. Hudson, J. J. Cooper-White, *Stem Cells Dev* **2012**, *21*, 2442.
[318] J. E. Scott, *Biochemistry* **1996**, *35*, 8795.
[319] C. N. Salinas, K. S. Anseth, *Ann Biomed Eng* **2009**, *90*, 456.
[320] H. Shen, H. Lin, A. X. Sun, S. Song, B. Wang, Y. Yang, J. Dai, R. S. Tuan, *Acta Biomater* **2020**, *105*, 44.
[321] S. Mahzoon, J. M. Townsend, T. N. Lam, V. Sjoelund, M. S. Detamore, *Ann Biomed Eng* **2019**, *47*, 2308.
[322] S. H. Park, J. Y. Seo, J. Y. Park, Y. B. Ji, K. Kim, H. S. Choi, S. Choi, J. H. Kim, B. H. Min, M. S. Kim, *NPG Asia Materials* **2019**, *11*, 1.
[323] C. Evans, *Int Orthop* **2014**, *38*, 1761.
[324] A. C. Daly, F. E. Freeman, T. Gonzalez-Fernandez, S. E. Critchley, J. Nulty, D. J. Kelly, *Adv Healthc Mater* **2017**, *6*, 1700298.
[325] T. Gonzalez-Fernandez, E. G. Tierney, G. M. Cunniffe, F. J. O'Brien, D. J. Kelly, *Tissue Eng Part A* **2016**, *22*, 776.

[326] J. M. Brunger, N. P. Huynh, C. M. Guenther, P. Perez-Pinera, F. T. Moutos, J. Sanchez-Adams, C. A. Gersbach, F. Guilak, *PNAS* **2014**, *111*, E798.
[327] J. Chen, H. Chen, P. Li, H. Diao, S. Zhu, L. Dong, R. Wang, T. Guo, J. Zhao, J. Zhang, *Biomaterials* **2011**, *32*, 4793.
[328] P. A. Parmar, S. C. Skaalure, L. W. Chow, J.-P. St-Pierre, V. Stoichevska, Y. Y. Peng, J. A. Werkmeister, J. A. M. Ramshaw, M. M. Stevens, *Biomaterials* **2016**, *99*, 56.
[329] L. Fu, Z. Yang, C. Gao, H. Li, Z. Yuan, F. Wang, X. Sui, S. Liu, Q. Guo, *Regen Biomater* **2020**, *7*, 527.
[330] T. K. Kim, B. Sharma, C. G. Williams, M. A. Ruffner, A. Malik, E. G. McFarland, J. H. Elisseeff, *Osteoarthritis Cartilage* **2003**, *11*, 653.
[331] M. Kim, M. J. Farrell, D. R. Steinberg, J. A. Burdick, R. L. Mauck, *Acta Biomater* **2017**, *58*, 1.
[332] R. Levato, W. R. Webb, I. A. Otto, A. Mensinga, Y. Zhang, M. van Rijen, R. van Weeren, I. M. Khan, J. Malda, *Acta Biomater* **2017**, *61*, 41.
[333] S. Schmidt, F. Abinzano, A. Mensinga, J. Teßmar, J. Groll, J. Malda, R. Levato, T. Blunk, *Int J Mol Sci* **2020**, *21*, 7071.
[334] S. McGivern, H. Boutouil, G. Al-Kharusi, S. Little, N. J. Dunne, T. J. Levingstone, *Bioengineering (Basel)* **2021**, *8*.
[335] K. Parratt, M. Smerchansky, Q. Stiggers, K. Roy, *J Mater Chem B* **2017**, *5*, 6237.
[336] H. A. Owida, R. Yang, L. Cen, N. J. Kuiper, Y. Yang, *J R Soc Interface* **2018**, *15*.
[337] Y. Zhu, H. Wu, S. Sun, T. Zhou, J. Wu, Y. Wan, *J Mech Behav Biomed Mater* **2014**, *36*, 32.
[338] J. Schiavi, L. Reppel, N. Charif, N. de Isla, D. Mainard, N. Benkirane-Jessel, J. F. Stoltz, R. Rahouadj, C. Huselstein, *J Tissue Eng Regen Med* **2018**, *12*, 360.
[339] H. Zhang, H. Huang, G. Hao, Y. Zhang, H. Ding, Z. Fan, L. Sun, *Adv Funct Mater* **2021**, *31*, 2006697.
[340] F. Gao, Z. Xu, Q. Liang, B. Liu, H. Li, Y. Wu, Y. Zhang, Z. Lin, M. Wu, C. Ruan, W. Liu, *Adv Funct Mater* **2018**, *28*, 1706644.
[341] C. Ding, Z. Qiao, W. Jiang, H. Li, J. Wei, G. Zhou, K. Dai, *Biomaterials* **2013**, *34*, 6706.
[342] T. B. Woodfield, M. Guggenheim, B. von Rechenberg, J. Riesle, C. A. van Blitterswijk, V. Wedler, *Cell Prolif* **2009**, *42*, 485.
[343] C. H. Lee, J. L. Cook, A. Mendelson, E. K. Moioli, H. Yao, J. J. Mao, *Lancet* **2010**, *376*, 440.
[344] M. B. Albro, R. J. Nims, K. M. Durney, A. D. Cigan, J. J. Shim, G. Vunjak-Novakovic, C. T. Hung, G. A. Ateshian, *Biomaterials* **2016**, *77*, 173.
[345] O. Jeon, D. S. Alt, S. W. Linderman, E. Alsberg, *Adv Mater* **2013**, *25*, 6366.
[346] X. Wang, E. Wenk, X. Zhang, L. Meinel, G. Vunjak-Novakovic, D. L. Kaplan, *J Control Release* **2009**, *134*, 81.
[347] S. Moeinzadeh, S. R. P. Shariati, E. Jabbari, *Biomaterials* **2016**, *92*, 57.
[348] W. Liu, Y. S. Zhang, M. A. Heinrich, F. De Ferrari, H. L. Jang, S. M. Bakht, M. M. Alvarez, J. Yang, Y. C. Li, G. Trujillo-de Santiago, *Adv Mater* **2017**, *29*, 1604630.

8. Annex

8.1. Declaration of authorship

Statement of individual author contributions and of legal second publication rights:

Publication: Hauptstein J, Böck T, Bartolf-Kopp M, Forster L, Stahlhut P, Nadernezhad A, Blahetek G, Zernecke-Madsen A, Detsch R, Jüngst T, Groll J, Teßmar J and Blunk T, Hyaluronic Acid-Based Bioink Composition Enabling 3D Bioprinting and Improving Quality of Deposited Cartilaginous Extracellular Matrix, Advanced Healthcare Materials, 2020, DOI: 10.1002/adhm.202000737[188]

Participated in	**Author Initials,** Responsibility decreasing from left to right				
Study Design Methods Development	JH JH	TB MB	JT TBö	JG, TJ	
Data Collection	JH	MB	AN, PS	JT, TBö	GB, AZ
Data Analysis and Interpretation	JH	TB	JT	RD	
Manuscript Writing Writing of Introduction Writing of Materials & Methods Writing of Discussion Writing of First Draft	 TBö JH JH JH	 TB TB TB TB	 MB 	 AN, PS 	

Publication: Hauptstein J[#], Forster L[#], Nadernezhad A, Horder H, Stahlhut P, Groll J, Blunk T* and Teßmar J*, Bioink Platform Utilizing Dual-stage Crosslinking of Hyaluronic Acid Tailored for Chondrogenic Differentiation of Mesenchymal Stromal Cells, Macromolecular Bioscience, 2021, DOI: 10.1002/mabi.202100331[223]

Participated in	**Author Initials,** Responsibility decreasing from left to right				
Study Design Methods Development	TB, JT JH	JH, LF LF	JG HH		
Data Collection	JH	LF	AN	HH	PS
Data Analysis and Interpretation	JH	LF	TB	JT	
Manuscript Writing Writing of Introduction Writing of Materials & Methods Writing of Discussion Writing of First Draft	 JH JH JH JH	 TB LF LF LF	 AN TB TB	 TB JT JT	 JT

Explanations: [#] equal contribution, * corresponding author

Publication: Hauptstein J, Forster L, Nadernezhad A, Groll J, Teßmar J and Blunk T, Tethered TGF-β1 in a Hyaluronic Acid-based Bioink for Bioprinting Cartilaginous Tissues, International Journal of Molecular Sciences, 2022, DOI: 10.3390/ijms23020924[244]					
Participated in	**Author Initials,** Responsibility decreasing from left to right				
Study Design Methods Development	JH JH	TB	JT	JG	
Data Collection	JH	LF	AN		
Data Analysis and Interpretation	JH	TB			
Manuscript Writing Writing of Introduction Writing of Materials & Methods Writing of Discussion Writing of First Draft	 JH JH JH JH	 TB LF TB TB	 AN 	 TB 	

The doctoral researcher confirms that she has obtained permission from both the publishers and the co-authors for legal second publication.

The doctoral researcher and the primary supervisor confirm the correctness of the above mentioned assessment.

Julia Hauptstein	17.01.2022	Würzburg	
Doctoral Researcher's Name	Date	Place	Signature

Prof. Dr. Torsten Blunk	17.01.2022	Würzburg	
Primary Supervisor's Name	Date	Place	Signature

Statement of individual author contributions to figures/tables included in the manuscripts:

Publication: Hauptstein J, Böck T, Bartolf-Kopp M, Forster L, Stahlhut P, Nadernezhad A, Blahetek G, Zernecke-Madsen A, Detsch R, Jüngst T, Groll J, Teßmar J and Blunk T, Hyaluronic Acid-Based Bioink Composition Enabling 3D Bioprinting and Improving Quality of Deposited Cartilaginous Extracellular Matrix, Advanced Healthcare Materials, 2020, DOI: 10.1002/adhm.202000737[188]					
Figure	**Author Initials,** Responsibility decreasing from left to right				
1	JH	TB			
2	JH	TB			
3	JH	TB			
4	JH	TB			
5	JH	TB			
6	JH	TB			
7	JH	JT	TB		
8	JH	MB	TBö	TB	
S1	LF	JT			
S2	JH	TB			
S3	AN	JH	TB		
S4	JH	TB			
S5	JH	TB			
S6	JH	TB			
S7	JH	TB			
S8	JH	TB			
S9	JH	PS	TB		
Table 1	JH	TB			

Publication: Hauptstein J#, Forster L#, Nadernezhad A, Horder H, Stahlhut S, Groll J, Blunk T* and Teßmar J*, Bioink Platform Utilizing Dual-stage Crosslinking of Hyaluronic Acid Tailored for Chondrogenic Differentiation of Mesenchymal Stromal Cells, Macromolecular Bioscience, 2021, DOI: 10.1002/mabi.202100331[223]					
Figure	**Author Initials,** Responsibility decreasing from left to right				
1	JH	TB	JT		
2	LF	JH	JT	TB	
3	JH	TB			
4	AN	LF	JT		
5	JH	HH	TB		
6	JH	PS	TB		
7	JH	TB			
8	JH	TB			
9	JH	TB	JT		
S1	LF	JT			
S2	LF	JT			

S3	LF	JT			
S4	JH	TB			
S5	JH	TB			
S6	JH	TB			
S7	JH	TB			
S8	JH	TB			
S9	JH	TB			
S10	JH	TB			
Table 1	LF	JT			
Table S1	LF	JT			
Table S2	LF	AN	JT		
Table S3	JH	TB			

Explanations: # equal contribution, * corresponding author

Publication: Hauptstein J, Forster L, Nadernezhad A, Groll J, Teßmar J and Blunk T, Tethered TGF-β1 in a Hyaluronic Acid-based Bioink for Bioprinting Cartilaginous Tissues, International Journal of Molecular Sciences, 2022, DOI: 10.3390/ijms23020924[244]					
Figure	**Author Initials,** Responsibility decreasing from left to right				
1	JH	TB			
2	JH	AN	TB		
3	JH	TB			
4	JH	TB			
5	JH	TB			
6	JH	TB			
7	JH	TB			
8	JH	TB	JT		
S1	LF	JH	JT		
S2	JH	TB			
S3	JH	TB			
S4	JH	TB			
S5	JH	TB			
S6	JH	TB			
S7	JH	TB			
Table S1	JH	TB			

I also confirm my primary supervisor's acceptance.

Julia Hauptstein	17.01.2022	Würzburg	
Doctoral Researcher's Name	Date	Place	Signature

8.2. Danksagung

In erster Linie will ich mich ganz besonders herzlich bei Herrn Prof. Dr. Torsten Blunk für die Möglichkeit bedanken, meine Doktorarbeit in seiner Arbeitsgruppe anzufertigen. Er hat nicht nur engagiert und fachlich kompetent diese Arbeit betreut, sondern hatte auch immer ein offenes Ohr für die Probleme des Alltags und war stets voller Vertrauen in meine Arbeit und meine Ideen. Die fachlichen Gespräche und Diskussionen auf Augenhöhe haben mir sehr geholfen, mich zu einer eigenständigen Wissenschaftlerin zu entwickeln. Ich bin außerdem sehr dankbar dafür, dass er mir die Möglichkeit eröffnet hat, an diversen nationalen und internationalen Konferenzen und persönlichen Weiterbildungen teilzunehmen.

Herrn Dr. Jörg Teßmar danke ich herzlich für die vielen wissenschaftlichen Gespräche im Projekt und bei Publikationen. Seine bildlichen Erklärungen von chemischen Sachverhalten haben nicht nur für schnelles Verständnis gesorgt, sondern auch für lustige Auflockerungen im Alltag. Herzlichen Dank für die gute Zusammenarbeit und die Übernahme meines Zweitgutachtens.

Bei Herrn Dr. Rainer Detsch will ich mich für die anregenden Diskussionen in unseren Mentoratsgesprächen und den projektübergreifenden Telefonkonferenzen bedanken. Vielen Dank für die Unterstützung meiner Promotion als Mitglied meines Thesis Komitees.

Prof. Dr. Carmen Villmann danke ich für die Übernahme des Prüfungsvorsitzes.

Mein besonderer Dank gilt meinem Projektpartner Leonard Forster. Seine chemischen Synthesen und Modifikationen, sowie die Charakterisierung aller Tintenkomponenten waren die Grundlage dieses Projekts. Herzlichen Dank für die gute Zusammenarbeit und die vielen fachlichen und persönlichen Gespräche in den letzten Jahren.
Auch den anderen Mitarbeitern des FMZ will ich herzlich für die freundliche Aufnahme in ihren Laboren sowie die fachliche Hilfe für mein Projekt danken. Dies gilt insbesondere für Ali Nadernezhad, Philipp Stahlhut, Dr. Thomas Böck, Michael Bartolf-Kopp und Dr. Tomasz Jüngst.

Herzlichen Dank an alle meine Kollegen der AG Blunk für das hervorragende Arbeitsklima, die gute Zusammenarbeit und stetige Unterstützung in den letzten Jahren. Weiterhin danke ich meinen Mitstreitern im SFB/TRR 225 in Würzburg, Erlangen und Bayreuth für die interdisziplinäre Zusammenarbeit, die anregenden Diskussionen auf allen Klausurtagungen und Summerschools, sowie für die fantastischen Abende nach dem offiziellen Programm.

Zum Schluss will ich mich von ganzem Herzen bei meinem Mann Niklas, meiner Familie und meinen Freunden bedanken. Eure bedingungslose Unterstützung hat meinen Werdegang und diese Arbeit überhaupt erst ermöglicht.

8.3. Affidavit – Eidesstattliche Erklärung

I hereby confirm that my thesis entitled *Hyaluronic Acid-based Multifunctional Bioinks for 3D Bioprinting of Mesenchymal Stromal Cells for Cartilage Regeneration* is the result of my own work. I did not receive any help or support from commercial consultants. All sources and/or materials applied are listed and specified in the thesis.

Furthermore, I confirm that this thesis has not yet been submitted as part of another examination process neither in identical nor in similar form.

Würzburg, 17.01.2022

Place, Date	Signature

Hiermit erkläre ich an Eides statt, die Dissertation *Hyaluronsäure-basierte multifunktionale Biotinten für den 3D Biodruck von mesenchymalen Stromazellen zur Knorpelregeneration* eigenständig, d.h. insbesondere selbstständig und ohne Hilfe eines kommerziellen Promotionsberaters, angefertigt und keine anderen als die von mir angegebenen Quellen und Hilfsmittel verwendet zu haben.

Ich erkläre außerdem, dass die Dissertation weder in gleicher noch in ähnlicher Form bereits in einem anderen Prüfungsverfahren vorgelegen hat.

Würzburg, 17.01.2022

Ort, Datum	Unterschrift

8.4. Curriculum vitae

8.5. Publications and conference contributions

Publications

1. **J. Hauptstein**, L. Forster, A. Nadernezhad, J. Groll, J. Teßmar, T. Blunk, Tethered TGF-β1 in a Hyaluronic Acid-based Bioink for Bioprinting Cartilaginous Tissues, International Journal of Molecular Sciences, 2022, DOI: 10.3390/ijms23020924
2. **J. Hauptstein**[#], L. Forster[#], A. Nadernezhad, J. Groll, T. Blunk*, J. Teßmar*, Bioink Platform Utilizing Dual-stage Crosslinking of Hyaluronic Acid Tailored for Chondrogenic Differentiation of Mesenchymal Stromal Cells, Macromolecular Bioscience, 2021, DOI: 10.1002/mabi.202100331
   [#] equal contribution, * corresponding author
3. **J. Hauptstein**, T. Böck, M. Bartolf-Kopp, L. Forster, P. Stahlhut, A. Nadernezhad, G. Blahetek, A. Zernecke-Madsen, R. Detsch, T. Jüngst, J. Groll, J. Teßmar, T. Blunk, Hyaluronic Acid-Based Bioink Composition Enabling 3D Bioprinting and Improving Quality of Deposited Cartilaginous Extracellular Matrix, Advanced Healthcare Materials, 2020, DOI: 10.1002/adhm.202000737
4. R. Schmid, S. Schmidt, J. Hazur, R. Detsch, E. Maurer, A. Boccaccini, **J. Hauptstein**, J. Teßmar, T. Blunk, S. Schrüfer, D. Schubert, R. Horch, A. Bosserhoff, A. Arkudas, A. Kengelbach-Weigand, Comparison of Hydrogels for the Development of Well-Defined 3D Cancer Models of Breast Cancer and Melanoma, Cancers, 2020, DOI: 10.3390/cancers12082320

Oral presentations at international conferences

1. **J. Hauptstein**, L. Forster, A. Nadernezhad, J. Groll, T. Blunk, J. Teßmar, Hyaluronic Acid-based Bioink with Dual-stage Crosslinking Mechanism Utilized for Cartilage Tissue Engineering, International Society for Biofabrication ISBF 2021, Wollongong, Australia, online conference
2. **J. Hauptstein**, T. Böck, M. Bartolf-Kopp, L. Forster, P. Stahlhut, A. Nadernezhad, G. Blahetek, A. Zernecke-Madsen, R. Detsch, T. Jüngst, J. Groll, J. Teßmar, T. Blunk, Hyaluronic Acid-based Bioink Composition Enabling 3D Bioprinting and Improving Quality of Deposited Cartilaginous Extracellular Matrix, Bioinspired Materials 2020, Irsee, Germany, online conference
3. **J. Hauptstein**, T. Böck, M. Bartolf-Kopp, L. Forster, P. Stahlhut, A. Nadernezhad, G. Blahetek, A. Zernecke-Madsen, R. Detsch, T. Jüngst, J. Groll, J. Teßmar, T. Blunk, Hyaluronic Acid-based Bioink Composition Enabling 3D Bioprinting and Improving Quality of Deposited Cartilaginous Extracellular Matrix, Materials Science and Engineering MSE 2020, Darmstadt, Germany, online conference
4. L. Forster, **J. Hauptstein**, A. Nadernezhad, J. Groll, T. Blunk, J. Teßmar, Hyaluronan-based Dual-stage Crosslinking Approach for 3D Bioprinting of Mesenchymal Stem Cells, World Biomaterials Congress WBC 2020, Glasgow, Scotland, online conference

Poster presentations at international conferences

1. **J. Hauptstein**, L. Forster, A. Nadernezhad, J. Groll, T. Blunk, J. Teßmar, Dual-stage Crosslinked Hyaluronic Acid-based Bioink Tailored for Chondrogenic Differentiation of Mesenchymal Stromal Cells, European Society for Biomaterials ESB 2021, Porto, Portugal, online conference
2. D. Janzen, E. Bakirci, **J. Hauptstein**, L. Forster, J. Teßmar, T. Blunk, P. Dalton, C. Villmann, Neuronal Networks in a Fiber-Reinforced Hyaluronic Acid-Based Matrix, European Society for Biomaterials ESB 2021, Porto, Portugal, online conference
3. L. Forster, **J. Hauptstein**, J. Weichhold, A. Nadernezhad, T. Böhm, T. Zorn, S. Schmidt, T. Blunk, J. Teßmar, Hyaluronan-based Dual-stage Crosslinking Approach for 3D Bioprinting of Mesenchymal Stem Cells, Bioinspired Materials 2020, Irsee, Germany, online conference
4. S. Schmidt, I.A.D. Mancini, T. Boeck, F. Abinzano, A. Mensinga, **J. Hauptstein**, J. Teßmar, P.R. van Weeren, J. Malda, J. Groll, R. Levato, T. Blunk, Mesenchymal Stem Cells and Articular Cartilage Progenitor Cells: Chondrogenic Differentiation in a Hyaluronic Acid Hydrogel, EUREKA! Symposium 2019, Würzburg, Germany
5. S. Schmidt, I.A.D. Mancini, T. Boeck, F. Abinzano, A. Mensinga, **J. Martini**, J. Teßmar, P.R. van Weeren, J. Malda, J. Groll, R. Levato, T. Blunk, Chondrogenic Differentiation of Mesenchymal Stem Cells and Chondroprogenitor Cells in a 3D-printable Hyaluronic acid Hydrogel, International Society for Biofabrication ISBF 2018, Würzburg, Germany